

LUND UNIVERSITY

Involvement of endosomal and synaptic Aβ in models of Alzheimer's disease.

Willén, Katarina

2017

Document Version:
Publisher's PDF, also known as Version of record

Link to publication

Citation for published version (APA):
Willén, K. (2017). *Involvement of endosomal and synaptic Aβ in models of Alzheimer's disease.* [Doctoral Thesis (compilation), Experimental Dementia Research]. Lund University: Faculty of Medicine.

Total number of authors:
1

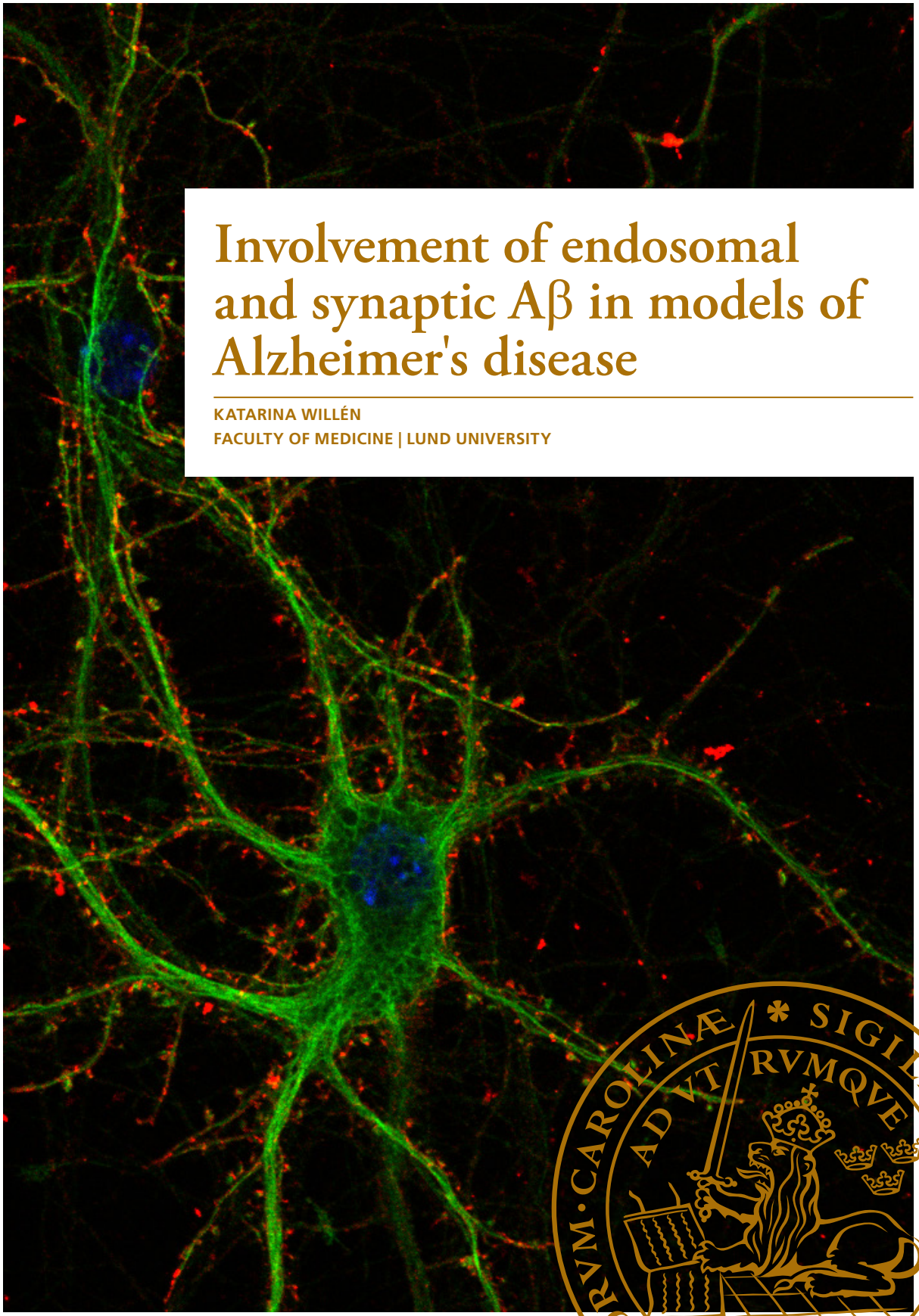
General rights
Unless other specific re-use rights are stated the following general rights apply:
Copyright and moral rights for the publications made accessible in the public portal are retained by the authors and/or other copyright owners and it is a condition of accessing publications that users recognise and abide by the legal requirements associated with these rights.
• Users may download and print one copy of any publication from the public portal for the purpose of private study or research.
• You may not further distribute the material or use it for any profit-making activity or commercial gain
• You may freely distribute the URL identifying the publication in the public portal

Read more about Creative commons licenses: https://creativecommons.org/licenses/

Take down policy
If you believe that this document breaches copyright please contact us providing details, and we will remove access to the work immediately and investigate your claim.

LUND UNIVERSITY

PO Box 117
221 00 Lund
+46 46-222 00 00



Involvement of endosomal and synaptic Aβ in models of Alzheimer's disease

KATARINA WILLÉN
FACULTY OF MEDICINE | LUND UNIVERSITY

Involvement of endosomal and synaptic Aβ in models of Alzheimer's disease

Involvement of endosomal and synaptic Aβ in models of Alzheimer's disease

Katarina Willén



LUND
UNIVERSITY

DOCTORAL DISSERTATION
by due permission of the Faculty of Medicine, Lund University, Sweden.
To be defended at Segerfalksalen, Wallenberg Neuroscience Center, Lund University. December 7th 2017 at 13:00.

Faculty opponent
Professor Tobias Hartmann

Saarland University, Homburg, Germany

Organization
LUND UNIVERSITY
Faculty of Medicine,
Dept. of Experimental Medical Science,
Experimental Dementia Research Unit

Author: Katarina Willén

Document name
Doctoral thesis

Date of issue
2017-11-16

Sponsoring organization

Title and subtitle: Involvement of endosomal and synaptic Aβ in models of Alzheimer's disease

Abstract

Alzheimer's disease (AD) is a devastating chronic neurodegenerative disease that accounts for 60-80% of all dementia cases. AD is characterized by progressive decline in cognitive function, aggregated β-amyloid (Aβ) in amyloid plaques, neurofibrillary tangles (NFTs), dystrophic neurites and loss of synapses and neurons. However, the earliest changes in the pathology of AD occur in the endocytic pathway with enlarged endosomes and accumulation of multivesicular bodies (MVBs), lysosomes and autophagic vacuoles. Aβ accumulates and aggregates particularly in MVBs in synaptic terminals, with signs of synaptic pathology. It is also well known that synaptic loss is a better correlate of cognitive decline than plaques or NFTs.

Hence, the aim of this thesis was to investigate the role of Aβ in the endocytic pathway and at synapses in AD. We found that extracellularly applied Aβ1-42 is taken up by primary neurons at synapses, and more by excitatory CAMKIIα-positive than inhibitory GAD67-positive ones. However, with no clear preference to the pre- or the post-synaptic site. Aβ1-42 uptake led to enlarged diameter of MVBs and aggregation of Aβ1-42 in endocytic vesicles. With time, loss of impermeability appeared in the endocytic pathway with oligomeric or fibrillar structures extending out extracellularly from late endocytic vesicles. Indicative of a role in plaque formation, markers of the endosomal sorting complexes required for transport (ESCRT)-components were found in plaques of AD-transgenic mouse models. We also show that APP traffics in the same subpopulation of MVBs as EGFR and is degraded in the lysosome. Depleting cells of ESCRT-components led to reduced secretion of Aβ and a marked intracellular accumulation of Aβ and APP. Hence, we suggest a scenario where disturbances in the MVB pathway, caused by Aβ, or vice versa, lead to a vicious circle of more Aβ accumulation and aggregation.

We further investigated the native state of this early Aβ aggregation in a mouse model of AD showing that focal β-sheet formation begins already before the onset of plaques. Here, we also confirmed the findings of Aβ accumulation leading to disrupted synaptic terminals in AD-transgenic mice brain. Additionally, we present data supporting the requirement of APP for normal synaptic composition of mature neurons.

Taken together, this work further strengthens the significance of Aβ accumulation and aggregation in the endocytic pathway at synapses, as an early event in AD pathogenesis.

Key words: Alzheimer's disease; Amyloid; Multivesicular body; APP

Classification system and/or index terms (if any)

Supplementary bibliographical information | Language

ISSN and key title 1652-8220 | ISBN 978-91-7619-559-8

Recipient's notes | Number of pages 80 | Price

Security classification

I, the undersigned, being the copyright owner of the abstract of the above-mentioned dissertation, hereby grant to all reference sources permission to publish and disseminate the abstract of the above-mentioned dissertation.

Signature Katarina Willén Date 2017-11-06

Involvement of endosomal and synaptic Aβ in models of Alzheimer's disease

Katarina Willén



LUND
UNIVERSITY

Coverphoto by Katarina Willén

Copyright Katarina Willén and the respective publishers

Faculty of Medicine
Department of Experimental Medical Science

Lund University, Faculty of Medicine Doctoral Dissertation Series 2017:177
ISBN 978-91-7619-559-8
ISSN 1652-8220

Printed in Sweden by Media-Tryck, Lund University
Lund 2017

’Truth in science can be defined as the working hypothesis best suited to open the way to the next one’

Konrad Lorenz

’Nothing in life is to be feared, it is only to be understood. Now is the time to understand more, so that we may fear less.’

Marie Curie

Content

Content 9
Original papers 11
Papers outside of this thesis 12
Abstract 13
Populärvetenskaplig sammanfattning 15
List of abbreviations 17
Introduction 21
Alzheimer's disease 21
APP and Aß 25
Aβ at synapses 30
Endo-lysosomal pathway dysfunction in Alzheimer's disease 31
Aims of the thesis 35
Methodological considerations 37
Animals 37
Cell culture 37
Cell lines 37
Primary neurons 37
Production of plasmids and transfection 38
Production of viral vectors and transduction 38
Western blot 39
Sodium dodecyl sulfate polyacrylamide gel electrophoresis (SDS-PAGE) 39
Blue native polyacrylamide gel electrophoresis (BN-PAGE) 40
Immunofluorescence 40
Brain 40
Cells 40
Confocal microscopy 41
List of antibodies 42
Electron microscopy 44

Exosome isolation 44
Image analysis and quantification 45
Statistical analysis 46
Results 47
Heterogeneous association of Aß and APP with synapses (Paper I) 47
ESCRTs regulate APP sorting in MVBs and intracellular Aβ accumulation (Paper II) 51
Aβ accumulation causes MVB enlargement (Paper III) 53
Conformational changes in Aβ and APP before plaques (Paper IV) 56
APP depletion alters selective pre- and post-synaptic proteins (Paper V) 59
Discussion and concluding remarks 61
Future perspectives 65
Acknowledgement 67
References 69

Original papers

This thesis is based on the following papers, which will be referred to by their Roman numerals:

I. **Willén K**, Szroka A, Takahashi R, Gouras GK. Heterogeneous association of Alzheimer's linked amyloid-β and amyloid-β protein precursor with synapses. Journal of Alzheimer's disease, 2017;60(2):511-524.

II. Edgar JE, **Willén K**, Gouras GK, Futter CE. ESCRTs regulate amyloid precursor protein sorting in multivesicular bodies and intracellular amyloid-β accumulation. Journal of Cell Science, 2015 Jul 15;128(14):2520-8.

III. **Willén K**, Edgar JE, Hasegawa T, Tanaka N, Futter CE, Gouras GK. Aβ accumulation causes MVB enlargement and is modelled by dominant negative VPS4A. Molecular Neurodegeneration, 2017 Aug 23;12(1):61.

IV. Klementieva O, **Willén K**, Martinsson I, Israelsson B, Engdahl A, Cladera J, Uvdal P, Gouras GK. Pre-plaque conformational changes in Alzheimer's disease-linked Aβ/APP. Nature Communications, 2017 Mar 13;8:14726.

V. Martinsson I*, Capetillo-Zarate E*, Faideau M*, **Willén K***, Esteras N, Lin M, Frykman S, Tjernberg LO, Gouras GK. APP depletion alters selective pre- and post-synaptic proteins * **Equal contribution.** Manuscript.

Papers outside of this thesis

1. Gouras GK, **Willén K**, Tampellini D. Critical role of intraneuronal Aβ in Alzheimer's disease: technical challenges in studying intracellular Aβ. Life Sciences, 2012 Dec 10;91(23-24):1153-8.

2. Dunning CJ, McGauran G, **Willén K**, Gouras GK, O'Connell DJ, Linse S. Direct High Affinity Interaction between Aβ42 and GSK3α Stimulates Hyperphosphorylation of Tau. A New Molecular Link in Alzheimer's Disease? ACS Chemical Neuroscience, 2016 Feb 17;7(2):161-70.

3. Gouras GK, **Willén K,** Faideau M. The inside-out amyloid hypothesis and synapse pathology in Alzheimer's disease. Neurodegenerative Diseases, 2014;13(2-3):142-6. Review.

Abstract

Alzheimer's disease (AD) is a devastating chronic neurodegenerative disease that accounts for 60-80% of all dementia cases. AD is characterized by progressive decline in cognitive function, aggregated β-amyloid (Aβ) in amyloid plaques, neurofibrillary tangles (NFTs), dystrophic neurites and loss of synapses and neurons. However, the earliest changes in the pathology of AD occur in the endocytic pathway with enlarged endosomes and accumulation of multivesicular bodies (MVBs), lysosomes and autophagic vacuoles. Aβ accumulates and aggregates particularly in MVBs in synaptic terminals, with signs of synaptic pathology. It is also well known that synaptic loss is a better correlate of cognitive decline than plaques or NFTs.

Hence, the aim of this thesis was to investigate the role of Aβ in the endocytic pathway and at synapses in AD. We found that extracellularly applied Aβ1-42 is taken up by primary neurons at synapses, and more by excitatory CAMKIIα-positive than inhibitory GAD67-positive ones. However, with no clear preference to the pre- or the post-synaptic site. Aβ1-42 uptake led to enlarged diameter of MVBs and aggregation of Aβ1-42 in endocytic vesicles. With time, loss of impermeability appeared in the endocytic pathway with oligomeric or fibrillar structures extending out extracellularly from late endocytic vesicles. Indicative of a role in plaque formation, markers of the endosomal sorting complexes required for transport (ESCRT)-components were found in plaques of AD-transgenic mouse models. We also show that APP traffics in the same subpopulation of MVBs as EGFR and is degraded in the lysosome.

Depleting cells of ESCRT-components led to reduced secretion of Aβ and a marked intracellular accumulation of Aβ and APP. Hence, we suggest a scenario where disturbances in the MVB pathway, caused by Aβ, or vice versa, lead to a vicious circle of more Aβ accumulation and aggregation. We further investigated the native state of this early Aβ aggregation in a mouse model of AD showing that focal β-sheet formation begins already before the onset of plaques. Here, we also confirmed the findings of Aβ accumulation leading to disrupted synaptic terminals in AD-transgenic mice brain. Additionally, we present data supporting the requirement of APP for normal synaptic composition of mature neurons.

Taken together, this work further strengthens the significance of Aβ accumulation and aggregation in the endocytic pathway at synapses, as an early event in AD pathogenesis.

Populärvetenskaplig sammanfattning

Alzheimers sjukdom (AS) är en kronisk neurodegenerativ sjukdom som leder till en succesiv försämring av minne och kognition. I världen beräknas 46.8 miljoner människor vara drabbade av demens, i Sverige 170 000 personer, varav 60–80% av AS. AS föregås i de flesta fall av en fas som kallas lindrig kognitiv störning, då rubbningarna ännu inte är så allvarliga att personen inte kan leva ett självständigt dagligt liv. Trots intensiv forskning finns det ännu inget läkemedel som på lång sikt kan bromsa eller stoppa sjukdomsutvecklingen av AS. Studier visar att förändringarna i hjärnan börjar långt innan dess att symptomen är så allvarliga att patienten diagnostiseras med AS. Det finns därför hopp om att tidigare upptäckt och behandling, tillsammans med utveckling av nya läkemedel, ska kunna bromsa sjukdomsförloppet i framtiden.

AS karakteriseras bl.a. av förlust av synapser (kopplingar mellan nervceller), nervcellsdöd samt plack i hjärnan. Dessa plack består till stor del av ett litet protein, en peptid, som kallas β-amyloid (Aβ). Aβ produceras och utsöndras av nervceller och har en tendens att lätt klumpa ihop sig, aggregera, och bilda mindre ansamlingar, oligomerer, som är toxiska för nervcellerna, samt större fibrer och slutligen plack. Tidigt i sjukdomsutvecklingen sker en onormal ansamling av Aβ i synapserna i speciella strukturer som kallas multivesikulära kroppar. Multivesikulära kroppar är en typ av vesiklar i det endosomala systemet, det intrikata transportsystem som sorterar material från cellytan till olika platser i cellen för nedbrytning i lysosomer eller åter till cellytan för återanvändning eller utsöndring genom exocytos.

I denna avhandling visar vi att Aβ tas upp av odlade nervceller, och ackumuleras framförallt vid synapser. Många excitatoriska nervceller hade prominent synaptisk ackumulering av Aβ medan de inhibitoriska nervcellerna inte hade upptag av Aβ. Upptag av Aβ ledde till förstorade multivesikulära kroppar och till störningar i det endosomala systemet. Vi såg även att Aβ aggregerade i vesiklarna och bildade oligomerer och fibrer, vilket främjas av det låga pH-värdet som finns i dessa strukturer. När vi undersökte modifierade möss som används som modell för AS, fann vi ESCRT (endosomal sorting complexes required for transport)-komponenterna Tsg101 och VPS4 i placken i deras hjärnor. Detta tyder på att oligomererna och fibrerna som bildas i det endosomala systemet, kan vara en möjlig startpunkt för plackbildningen. Vi har även experimentellt inducerat störningar i det endosomala systemet, i ESCRT–komponenterna Hrs, Tsg101 och VPS4A, för att i

sin tur undersöka hur detta påverkar Aβ-ansamling i cellen. Vi fann att det ledde till en markant ökning av Aβ inne i cellen, medan utsöndringen av Aβ minskade. Vi såg även ökad fosforylering av proteinet tau vilket är ett utmärkande kännetecken i AS. Genom en typ av absorbtionsspektroskopi, FTIR, som tillåter oss att studera aggregationen i sin naturliga form, kunde vi upptäcka aggregation redan innan plack bildats, i hjärnsnitt från genetiskt modifierade möss. Dessutom presenterar vi data som visar på att proteinet APP (amyloid precursor protein), som kan klyvas till Aβ, är viktigt för normal proteinsammansättning i synapserna.

Tillsammans visar de arbeten som ingår i denna avhandling att det sker en skadlig ackumulering och aggregering av Aβ i det endosomala systemet i synapser, i tidiga skeden i modeller av AS.

List of abbreviations

α-CTF	α-C-terminal fragment of APP
β-CTF	β-C-terminal fragment of APP
μFTIR	Fourier transform infrared micro-spectroscopy
Aβ	β-amyloid
AD	Alzheimer's disease
AICD	APP intracellular domain
APP	amyloid precursor protein
APP KO	APP knockout
APPL1	APP-like protein 1
APPL2	APP-like protein 2
APP/PS1	B6.Cg-Tg(APPswe,PSEN1dE9)85Dbo/Mmjax mice
BACE1	β-site amyloid precursor protein cleaving enzyme
BIN1	bridging integrator 1
BN-PAGE	blue native polyacrylamide gel electrophoresis
BSA	bovine serum albumin
CD2AP	CD2-associated protein
CLEM	correlative light electron microscopy
CSF	cerebrospinal fluid
DIV	days in vitro
dnVPS4A	dominant negative form of VPS4A
EGFR	epidermal growth factor receptor
EM	electron microscopy
ER	endoplasmic reticulum

ERC	entorhinal cortex
ESCRT	endosomal sorting complexes required for transport
FBS	fetal bovine serum
FTD	frontotemporal dementia
GSK3	glycogen synthase kinase 3
GVD	granulovacuolar degeneration
GWAS	genome-wide association studies
H4-APP	H4 neuroglioma cells stably expressing human APP
IDE	insulin degrading enzyme
ILV	intraluminal vesicle
iNs	induced neurons
iPSCs	induced pluripotent stem cells
ISF	interstitial fluid
KO	knockout
LTD	long-term depression
LTP	long-term potentiation
MCC	Manders' colocalization coefficients
MCI	mild cognitive impairment
MOI	multiplicity of infection
MVB	Multivesicular body
NFTs	neurofibrillary tangles
NGS	normal goat serum
NMDA	N-methyl-D-aspartate
p3	3 kDa peptide
PBS	phosphate buffered saline
PBST	PBS with 0.1% Tween-20
PCC	Pearson's correlation coefficient
PFA	paraformaldehyde
PI3P	phosphatidylinositol 3-phosphate

PICALM	phosphatidylinositol-binding clathrin assembly protein
PMEL	premelanosome protein
PSEN1	presenilin 1
PSEN2	presenilin 2
PrPC	cellular prion protein
sAPPα	α-secretase cleaved soluble fragment of APP
sAPPβ	β-secretase cleaved soluble fragment of APP
SDS	sodium dodecyl sulfate
SDS-PAGE	Sodium dodecyl sulfate polyacrylamide gel electrophoresis
shRNA	short hairpin RNA
SORL1	sortilin-related receptor 1
TCA	trichloroacetic acid
TGN	trans-Golgi network
VPS4	vacuolar protein sorting-associated protein 4

Introduction

Alzheimer's disease

The first case of Alzheimer's disease (AD) was described in 1906 by Alois Alzheimer, but it took 60 years before AD was recognized as a common cause of dementia. Since then extensive research has been carried out.

Prevalence

AD is a chronic neurodegenerative disease that accounts for 60-80% of all dementia cases. The World Alzheimer Report 2015 estimated that 46.8 million people worldwide were living with dementia (Alzheimer's Disease International 2015). AD is characterized by progressive decline in cognitive function. Clinical AD is mostly preceded by a phase called mild cognitive impairment (MCI) when the individual experience cognitive changes, but the changes are not severe enough to interfere with daily life or independent function. However, MCI does not always lead to AD or other types of dementia (Petersen et al., 2001).

A growing number of studies indicate that age-specific risk of AD and other dementias in higher-income Western countries may have decreased the past 25 years. The declines have been ascribed to increased levels of education and improved management of cardiovascular diseases. However, the total number of cases with AD is expected to increased dramatically as the population grows older. It is also unclear if this positive trend will continue given world-wide trends of increased mid-life diabetes and obesity which are potential risk factors for AD (reviewed in Alzheimer's Association, 2017).

Treatment

Despite the advances in unravelling the biological underpinnings in AD, to date there are still no disease-modifying therapies available for the people affected. Today the only medications that have some impact on the symptoms of patients with mild to moderate AD are N-methyl-D-aspartate (NMDA) receptor antagonists and acetylcholinesterase inhibitors. And these effects are both modest and transient. The pathology of AD appears to develop 10-20 years or more before the clinical signs of AD, as they are currently defined. Hence by the time the patient receives their diagnosis there has already been substantial degeneration of synapses and neurons

as well as inflammatory changes. Advances in the biomarker field and more sensitive and longitudinal tests for measuring cognitive impairment gives hope that earlier intervention, together with new therapeutic targets, will be able to delay or even prevent the disease (Figure 1). Recently, a small Phase 1b clinical trial of a human IgG1 monoclonal antibody Aducanumab showed some promising results in slowing cognitive decline and in plaque reduction (Sevigny et al., 2016). The antibody, which binds plaques and oligomers but not monomers, was derived from healthy, aged donors who were cognitively normal. The rationale was that these donors' immune systems had successfully resisted Alzheimer's disease and that the operative antibodies could be turned into therapeutics. However, we still await the results from the Phase 3 clinical trial.

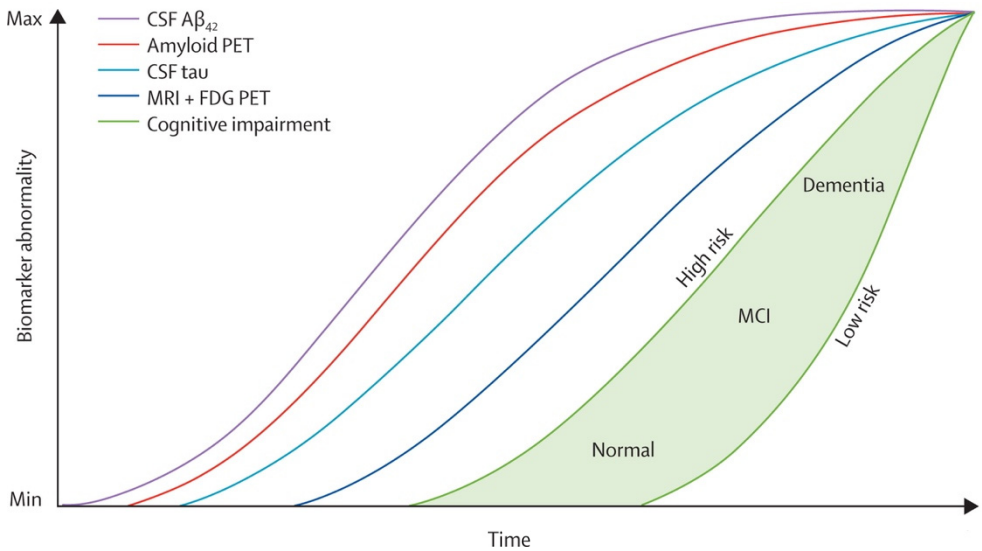


Figure 1. A temporal model of AD biomarkers. CSF Aβ42, cerebrospinal fluid (CSF) levels of Aβ42; Amyloid PET, positron-emission tomography (PET) imaging of amyloid deposition in brain; CSF tau, CSF levels of tau; MRI + FDG PET, magnetic resonance imaging (MRI) of atrophy and fluorodeoxyglucose (FDG) PET of hypometabolism as markers of neurodegeneration; MCI, mild cognitive impairment. Cognitive impairment is illustrated as a zone (green) with low-risk and high-risk borders, illustrating that two patients with the same biomarker profile can have different cognitive outcomes. Note that increased CSF Aβ42 abnormality represents a decrease in CSF Aβ42 levels. Adapted from Jack et al., 2013, with permission.

Neuropathological alterations

The neuropathological hallmarks of AD consist of aggregation of the β-amyloid peptide (Aβ) in amyloid plaques, hyperphosphorylation of the microtubule binding protein tau in neurofibrillary tangles (NFTs) and dystrophic neurites, as well as anatomical selective loss of synapses and neurons. These neuropathological changes are accompanied by astrogliosis and microglial activation (Rogers et al. 1988;

Beach et al. 1989; Itagaki et al. 1989). There are also distinctive lesions found mainly in the cell bodies of hippocampal pyramidal neurons, such as Hirano bodies and granulovacuolar degeneration (GVD) (Ball, 1978; Xu et al., 1992).

Amyloid plaques can be classified as diffuse or dense core plaques based on their staining with dyes specific for β-sheet confirmation, such as Thioflavin S. Thioflavin S positive dense core plaques are associated with dystrophic neurites, synaptic loss and activated astrocytes and microglia (Itagaki et al., 1989; Vehmas et al., 2003). The origin of dystrophic neurites can be either axonal or dendritic and show immunoreactivity for both aggregated and phosphorylated tau as well as for the amyloid precursor protein (APP) (Su et al., 1998). Although plaques are extracellular aggregates of Aβ, the first signs of Aβ accumulation in AD is within neurons both in human brain (Gouras et al., 2000; D'Andrea et al., 2001; Cataldo et al., 2004) and in AD transgenic mouse models (Oakley et al., 2006; Takahashi et al., 2002; Wirths et al., 2001). Aβ accumulates and aggregates particularly in endocytic vesicles in synaptic terminals, also showing signs of pathology (Takahashi et al., 2002). This suggests that accumulation of intraneuronal Aβ peptides is one of the earliest events in AD pathogenesis. Recently, it was shown that Aβ oligomers accumulated in synaptosomes (resealed nerve terminals) of postmortem human subjects with early AD, in the beginning of plaque pathology. Additionally, Aβ oligomers in synaptic terminals were elevated in early AD cases compared with non-demented controls with plaque pathology, indicating an association of synaptic Aβ oligomers with dementia (Bilousova et al., 2016).

Synapse loss is a better correlate of cognitive decline than plaques or NFTs (DeKosky and Scheff, 1990; Terry, 1991). Interestingly, the remaining synapses have been shown to be enlarged, which is believed to be a compensatory response (Scheff et al., 1990). Synapse damage is an early feature of the neurodegenerative process, with subsequent retrograde degeneration of the axons and atrophy of the dendritic tree and the cell body. However, the anatomical and neurotransmitter specificity of synaptic damage in AD is not well understood. Studies on post-mortem brain have shown special loss of basal forebrain cholinergic neurons and loss of the neurotransmitter acetylcholine (Davies and Maloney, 1976; DeKosky et al., 2002; Mesulam, 2004; Perry et al., 1981).

Amyloid plaque deposition in the AD brain generally follows a similar pattern during the progression of the disease. Starting with the neocortex in phase 1, progressing to allocortical brain regions in phase 2, and continuing with diencephalic nuclei, the striatum, and the cholinergic nuclei of the basal forebrain in phase 3. In phase 4 several brainstem nuclei become involved and finally in phase 5 cerebellum also has amyloid plaques (Braak and Braak, 1991; Thal et al., 2002).

When it comes to intraneuronal Aβ accumulation in human brain, Aβ42 was seen especially in layer II neurons of entorhinal cortex (ERC), CA1 pyramidal neurons

of hippocampus and basal forebrain cholinergic neurons; regions that are known to be vulnerable in AD. This accumulation increased with age but then decreased with plaque deposition and severity of dementia (Gouras et al., 2000). A more recent report described Aβ42 immunoreactivity in the cholinergic neuronal population of the basal forebrain, with increased levels of Aβ oligomers in aged and AD brains compared to young (Baker-Nigh et al., 2015). In CA1 pyramidal neurons isolated by laser capture microdissection, the intracellular Aβ42/Aβ40 ratio was increased in late onset AD cases compared to controls suggesting that the intracellular accumulation of Aβ42 increases the vulnerability of neurons (Aoki et al., 2008). Additionally, the concentration of Aβ42 was much higher in the vulnerable CA1 pyramidal neurons compared to cerebellar Purkinje neurons that are known to be relatively spared in AD (Hashimoto et al., 2010). Early accumulation of Aβ42 was also recently reported in Reelin-positive neurons in ERC layer II (Kobro-Flatmoen et al., 2016). These glutamatergic Reelin-positive ERC layer II neurons are destined for early tangle pathology and neuronal loss in AD (Braak and Braak, 1995; Gómez-Isla et al., 1996). The initial plaques in the hippocampus develop in their terminal fields in the outer molecular layer of the dentate, explaining the apparent anatomical separation between amyloid plaques and tau pathologies.

Risk factors and mutations

The greatest risk factor is age, with only ~5% of all AD cases carrying the rare mutations in APP, PSEN1 and PSEN2 causing the dominantly inherited forms of early-onset AD (<65 years). Still, the rare mutations causing early-onset AD give us very valuable clues on the etiology of the disease. They point at which proteins, processes and cellular pathways that play important roles in the development of AD. Most of the more than 200 early-onset AD mutations lead to increased Aβ42/Aβ40 ratio. The Swedish mutation in APP increases all species of Aβ, and several other early-onset mutations are due to mutations within the Aβ domain that lead to increased tendency of Aβ to aggregate.

However, twin and family studies indicate that genetic factors play a role in at least 80% of all AD cases (Gatz et al., 2006). The ε4 isoform of apolipoprotein E (ApoE4), which is present in almost 20% of the population, is by far the strongest risk factor for late-onset AD (>65 years). The risk of developing AD increases approximately fourfold when inheriting one copy of ApoE4 and by greater than tenfold for two copies of the ε4 allele compared to the ε3 allele. ApoE modulates multiple pathways in AD pathology including production, clearance, aggregation and toxicity of Aβ, as well as tauopathy, synaptic plasticity, lipid transport and neuroinflammation (Holtzman et al., 2012; Huang et al., 2017; Shi et al., 2017; Zhao et al., 2017). Genome-wide association studies (GWAS), as well as more recently exome and genome sequencing, have since led to the identification of additional AD candidate genes for late-onset AD. Although these loci generally have a much

weaker effect or are much rarer than ApoE (Lambert et al., 2013; Guierro et al., 2013; Jonsson et al., 2013) they help outline additional cell biological processes or pathways that are important in AD pathogenesis. Three main areas have emerged: the endosomal pathway, the immune system and cholesterol/sterol metabolism (Jones et al., 2010; Ubelmann et al., 2017).

APP and Aß

The 37-44 amino acid long Aβ is a normal product produced by sequential cleavage of APP by the β- and γ-secretases.

APP

APP is a type-I oriented transmembrane glycoprotein with its amino terminus within the lumen/extracellular space and its carboxyl terminus within the cytosol (Kang et al. 1987). APP has two homologs in mammals, the APP-like proteins 1 and 2 (APLP1 and APLP2). Functional redundancy has been described in knockout (KO) animals pointing at similar functional roles of the homologs, in addition to shared conserved amino acid sequences and protein subdomains (Wasco et al., 1992, 1993; Coulson et al., 2000). However, it is only APP that contains the sequence encoding the Aβ domain. As a result of alternative splicing, APP exists in different isoforms, with the APP695 being the isoform predominantly expressed in neurons. The extracellular domain of APP can self-dimerize and bind to several proteins in the extracellular matrix (Soba et al., 2005; Deyts et al., 2016; Müller et al., 2017). The cytoplasmic domain interacts with cytoskeleton-associated scaffold proteins (van der Kant and Goldstein, 2015). This suggests a role for APP as an adhesion protein and APP is concentrated in dynamic parts of the neurons such as dendritic spines and in the outer leading edge of the growth cone (Sabo et al., 2003; Sosa et al., 2013). Evidence also supports that APP has trophic properties in neurons and synapses, particularly for the α-secretase cleaved soluble fragment of APP (sAPPα). Hence apart from its well-established role in AD pathogenesis, APP also has important physiological functions during brain development as well as in the mature brain in regards to neuronal plasticity, memory and neuroprotection (reviewed in Thinakaran and Koo, 2008; Müller et al., 2017).

APP processing and Aβ generation

Like many other type-I transmembrane proteins, APP is transported to the plasma membrane from the biosynthetic and secretory pathways, where it can be processed by α-secretases in the non-amyloidogenic pathway (Figure 2 and 3). In the non-amyloidogenic pathway, α-secretases cleaves APP within the Aβ domain (Esch et al., 1990; Sisodia et al., 1990) thereby preventing the formation of Aβ. The cleavage

results in the soluble sAPPα and the membrane bound α-C-terminal fragment (α-CTF). The α-CTF is then subsequently cleaved by γ-secretase to release the p3 (3 kDa) peptide into the extracellular milieu and the APP intracellular domain (AICD) (Gu et al., 2001; Sastre et al., 2001) into the cytosol that has a function in nuclear signalling. AICD has been reported to regulate the transcription of several genes, among them APP and enzymes involved in lipid metabolism (von Rotz et al., 2004; Grimm et al., 2017).

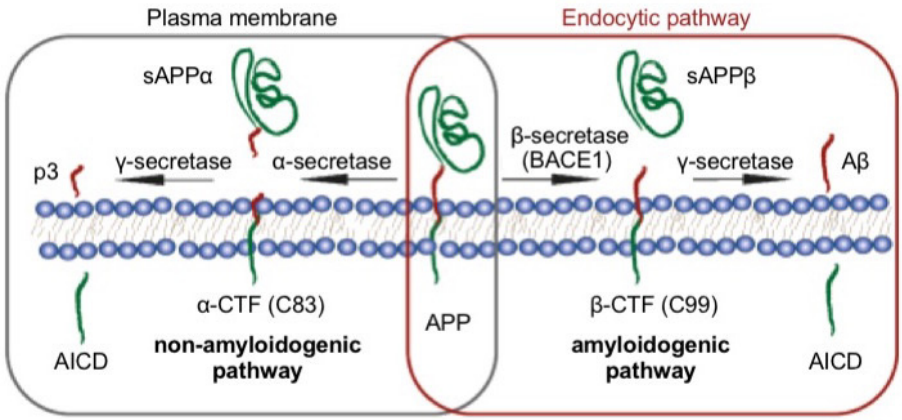


Figure 2. APP cleavage pathways. APP is processed by two alternative pathways, the non-amyloidogenic, mainly taking place at the cell surface, and the amyloidogenic, that preferentially occurs in the endocytic pathway. α-secretase cleaves in the Aβ-region of APP producing sAPPα and the 83-amino acid long α-CTF. γ-secretase then cleaves α-CTF to produce p3 and AICD. BACE1, on the other hand, cleaves APP to produce sAPPβ and the 99-amino acid long β-CTF. β-CTF is further cleaved by γ-secretase into Aβ and AICD. Adapted from Rajendran and Annaert 2012 with permission. © 2012 John Wiley & Sons A/S.

Alternatively, APP is rapidly endocytosed in a clathrin-dependent manner into endosomes where the amyloidogenic cleavage of APP by β-site amyloid precursor protein cleaving enzyme 1 (BACE1) mainly occurs (Vassar et al., 1999; Zou et al., 2007; Cirrito et al., 2008; Sannerud et al., 2011; Rajendran and Annaert, 2012). This results in the soluble β-cleaved fragment (sAPPβ) in the endosomal lumen and the membrane bound β-C-terminal fragment (β-CTF). BACE1 is an aspartyl protease with a pH optimum of pH 4.5 (Vassar et al., 1999) and is trafficked and recycled within the endosomal pathway (Udayar et al., 2013) which is consistent with endosomes being the major site for β-secretase activity. Amyloidogenic processing appears to be favoured in neurons due to the greater abundance of BACE1 (Gouras et al., 1998; Vassar et al., 1999), while the anti-amyloidogenic pathway is favoured in all other cell types. The β-cleavage is the initial and rate-limiting step in the amyloidogenic pathway (Vassar, 2004), β-CTF is then cleaved by γ-secretase within the transmembrane domain, producing Aβ on the luminal side as well as AICD. The

γ-secretases are a family of intramembrane-cleaving proteases consisting of four subunits, with the catalytic activity in the presenilin (PSEN)1 or PSEN2 subunits (De Strooper et al., 1998; Wolfe et al., 1999). γ-secretase cleaves β-CTF in a sequential fashion giving rise to Aβ peptides of different lengths (Wolfe et al., 2012). Aβ40 is the most abundant, while Aβ42, Aβ43 and longer Aβ peptides are more hydrophobic and prone to aggregate into oligomers and fibrils. Aβ42 is believed to be building blocks of the toxic Aβ oligomers, while Aβ40 even has been suggested to be anti-amyloidogenic (Kim et al., 2007).

Neurons are highly polarized cells with axons and dendrites far away from the soma, performing different functions and therefore having different sets of lipids and proteins. To make it even more complicated, the dendrites and axons are compartmentalized into specialised compartments such as the dendritic shaft, dendritic spines, axonal shaft the axonal presynaptic terminals, etc. Given the complex morphology of neurons the precise subcellular sites of APP processing are not well defined. APP is known to be transported down both axons and dendrites and BACE1 and γ-secretases have been localized to both pre- and post-synaptic compartments (Koo et al., 1990; DeBoer et al., 2014; Lundgren et al., 2015; Schedin-Weiss et al., 2016). Conditional knockout of PSEN1 has been reported to cause accumulation of β-CTF in pre-synapses in hippocampus CA1 area (Saura et al., 2005). More recently, PSEN1 and PSEN2 were shown to differ in their trafficking and relative cleavage of APP in axons and dendrites, with PSEN2 being exclusively in the somatodendritic compartments, while PSEN1 localized to both axons and dendrites (Sannerud et al., 2016). Interestingly, they showed that PSEN2 only cleaved APP in the late endosomal/lysosomal compartments generating an increased intracellular pool of Aβ42 and increased ratio of Aβ42/40. Sannerud et al also discovered that familial early-onset mutations in PSEN2 dramatically increased intracellular Aβ42/40 ratios and over all increased intracellular Aβ levels and decreased Aβ in the medium. In addition, they found familial early-onset PSEN1 mutations that phenocopied PSEN2 mutations, shifting PSEN1 localization to late endosomes/lysosomes and increasing intracellular Aβ42/40 ratios. Still, many questions remain unknown regarding APP trafficking and its relative processing in pre- versus post-synaptic terminals.

Activity dependent APP processing

Both human and animal studies support that Aβ levels and metabolism is regulated by neuronal activity. Patients with temporal lobe epilepsy develop Aβ-containing plaques as early as 30 years of age (Mackenzie and Miller, 1994; Gouras et al., 1997). The distribution of plaque pathology in the brain resembles the pattern of metabolic activity in the default network, which has led to the hypothesis that synaptic activity may drive Aβ plaque deposition (Buckner et al., 2005). Synaptic activity stimulates Aβ generation and secretion in cultures of hippocampal slices or

primary neurons (Kamenetz et al., 2003) as well as degradation (Tampellini et al., 2009).

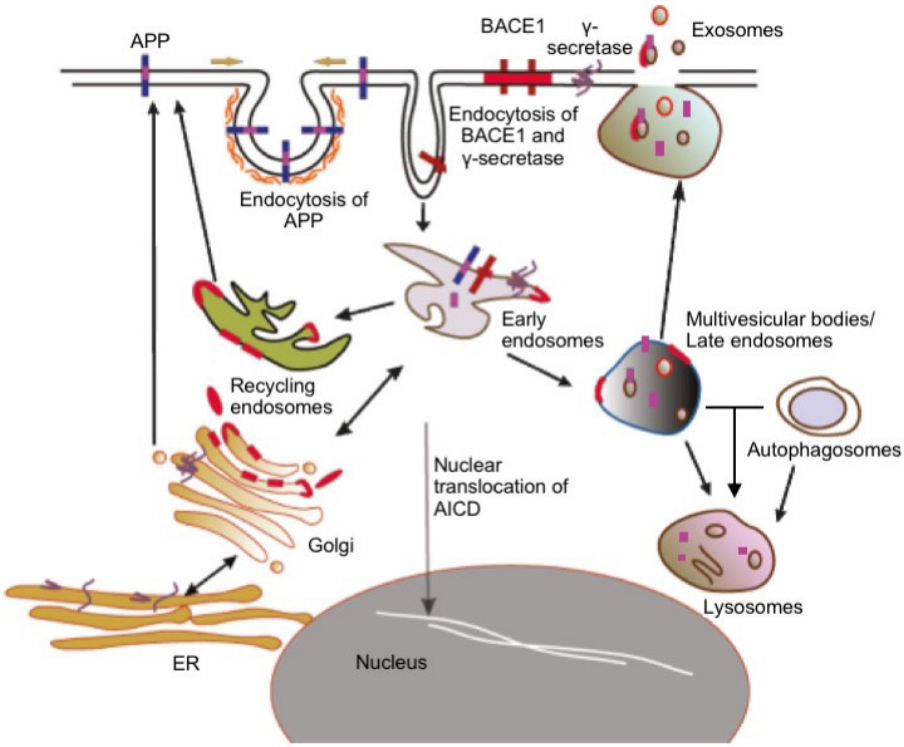


Figure 3. Model of APP trafficking pathways in APP processing and degradation. The transmembrane proteins APP (blue with the Aβ-domain shown in pink), BACE1 (red) and γ-secretase (purple) involved in production of Aβ, all traffic through the secretory- and the endocytic pathways. APP is internalized from the plasma membrane by clathrin-mediated endocytosis and sorted to early endosomes where BACE1 can cleave APP into β-CTF and sAPPβ. β-CTF becomes substrate for γ-secretase to produce AICD and Aβ in the early endosome/MVB/lysosome-pathway. AICD can be transported to the nucleus. MVBs can fuse with the plasma membrane to release ILVs as exosomes. Alternatively, MVBs can be sorted to lysosomes for degradation. Autophagosomes have also been reported to contribute to Aβ release and degradation. Raft domains in the membrane are shown in red. Adapted from Rajendran and Annaert, 2012, with permission. © 2012 John Wiley & Sons A/S.

Aβ clearance

While the early-onset familial forms of AD are caused by (a direct or indirect) increased tendency for Aβ to aggregate, it has been suggested that the late-onset forms of AD are due to defective clearance of Aβ (Selkoe, 2001; Tanzi et al., 2004). In year 2000, neprilysin was identified as one of the major Aβ-degrading proteases (Iwata et al., 2000). Since then the list has grown long and it is known today that Aβ

can be degraded by many proteases with different characteristics and subcellular locations. A knockout study of neprilysin, which is normally found in the extracellular space, ER and Golgi, showed a doubling of steady-state levels of both Aβ40 and Aβ42 (Iwata et al., 2001). Knockout of the Aβ-degrading protease Cathepsin D, that resides in the endo-lysosomal pathway, showed a tripling of Aβ42 but no significant change in Aβ40, resulting in increased Aβ42/Aβ40 ratio (Leissring et al., 2009). Insulin degrading enzyme (IDE), another major Aβ-degrading protease, has been reported to localize both in extracellular space, endoplasmic reticulum (ER), endosomes, lysosomes, mitochondria and the cytosol. However, IDE is believed to exclusively degrade monomeric Aβ (reviewed in Saido and Leissring, 2012; Leissring, 2016). It has been suggested that Aβ also can be degraded by the proteasome (Lopez Salon et al., 2003). Given that Aβ is produced in luminal compartments in neurons, it is not likely that the proteasome plays a major physiological role in the degradation of Aβ. However, loss of endosomal/lysosomal impermeability has been reported in non-neuronal cells after incubation with Aβ1-42 (Yang et al., 1998) suggesting that Aβ might leak into the cytoplasm under pathological conditions. There are studies in cultured cells that suggests that cytosolic Aβ is particularly cytotoxic. Hence this could be a small but important pool of Aβ in the pathology of AD (Zhang et al., 2002; Lee et al., 2006).

As mentioned above, Aβ can be degraded both in extracellular compartments (interstitial fluid, ISF) as well as in intracellular compartments. Microglia and astrocytes can internalize extracellular Aβ and degrade it in the lysosome. Neurons, on the other hand, can eliminate Aβ via lysosomal degradation both through uptake of extracellular Aβ and directly after production of Aβ in the endo-lysosomal pathway. Extracellular Aβ is also cleared from the brain through the blood-brain barrier into the blood or through ISF bulk flow via perivascular drainage, the cerebrospinal fluid (CSF) sink or the perivascular glymphatic pathway (reviewed in Tarasoff-Conway et al. 2015). The meningeal lymphatic vessels, discovered in 2015, might provide another clearance route (Louveau et al., 2015). Aβ is continuously generated and degraded, and the concentration of Aβ within a given compartment at a given time point is determined jointly by these opposing processes. As well, Aβ exists in a dynamic equilibrium being transported between different compartments. Hence, degradation of Aβ in one compartment could result in lowering concentrations of Aβ in the others.

Aβ uptake and secretion

A recent paper showed that Aβ1-40 and Aβ1-42 were taken up by human neuroblastoma cells by a constitutive mechanism independent of clathrin and dynamin, but dependent on actin polymerisation and micropinocytosis. Interestingly, Aβ1-42 was shown to be taken up approximately twice as efficiently as Aβ1-40 (Wesén et al., 2017). Although it is well established that neuronal activity

stimulates Aβ secretion, the identity of the intracellular compartment whereby Aβ is released into the extracellular milieu still remains elusive. A small portion (<1%) of Aβ has been found associated to secreted exosomes, suggesting that Aβ can be released into the extracellular space via fusion of multivesicular bodies (MVBs; also called multivesicular endosomes, MVEs) to the plasma membrane in N2a cells (Rajendran et al., 2006). It is not unlikely that a larger portion of Aβ was released from the lumen of the MVB when fusing to the plasma membrane, but that only a small fraction of the hydrophobic Aβ was attached to the intraluminal vesicles (ILVs) after ultracentrifugation (Figure 3). Other papers have suggested autophagy-dependent Aβ secretion, with impairment in autophagosome clearance resulting in reduced Aβ secretion and accumulation of intracellular Aβ and autophagosomes (Nilsson et al., 2013). It is interesting to note that secretion of Aβ is impaired with time in culture in AD-transgenic but not in wild-type neurons. Additionally, the ability of synaptic activity to elevate secreted Aβ and reduce intraneuronal Aβ is also reduced in AD-transgenic neurons with time in culture (Tampellini et al., 2011), suggesting impaired ability of familial AD-transgenic neurons to efficiently modulate levels of secreted and intraneuronal Aβ.

Aβ at synapses

As described, synapse loss is an early feature of AD and a better correlate of cognitive decline than other neuropathological markers. Synaptotoxic effects have been described with soluble Aβ oligomers prepared from multiple sources (Shankar et al. 2008). Aβ oligomers impair excitatory synaptic transmission, inhibit long-term potentiation (LTP), induce loss of dendritic spines, and impair rodent spatial memory (Selkoe, 2002; Haass and Selkoe, 2007; Crews and Masliah, 2010). It has been suggested that Aβ has different effects on the pre- and post-synaptic sides depending on the concentration (Palop and Mucke, 2010). At physiological concentrations Aβ could facilitate pre-synaptic potentiation (Abramov et al., 2009; Puzzo et al., 2008), while at abnormally high levels Aβ would lead to post-synaptic depression and loss of dendritic spines (Walsh et al., 2002; Wang et al., 2000).

Aβ has been reported to interact with a number of different receptors present at the synapse, including the cellular prion protein (PrPC) receptor (Laurén et al., 2009), metabotropic glutamate receptor 5 (Renner et al., 2010), a7 nicotinic acetylcholine receptor (Wang et al., 2000), NMDA receptors (De Felice et al., 2007) and glutamate transporters (Li et al., 2009). Some of these putative receptors could potentially explain the synaptotoxic effects of Aβ, however considerable controversy exists.

It is possible that the specific vulnerability of certain brain areas and neurons in AD is caused by a preference of Aβ to bind to and accumulate in specific types of neurons. For example, it has been shown that synaptosomes prepared from cerebellar synapses bind less Aβ oligomers compared to cortical synaptosomes (Lacor et al., 2007).

Endo-lysosomal pathway dysfunction in Alzheimer's disease

Abnormalities in the endosomal-lysosomal pathway, including the autophagic system, are signature features of AD, preceding Aβ plaques and NFTs (Peric and Annaert, 2015). Endo-lysosomal pathway dysfunction and β-amyloidogenesis are intertwined, given the pivotal roles of endosomes and lysosomes in processing, trafficking and clearance of APP and its metabolites. There is also increasing evidence that APP metabolites can have pathogenic effects on this pathway. The endo-lysosomal pathway is a dynamic system of communicating vesicles, sorting and trafficking internalized extracellular or membrane-bound material to sites through-out the cell. Surface receptors important in e.g. neurotransmission and synaptic plasticity are endocytosed and recycled back to the plasma membrane in recycling endosomes or degraded in the lysosome. The endosomal-lysosomal pathway is also vital for cell signalling (Di Fiore and von Zastrow, 2014). Additionally, the endo-lysosomal compartments undertake exocytosis to repair the plasma membrane, to communicate between cells or to eliminate unwanted material (Eitan et al., 2016).

Enlargement of endo-lysosomal compartments

Enlarged Rab5-positive early endosomes and Rab7-positive late endosomes have been reported before plaques and tangles in AD and the related pathology in Down syndrome (Cataldo et al., 2000; Cataldo et al., 2008). Additionally, with electron microscopy (EM), MVBs, lysosomes and autophagic vacuoles were progressively seen to accumulate in AD (Nixon et al., 2005). It was recently suggested that enlarged early endosomes and lysosomes were caused by β-CTFs, independent of Aβ (Kim et al., 2016; Lauritzen et al., 2016). However, other studies have pointed at Aβ also being an important player in the dysfunction of the endo-lysosomal pathway. In a study with early stage AD cases (Braak stage I–II) and DS brain, Aβ immunolabelling colocalized with Rab5-positive early endosomes in pyramidal neurons. This colabelling was more frequently associated with larger Rab5-positive compartments compared to smaller ones (Cataldo et al., 2004). In an immuno-EM study, Aβ1-42 was found to localize to the limiting membrane of MVBs at synapses,

where it accumulated during AD pathogenesis and was associated with synaptic pathology (Langui et al., 2004; Takahashi et al., 2002). A more mechanistic study, found that epidermal growth factor receptor (EGFR)-sorting via the MVB was impaired by Aβ accumulation in cultured AD transgenic neurons. Translocation onto the ILVs of MVBs appeared to be affected, suggesting Aβ dependent dysfunction of the late endosomal sorting complexes required for transport (ESCRT) pathway in AD (Almeida et al., 2006).

MVBs and the ESCRT machinery

MVBs originate from endosomes that have undergone invagination of their limiting membrane creating ILVs. The ESCRTs are a set of highly conserved proteins that can regulate and drive the formation of the ILVs of MVBs (Figure 4). They assemble into four subcomplexes, ESCRT 0-III, composed of several subunits each, that sequentially act to deliver ubiquitinated transmembrane proteins to endosomes, recruit necessary molecules such as phosphatidylinositols and respective kinases, and promote invagination and cleavage to form the ILVs in the lumen of endosomes thereby generating MVBs (Babst, 2011). ESCRT-III subunits, among them CHMP2B, are inactive monomers in the cytoplasm (Babst et al., 2002), that assemble on endosomal membranes in an ordered manner to generate the transient ESCRT-III complex. CHMP2B recruits the vacuolar protein sorting-associated protein 4 (VPS4) AAA–ATPase complex to dissociate the ESCRT-III complex which is essential for the recycling of the ESCRT machinery (Babst et al., 1998; Lata et al., 2008; Wollert et al., 2009) and may also be involved in the scission of the vesicle. The MVBs can then either deliver their cargo to the lysosome for degradation or release the intraluminal vesicles (then called exosomes) via fusion with the plasma membrane. It should be noted though, that in mammalian cells several mechanisms of ILV formation have been identified. It has been suggested that ESCRT-independent (CD63 dependent) ILV formation might work in a competitive fashion within a single MVB, with upregulation of CD63 dependent ILV formation with ESCRT depletion (Stuffers et al., 2009; van Niel et al., 2011; Edgar et al., 2014).

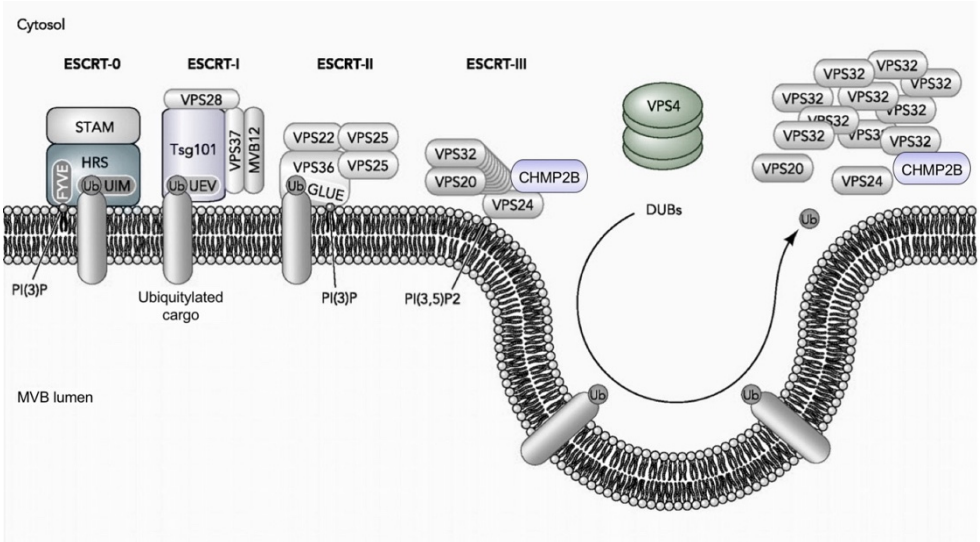


Figure 4. Schematic representation of the ESCRT machinery. The ESCRT machinery acts in a sequential manner to deliver ubiquitinated transmembrane proteins to endosomes and promote invagination and cleavage to form the ILVs in the lumen of endosomes, thereby generating MVBs. The ESCRT machinery consists of four subcomplexes, ESCRT-0, -I, -II and –III, plus the ATPase VPS4 that promotes disassembly and recycling of ESCRT-III oligomers. ESCRT-0, -I and –II form stable hetero-oligomers that recognize ubiquitin and the endosome-enriched phosphatidylinositol 3-phosphate (PI(3)P) at the endosomal surface. In addition, ESCRT-II initiates the assembly of the ESCRT-III complex. ESCRT-III does not form a stable complex, but rather assembles transiently during membrane sculpting and fission events. CHMP2B recruits VPS4 to dissociate the ESCRT-III complex and may also be involved in the scission of the vesicle. The ESCRT components investigated in this thesis are highlighted: Hrs, Tsg101, CHMP2B and VPS4. Adapted from Lobert and Stenmark, 2011.

Genetic links

As mentioned above, GWAS studies have identified novel loci with increased risk for late-onset AD. These unbiased analyses converge with the pathological observations of endo-lysosomal abnormalities in early, preclinical stages of the disease. Variants of endocytic regulators increasing the risk for AD include sortilin-related receptor 1 (SORL1), phosphatidylinositol-binding clathrin assembly protein (PICALM), bridging integrator 1 (BIN1), and CD2-associated protein (CD2AP) (Peric and Annaert, 2015). One report recently showed that Bin1 promote axonal Aβ production in endosomes, while CD2AP, promote Aβ generation in dendrites (Ubelmann et al., 2017). Knocking down Bin1 prevents BACE1 from being recruited to recycling tubules resulting in its retention in Rab5-positive axonal endosomes. CD2AP appears to regulate sorting to ILVs as its knockdown traps APP on the limiting membrane of maturing endosomes and prevents it from being degraded in the lysosome. The net result for both risk factors would be APP and BACE1 co-residing for an extended period. This would increase amyloidogenic

processing, suggesting that Aβ generation mainly occurs at the limiting endosomal membrane. Interference with APP ubiquitination (Williamson et al., 2017) as well as deficiencies in ESCRT functions via different mechanisms such as decreased levels of phosphatidylinositol 3-phosphate (PI3P) (Morel el at., 2013), via effects of Aβ (Almeida et al., 2006) or by direct interference of ESCRT components could all prolong the residence time of APP on the limiting membrane of endosomes/MVBs. Additionally, ESCRT dysfunction would interfere with degradation of membrane bound molecules, including APP and lipids, in the lysosome.

The ESCRT-III protein CHMP2B is genetically linked to frontotemporal dementia (FTD), which is the second most common cause of presenile dementia (Skibinski et al., 2005). A copy number variation of CHMP2B has also been reported in a family with early onset AD (Hooli et al., 2014) and immunoreactivity for CHMP2B is known to be increased in GVD in hippocampus in AD (Yamazaki et al., 2010). Additionally, GWAS for late onset AD identified an association with VPS4B (Jones et al., 2010). Interestingly, specific reductions in the lipid PI3P, that regulates endosomal signalling and binds to the ESCRT-0 protein Hrs, has been found in both brains of AD patients as well as AD mouse models (Chan et al., 2012).

Together this suggests that the ESCRT pathway may be vulnerable in the pathogenesis in AD and can affect degradation of Aβ and APP. Clarifying the endosomal trafficking route of APP and Aβ is essential in understanding the pathophysiology of AD and why promising new drugs have been unsuccessful. Furthermore, the recognition of the endosome/MVB as a crucial decision point in the amyloidogenic pathway opens the door for discovery of much needed novel therapeutic targets.

Aims of the thesis

The overall aim of this thesis was to investigate the role of Aβ in the endocytic pathway and at synapses in Alzheimer's disease.

More specifically, the aims were as follows:

Paper I

The aim was to investigate the anatomic and synaptic selectivity of APP processing and Aβ accumulation in primary neurons. This was pursued to better define the subcellular site of Aβ within neurons as well as the selective vulnerability of certain neurons in AD.

Paper II

APP has been localized to MVBs where sorting of APP onto intraluminal vesicles ILVs could potentially either promote amyloidogenic processing, or reduce Aβ production or accumulation by sorting APP and processing products to lysosomes for degradation. Paper II aimed to inhibit the ILV sorting machinery and analyse the effects on Aβ levels.

Paper III

In this paper, we set out to test whether Aβ causes the abnormal endosomal phenotype seen in AD. Could Aβ act via dysfunction of the ESCRT pathway? And does late ESCRT dysfunction recapitulate AD related cellular phenotypes such as Aβ accumulation?

Paper IV

The aim of this paper was to analyse the early changes in Aβ structure in brains of AD transgenic mouse models. This was done by using non-destructive techniques of synchrotron-based two-dimensional Fourier transform infrared micro-spectroscopy imaging (μFTIR) and blue native polyacrylamide gel electrophoresis (BN-PAGE).

Paper V

The aim of paper V was to investigate the effect of APP and its proteolytic cleavage products on normal synaptic composition.

Methodological considerations

A brief overview of the methods will be given in this section, in particular the methods I have utilized myself. For more detailed descriptions, please see the papers included in the thesis.

Animals

Animals were kept under a 12 h light/dark cycle with ad libitum access to food and water. Procedures were approved and performed according to the guidelines of the ethical committee for use of laboratory animals at Lund University (paper I-V) and Cornell University (paper V).

Cell culture

Cell lines

Mouse N2a neuroblastoma cells were used in several experiments as they have higher transfection efficiency compared to primary mouse neurons. The N2a cells used were stably transfected with the human APP (paper II), the 670/671 Swedish mutation human APP (paper III) (Thinakaran et al., 1996) or wild-type α-synuclein with HA-Tag (paper III). In paper II, human H4 neuroglioma cells stably expressing human APP (ATCC) was used in the initial part of the paper as this cell line was available in the lab performing that set of experiments. When changing between cell lines or between cell lines and primary mouse neurons, bridging experiments were performed.

Primary neurons

Primary neuronal cultures were prepared from cortices including hippocampi of embryonic day 15-17 mice embryos. Briefly, dissected cortices were incubated with

0.25% trypsin for 15 minutes, washed with Hanks Buffer Solution and triturated in 10% fetal bovine serum (FBS) media with glass pipettes until neurons were dissociated. Neurons to be analysed by immunofluorescent microscopy were plated on poly-D-lysine-treated (Sigma) coverslips (Bellco glass) in 10% FBS media for 5 h and then changed into serum-free Neurobasal media with B27 supplement (Invitrogen) and 2 mM L-glutamine. Neurons to be analysed by Western blot were plated directly in serum-free Neurobasal media with B27 supplement and 2 mM L-glutamine on poly-D-lysine-treated 100 mm or 60 mm plastic petri dishes (Corning). The neurons were analysed at 12-19 days in vitro (DIV). Primary neuronal cultures in papers I-IV were generated from B6.Cg-Tg(APPswe,PSEN1dE9)85Dbo/Mmjax mice (APP/PS1) AD transgenic (MMRRC) and wild-type C57Bl/6J (Charles River/Janvier Labs) mouse embryos. In paper V, C57Bl/6J (Jackson Labs/Charles River) and APP knockout (APP KO) mice (Jackson Labs) (Zheng et al. 1995) mouse embryos were used.

Production of plasmids and transfection

Paper II: Mammalian AllStar negative siRNA, human Hrs or Tsg101 siRNA (Razi and Futter, 2006), murine Hrs ON-TARGETplus SMARTpool siRNA or murine Tsg101 ON-TARGETplus SMARTpool siRNA sequences (Qiagen).

Paper III: p3xFLAG-CMV-10-hVPS4A-wt and p3xFLAG-CMV-10-hVPS4A-dn E228Q were generated as described (Hasegawa et al., 2011). The control plasmids p3xFLAG-CMV-7-BAP Control Plasmid was purchased from Sigma-Aldrich and pcDNA3-CMV-GFP from Addgene. In order to change the strong CMV promoter into a weaker promoter more tolerable to primary neurons, the “wtVPS4” sequence in p3xFLAG-CMV-10-hVPS4A-wt and the “dnVPS4A” sequence in pcDNA3-synapsin-FLAG-wtVPS4A were amplified by PCR using primers from Eurofin. The sequences were then inserted into pcDNA3-synapsin-FLAG to create p3xFLAG-CMV-10-hVPS4A-wt and p3xFLAG-CMV-10-hVPS4A-dn respectively.

Production of viral vectors and transduction

Viral vectors used in paper V with short hairpin RNA (shRNA) targeting mouse APP (Young-Pearse et al., 2007) were created by restriction digestion and ligation into a modified pENTR plasmid (Campeau et al., 2009). Gateway recombination was used to transfer the shRNA and scrambled control RNA into a pLenti (Campeau et al., 2009) acceptor plasmid. Lentiviral vectors were prepared by a viral vector

core facility, Lund University. Primary mouse neurons were transduced with lentiviral vectors containing either shRNA targeting APP or scrambled control at multiplicity of infection (MOI) of 5 at 10 DIV and either fixed for fluorescence microscopy or harvested for WB analysis at 14 DIV.

Western blot

Western blot analysis was performed to analyse changes in relative protein content or protein structure of cells or brain. The advantage of using Western blot compared to ELISA and similar techniques, is the ability to analyse several APP cleavage products of different sizes from the same sample (such as APP, CTFs, and Aβ), as well as being able to assess their aggregation state.

Cell medium was collected and centrifuged to remove cell debris. To concentrate proteins in low concentration in the medium, such as α-synuclein, total protein was extracted using a trichloroacetic acid (TCA)/acetone precipitation protocol.

Cells were washed twice and harvested in ice cold phosphate-buffered saline (PBS) by scraping and pelleted by centrifugation. Lysates were loaded in equal protein concentration according to total protein content with BCA assay (ThermoFisher Scientific) and/or, in the case of lysates with sodium dodecyl sulfate (SDS) and ß-mercaptoethanol, normalized against ß-actin or tubulin. Cell medium was normalized according to the total protein content/actin/tubulin of its corresponding lysate.

Samples were subjected to electrophoresis and transferred to polyvinylidine difluoride membranes (Invitrogen). Membranes were blocked in phosphate buffered saline (PBS) containing 0.1% Tween-20 (PBST) and 5% milk, and incubated in primary antibodies listed in Table 1 overnight and then with HRP-conjugated secondary antibodies for 1 h diluted in PBST and 5% milk. The immunoreaction was visualized by a chemiluminescence system (Pierce or BioRad).

Sodium dodecyl sulfate polyacrylamide gel electrophoresis (SDS-PAGE)

For the detection of Aß cell pellets were lysed with 6% SDS containing 10 µl/ml β-mercaptoethanol, sonicated, and then heated at 95 °C for 6 min. After centrifugation, supernatants and medium were mixed with loading buffer, heated at 95 °C for 5 min and loaded into 10–20% Tricine gels (Invitrogen). For visualization of Aβ, membranes were boiled in PBS for 5 min prior to blocking.

For lysis with a milder detergent, cells were lysed in RIPA buffer (Thermo Fisher Scientific) with protease inhibitor and phosphatase inhibitor (Thermo Fisher Scientific). Lysates, with NuPAGE LDS sample buffer and NuPAGE reducing agent, were loaded on NuPAGE 4-12% BisTris gels and run with NuPAGE MES SDS buffer (Invitrogen).

Blue native polyacrylamide gel electrophoresis (BN-PAGE)

For native conditions, cell pellets were lysed on ice in NativePAGE sample buffer (1X, Life Technologies) containing 1% digitonin (Life Technologies) and Halt proteinase inhibitor cocktail (1X, Thermo Scientific) by pipetting up and down and incubating on ice for 15 min. Lysates were centrifuged at 20000 x g for 30 min at 4 °C. Equal amounts of protein were loaded on a 3-12% NativePAGE Novex Bis-Tris gel (Life Technologies).

Immunofluorescence

Brain

Mice were anesthetized and fixed by transcardial perfusion with PBS followed by 4% paraformaldehyde (PFA) in 0.1 M PBS (pH 7.4) at RT. After dissection, brains were postfixed by immersion in 4% PFA in 0.1M PBS (pH 7.4) at 4 °C for 2 h or overnight. After fixation, brains were cut in 40 μm thick sections with a Leica SM 2010R sliding microtome. Sections were kept in storage buffer composed of 30% sucrose and 30% ethylene glycol in PBS at −20 °C until use. Free-floating sections were blocked for 1 h in RT with normal goat serum (NGS) and triton-X and then incubated in primary antibodies overnight at 4 °C, see Table 1, followed by appropriate fluorescent Alexa secondary antibodies for 1 h at RT. Sections were mounted in SlowFade Gold antifade reagent (Invitrogen).

Cells

With the drawback of cultured neurons not being in their natural environment and context, using cultured cells for immunofluorescent analysis has several advantages. First of all, the cells can easily be manipulated and accessed for more complex experimental setups. Secondly, the complete neuron can easily be visualized to analyse both synapses, processes and soma. Cells were grown on coverslips and fixed in 4% PFA in PBS with 0.12 M sucrose for 20 min, permeabilized and blocked

in PBS containing 2% NGS, 1% bovine serum albumin, and 0.1% saponin at room temperature for 1 h, and then immunolabelled with primary antibodies (see Table 1) in 2% NGS in PBS overnight at 4°C followed by appropriate fluorescent Alexa secondary antibodies for 1 h at RT. Coverslips were mounted in SlowFade Gold antifade reagent (Invitrogen).

Confocal microscopy

Immunofluorescence was examined by confocal laser scanning microscopy (Leica TCS SP8, Leica TCS SP2 or Zeiss LSM 510). Channels were imaged sequentially to avoid bleed-through. Images were taken with Leica Confocal Software or Zeiss ZEN software.

List of antibodies

Tabel 1. List of primary antibodies used in this thesis.

Antibody	Target epitope	Host	Dilution WB	Dilution IF	Source	Catalog number
369	Human/mouse full length APP, α/β-CTFs, APP C-terminus	Rabbit	1:1000	1:500	Buxbaum et al., 1990	
6E10	Human Aβ, full length APP, sAPPα, β-CTF, a.a. 3-8 of Aβ	Mouse	1:1000	1:500	BioLegend	Previously Covance SIG-39320
12F4	Human/mouse Aβx-42, C-terminus specific	Mouse		1:250	BioLegend	Previously Covance SIG-39142
22C11	Human APP, N-terminus, a.a. 66-81 of APP	Mouse	1:1000		BioLegend	ab348
82E1	Human Aβ1-x, N-terminus specific, a.a. 1-4 of Aβ	Mouse	1:1000	1:200	IBL International	10323
Amyloidβ (1-42)		Rabbit		1:250	IBL International	18582
Amyloidβ (1-42)	Human/mouse Aβx-42, C-terminus specific	Rabbit		1:1000	Invitrogen	700254
β-actin		Mouse	1:2000		Sigma	A 5316
CAMKIIα		Mouse		1:500	Millipore	05-532
Cathepsin D		Rabbit			Upstate	
CD63		Mouse	1:1000		ThermoFisher Scientific	MA1-19281
CHMP2B		Rabbit	1:1000	1:250	Abcam	ab33174
Cholera toxin Subunit B, Alexa-488	Binds to ganglioside GM1			1:1000	Molecular Probes	C-34775
Clavestin-1+2		Rabbit		1:250	Bioss	bs-6569R-A647
DAPI				1:1500	Sigma	D9542
Drebrin		Rabbit		1:1000	Abcam	ab11068
FLAG	DYKDDDDK	Rat	1:1000	1:1000	Biolegend	637302
Flotillin-1		Mouse		1:400	BD Biosciences	610821
G2-10	Aβ40	Mouse			Millipore	MABN11
GAD67		Mouse		1:1000	Millipore	MAB5406

Tabel 1 Cont. List of primary antibodies used in this thesis.

Antibody	Target epitope	Host	Dilution WB	Dilution IF	Source	Catalog number
GM130		Mouse		1:500	BD Biosciences	610822
GSK3β		Rabbit	1:1000	1:400	Cell Signaling Technology	12456
pGSKα/β		Rabbit	1:1000		Cell Signaling Technology	9331S
HA-Tag		Rabbit	1:1000		Cell Signaling Technology	3724
Hrs and Hrs-2		Mouse		1:100	Enzo	ALX-804-382-C050
LAMP1		Rabbit		1:1000	Abcam	ab24170
LAMP1		Rat		1:1500	Abcam	ab25245
LC3β		Rabbit	1:1000		Cell Signaling Technology	2775
MAP2		Mouse		1:1000	Sigma	M4403
MAP2		Chicken		1:1500	Abcam	Ab5392
MBC A β42	Human/mouse Aβx-42, C-terminus specific	Mouse	1:1000		Kindly provided by Dr. Haruyasu Yamaguchi	
Myc tag		Rabbit			Abcam	ab9106
NR1		Mouse			Upstate	05-432
OC	Amyloid fibrillar oligomers/ fibrils	Rabbit		1:1000	Merck Millipore	AB2286
P2:1	Human APP, N-terminus, a.a. 104-118 of APP	Mouse		1:500	ThermoFisher Scientific	OMA1-03132
Phospho-tau pSer396		Rabbit	1:1000		ThermoFisher	44-752G
PSD-95		Mouse	1:1000	1:200	Millipore	MAB1596
Rab7		Mouse		1:500	Abcam	ab50533
Synapsin I		Rabbit	1:1000	1:500	Sigma	S193
Somatostatin		Rat		1:200	Millipore	MAB354
Synaptophysin		Mouse	1:1000	1:1000	Merck Millipore	MAB5258
Tau-1		Mouse		1:500	Chemicon	MAB3420
TGN46		Sheep			AbD Serotec	APH
Tsg101		Mouse		1:250	Genetex	GTX70255
VPS4		Mouse	1:1000	1:100	SantaCruz	sc-133122

Abbreviations: WB, Western blot; IF, immunoflourescence.

Electron microscopy

In paper I paraffin embedded brain sections (10 µm) of PS1cKO; APP Tg mice were deparaffinised and alcohol-dehydrated. Free-floating sections were incubated with 369 antibody (APP C-terminal epitope) by the immune-gold silver procedure with goat anti-rabbit IgG conjugated to 1 nm gold particles (Amersham Biosciences, Arlington, IL) in 1.01% gelatin and 0.08% bovine serum albumin in PBS. Transmission electron microscopy was performed on a Philips CM10 electron microscope. Immunogold electron microscopic analysis was performed as previously described (Takahashi et al., 2002).

For paper II PFA-fixed, 50-µm vibratome sections of hippocampus 10-month-old Tg2576 mice and wild-type littermates were dissected and embedded in 12% gelatin. Sections were immunogold labelled (Slot et al., 1991) and visualized with a JEOL1010 transmission electron microscope with a Gatan digital camera and Digital Micrograph software.

For the electron microscopy of cells in paper III, primary neurons were grown on Thermanox coverslips (Nalgene, Nunc) and fixed with 2% PFA, 2.5% glutaraldehyde in 0.1M cacodylate. Cells were then secondarily fixed with 1% osmium tetroxide followed by incubation with 1% tannic acid to enhance contrast. Cells were dehydrated using increasing percentages of ethanol before being embedded in Epoxy resin (Agar scientific, UK) stubs. Coverslips were cured overnight at 65°C. Ultrathin sections were cut using a diamond knife mounted to a Reichert ultracut S ultramicrotome and sections were collected onto copper grids. Grids were post-stained with drops of lead citrate. Sections were viewed on a FEI Tecnai transmission electron microscope (Eindhoven, The Netherlands) at a working voltage of 80kV. Bovine serum albumin (BSA)-gold was prepared as previously described (Slot et al., 1991). For quantification of MVB diameter, MVBs were defined as organelles containing intraluminal vesicles and monomeric rather than flocculated BSA-gold.

Exosome isolation

To examine changes in exosomal secretion with expression of dnVPS4A exosomes were purified from cell culture medium by differential ultracentrifugation (Théry et al., 2006). Briefly, Swe N2a cells were cultured and transfected for 48 h in exosome-free medium with either dnVPS4A, wtVPS4A or ctrGFP. Collected medium was depleted of cells and cellular debris by sequential low speed centrifugation. Exosomes were isolated by centrifugation of the collected supernatant at 100,000 ×

g at 4°C for 70 min. The resultant pellet was washed in PBS and centrifuged for 70 min at 100,000 × g at 4°C.

Image analysis and quantification

Imaris software (Bitplane) was used to analyse colocalization between two fluorescently labelled proteins imaged on cells or tissue by confocal microscopy at a single z-plane. The colocalization channel displays the intensity of colocalized voxels as the square root of the product of the intensities of the original channels, hence the brightest pixels in the colocalization channel represent the pixels with the highest colocalization. Quantification of colocalization was done with automatic thresholding, based on point spread function width, and reported as percentage of colocalized material above threshold. Pearson's correlation coefficient (PCC) values range from 1 for two images whose fluorescence intensities are perfectly linearly related, to -1 for two images whose fluorescence intensities are perfectly, but inversely, related to one another. Values near zero reflect distributions that are uncorrelated with one another. Manders' colocalization coefficients (MCC) is the fraction of the total probe fluorescence of one protein that colocalizes with the fluorescence of a second protein. MCC strictly measures co-occurrence independent of signal proportionality. Colocalization can also be visualised as a scatter plot. Under conditions of proportional codistribution, the points of the scatter plot cluster around a straight line. However, lack of colocalization is reflected by distribution of points onto two separate groups, each showing varying levels of one probe with little or no signal from the other probe.

In Paper I, Image J was used for analysis of localization of γ-secretase cleaved APP (detected by antibody 369). Thresholds were set by automatic thresholding by default on confocal images in the MAP2 or tau-1 channel. The mean intensity of the 369 channel was subsequently measured in the pixels that were above threshold in the MAP2 or tau-1 channel, respectively. In paper II images were analysed using Methamorph Image Analysis or Velocity software. In paper III and IV, two-dimensional images from confocal microscopy were quantified and reconstructed into 3D volumetric data sets. LAMP1-positive vesicles in pyramidal neurons were quantified by measuring the diameter of the five largest LAMP1-positive vesicles per cell, imaged by confocal microscopy in z-stacks. In paper V, quantifications of fluorescence intensities and puncta densities were performed using the integrated morphometric analysis feature in Metamorph. Images were thresholded to quantify only puncta with intensities (2x) brighter than the neuritic shafts. Analysis of spine density and length were performed blinded manually using ImageJ. Western blots

were quantified using Image Lab Software (Bio-Rad Laboratories) or, for paper IV, Image J.

Statistical analysis

Statistical analyses were performed using GraphPad Prism. Statistical comparisons were made using two-tailed unpaired t-tests for comparisons between two groups, and one-way Anova when comparing multiple groups.

Results

Below follows a brief description of the main results found in the five papers included in this thesis. For more detail, see the full papers at the end of the thesis.

Heterogeneous association of Aß and APP with synapses (Paper I)

Amyloid deposition in the AD brain during the progression of the disease generally follows a similar pattern (Braak et al., 1991; Thal et al., 2002). It is possible that the specific vulnerability of certain brain areas and neurons in the AD brain are attributed to a preference of Aβ to accumulate in and/or bind to specific types of neurons. In this paper we set out to investigate the anatomic and synaptic selectivity of APP processing and Aβ accumulation in primary neurons.

We found that Aβ does not bind to and accumulate equally in all neurons in culture. Exogenously added synthetic Aβ1-42 bound to excitatory CAMKIIα-positive neurons but not to inhibitory GAD67-positive primary neurons (Figure 5). However, neurons are vastly heterogeneous in their properties. In line with this, not all CAMKIIα-positive neurons had strong Aβ1-42 labelling and not all Aβ1-42-positive neurons co-labelled with CAMKIIα.

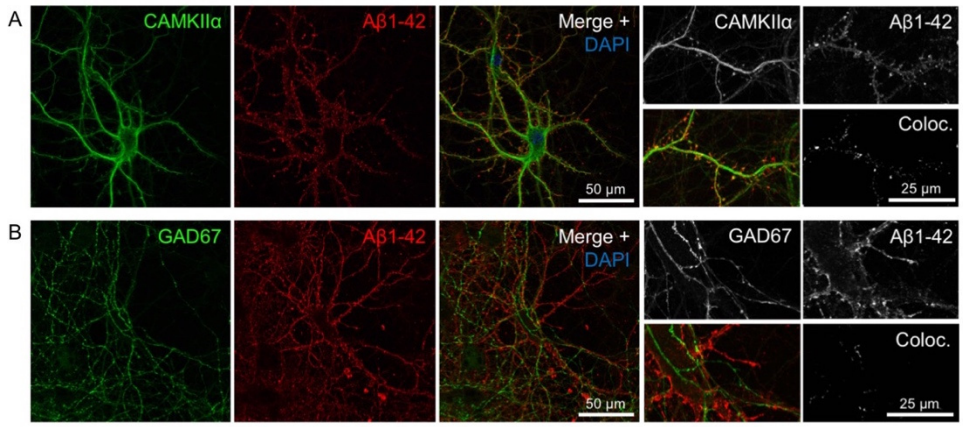


Figure 5. Accumulation of exogenously added Aβ1-42 for 30 min is more pronounced in excitatory CamKII-positive compared to inhibitory GAD67-positive neurons. (A) Aβ1-42 accumulation in some but not all, and not exclusively in, neurons labelled with CamKIIα. Higher magnification images (right) with Aβ1-42 in CamKIIα-positive synaptic terminals. (B) Aβ1-42 was not seen accumulating in any GAD67-positive neurons. Higher magnification images (right) showing no colocalization of Aβ1-42 in GAD67-positive synaptic terminals. Modified from Paper I.

To test whether Aβ1-42 has a preference to the pre- or post-synaptic side, neurons were labelled with two sets of pre- and post-synaptic markers, respectively: synapsin I and PSD-95 (Figure 6A) or synaptophysin and drebrin (Figure 6B). The intensity and prevalence of a specific marker at the synaptic site can potentially influence the colocalization analysis, and therefore two different sets of markers were used. Quantification of colocalization revealed that there was no significant difference in the percentage of material above threshold colocalized with Aβ1-42 between these pre- and post-synaptic markers (Figure 6C).

As well as being endocytosed from the extracellular compartment, Aβ is also produced within neurons after γ-secretase cleavage of β-CTFs. Here we showed by immuno-gold EM that β-CTF accumulated mainly in post-synaptic compartments in the CA3 region of hippocampus in PS1 cKO; APP Tg mice lacking γ-secretase cleavage (Figure 7A). A previous report focusing on CA1 hippocampus described pre-synaptic accumulation in the same mouse model (Saura et al., 2005). Hence, β-CTF accumulation due to lack of PS1 activity can occur both at the pre- and post-synaptic sites. To further explore this selective accumulation of β-CTF, we used immunofluorescent labelling of APP/PS1 cortical primary neurons treated with the γ-secretase inhibitor DAPT. After 2h with DAPT there was a marked increase of β-CTFs in pre-synaptic compartments of treated compared to untreated neurons (223% of untreated control). After 17h of DAPT treatment, β-CTFs were further increased in pre-synaptic compartments (324% of untreated control) and was now also evident in post-synaptic compartments (202% of untreated control) (Figure 7 B-C). To sum up, β-CTF-accumulation after γ-secretase inhibition, occurs in general

earlier and/or to a larger extent in pre-synaptic compartments compared to post-synaptic compartments in cortical primary neurons. However, there are anatomical differences in the pre- versus post-synaptic build-up of β-CTF in the brain.

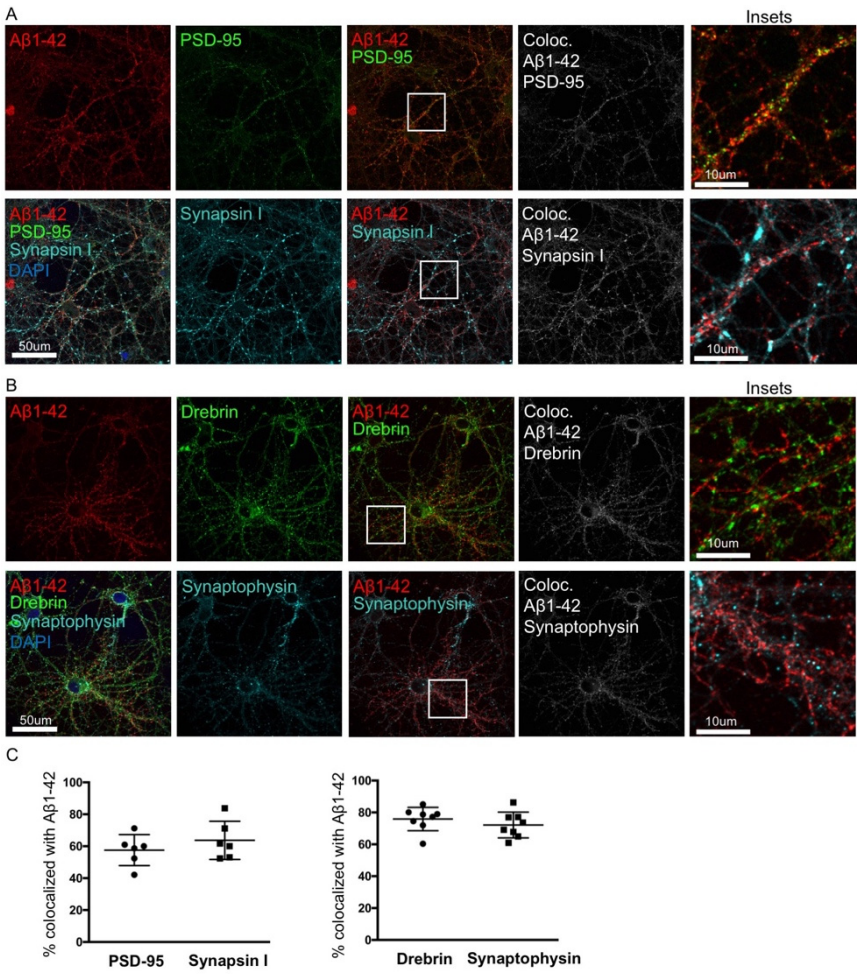


Figure 6. Aβ binds and accumulates at both pre- and post-synaptic sites. (A-B) Double-labelling of primary neurons treated with 0.5 μM of fluorescently tagged Aβ1-42 for 30 min, with two different sets of pre-synaptic and post- synaptic markers, synapsin I and PSD-95 (A) and synaptophysin and drebrin (B). In the colocalization channel (right panel) the amount of colocalization is represented as the brighter the pixels, the higher the colocalization at that particular pixel. (C) Quantification of colocalization showed no significant difference in the percentage of colocalization above threshold between Aβ555 and pre- or post-synaptic markers. Modified from Paper I.

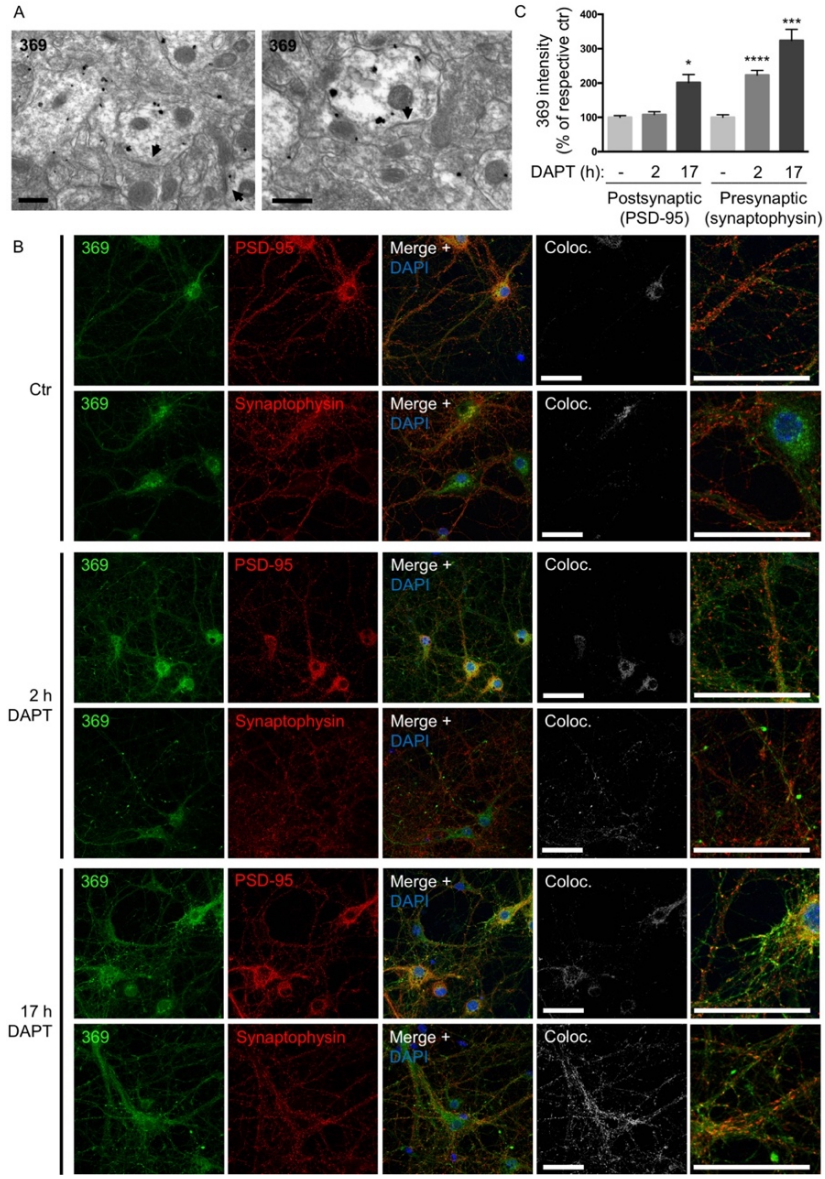


Figure 7. γ-secretase inhibition leads to earlier β-CTF accumulation at pre-synaptic compared to post-synaptic sites. (A) In the CA3 region of hippocampus β-CTFs were mainly accumulating in post-synaptic compartments in PS1 cKO; APP Tg mice. Arrowheads denote post-synaptic densities. Scale bars 500 nm. (B) Immunofluorescent labelling of APP/PS1 primary cortical neurons treated with γ-secretase inhibitor DAPT. Scale bars 50 µm. (C) Quantification of B. The intensity of antibody 369 labelling in post-synaptic compared to pre-synaptic compartments with DAPT-treatment indicated a relatively greater increase in pre-synapses, which was also evident earlier (at 2h). Values are percentage of respective untreated control. *p<0.05, ***p<0.001, ****p<0.0001 From Paper I.

ESCRTs regulate APP sorting in MVBs and intracellular Aβ accumulation (Paper II)

We knew from previous work in the lab that Aβ predominantly is found at the limiting membrane of MVBs in human cortical AD brain (Takahashi et al., 2002), and particularly at synapses. We also knew that Aβ42 traffics in the same MVBs as EGFR (Almeida et al., 2006).

To further explore the trafficking of APP in the endocytic pathway, we investigated H4 neuroglioma cells stably expressing human APP (H4-APP) by immunoelectron microscopy with antibody 6E10. We found the majority of APP/β-CTF/Aβ in Golgi and MVBs. On the MVBs most of the labelling was on ILVs but some was on the limiting membrane. The labelling was confined to a subset (39%) of MVBs, while a second population of MVBs was 6E10-negative. Lysosomes were not stained. Also, 6E10 and Aβ40-specific antibodies localized to the ILVs of a subset of MVBs in the Tg2576 mice. It is known that EGFR traffics in a subpopulation of MVBs destined for the lysosome (White et al., 2006). We found that APP is trafficked in the same population of MVBs that deliver EGFR to the lysosome for degradation. APP is trafficked to the lysosome but is rapidly degraded and is only detectable there following inhibition of lysosomal degradation by leupeptin.

Depletion by siRNA of the ESCRT-0 component Hrs, caused APP to redistribute from ILVs to the limiting membrane of enlarged endosomes. Immunofluorescence analysis showed that the 6E10-positive punctae were clearly enlarged in Hrs-depleted cells and sometimes 6E10-positive 'rings' could be observed. Some Hrs-depleted MVBs contained a population of unusually small ILVs.

In order to determine whether depleting the early ESCRT components Hrs or Tsg101 affected delivery of APP to lysosomes, we analysed the colocalization of APP with LAMP1 with immunofluorescent labelling. We found that with leupeptin treatment, colocalization between LAMP1 and APP decreased in Hrs or Tsg101 depleted cells compared to control cells. This indicates that early ESCRT components Hrs and Tsg101 are needed in the process of delivering APP in MVBs to lysosomes for degradation.

To investigate the effect of Hrs and Tsg101 depletion on Aβ secretion and accumulation, we used a mouse neuroblastoma cell line overexpressing human APP (N2a APP) that produce higher levels of Aβ compared to H4-APP. Depletion of Hrs or Tsg101 (Figure 8A) led to a marked reduction in secreted Aβ40 levels in cell medium by ELISA and Western blot. Cell lysates showed an increase in APP levels upon Hrs or Tsg101 depletion, consistent with reduced delivery of APP to the lysosome. Although α-CTF and β-CTF levels were unchanged by Hrs or Tsg101 depletion, the intracellular levels of Aβ were increased following Hrs depletion

(Figure 8B-E). Thus, in conclusion, the early ESCRT machinery has a dual role in limiting intracellular Aβ accumulation through targeting of APP and processing products to the lysosome for degradation, and promoting Aβ secretion.

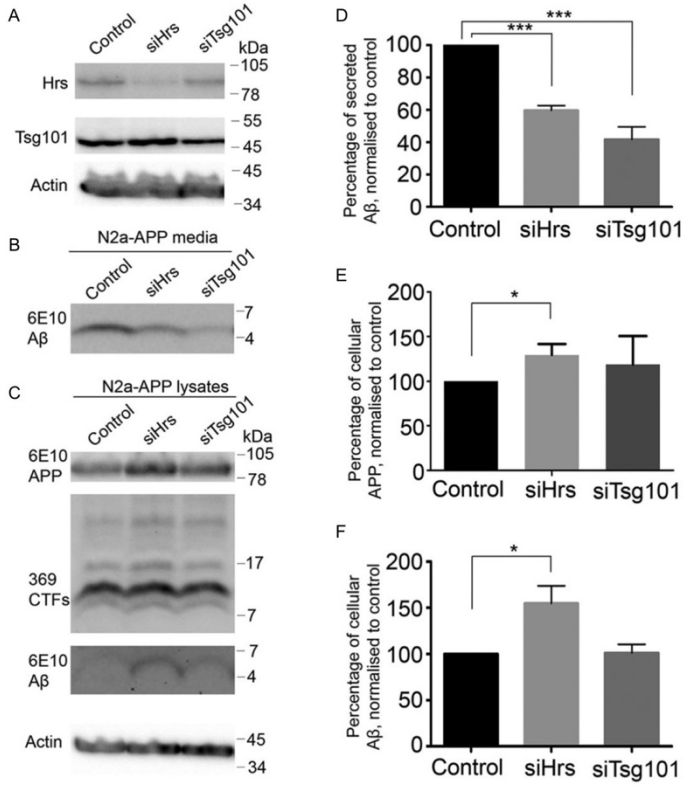


Figure 8. Reduced Aβ secretion after depletion of Hrs or Tsg101 and increased intracellular APP and Aβ after Hrs depletion. (A) Representative blots of cell lysates of N2a-APP cells depleted of Hrs (siHrs) or Tsg101 (siTsg101). (B) Hrs or Tsg101 depletion led to reduced Aβ secretion. (C) Cell lysates displayed increased Aβ and APP levels after Hrs depletion. (D) Quantification of B. (E-F) Quantification of C. * $p < 0.05$, *** $p < 0.005$. Modified from Paper II.

Aβ accumulation causes MVB enlargement (Paper III)

Among the earliest pathological features in AD, preceding Aβ plaques and NFTs, are abnormalities in the endocytic pathway. These include enlarged early and late endosomes (Cataldo et al., 2000, 2008) as well as accumulation of MVBs, lysosomes and autophagosomes (Nixon et al., 2005). In paper III we set out to test what causes the abnormal endosomal phenotype seen in AD.

We found that increased levels of Aβ can lead to the enlarged endosomal phenotype seen in AD. MVB size was compared between wild-type and APP/PS1 transgenic primary mouse neurons as well as wild-type neurons treated with human synthetic Aβ1-40 or Aβ1-42 for 48 h (Figure 9A-D). The cells were fed with BSA-gold to delineate endocytic compartments and MVBs were defined as organelles containing intraluminal vesicles and monomeric BSA-gold. We also detected leakage of the endo-lysosomal compartments as cytosolic BSA-gold could be seen in the Aβ1-42 treated cells.

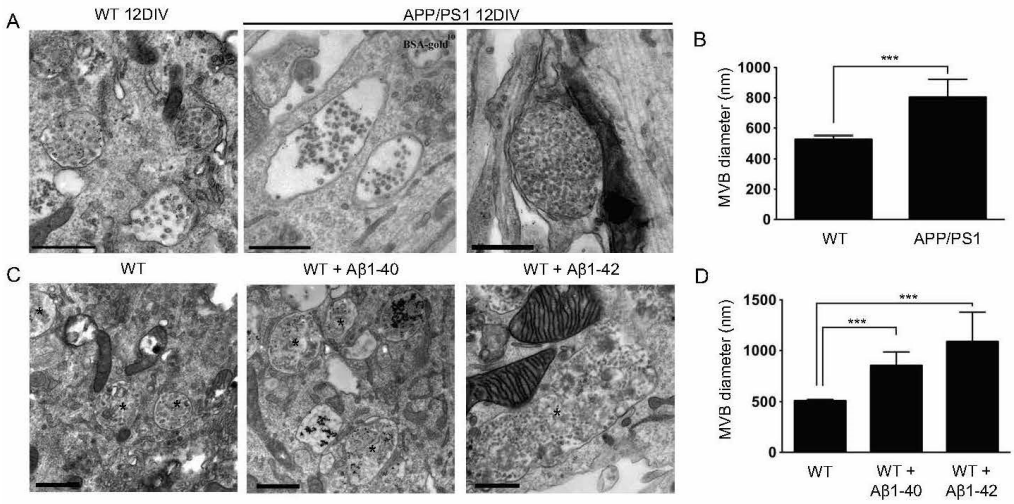


Figure 9. Aβ increases MVB diameter in primary neurons. (A) Electron microscopy revealed that APP/PS1 AD transgenic compared to wild-type mouse primary neurons have significantly larger MVBs at 12 DIV. Scale bar 500 nm. (B) Quantification of A showed an increase of 52% in MVB diameter in Tg compared to wild-type neurons, n > 94 MVBs per group; *** $p < 0.001$. (C) Exogenously added monomeric Aβ1-40 or Aβ1-42 to wild-type primary neurons at 12 DIV led to increased MVB diameter at 48 h on EM images. MVBs are marked with an asterisk. Scale bar 500 nm. (D) Quantification of C, n >45 MVBs per group; *** $p < 0.001$. Modified from Paper III.

The added synthetic Aβ1-42 was rapidly taken up by neurons and started to aggregate within the acidic endocytic compartments in the neuronal processes. After 48 h amyloid fibrils or amyloid oligomers, labelled with OC antibody, were seen in

the processes extending out from enlarged late endosomes labelled with LAMP1 (Figure 10A). Surface labelling showed that a portion of the amyloid structures now also could be seen on the extracellular side of the plasma membrane (Figure 10B).

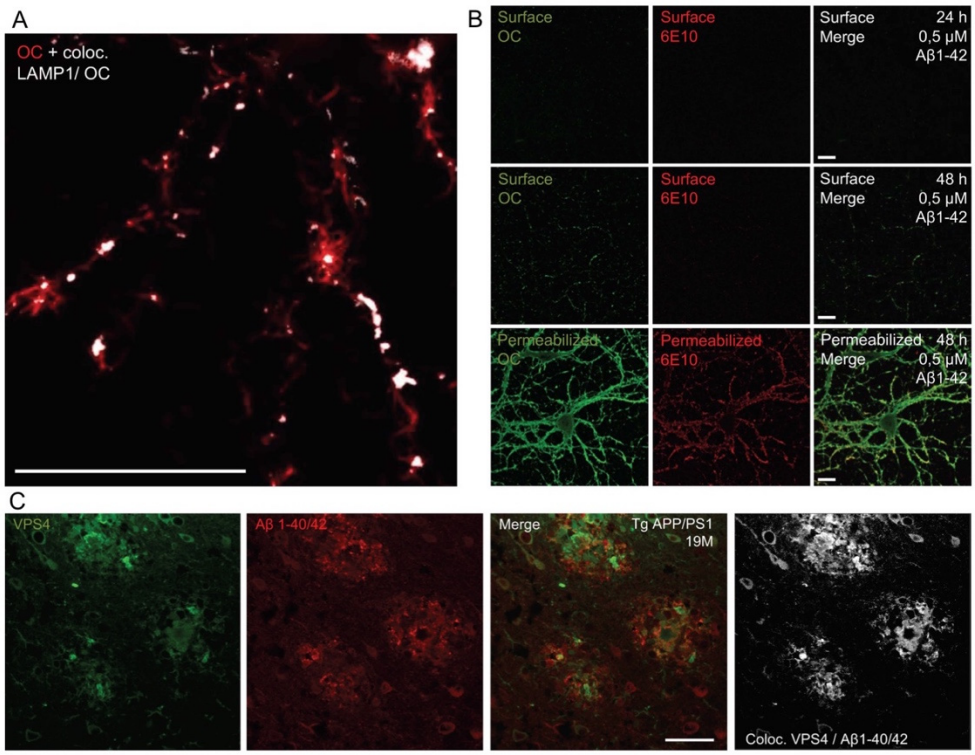


Figure 10. (A) After 48 h of treatment with Aβ1-42, OC antibody, labelling amyloid fibrils or amyloid oligomers, was seen extending out from LAMP1-positive structures in the processes. The image shows OC with the superimposed colocalizing channel for LAMP1 and OC. Scale bar 20 µm. (B) Weak surface labelling of non-permeabilized neurons shows that OC and 6E10 antibody positive structures were intracellular after 24 h of treatment with Aβ1-42 (upper panel). At 48 h extracellular OC antibody labelling was now more visible consistent with penetration of the plasma membrane by the elongated OC positive fibrils (middle panel). Strong OC and 6E10 antibody labelling of permeabilized cells after fixation but before immunolabelling, shows that the majority of added human Aβ1-42 (antibody 6E10) and OC antibody positive fibrils and/or fibrillar oligomers are inside neurons (lower panel). Scale bar 20 µm. (C) VPS4 colocalizes with Aβ42 in amyloid plaques of 19-month-old APP/PS1 mice. Scale bar 40 µm. Modified from Paper III.

These small seeds could potentially act as the initiation sites for plaques. We found ESCRT components VPS4 (Figure 10C) and Tsg101 in plaques of two different mouse models of AD, partially colocalizing with Aβ.

Prior data from the lab suggested that Aβ might impair ESCRT dependent sorting of EGFR in the MVB pathway (Almeida et al., 2006). Expression of VPS4 mutants deficient in ATP hydrolysis, such as the dominant negative VPS4 used in this study,

is known to lead to enlarged vesicles resulting from disrupted recycling of ESCRT-III components such as CHMP2B (Babst et al., 1998; Bishop et al., 2000; Dores et al., 2012). CHMP2B is genetically linked to FTD and AD (Skibinski et al., 2005; Hooli et al., 2014), and interacts directly with and recruits VPS4 that then disassembles the ESCRT-III complex. We therefore asked ourselves if Aβ could act via the ESCRTs to cause enlarged MVBs and further intracellular accumulation of Aβ. We found increased levels of high molecular weight complexes of CHMP2B on blue native polyacrylamide gel electrophoresis in APP/PS1 neurons treated with Aβ1-42 for 3 h, suggesting that Aβ might affect ESCRT-III recycling.

In paper II we found that the early ESCRT components Hrs and Tsg101 were important for the secretion of Aβ and that Hrs depletion led to intracellular accumulation of Aβ. In paper III we instead used the dominant negative form of VPS4A (dnVPS4A) to model dysfunction of the late ESCRT pathway. Apart from the mentioned close interaction with CHMP2B, VPS4B itself has been associated with late-onset AD in a genome-wide association study (Jones et al., 2010). DnVPS4A reduced Aβ secretion into the medium by 87% and caused a marked increase of intracellular Aβ by 424% in Swe N2a cells. Amyloid fibrils/oligomers and Aβ42 labelling were visible in association with enlarged endocytic vesicles in dnVPS4A positive Swe N2a cells. We also confirmed the intracellular accumulation of Aβ42 in neurons by constructing a dnVPS4A plasmid with a synapsin promoter suitable for the more sensitive primary neurons. However, as neurons have very low transfection efficiency, the succeeding WB experiments were conducted in N2a cells.

In accordance with the result of ESCRT dependent APP trafficking to the lysosomes in paper II, we found in paper III that Aβ also traffics to the lysosomes via ESCRT dependent MVBs. Blocking acidification of lysosomes with the vacuolar H+ ATPase inhibitor Bafilomycin A1 led to the same intracellular Aβ accumulation and decreased secretion as dnVPS4 expression. However, the reduced secretion of Aβ with both dnVPS4 and Bafilomycin A1 is not as straightforward to explain with the current views of secretion routes for Aβ. One possible scenario could be reduced fusion of MVBs with the plasma membrane and hence reduced release of exosomes. To test this, exosomes were purified from conditioned media from dnVPS4 expressing cells. However, the exosomal markers flotillin-1 and CD63 was found to be increased in exosomal preparations from dnVPS4A expressing cells compared to controls. A competitive relationship between ESCRT dependent and ESCRT independent (CD63 dependent) mechanisms of ILV formation has been suggested, with upregulation of CD63 dependent ILV formation from ESCRT depletion (Stuffers et al., 2009; van Niel et al., 2011; Edgar et al., 2014). Hence it could be that ESCRT dependent MVBs, containing APP and Aβ, accumulate in the cell not being able to fuse with the plasma membrane or the lysosome, while ESCRT independent MVBs, not trafficking APP and Aβ, fuse with the plasma membrane

releasing their exosomes. Alternatively, it has been reported that formation of ILVs destined for exosomal release is not ESCRT dependent, while ESCRTs were necessary for ILVs destined for degradation in the lysosome (Trajkovic et al., 2008). Hence it could be that ESCRT depletion only blocks MVBs destined for the lysosome. A possible fate of MVBs is fusion with autophagosomes before degradation in lysosomes (Lamb et al., 2013). Interestingly, a paper also reported reduced Aβ secretion and accumulation of intracellular Aβ with depletion of autophagy-related gene 7 (Atg7) (Nilsson et al., 2013). We found that autophagic marker LC3β-II, which correlates with increased numbers of autophagosomes (or amphisomes) in the cell, and p62, a substrate for degradation by autophagy, were both increased with expression of dnVPS4A. However, the relationship between ESCRT-mediated sorting of APP onto ILVs, autophagy and Aβ secretion requires further studies.

Interestingly, we also demonstrated that tau phosphorylation at residue S396 was significantly increased by 56% with dnVPS4A. This could be explained by MVBs being necessary for the sequestration of glycogen synthase kinase 3 (GSK3) which phosphorylates tau at serine 396 (S396) (Taelman et al., 2010).

Conformational changes in Aβ and APP before plaques (Paper IV)

As demonstrated in paper III, MVB dysfunction may lead to intracellular Aβ accumulation and aggregation in cultured cells. In addition, elevated levels of Aβ can aggregate in the acidic vesicles of the endocytic pathway eventually leading to Aβ-aggregates extending out to the extracellular compartment. In paper IV we wanted to further investigate this early Aβ aggregation in the brain as well as examining the specific aggregation state under physiological conditions. This still remains unclear since many of the available techniques used to process brain tissue potentially in themselves may change the structure of the aggregates.

We used synchrotron-based two-dimensional Fourier transform infrared micro-spectroscopy imaging (μFTIR) which can specifically detect β-sheet structure without any need of chemical tissue processing or labelling. In order to focus on the development amyloid pathology, Tg19959 mice was chosen, which develop plaques at or just before 3 months, at ages 1, 2 and 3 months. We found an increase with age in the intensity of the band around 1,627cm^{-1} in the amide I region of the infrared spectra. This suggests increased β-sheet structures developing already between 1 and 2 months in Tg19959 mice (Figure 11A). A second derivative analysis was performed for better resolution of the peaks for inter-molecular β-sheet structures and α-helical structures (Figure 11B-G). The inter-molecular β-sheet content

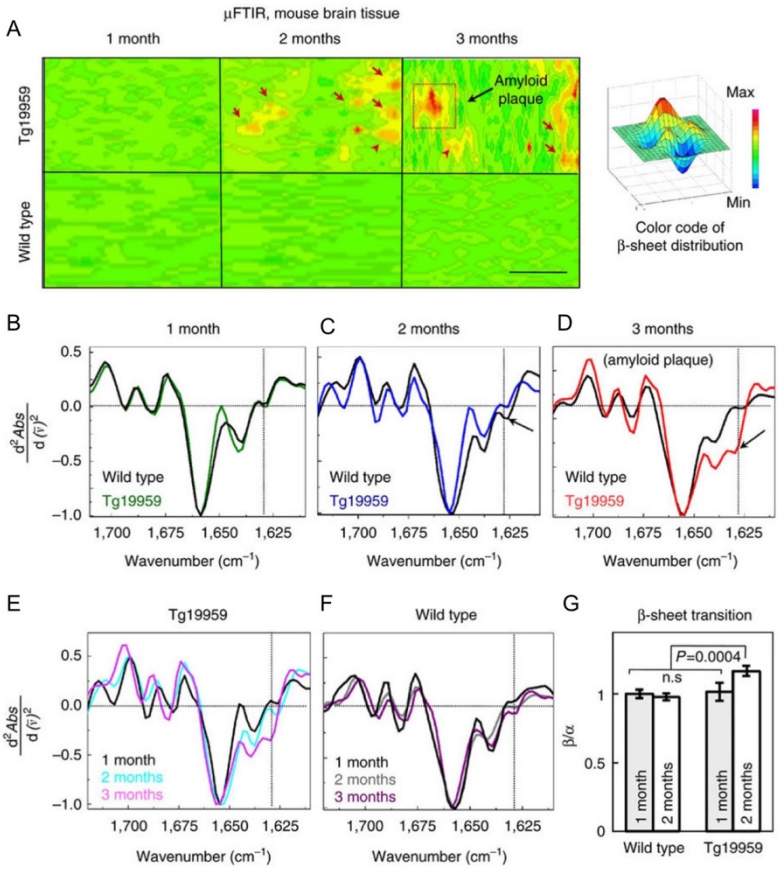


Figure 11. Early β-structural transition in transgenic AD mouse brains. (A) Absorption intensities for the β-sheet content in brain sections of Tg19959 (upper panels) and wild-type (lower panels) mice at 1, 2 and 3 months, respectively. β-sheet content is shown in red (arrows). FTIR maps were integrated for the β-sheet spectral region at 1,635–1,620cm^{-1}. Maps are representative; n=3; n represents the number of animals per genotype/age. Scale bar, 50 μm. (B) β-sheet structures in 1-month Tg19959 mice are similar to those in wild-type mice. Values are averaged and normalized 2nd derivatives of the Amide I absorption band; averages were taken from 20 to 40 FTIR measurement positions per brain section and 3 brain sections per genotype/age. (C) The arrow shows an increase in β-sheet content in 2-month Tg19959 mouse brain. Averaged and normalized 2nd derivatives of FTIR spectra taken from areas with increased β-sheet content in the corresponding μFTIR maps in A. (D) Same as in C, but for 3-month Tg19959 mice, with spectra taken from an area with high β-sheet content (indicated by red dotted square on the corresponding μFTIR map). (E) The overlap of the second derivatives corresponding to Tg19959 mice at different ages more clearly shows the progressive increase in β-content with age. (F) In comparison, the overlap of the second derivatives corresponding to wild-type mice at different ages is similar. FTIR spectra in B-F are representative. (G) Statistical analysis of β-sheet content measured as the average of the ratio of peak intensities between 1,635 and 1,620cm^{-1} (β-sheet) to 1,656cm^{-1} (α-helix) in Tg19959 and wild-type mice as a function of age. Protein aggregation in wild-type mice is taken as 100%. N=9; N represents the number of brain sections. Modified from Paper IV.

increased only in Tg19959 mouse brains and not in wild-type mouse brains, with the β-sheet content of 1-month-old AD transgenic brain being similar to those of wild-type. Next, we examined Aβ aggregation in AD transgenic neurons in culture, which have been shown to accumulate Aβ with time in culture (Takahashi et al., 2004). Consistently, μFTIR revealed elevation of β-sheet structures in AD transgenic APP/PS1 neurons between 12 and 19 DIV, compared to wild-type neurons, respectively.

With immunofluorescent labelling, progressive Aβ42 accumulation in synaptic compartments was demonstrated in 1, 2 and 3-month-old Tg19959 mouse brain sections. Signs of disrupted cytoarchitecture of dendritic spines with accumulating Aβ42 was also found, in line with the results from paper III.

BN-PAGE was performed to analyse the native conformation of Aβ and APP in Tg19959 mouse brain tissue at the early ages where changes in β-sheet structures were seen with μFTIR. For molecular weight estimation of native Aβ on BN-PAGE, we used synthetic Aβ1-42 which runs as a mixture of monomers, dimers, trimers and tetramers. Aβ in wild-type and 1-month-old Tg19959 brain was found to run as a band corresponding to the molecular weight of synthetic Aβ1-42 tetramer. However, at 2 months of age, the intensity of this band decreased as a high molecular weight smear between 100-500 kDa increased, indicative of Aβ aggregation. These results support the conclusion that under physiological conditions Aβ in brain initially may exists as a low molecular weight protein complex running at the same speed in the native gel as Aβ1-42 tetramers.

APP depletion alters selective pre- and post-synaptic proteins (Paper V)

The normal physiological role of APP and its cleavage products is still not fully understood. APP has been described to be important in synaptic pruning during development. However, studying the role of APP in the mature neuron has been complicated by its role in development. Therefore, we used both APP KO mice brains and APP KO neurons, as well as APP RNAi knockdown in mature wild-type neurons to study the role of APP in synaptic composition. We chose to investigate the pre-synaptic proteins synapsin I and synaptophysin and the post-synaptic proteins GluA1, drebrin, NR1 and PSD-95. Previous work in the lab have shown reductions in synaptophysin, GluA1 and PSD-95 in AD transgenic Tg2576 neurons compared to wild-type at 19 DIV (Almeida et al., 2005).

First, we examined changes in total levels of synaptic proteins in APP KO neurons compared to wild-type with western blot. At 12 DIV levels of AMPA receptor subunit GluA1 was significantly increased. At 19 DIV the increase in total protein levels of synaptophysin and PSD-95 reached significance. To more specifically study the changes in protein composition at the level of synapses, without the impact of newly synthesised synaptic proteins in the Golgi in the cell body, we measured relative immunofluorescence in neurites of APP KO neurons compared to wild-type. At 12 DIV APP KO neurons had significantly increased labelling of synapsin I, synaptophysin and GluA1. At 19 DIV only drebrin was significantly changed, with decreased levels of immunofluorescence.

Frontal cortex brain homogenates of 3-month-old APP KO mice showed significant increases in synapsin I, synaptophysin and GluA1. At 12 months, however, similar to the results from immunofluorescent labelling in 19 DIV KO neurons, there was no statistical difference in synapsin I, synaptophysin or GluA1, while a marked decrease was now evident in levels of drebrin. PSD-95 was now also significantly increased.

Given the evidence for APP in brain development, we next used RNAi to knockdown APP in cultured neurons in order to investigate roles for APP in mature synapses. Lentiviral vectors containing shAPP targeting APP or a scrambled control were prepared and used to transduce wild-type primary neurons at 10 DIV. At 14 DIV cells were fixed or collected for further analysis. We verified the knockdown of APP using western blot with the C-terminal APP antibody 369, whereas there was no effect on APP levels with scrambled control compared to non-transduced control. Western blot analysis revealed significantly increased protein levels of PSD-95 with APP knockdown compared to scrambled control.

Discussion and concluding remarks

The understanding of Aβ's role in Alzheimer's disease is progressively changing. While focus traditionally has been on the aggregation of extracellular Aβ into plaques, a complex picture of intracellular and extracellular pools of Aβ and other cleavage products of APP is emerging.

In paper I, we focused on how the extracellular pool of Aβ targets synapses, as well as where Aβ is produced within synapses. Aβ in brain accumulates and aggregates particularly in synaptic terminals with Aβ pathogenesis (Takahashi et al., 2002), which occurs even prior to plaques, and synapse loss is the best pathological correlate of cognitive deficits (Terry et al., 1991). We showed that exogenous Aβ1-42 accumulates in processes in a subset of CamKII-positive neurons but not in GAD67-positive neurons. Colocalization analysis with pre- and post-synaptic markers demonstrated that exogenous Aβ1-42 does not have a clear preference for the pre- or post-synaptic site. It is important to note that colocalization analysis of Aβ with the pre- or post-synaptic site is very much dependent on the particular markers chosen to represent the synaptic sites. It is also likely that the concentration and conformation of Aβ will have an impact on the precise spatial targeting of added Aβ to synapses. It has been suggested that Aβ might have differential effects on the pre- and post-synaptic sides and that this effect depends on the concentration of Aβ (Palop and Mucke, 2010). Within a physiological range, small increases in Aβ might primarily facilitate pre-synaptic functions, resulting in synaptic potentiation (Abramov et al., 2009; Puzzo et al., 2008). However, at abnormally high levels, Aβ could enhance long-term depression (LTD)-related mechanisms, resulting in post-synaptic depression and loss of dendritic spines (Walsh et al., 2002; Wang et al., 2002). Aβ is produced within neurons after γ-secretase cleavage of β-CTFs. Blocking this cleavage by treatment with the chemical γ-secretase inhibitor DAPT leads to β-CTFs accumulation. We investigated where this accumulation occurs as a proxy of where in the neuron the γ-secretase cleavage occurs to produce Aβ. Our data shows that β-CTFs accumulation after DAPT treatment occurs earlier and/or to a larger extent in pre-synaptic compartments compared to post-synaptic compartments in cortical primary neurons.

In H4 neuroglioma cells stably expressing human APP, used in paper II, APP/β-CTF/Aβ was found mainly in the trans-Golgi network (TGN) and in the endosomes, in line with previous studies. In the endocytic pathway APP/β-CTF/Aβ was found

on the ILVs of a subset of MVBs. APP being sorted to ILVs could potentially have two outcomes. It could (1) lead to increased amyloidogenic processing, as is the case for premelanosome protein (PMEL) with ILV sorting in melanogenic cells (Theos et al., 2006; van Niel et al., 2011), and increase Aβ production. It could also (2) prevent accumulation of Aβ by directing APP to the lysosome. Consistent with the second possibility, lysosomal protease inhibitors led to the accumulation of APP/β-CTF/Aβ in cells and APP/β-CTF/Aβ was found in the EGFR-containing MVBs that are known to fuse with lysosomes. We also found that depletion of the early ESCRT component Hrs increased intracellular levels of APP/β-CTF/Aβ and inhibited its delivery to the lysosome. However, in line with the first scenario, we found reduced secretion of Aβ with Hrs and Tsg101 depletion. We can hence not rule out the possibility that depletion of the early ESCRTs affects Aβ production. Still, the elevated levels of intracellular Aβ with Hrs depletion, suggests that Hrs-dependent sorting of APP to ILVs does not promote Aβ production. The accumulation of intracellular Aβ with Hrs depletion could be caused by both inhibited delivery of APP and its cleavage products to the lysosome, by increasing the time that they reside on the MVBs, but also by reduced Aβ secretion. Overall, in paper II we revealed a role for early ESCRT components in limiting intracellular Aβ accumulation by sorting APP onto ILVs of MVBs for lysosomal degradation and by promoting Aβ secretion.

We continued to investigate the endocytic pathway in models of AD in paper III, demonstrating that increased levels of Aβ lead to enlarged MVB size. However, it is important to note that these results do not exclude previously reported effects of β-CTFs on early endosomal enlargement (Kim et al., 2016; Lauritzen et al., 2016). Neuropathological findings have shown early intraneuronal accumulation and aggregation of Aβ in AD, especially within dystrophic neurites. Our results point to a model, where increased levels of Aβ leads to enlarged and defective MVBs, possibly via effects on ESCRT components. Alternatively, age and other risk factors could act as the starting point for MVB dysfunction, which then in turn results in accumulation of Aβ in enlarged endocytic vesicles. Hence, we suggest a scenario where disturbances in the MVB pathway, caused by Aβ, or vice versa, leads to a vicious circle of more Aβ accumulation and aggregation. Aggregated Aβ in MVBs could potentially serve as seeds for plaques, as supported by our findings of ESCRT components in plaques in mouse models on AD.

In paper IV we uncovered an early increase in β-sheet content by FTIR, concomitant with a change in the native Aβ conformation on BN-PAGE before plaque in AD transgenic mouse brain. Stabilizing the physiological structure of Aβ might therefore be considered as an interesting therapeutic strategy. This type of pharmacological stabilization of a physiological tetramer has successfully been developed for patients with transthyretin amyloidosis and led to the approval of a drug that slows down the progression of the disease. The strategy of stabilizing Aβ

could potentially also have the benefit, compared to many other therapeutic approaches, of not interfering with a physiological role of APP and Aβ.

We investigated the physiological role of APP and its cleavage products at synapses in paper V by comparing the synaptic composition in neurons devoid of APP with wild-type neurons. Although the data is not completely consistent between different analysis methods and time points, it is interesting to note that with Western blot analysis we found increased or a trend for increased levels of the same synaptic markers that previously was shown to be reduced in AD transgenic neurons, that is GluR1, PSD-95 and synaptophysin (Almeida et al., 2005). In the knockdown approach, where we depleted wild-type neurons of APP when synapses were mature, we only detected increased levels of PSD-95 with Western blot. However, with increased n, comparable to the number used in the analysis of APP KO neurons, it is possible that additional synaptic markers also would have reached significantly changed levels, as GluA1 showed a trend for increased levels. In conclusion, our results demonstrate that APP and/or its cleavage are required for normal synaptic composition of mature neurons.

In the studies constituting this thesis, we have investigated the role of Aβ and APP in neurons, with focus on the synapse and the endocytic pathway. The complexity of APP trafficking and the relative significance of the multitude of cleavage products produced, are still not fully understood. Increasing our knowledge will be important to understand the development of the disease and to find effective therapeutic target(s) for AD.

Future perspectives

In this thesis, we have explored certain aspects of the cell biology of Aβ and APP in neurons. Aspects that we believe are important in the early development of the disease. However, many questions remain. Below follows a brief description of experiments and questions that we would like to continue to work on in the future.

Aβ is not only degraded within neurons, but microglia also play a major role. Additionally, there is an increasing awareness in the field of the important role of astrocytes in synaptic regulation. As such I believe it is important to study the interplay between these three cell types in the accumulation of Aβ and loss of synapses during AD.

Working with cell lines overexpressing human AD-related proteins have clear advantages in their ease of manipulation. However, for future studies, a more relevant model would be human patient derived induced pluripotent stem cells (iPSCs) or induced neurons (iNs), given that they are able to differentiate into fully mature neurons. Instead of primary mouse neurons overexpressing human AD-related proteins, as used in this thesis, the newly developed knock-in mouse where human AD related proteins are expressed at physiological levels under their endogenous promoter could be used. I believe this is particularly important when studying abnormalities in the endo-lysosomal pathway.

For further investigation of cell-type specific uptake of exogenously added Aβ, explored in paper I, the use of organotypic brain slices would add an important anatomic dimension to the study. The drawback would be to account for the effect of axotomy. In addition, application of lower non-pathological concentrations of Aβ would likely increase the selectivity of Aβ uptake, allowing us to more specifically pinpoint the cell type and subcellular location most prone to take up and/or accumulate Aβ.

In paper II and III we investigated Aβ and the endo-lysosomal system focusing on the MVB pathway. It would be highly interesting to further study the effect of Aβ on ILV-formation using already existing model systems in yeast. In addition to enlarged MVBs, we also noticed double-membraned structures in the Aβ1-42 treated neurons with EM. This asks for a more thorough EM examination of the interplay between Aβ, the MVB pathway and autophagy. Another line of investigation would be to further examine pathways of Aβ secretion in neurons.

Here compartmentalised neuronal chambers and live imaging could be utilized as well as specific inhibitors of different routes of secretion. Lastly, to further study the details of Aβ aggregation in the endosomal pathway, correlative light electron microscopy (CLEM) would potentially be a very useful tool. In broader terms, it would be highly relevant to study these pathways in context of ApoE and lipid composition.

Acknowledgement

I would like to thank everyone who has contributed to the work represented in this thesis. First of all, my supervisor **Prof. Gunnar Gouras**. I am very grateful to you for giving me the opportunity to do my PhD under your supervision and for introducing me to the field of Alzheimer's disease. Your dedication is inspirational! I would also like to express my gratitude towards **Dr. Davide Tampellini** who started out as my co-supervisor but then left for new adventures in Paris. You made me feel very welcome to our new little group, and I am most grateful for everything you taught me.

Bodil, thank you for your assistance in the animal facility, as well as for your support and calm temper. **Mathilde**, thank you for introducing me to the hands-on work of cloning and plasmids. And of course, I am very grateful for sharing time with you both in and outside of the lab. **Oxana**, my officemate, thank you for our nice discussions, both scientific and political ones. I also value your expertise in biochemistry and your eagerness to test new methods. **Isak**, thank you for your contributions to paper V as well as for opening my ears to the world of runes, Klingon and Elvish (and much more). **Tomas**, I value your creative thinking regarding experiments and that you openly speak your mind. **Sabine**, although you have not been in the lab for that long, thank you for being such a nice person and for always keeping things tidy in the lab. **Vladimir**, thank you for contributing to scientific discussions and offering new perspectives (as well as small chocolate treats).

Agnes, thank you for your contributions to the first paper of this thesis, as well as for your effectiveness and helpfulness. I would also like to thank the other former students that have passed through the lab for longer or shorter periods: **Sofia**, **Una**, **Sofie**, **Efraim**, **Elisabeth**, **Michiel** and **Esther**. Thank you for spreading your good spirits around the lab as well as for your curiosity and your enthusiastic questions.

Dr. James Edgar and **Prof. Clare Futter**, I am very grateful for our collaboration and for being able to take part of your expertise in EM, ESCRTs and the endocytic pathway.

I would also like to warmly thank **everyone at B11** for contributing to such a nice atmosphere on the floor. For all the interesting, important (and sometimes disgusting) discussions during lunch and the delicious pastries that you have made

for the fikas! A special thanks to **Agnes P.**, **Alexander**, **Andreas**, **Antonio, Chris**, **Emelie**, **Emma**, **Jonathan**, **Marina**, **Martina**, **Nadja**, **Oscar**, **Patrik**, **Ulrikke, Yiyi**, **Yoatzin** and many more for organizing and joining game nights, movie nights, wine tastings, volleyball games, parties and after works. Additionally, I would also like to thank **Chris** for your advice regarding exosomal isolation.

I would also like to thank previous and present PhD students and post docs mainly at A10 for including me and making me feel welcome when I started my PhD. I had many great parties with you guys! Thanks **Edina, Reena, Wen, Andrew, Oldriska, Sonja, Trevor, Amelie, Zuzanna, Staffan, Medhi, Nolwen, Christian, Ilknur, Juan, Marcus, Patrick** and many more!

To my **friends**, you are invaluable! Some of you I don't see that often, but I know you are there and you are important to me. To **Samir**, for inspiring me to be stronger. To **Johanna**, for being a superb travel buddy on well needed breaks and adventures during my time as a PhD student.

I would like to thank my family for always being there for me. My sister **Anna** for being the best listener when I needed it the most. My mother **Gudrun**, for your endless love, unselfishness and encouragement. My father **Hans**, for your interest in discussing science and for believing in me and my abilities.

The studies in this thesis were funded by **Swedish Brain Power**, **MultiPark**, **Parkinsonsfonden**, **the Swedish Research Council**, **Alzheimerfonden**, **NIH grant R01-AG027140**, **Alzheimer's Society**, **Hjärnfonden**, **the Welcome Trust**, **Interreg Öresund-Kattegat-Skagerrak (EU)**, **the Segerfalk foundation**, **Anna-Lisa Rosenberg foundation** and **Åhléns foundation**. Finally, I would also like to thank **MultiPark** for rewarding me travel grants that have enabled me to go to many inspiring conferences.

References

Abramov E, Dolev I, Fogel H, Ciccotosto GD, Ruff E, Slutsky I. (2009) Amyloid-beta as a positive endogenous regulator of release probability at hippocampal synapses. Nat Neurosci 12, 1567-1576.

Almeida CG, Tampellini D, Takahashi RH, Greengard P, Lin MT, Snyder EM, Gouras GK. (2005) Beta-amyloid accumulation in APP mutant neurons reduces PSD-95 and GluR1 in synapses. Neurobiol disease 20, 187-198.

Almeida C, Takahashi H, Gouras GK. (2006) Beta-amyloid accumulation impairs multivesicular body sorting by inhibiting the ubiquitin-proteasome system. J Neurosci 26, 4277–88.

Alzheimer's Association. (2017) 2017 Alzheimer's disease facts and figures. Alzheimers Dement 13, 325–73.

Alzheimer's Disease International. (2015) World Alzheimer Report 2015. The global impact of dementia. An analysis of prevalence, incidence, cost and trends. https://www.alz.co.uk/research/WorldAlzheimerReport2015.pdf

Aoki M, Volkmann I, Tjernberg LO, Winblad B, Bogdanovic N (2008) Amyloid β-peptide levels in laser capture microdissected cornu ammonis 1 pyramidal neurons of Alzheimer's brain. Neuroreport 19, 1085–1089.

Babst M, Wendland B, Estepa EJ, Emr SD. (1998) The Vps4p AAA ATPase regulates membrane association of a Vps protein complex required for normal endosome function. EMBO J 11, 2982–93.

Babst M, Katzmann DJ, Estepa-Sabal EJ, Meerloo T, Emr SD. (2002) Escrt-III: an endosome-associated heterooligomeric protein complex required for mvb sorting. Dev Cell 3, 271–82.

Babst M. (2011) MVB vesicle formation: ESCRT-dependent, ESCRT-independent and everything in between. Curr Opin Cell Biol 23, 452-7.

Baker-Nigh A, Vahedi S, Davis EG, Weintraub S, Bigio EH, Klein WL, Geula C. (2015) Neuronal amyloid-β accumulation within cholinergic basal forebrain in ageing and Alzheimer's disease. Brain 138, 1722-1737.

Ball MJ, Nuttal K. (1978) Topographic distribution of neuro- fibrillary tangles and granulovacuoles in hippocampal cortex of aging and demented patients. A quantitative study. Acta Neuropathol 42, 73–80.

Beach T, Walker R, McGeer E. (1989) Patterns of gliosis in Alzheimer's disease and aging cerebrum. Glia 2, 420–436.

Bilousova T, Miller CA, Poon WW, Vinters HV, Corrada M, Kawas C, Hayden EY, Teplow DB, Glabe C, Albay R, 3rd, Cole GM, Teng E, Gylys KH (2016) Synaptic amyloid-β

oligomers precede p-Tau and differentiate high pathology control cases. Am J Pathol 186, 185-198.

Bishop N, Woodman P. (2000) ATPase-defective mammalian VPS4 localizes to aberrant endosomes and impairs cholesterol trafficking. Mol Biol Cell 11, 227–39.

Braak H, Braak E (1991) Neuropathological stageing of Alzheimer-related changes. Acta Neuropathol 82, 239-259.

Braak H, Braak E (1995) Staging of Alzheimer's disease- related neurofibrillary changes. Neurobiol Aging 16, 271-278.

Buckner RL, Snyder AZ, Shannon BJ, LaRossa G, Sachs R, Fotenos AF, Sheline YI, Klunk WE, Mathis CA, Morris JC, Mintun MA (2005) Molecular, structural, and functional characterization of Alzheimer's disease: Evidence for a relationship between default activity, amyloid, and memory. J Neurosci 25, 7709-7717.

Buxbaum JD, Gandy SE, Cicchetti P, Ehrlich ME, Czernik AJ, Fracasso RP, Ramabhadran TV, Unterbeck AJ, Greengard P. (1990) Processing of Alzheimer beta/A4 amyloid precursor protein: Modulation by agents that regulate protein phosphorylation. Proc Natl Acad Sci U S A 87, 6003-6006.

Campeau E, Ruhl VE, Rodier F, Smith CL, Rahmberg BL, Fuss JO, Campisi J, Yaswen P, Cooper PK, Kaufman PD. (2009) A Versatile Viral System for Expression and Depletion of Proteins in Mammalian Cells. PloS one, 4, e6529.

Cataldo AM, Peterhoff CM, Troncoso JC, Gomez-Isla T, Hyman BT, Nixon RA. (2000) Endocytic pathway abnormalities precede amyloid beta deposition in sporadic Alzheimer's disease and down syndrome: differential effects of APOE genotype and presenilin mutations. Am J Pathol 157, 277–86.

Cataldo AM, Petanceska S, Terio NB, Peterhoff CM, Durham R, Mercken M, Mehta PD, Buxbaum J, Haroutunian V, Nixon RA. (2004) Abeta localization in abnormal endosomes: association with earliest Abeta elevations in AD and down syndrome. Neurobiol Aging. 25, 1263–72.

Cataldo AM, Mathews PM, Boiteau AB, Hassinger LC, Peterhoff CM, Jiang Y, Mullaney K, Neve RL, Gruenberg J, Nixon RA. (2008) Down syndrome fibroblast model of Alzheimer-related endosome pathology: accelerated endocytosis promotes late endocytic defects. Am J Pathol 173, 370–84.

Chan RB, Oliveira TG, Cortes EP, Honig LS, Duff KE, Small SA, Wenk MR, Shui G, Di Paolo, G. (2012) Comparative lipidomic analysis of mouse and human brain with Alzheimer disease. J Biol Chem 287, 2678–88.

Cirrito JR, Kang JE, Lee J, Stewart FR, Verges DK, Silverio LM, Bu G, Mennerick S, Holtzman DM. (2008) Endocytosis is required for synaptic activity-dependent release of amyloid-β In vivo. Neuron 58, 42–51.

Coulson EJ, Paliga K, Beyreuther K, Masters CL. (2000) What the evolution of the amyloid protein precursor supergene family tells us about its function. Neurochem Int 36, 175-84.

Crews L, Masliah E. (2010) Molecular mechanisms of neuro-degeneration in Alzheimer's disease. Hum Mol Genet 19, 12–20.

D'Andrea MR, Nagele RG, Wang HY, Peterson PA, Lee DHS. (2001) Evidence that neurones accumulating amyloid can undergo lysis to form amyloid plaques in Alzheimer's disease. Histopathology 38, 120–34.

Davies P, Maloney AJ (1976) Selective loss of central cholinergic neurons in Alzheimer's disease. Lancet 2, 1403.

DeBoer, SR, Dolios G, Wang R, Sisodia SS. (2014) Differential release of beta-amyloid from dendrite- versus axon-targeted APP. J Neurosci 34, 12313-12327.

De Felice FG, Velasco PT, Lambert MP, Viola K, Fernandez SJ, Ferreira ST, Klein WL. (2007) Ab oligomers induce neuronal oxidative stress through an N-methyl-D-aspartate receptor-dependent mechanism that is blocked by the Alzheimer drug memantine. J Biol Chem 282, 11590–11601.

DeKosky ST, Scheff SW. (1990) Synapse loss in frontal cortex biopsies in Alzheimer's disease: Correlation with cognitive severity. Ann Neurol 27, 457-464.

DeKosky ST, Ikonomovic MD, Styren SD, Beckett L, Wisniewski S, Bennett DA, Cochran EJ, Kordower JH, Mufson EJ. (2002) Upregulation of choline acetyltransferase activity in hippocampus and frontal cortex of elderly subjects with mild cognitive impairment. Ann Neurol 2, 145-155.

De Strooper B, Saftig P, Craessaerts K, Vanderstichele H, Gundula G, Annaert W, Von Figura K, Van Leuven F. (1998) Deficiency of presenilin-1 inhibits the normal cleavage of amyloid precursor protein. Nature 391, 387 – 390.

Deyts C, Thinakaran G, Parent AT. (2016) APP receptor? to be or not to be. Trends Pharmacol Sci 37, 390–411.

Di Fiore PP, von Zastrow M. (2014) Endocytosis, signaling, and beyond. Cold Spring Harb Perspect Biol 1, 6-8.

Dores MR, Chen B, Lin H, Soh UJ, Paing MM, Montagne WA, Meerloo T, Trejo J. (2012) ALIX binds a YPX(3)L motif of the GPCR PAR1 and mediates ubiquitin-independent ESCRT-III/MVB sorting. J Cell Biol 197, 407–19.

Edgar JR, Eden ER, Futter CE. (2014) Hrs- and CD63-dependent competing mechanisms make different sized endosomal intraluminal vesicles. Traffic. 15,197–211.

Eitan E, Suire C, Zhang S, Mattson MP. (2016) Impact of lysosome status on extracellular vesicle content and release. Ageing Res Rev 32, 65–74.

Esch FS, Keim PS, Beattie EC, Blacher RW, Culwell AR, Oltersdorf T, McClure D, Ward PJ. (1990) Cleavage of amyloid beta peptide during constitutive processing of its precursor. Science 248, 1122–1124.

Gatz M, Reynolds CA, Fratiglioni L, Johansson B, Mortimer JA, Berg S, Fiske A, Pedersen NL. 2006. Role of genes and environments for explaining Alzheimer disease. Arch Gen Psychiatry 63, 168–174.

Gómez-Isla T, Price JL, McKeel DWJr, Morris JC, Growdon JH, Hyman BT. (1996) Profound loss of layer II entorhinal cortex neurons occurs in very mild Alzheimer's disease. J Neurosci 16, 4491-4500.

Gouras GK, Relkin NR, Sweeney D, Munoz DG, Mackenzie IR, Gandy S. (1997) Increased apolipoprotein E epsilon 4 in epilepsy with senile plaques. Ann Neurol 41, 402–404.

Gouras GK, Xu H, Jovanovic JN, Buxbaum JD, Wang R, Greengard P, Relkin NR, Gandy S. (1998) Generation and regulation of beta-amyloid peptide variants by neurons. J Neurochem. 71, 1920-5.

Gouras GK, Tsai J, Naslund J, Vincent B, Edgar M, Checler F, Greenfield JP, Haroutunian V, Buxbaum JD, Xu H, Greengard P, Relkin NR. (2000) Intraneuronal Ab42 accumulation in human brain. Am J Pathol 156, 15–20.

Grimm MO, Mett J, Grimm HS, Hartmann T. (2017) APP Function and Lipids: A Bidirectional Link. Front Mol Neurosci 10, 63.

Gu Y, Misonou H, SatoT, Dohmae N, Takio K, Ihara Y. (2001) Distinct intramembrane cleavage of the beta-amyloid precursor protein family resembling gamma-secretase-like cleavage of Notch. J Biol Chem 276, 35235–35238.

Guerreiro R, Wojtas A, Bras J, Carrasquillo M, Rogaeva E, Majounie E, Cruchaga C, Sassi C, Kauwe JS, Younkin S et al (2013) TREM2 variants in Alzheimer's disease. N Engl J Med 368, 117 – 127.

Haass C, Selkoe DJ. (2007) Soluble protein oligomers in neurodegeneration: Lessons from the Alzheimer's amyloid b-peptide. Nat Rev 8, 101–112.

Hasegawa T, Konno M, Baba T, Sugeno N, Kikuchi A, Kobayashi M, Miura E, Tanaka N, Tamai K, Furukawa K, Arai H, Mori F, Wakabayashi K, Aoki M, Itoyama Y, Takeda A. (2011) The AAA-ATPase VPS4 regulates extracellular secretion and lysosomal targeting of α-synuclein. PLoS One 6, e29460.

Hashimoto M, Bogdanovic N, Volkmann I, Aoki M, Winblad B, Tjernberg LO (2010) Analysis of microdissected human neurons by a sensitive ELISA reveals a correlation between elevated intracellular concentrations of Abeta42 and Alzheimer's disease neuropathology. Acta Neuropathol 119, 543-554.

Holtzman DM, Herz J, Bu G. (2012) Apolipoprotein E and apolipoprotein E receptors: normal biology and roles in Alzheimer disease. Cold Spring Harb Perspect Med 2, a006312.

Hooli BV, Kovacs-Vajna ZM, Mullin K, Blumenthal MA, Mattheisen M, Zhang C, Lange C, Mohapatra G, Bertram L, Tanzi RE. (2014) Rare autosomalcopy number variations in early-onset familial Alzheimer's disease. Mol Psychiatry 19, 676–81.

Huang YA, Zhou B, Wernig M, Südhof TC. (2017) ApoE2, ApoE3, and ApoE4 Differentially Stimulate APP Transcription and Aβ Secretion. Cell 168, 427-441.

Itagaki S, McGeer PL, Akiyama H, Zhu S, Selkoe D. (1989) Relationship of microglia and astrocytes to amyloid deposits of Alzheimer disease. J Neuroimmunol 24, 173–182.

Iwata N, Tsubuki S, Takaki Y, Watanabe K, Sekiguchi M, Hosoki E, Kawashima-Morishima M, Lee HJ, Hama E, Sekine-Aizawa Y, SAido TC. (2000) Identification of the major Abeta1–42-degrading catabolic pathway in brain parenchyma: Suppression leads to biochemical and pathological deposition. Nat Med 6, 143–150.

Iwata N, Tsubuki S, Takaki Y, Shirotani K, Lu B, Gerard NP, Gerard C, Hama E, Lee HJ, Saido TC. (2001) Metabolic regulation of brain Abeta by neprilysin. Science 292, 1550–1552.

Jack CR Jr, Knopman DS, Jagust WJ, Petersen RC, Weiner MW, Aisen PS, Shaw LM, Vemuri P, Wiste HJ, Weigand SD, Lesnick TG, Pankratz VS, Donohue MC, Trojanowski JQ. (2013) Tracking pathophysiological processes in Alzheimer's

disease: an updated hypothetical model of dynamic biomarkers. Lancet Neurol 12, 207-16.

Jones L, Holmans PA, Hamshere ML, Harold D, Moskvina V, Ivanov D, Pocklington A, Abraham R, Hollingworth P, Sims R, Gerrish A, Pahwa JS, Jones N, Stretton A, Morgan AR, Lovestone S, Powell J, Proitsi P, Lupton MK, Brayne C, Rubinsztein DC, Gill M, Lawlor B, Lynch A, Morgan K, Brown KS, Passmore PA, Craig D, McGuinness B, Todd S, Holmes C, Mann D, Smith AD, Love S, Kehoe PG, Mead S, Fox N, Rossor M, Collinge J, Maier W, Jessen F, Schürmann B, Heun R, Kölsch H, van den Bussche H, Heuser I, Peters O, Kornhuber J, Wiltfang J, Dichgans M, Frölich L, Hampel H, Hüll M, Rujescu D, Goate AM, Kauwe JS, Cruchaga C, Nowotny P, Morris JC, Mayo K, Livingston G, Bass NJ, Gurling H, McQuillin A, Gwilliam R, Deloukas P, Al-Chalabi A, Shaw CE, Singleton AB, Guerreiro R, Mühleisen TW, Nöthen MM, Moebus S, Jöckel KH, Klopp N, Wichmann HE, Rüther E, Carrasquillo MM, Pankratz VS, Younkin SG, Hardy J, O'Donovan MC, Owen MJ, Williams J. (2010) Genetic evidence implicates the immune system and cholesterol metabolism in the aetiology of Alzheimer's disease. PLoS One 5, e13950.

Jonsson T, Stefansson H, Steinberg S, Jonsdottir I, Jonsson PV, Snaedal J, Bjornsson S, Huttenlocher J, Levey AI, Lah JJ, Rujescu D, Hampel H, Giegling I, Andreassen OA, Engedal K, Ulstein I, Djurovic S, Ibrahim-Verbaas C, Hofman A, Ikram MA, van Duijn CM, Thorsteinsdottir U, Kong A, Stefansson K. (2013) Variant of TREM2 associated with the risk of Alzheimer's disease. N Engl J Med 368, 107 – 116.

Kamenetz F, Tomita T, Hsieh H, Seabrook G, Borchelt D, Iwatsubo T, Sisodia S, Malinow R. (2003) APP processing and synaptic function. Neuron 37, 925-937.

Kang J, Lemaire HG, Unterbeck A, Salbaum JM, Masters CL, Grzeschik KH, Multhaup G, Beyreuther K, Muller-Hill B. (1987) The precursor of Alzheimer's disease amyloid A4 protein resembles a cell-surface receptor. Nature 325, 733–736.

Kim J, Onstead L, Randle S, Price R, Smithson L, Zwizinski C, Dickson DW, Golde T, McGowan E. (2007) Abeta40 inhibits amyloid deposition in vivo. J Neurosci 27, 627 – 633.

Kim S, Sato Y, Mohan PS, Peterhoff C, Pensalfini A, Rigoglioso A, Jiang Y, Nixon RA. (2016) Evidence that the rab5 effector APPL1 mediates APP-βCTF-induced dysfunction of endosomes in down syndrome and Alzheimers disease. Mol Psychiatry 21, 707–16.

Kobro-Flatmoen A, Nagelhus A, Witter MP. (2016) Reelin-immunoreactive neurons in entorhinal cortex layer II selectively express intracellular amyloid in early Alzheimer's disease. Neurobiol Dis 93, 172-183.

Koo, EH, Sisodia, SS, Archer DR, Martin LJ, Weidemann A, Beyreuther K, Fischer P, Masters CL, Price DL. (1990) Precursor of amyloid protein in Alzheimer disease undergoes fast anterograde axonal transport. Proc Natl Acad Sci U S A 87, 1561-1565.

Lacor PN, Buniel MC, Furlow PW, Clemente AS, Velasco PT, Wood M, Viola KL, Klein WL. (2007) Abeta oligomer- induced aberrations in synapse composition, shape, and density provide a molecular basis for loss of connectivity in Alzheimer's disease. J Neurosci 27, 796-807.

Lamb CA, Dooley HC, Tooze SA. (2013) Endocytosis and autophagy: Shared machinery for degradation. BioEssays 35, 34-45.

Lambert JC, Ibrahim-Verbaas CA, Harold D, Naj AC, Sims R, Bellenguez C, DeStefano AL, Bis JC, Beecham GW, Grenier-Boley B et al (2013) Meta-analysis of 74,046 individuals identifies 11 new susceptibility loci for Alzheimer's disease. Nat Genet 45, 1452 – 1458.

Langui D, Girardot N, El Hachimi KH, Allinquant B, Blanchard V, Pradier L, Duyckaerts C. (2004) Subcellular topography of neuronal Abeta peptide in APPxPS1 transgenic mice. Am J Pathol 165, 1465–77.

Lata S, Schoehn G, Jain A, Pires R, Piehler J, Gottlinger HG, Weissenhorn W. (2008) Helical structures of ESCRT-III are disassembled by VPS4. Science 321, 1354–1357.

Laurén J, Gimbel DA, Nygaard HB, Gilbert JW, Strittmatter SM. (2009) Cellular prion protein mediates impairment of synaptic plasticity by amyloid-beta oligomers. Nature 457, 1128-1132.

Lauritzen I, Pardossi-Piquard R, Bourgeois A, Pagnotta S, Biferi MG, Barkats M, Lacor P, Klein W, Bauer C, Checler F. (2016) Intraneuronal aggregation of the β-CTF fragment of APP (C99) induces Aβ-independent lysosomal-autophagic pathology. Acta Neuropathol 132, 257–76.

Lee EK, Park YW, Shin DY, Mook-Jung I, Yoo YJ. (2006) Cytosolic amyloid-beta peptide 42 escaping from degradation induces cell death. Biochem Biophys Res Commun 344, 471–477.

Leissring MA, Reinstatler L, Sahara T, Roman R, SevleverD, SaftigP, LevitesY, Golde TE, BurgessJD, Ertekin-Taner N, et al. (2009) Cathepsin D selectively degrades Ab42 and tau: Implications for Alzheimer disease pathogenesis. In Society for Neuroscience, Program No. 139108. Society for Neuroscience, Chicago.

Leissring MA. (2016) Aβ-Degrading Proteases: Therapeutic Potential in Alzheimer Disease. CNS Drugs. 30, 667-75.

Li S, Hong S, Shepardson NE, Walsh DM, Shankar GM, Selkoe D. (2009) Soluble oligomers of amyloid β protein facilitate hippocampal long-term depression by disrupting neuronal glutamate uptake. Neuron 62, 788–801.

Lobert VH, Stenmark H. (2011) Cell polarity and migration: emerging role for the endosomal sorting machinery. Physiology (Bethesda) 26, 171-80.

Lopez Salon M, Pasquini L, BesioMoreno M, Pasquini JM, Soto E. (2003) Relationship between beta-amyloid degradation and the 26S proteasome in neural cells. ExpNeurol 180, 131–143.

Louveau A, Smirnov I, Keyes TJ, Eccles JD, Rouhani SJ, Peske JD, Derecki NC, Castle D, Mandell JW, Lee KS, Harris TH, Kipnis J. (2015) Structural and functional features of central nervous system lymphatic vessels. Nature 523, 337-41.

Lundgren JL, Ahmed S, Schedin-Weiss S, Gouras GK, Winblad B, Tjernberg LO, Frykman S. (2015) ADAM10 and BACE1 are localized to synaptic vesicles. J Neurochem 135, 606-615.

Mackenzie IR. Miller LA. (1994) Senile plaques in temporal lobe epilepsy. Acta Neuropathol 87, 504–510.

Mesulam M. (2004) The cholinergic lesion of Alzheimer's disease: Pivotal factor or side show? Learn Mem 11, 43-49.

Morel E, Chamoun Z, Lasiecka ZM, Chan RB, Williamson RL, Vetanovetz C, Dall'Armi C, Simoes S, Point Du Jour KS, McCabe BD, Small SA, Di Paolo G. (2013) Phosphatidylinositol-3-phosphate regulates sorting and processing of amyloid precursor protein through the endosomal system. Nat Commun 4, 2250.

Müller UC, Deller T, Korte M. (2017) Not just amyloid: physiological functions of the amyloid precursor protein family. Nat Rev Neurosci 18, 281–298.

Nilsson P, Loganathan K, Sekiguchi M, Matsuba Y, Hui K, Tsubuki S, Tanaka M, Iwata N, Saito T, Saido TC. (2013) Abeta secretion and plaque formation depend on autophagy. Cell Rep 5, 61-69.

Nixon RA, Wegiel J, Kumar A, Yu WH, Peterhoff C, Cataldo A, Cuervo AM. (2005) Extensive involvement of autophagy in Alzheimer disease: an immunoelectron microscopy study. J Neuropathol Exp Neurol 64, 113–22.

Oakley H, Cole SL, Logan S, Maus E, Shao P, Craft J, Guillozet-Bongaarts A, Ohno M, Disterhoft J, Van Eldik L, Berry R, Vassar R. (2006) Intraneuronal beta-amyloid aggregates, neurodegeneration, and neuron loss in transgenic mice with five familial Alzheimer's disease mutations: potential factors in amyloid plaque formation. J Neurosci 26, 10129–40.

Palop JJ, Mucke L. (2010) Amyloid-beta-induced neuronal dysfunction in Alzheimer's disease: From synapses toward neural networks. Nat Neurosci 13, 812-818.

Peric A, Annaert W. (2015) Early etiology of Alzheimer's disease: tipping the balance toward autophagy or endosomal dysfunction? Acta Neuropathol 129, 363–81.

Perry EK, Blessed G, Tomlinson BE, Perry RH, Crow TJ, Cross AJ, Dockray GJ, Dimaline R, Arregui A. (1981) Neurochemical activities in human temporal lobe related to aging and Alzheimer-type changes. Neurobiol Aging 2, 251-256.

Petersen RC, Stevens JC, Ganguli M, Tangalos EG, Cummings JL, DeKosky ST. (2001) Practice parameter: early detection of dementia: mild cognitive impairment (an evidence-based review). Report of the quality standards subcommittee of the American Academy of Neurology. Neurology 56, 1133–1142.

Puzzo D, Privitera L, Leznik E, Fà M, Staniszewski A, Palmeri A, Arancio O. (2008) Picomolar amyloid-beta positively modulates synaptic plasticity and memory in hippocampus. J Neurosci 28, 14537-14545.

Rajendran L, Honsho M, Zahn TR, Keller P, Geiger KD, Verkade P, Simons K. (2006) Alzheimer's disease beta-amyloid peptides are released in association with exosomes. Proc Natl Acad Sci U S A 103, 11172-7.

Rajendran L, Annaert W. (2012) Membrane trafficking pathways in Alzheimer's disease. Traffic 13, 759–70.

Renner M, Lacor PN, Velasco PT, Xu J, Contractor A, Klein WL, Triller A. (2010) Deleterious effects of amyloid-β oligomers acting as an extracellular scaffold for mGluR5. Neuron 66, 739-754.

Rogers J, Luber-Narod J, Styren S, CivinW. (1988) Expression of immune system-associated antigens by cells of the human central nervous system: Relationship to the pathology of Alzheimer's disease. Neurobiol Aging 9, 339–349.

Sabo SL, Ikin AF, Buxbaum JD, Greengard P. (2003) The amyloid precursor protein and its regulatory protein, FE65, in growth cones and synapses and in vivo. J Neurosci 23, 5407–5415.

Saido T, Leissring MA. (2012) Proteolytic degradation of amyloid β-protein. Cold Spring Harb Perspect Med 2, a006379.

Sannerud R, Declerck I, Peric A, Raemaekers T, Menendez G, Zhou L, Veerle B, Coen K, Munck S, De Strooper B, Schiavo G, Annaert W. (2011) ADP ribosylation factor 6 (ARF6) controls amyloid precursor protein (APP) processing by mediating the endosomal sorting of BACE1. Proc Natl Acad Sci U S A 108, E559-68.

Sannerud R, Esselens C, Ejsmont P, Mattera R, Rochin L, Tharkeshwar AK, De Baets G, De Wever V, Habets R, Baert V, Vermeire W, Michiels C, Groot AJ, Wouters R, Dillen K, Vints K, Baatsen P, Munck S, Derua R, Waelkens E, Basi GS, Mercken M, Vooijs M, Bollen M, Schymkowitz J, Rousseau F, Bonifacino JS, Van Niel G, De Strooper B, Annaert W. (2016) Restricted location of PSEN2/γ- Secretase determines substrate specificity and generates an intracellular Aβ pool. Cell 166, 193–208.

Sastre M, Steiner H, Fuchs K, Capell A, Multhaup G, Condron MM, Teplow DB, Haass C. (2001) Presenilin-dependent gamma-secretase processing of beta-amyloid precursor protein at a site corresponding to the S3 cleavage of Notch. EMBO Rep 2, 835–841.

Saura CA, Chen G, Malkani S, Choi SY, Takahashi RH, Zhang D, Gouras GK, Kirkwood A, Morris RG, Shen J. (2005) Conditional inactivation of presenilin 1 prevents amyloid accumulation and temporarily rescues contextual and spatial working memory impairments in amyloid precursor protein transgenic mice. J Neurosci 25, 6755-6764.

Schedin-Weiss S, Caesar I, Winblad B, Blom H, Tjernberg LO. (2016) Super-resolution microscopy reveals gamma-secretase at both sides of the neuronal synapse. Acta Neuropathol Commun 4, 29.

Scheff SW, DeKosky ST, Price DA. (1990) Quantitative assessment of cortical synaptic density in Alzheimer's disease. Neurobiol Aging 11, 29–37.

Selkoe DJ. (2001) Clearing the brain's amyloid cobwebs. Neuron 32, 177–180.

Selkoe DJ. (2002) Alzheimer's disease is a synaptic failure. Science 298, 789–791.

Sevigny J, Chiao P, Bussière T, Weinreb PH, Williams L, Maier M, Dunstan R, Salloway S, Chen T, Ling Y, O'Gorman J, Qian F, Arastu M, Li M, Chollate S, Brennan MS, Quintero-Monzon O, Scannevin RH, Arnold HM, Engber T, Rhodes K, Ferrero J, Hang Y, Mikulskis A, Grimm J, Hock C, Nitsch RM Sandrock, A. (2016) The antibody aducanumab reduces Aβ plaques in Alzheimer's disease. Nature 537, 50–6.

Shankar GM, Li S, Mehta TH, Garcia-Munoz A, Shepardson NE, Smith I, Brett FM, Farrell MA, Rowan MJ, Lemere CA, Regan CM, Walsh DM, Sabatini BL, Selkoe DJ. (2008) Amyloid-beta protein dimers isolated directly from Alzheimer's brains impair synaptic plasticity and memory. Nat Med 14, 837–842.

Shi Y, Yamada K, Liddelow SA, Smith ST, Zhao L, Luo W, Tsai RM, Spina S, Grinberg LT, Rojas JC, Gallardo G, Wang K, Roh J, Robinson G, Finn MB, Jiang H, Sullivan PM, Baufeld C, Wood MW, Sutphen C, McCue L, Xiong C, Del-Aguila JL, Morris JC, Cruchaga C; Alzheimer's Disease Neuroimaging Initiative, Fagan AM, Miller BL, Boxer AL, Seeley WW, Butovsky O, Barres BA, Paul SM, Holtzman DM. (2017)

ApoE4 markedly exacerbates tau-mediated neurodegeneration in a mouse model of tauopathy. Nature, 549, 523-527.

Sisodia SS, Koo EH, Beyreuther K, Unterbeck A, Price DL. (1990) Evidence that β-amyloid protein in Alzheimer's disease is not derived by normal processing. Science 248, 492–495.

Skibinski G, Parkinson NJ, Brown JM, Chakrabarti L, Lloyd SL, Hummerich H, Nielsen JE, Hodges JR, Spillantini MG, Thusgaard T, Brandner S, Brun A, Rossor MN, Gade A, Johannsen P, Sørensen SA, Gydesen S, Fisher EM, Collinge J. (2005) Mutations in the endosomal ESCRTIII-complex subunit CHMP2B in frontotemporal dementia. Nat Genet 37, 806–8.

Slot JW, Geuze HJ, Gigengack S, Lienhard GE, James, DE. (1991) Immuno-localization of the insulin regulatable glucose transporter in brown adipose tissue of the rat. J Cell Biol 113, 123-135.

Soba P, Eggert S, Wagner K, Zentgraf H, Siehl K, Kreger S, Löwer A, Langer A, Merdes G, Paro R, Masters CL, Müller U, Kins S, Beyreuther K. (2005) Homo- and heterodimerization of APP family members promotes intercellular adhesion. EMBO J 24, 3624–3634.

Sosa LJ, Bergman J, Estrada-Bernal A, Glorioso TJ, Kittelson JM, Pfenninger KH. (2013) Amyloid precursor protein is an autonomous growth cone adhesion molecule engaged in contact guidance. PLoS ONE 8, e64521.

Stuffers S, Sem Wegner C, Stenmark H, Brech A. (2009) Multivesicular endosome biogenesis in the absence of ESCRTs. Traffic 10, 925–37.

Su JH, Cummings BJ, Cotman CW. (1998) Plaque biogenesis in brain aging and Alzheimer's disease. II. Progressive transformation and developmental sequence of dystrophic neurites. Acta Neuropathol 96, 463–471.

Taelman VF, Dobrowolski R, Plouhinec JL, Fuentealba LC, Vorwald PP, Gumper I, Sabatini DD, De Robertis EM. (2010) Wnt signaling requires sequestration of glycogen synthase kinase 3 inside multivesicular endosomes. Cell 143, 1136–48.

Takahashi RH, Milner TA, Li F, Nam EE, Edgar MA, Yamaguchi H, Beal MF, Xu H, Greengard P, Gouras GK. (2002) Intraneuronal Alzheimer abeta42 accumulates in multivesicular bodies and is associated with synaptic pathology. Am J Pathol 161, 1869-79.

Takahashi RH, Almeida CG, Kearney PF, Yu F, Lin MT, Milner TA, Gouras GK. (2004) Oligomerization of Alzheimer's beta-amyloid within processes and synapses of cultured neurons and brain. J Neurosci 24, 3592–3599.

Tampellini D, Rahman N, Gallo EF, Huang Z, Dumont M, Capetillo-Zarate E, Ma T, Zheng R, Lu B, Nanus DM, LinMT, Gouras GK. (2009) Synaptic activity reduces intraneuronal Abeta, promotes APP transport to synapses, and protects against Abeta-related synaptic alterations. J Neurosci 29, 9704-9713.

Tampellini D, Rahman N, Lin MT, Capetillo-Zarate E, Gouras GK. (2011) Impaired beta-amyloid secretion in Alzheimer's disease pathogenesis. J Neurosci 31, 15384–90.

Tanzi RE, Moir RD, Wagner SL. (2004) Clearance of Alzheimer's Abeta peptide: The many roads to perdition. Neuron 43, 605–608.

Tarasoff-Conway JM, Carare RO, Osorio RS, Glodzik L, Butler T, Fieremans E, Axel L, Rusinek H, Nicholson C, Zlokovic BV, Frangione B, Blennow K, Ménard J, Zetterberg H, Wisniewski T, de Leon MJ. (2015) Clearance systems in the brain-implications for Alzheimer disease. Nat Rev Neurol 11, 457-70.

Terry RD, Masliah E, Salmon DP, Butters N, DeTeresa R, Hill R, Hansen LA, Katzman R. (1991) Physical basis of cognitive alterations in Alzheimer's disease: Synapse loss is the major correlate of cognitive impairment. Ann Neurol 30, 572-580.

Thal DR, Rüb U, Orantes M, Braak H. (2002) Phases of Abeta-deposition in the human brain and its relevance for the development of AD. Neurology 58, 1791-1800.

Theos AC, Truschel ST, Tenza D, Hurbain I, Harper DC, Berson JF, Thomas PC, Raposo G, Marks MS. (2006) A lumenal domain-dependent pathway for sorting to intralumenal vesicles of multivesicular endosomes involved in organelle morphogenesis. Dev Cell 10, 343-354.

Théry C, Amigorena S, Raposo G, Clayton A. (2006) Isolation and characterization of exosomes from cell culture supernatants and biological fluids. Curr Protoc Cell Biol 30, 3.22:3.22.1–3.22.29.

Thinakaran G, Teplow DB, Siman R, Greenberg B, Sisodia SS. (1996) Metabolism of the "Swedish" amyloid precursor protein variant in neuro2a (N2a) cells. Evidence that cleavage at the "beta-secretase" site occurs in the golgi apparatus. J Biol Chem 271, 9390–9397.

Thinakaran G, Koo EH. (2008) Amyloid precursor protein trafficking, processing, and function. J Biol Chem. 283, 29615-9.

Trajkovic K, Hsu C, Chiantia S, Rajendran L, Wenzel D, Wieland F, Schwille P, Brügger B, Simons M. (2008) Ceramide triggers budding of exosome vesicles into multivesicular endosomes. Science 319, 1244–7.

Ubelmann F, Burrinha T, Salavessa L, Gomes R, Ferreira C, Moreno N, Guimas AC. (2017) Bin1 and CD2AP polarise the endocytic generation of beta-amyloid. EMBO Rep 18, 102–22.

Udayar V, Buggia-Prévot V, Guerreiro RL, Siegel G, Rambabu N, Soohoo AL, Ponnusamy M, Siegenthaler B, Bali J; AESG, Simons M, Ries J, Puthenveedu MA, Hardy J, Thinakaran G, Rajendran L. (2013) A paired RNAi and RabGAP overexpression screen identifies Rab11 as a regulator of β-amyloid production. Cell Rep 5, 1536-51.

van der Kant R, Goldstein LS. (2015) Cellular functions of the amyloid precursor protein from development to dementia. Dev Cell 32, 502-15.

van Niel G, Charrin S, Simoes S, Romao M, Rochin L, Saftig P, Marks MS, Rubinstein E, Raposo G. (2011) The tetraspanin CD63 regulates ESCRT-independent and -dependent endosomal sorting during melanogenesis. Dev Cell 21, 708–21.

Vassar R, Bennett BD, Babu-Khan S, Kahn S, Mendiaz EA, Denis P, Teplow DB, Ross S, Amarante P, Loeloff R, Luo Y, Fisher S, Fuller J, Edenson S, Lile J, Jarosinksi M, Biere AL, Curran E, Burgess T, Louis JC, Collins F, Treanor J, Rogers G, Citron M. (1999) β-secretase cleavage of Alzheimer's amyloid precursor protein by the transmembrane aspartic protease BACE. Science 286, 735–741

Vassar R. (2004) BACE1: The beta-secretase enzyme in Alzheimer's disease. J Mol Neurosci 23, 105–114.

Vehmas AK, Kawas CH, Stewart WF, Troncoso JC. (2003) Immune reactive cells in senile plaques and cognitive decline in Alzheimer's disease. Neurobiol Aging 24, 321–331.

von Rotz RC, Kohli BM, Bosset J, Meier M, Suzuki T, Nitsch RM, Konietzko U. (2004). The APP intracellular domain forms nuclear multiprotein complexes and regulates the transcription of its own precursor. J Cell Sci 117, 4435–4448.

Walsh DM, Klyubin I, Fadeeva JV, Cullen WK, Anwyl R, Wolfe MS, Rowan MJ, Selkoe DJ. (2002) Naturally secreted oligomers of amyloid beta protein potently inhibit hippocampal long-term potentiation in vivo. Nature 416, 535-539.

Wang HW, Pasternak JF, Kuo H, Ristic H, Lambert MP, Chromy B, Viola KL, Klein WL, Stine WB, Krafft GA, Trommer BL. (2002) Soluble oligomers of β-amyloid (1-42) inhibit long-term potentiation but not long-term depression in rat dentate gyrus. Brain Res 924, 133-140.

Wang HY, Lee DH, D'Andrea MR, Peterson PA, Shank RP, Reitz AB. (2000) beta-Amyloid(1-42) binds to alpha7 nicotinic acetylcholine receptor with high affinity. Implications for Alzheimer's disease pathology. J Biol Chem 275, 5626-5632.

Wasco W, Bupp K, Magendantz M, Gusella JF, Tanzi RE, Solomon F. (1992) Identification of a mouse brain cDNA that encodes a protein related to the Alzheimer disease-associated amyloid beta protein precursor. Proc Natl Acad Sci U S A 89, 10758-62.

Wasco W, Gurubhagavatula S, Paradis MD, Romano DM, Sisodia SS, Hyman BT, Neve RL, Tanzi RE. (1993) Isolation and characterization of APLP2 encoding a homologue of the Alzheimer's associated amyloid beta protein precursor. Nat Genet 5, 95-100.

Wesén E, Jeffries GDM, Matson Dzebo M, Esbjörner EK. (2017) Endocytic uptake of monomeric amyloid-β peptides is clathrin- and dynamin-independent and results in selective accumulation of Aβ(1-42) compared to Aβ(1-40). Sci Rep 7, 2021.

White IJ, Bailey LM, Aghakhani MR, Moss SE, Futter CE. (2006) EGF stimulates annexin 1-dependent inward vesiculation in a multivesicular endosome subpopulation. EMBO J 25, 1-12.

Williamson RL, Laulagnier K, Miranda AM, Fernandez MA, Wolfe MS, Sadoul R, Di Paolo G. (2017) Disruption of amyloid precursor protein ubiquitination selectively increases amyloid beta (Aβ) 40 levels via presenilin 2-mediated cleavage. J Biol Chem. Epub ahead of print.

Wirths O, Multhaup G, Czech C, Blanchard V, Moussaoui S, Tremp G, Pradier L, Beyreuther K, Bayer TA. (2001) Intraneuronal Abeta accumulation precedes plaque formation in beta-amyloid precursor protein and presenilin-1 double-transgenic mice. Neurosci Lett 306, 116–20.

Wolfe MS, Xia W, Ostaszewski BL, Diehl TS, Kimberly WT, Selkoe DJ. (1999) Two transmembrane aspartates in presenilin-1 required for presenilin endoproteolysis and g-secretase activity. Nature 398, 513 – 517.

Wolfe, MS. (2012) Processive proteolysis by γ-secretase and the mechanism of Alzheimer's disease. Biol Chem 393, 899–905.

Wollert T, Wunder C, Lippincott-Schwartz J, Hurley JH. (2009) Membrane scission by the ESCRT-III complex. Nature 458, 172–7.

Xu M, Shibayama H, Kobayashi H, Yamada K, Ishihara R, Zhao P, Takeuchi T, Yoshida K, Inagaki T, Nokura K. (1992) Granulovacuolar degeneration in the hippocampal cortex of aging and demented patients: A quantitative study. Acta Neuropathol 85, 1–9.

Yamazaki Y, Takahashi T, Hiji M, Kurashige T, Izumi Y, Yamawaki T, Matsumoto M. (2010) Immunopositivity for ESCRT-III subunit CHMP2B in granulovacuolar degeneration of neurons in the Alzheimer's disease hippocampus. Neurosci Lett 477, 86–90.

Yang AJ, Chandswangbhuvana D, Margol L, Glabe CG. (1998) Loss of endosomal/ lysosomal membrane impermeability is an early event in amyloid Abeta1-42 pathogenesis. J Neurosci Res 52, 691–698.

Young-Pearse TL, Bai J, Chang R, Zheng JB, LoTurco JJ, Selkoe DJ. (2007) A critical function for beta-amyloid precursor protein in neuronal migration revealed by in utero RNA interference. J Neurosci 27, 14459-14469.

Zhang Y, McLaughlin R, Goodyer C, LeBlanc A. (2002) Selective cytotoxicity of intracellular amyloid beta peptide1-42 through p53 and Bax in cultured primary human neurons. J Cell Biol 156, 519–529.

Zheng H, Jiang M, Trumbauer ME, Sirinathsinghji DJ, Hopkins R, Smith DW, Heavens RP, Dawson GR, Boyce S, Conner MW, Stevens KA, Slunt HH, Sisoda SS, Chen HY, Van der Ploeg LH. (1995) β-amyloid precursor protein-deficient mice show reactive gliosis and decreased locomotor activity. Cell 81, 525-531.

Zhao N, Liu CC, Qiao W, Bu G. (2017) Apolipoprotein E, Receptors, and Modulation of Alzheimer's Disease. Biol Psychiatry. Epub ahead of print.

Zou L, Wang Z, Shen L, Bao GB, Wang T, Kang JH, Pei G. (2007) Receptor tyrosine kinases positively regulate BACE activity and amyloid-β production through enhancing BACE internalization. Cell Res 17, 389–401.

Paper I

Journal of Alzheimer's Disease 60 (2017) 511–524
DOI 10.3233/JAD-170262
IOS Press

Heterogeneous Association of Alzheimer's Disease-Linked Amyloid-β and Amyloid-β Protein Precursor with Synapses

Katarina Willén[a], Agnieszka Sroka[a], Reisuke H. Takahashi[b] and Gunnar K. Gouras[a,*]
[a]*Department of Experimental Medical Science, Lund University, Lund, Sweden*
[b]*Department of Anatomic Pathology, Tokyo Medical University, Tokyo, Japan*

Handling Associate Editor: P. Hemachandra Reddy

Accepted 7 July 2017

Abstract. Alzheimer's disease (AD) is increasingly viewed as a disease of synapses. Loss of synapses correlates better with cognitive decline than amyloid plaques and neurofibrillary tangles, the hallmark neuropathological lesions of AD. Soluble forms of amyloid-β (Aβ) have emerged as mediators of synapse dysfunction. Aβ binds to, accumulates, and aggregates in synapses. However, the anatomical and neurotransmitter specificity of Aβ and the amyloid-β protein precursor (AβPP) in AD remain poorly understood. In addition, the relative roles of Aβ and AβPP in the development of AD, at pre- versus post-synaptic compartments and axons versus dendrites, respectively, remain unclear. Here we use immunogold electron microscopy and confocal microscopy to provide evidence for heterogeneity in the localization of Aβ/AβPP. We demonstrate that Aβ binds to a subset of synapses in cultured neurons, with preferential binding to glutamatergic compared to GABAergic neurons. We also highlight the challenge of defining pre- versus post-synaptic localization of this binding by confocal microscopy. Further, endogenous $A\beta_{42}$ accumulates in both glutamatergic and GABAergic AβPP/PS1 transgenic primary neurons, but at varying levels. Moreover, upon knock-out of presenilin 1 or inhibition of γ-secretase AβPP C-terminal fragments accumulate both pre- and post-synaptically; however earlier pre-synaptically, consistent with a higher rate of AβPP processing in axons. A better understanding of the synaptic and anatomical selectivity of Aβ/AβPP in AD can be important for the development of more effective new therapies for this major disease of aging.

Keywords: Alzheimer's disease, amyloid-beta, gamma-secretase, synapse

INTRODUCTION

Synapses are a unique characteristic of nerve cells and are increasingly seen as critical sites of pathogenesis in neurodegenerative diseases of aging. In Alzheimer's disease (AD), it has long been known that loss of synapses is a better brain correlate of cognitive decline than the number of amyloid plaques or neurofibrillary tangles [1, 2], the two neuropathological hallmark lesions. The high metabolic demands of the brain relate to the large amount of energy consumed by synaptic function. It has been hypothesized that this high-energy consumption at synapses could lead to their age-related vulnerability from reactive oxidant species [3, 4]. Further, synaptic activity stimulates amyloid-β (Aβ) generation and secretion [5], as well as degradation [6]. The observation that the anatomy of amyloid plaque pathology in the brain resembles metabolic activity in the default network has led to a hypothesis that synaptic activity via stimulated generation and secretion of Aβ may drive Aβ accumulation and

*Correspondence to: Gunnar K. Gouras, Department of Experimental Medical Science, Experimental Dementia Research Unit, Lund University, 221 84 Lund, Sweden. Tel.: +46 46 222 03 09; E-mail: gunnar.gouras@med.lu.se.

ISSN 1387-2877/17/$35.00 © 2017 – IOS Press and the authors. All rights reserved
This article is published online with Open Access and distributed under the terms of the Creative Commons Attribution Non-Commercial License (CC BY-NC 4.0).

thereby AD pathogenesis [7]. Several other findings point to synapses as critical mediators of the disease. Aβ in brain accumulates and aggregates particularly in synaptic terminals with Aβ pathogenesis, which occurs even prior to plaques [8, 9]. Aβ selectively binds to synapses when added to cultured neurons [10]. Further, Aβ oligomers in synaptosomes were shown to be increased in early AD but not in brains of cognitively normal individuals who showed amyloid pathology [11].

In contrast to several other neurodegenerative diseases, such as Parkinson's disease, the anatomic and neurotransmitter specificity of synaptic damage in AD remains poorly understood. Neurochemical and neuropathological studies on postmortem brain have provided some insights into the selective vulnerability in AD with evidence for preferential loss of the neurotransmitter acetylcholine and basal forebrain cholinergic neurons [12–15]. Region-specific accumulation of intraneuronal $A\beta_{42}$ was noted particularly in AD vulnerable neurons, such as layer II neurons of entorhinal cortex (ERC), CA1 pyramidal neurons of hippocampus and basal forebrain cholinergic neurons, which appeared to increase with age, but then decreased with severity of dementia and plaque deposition [16]. More recently, intracellular $A\beta_{42}$ immunoreactivity was more carefully described in the cholinergic neuronal population in the basal forebrain and shown to be stronger compared to in the pyramidal neurons of the superior temporal and insular cortices [17]. Moreover, it is well known that tangle pathology in the hippocampal formation initiates in a set of projection neurons in layer II of ERC that then degenerate early in the disease [18, 19]. Early accumulation of $A\beta_{42}$ in Reelin-positive neurons of ERC layer II was recently reported [20]. While these glutamatergic Reelin-positive ERC layer II neurons are destined for early tangle pathology and loss in AD, initial plaques in the hippocampus develop in their terminal fields in the outer molecular layer of the dentate, providing an explanation for the apparent anatomical disconnect between amyloid and tau pathologies. Studies on the subcellular distribution of intracellular Aβ accumulation in brain have emphasized post-synaptic accumulation and aggregation of Aβ, although marked pre-synaptic localization was also reported [8]. When it comes to extracellular Aβ, it was shown that added exogenous oligomeric $A\beta_{1\text{-}42}$ appears to bind particularly to the post-synapse, where it overlapped with the post-synaptic marker PSD-95 [10], although this Aβ did not bind equally to all neurons. Further evidence for such selectivity of Aβ came from a report showing that not all neurons are equally sensitive to Aβ-induced synapse damage [21].

It also remains unclear whether amyloid-β protein precursor (AβPP) trafficking and generation of Aβ, occurs more in pre- compared to post-synaptic terminals [22, 23]. AβPP is known to be transported down both axons and dendrites and the proteases that cleave AβPP to generate Aβ have been localized to both pre- and post-synaptic sites. One recent report in primary neurons showed that one genetic risk factor for late onset AD, Bin1, promoted axonal Aβ generation in endosomes, while another genetic risk factor, CD2AP, promoted Aβ generation in dendrites [24]. Evidence also supports pre-synaptic Aβ generation in certain anatomical pathways such as the mossy fibers of the hippocampus, given accumulation of BACE1 and Aβ at these sites [25]. More than 150 familial AD-causing mutations in presenilin 1 (PS1), critical for the final cleavage to generate Aβ, have been identified and approximately 10 additional mutations have been found in the homologous gene PS2 (http://www.molgen.ua.ac.be/ADMutations). Conditional knock-out of PS1 was reported to lead to accumulation of AβPP CTFs to pre-synaptic sites of CA1 in hippocampus [26]. Interestingly, a recent report highlighted that PS1 and PS2 appear to differ in their trafficking and relative cleavage of AβPP in axons compared to dendrites [27]. Thus, current evidence supports that at anatomical, neuron-type and subcellular levels, there are differences in AβPP processing, Aβ generation and AD-related pathogenesis.

Here we set out to provide new evidence pertaining to the anatomic and synaptic selectivity of AβPP processing and Aβ accumulation. We also aim to highlight work that will be necessary to better define the subcellular site of Aβ involvement within neurons as well as the selective vulnerability of certain neurons in AD.

MATERIALS AND METHODS

Cell culture

Primary neuronal cultures were generated from B6.Cg-Tg(AβPP swe,PSEN1dE9) 85Dbo/Mmjax mice (AβPP/PS1) AD transgenic (tg) and wild-type (wt) mouse embryos. The AβPP sequence in AβPP/PS1 encodes a chimeric mouse/human AβPP (Mo/Hu AβPP 695swe) that was humanized by modifying three amino acids, and introducing the Swedish

AD mutation. The PS1 sequence encodes human presenilin 1 lacking exon 9 (dE9) that models AD-associated mutations in PS1. Both AβPPswe and PS1 are independently controlled by the prion protein promoter. Primary neuronal cultures were prepared from cortices including hippocampi of embryonic day 15 embryos as previously described [9]. In brief, E15 brain tissue was dissociated by trypsinization and trituration in DMEM with 10% fetal bovine serum (Gibco). Dissociated neurons were cultured on poly-D-lysine (Sigma) coated plates or glass coverslips (Bellco Glass Inc.) and were maintained in neurobasal medium (Gibco), B27 supplement (Gibco), glutamine (Invitrogen) and antibiotics (ThermoScientific). All animal experiments were approved by the Animal Ethical Committee of Lund University.

Mice

PS1 cKO; AβPP Tg mice were generated as described [26].

Cell immunofluorescence

Cultured neurons at 12 and 19 DIV or N2a cells were fixed in 4% paraformaldehyde (PFA) in PBS with 0.12 M sucrose for 20 min, permeabilized and blocked in PBS containing 2% normal goat serum (NGS), 1% bovine serum albumin, and 0.1% saponin at room temperature for 1 h, and then immunolabeled in 2% NGS in PBS overnight at 4°C. After appropriate washing, coverslips were mounted with SlowfadeGold (Invitrogen). For PSD-95 labeling cells were fixed 10 min in 4% PFA in PBS with 0.12 M sucrose followed by 5 min in ice-cold methanol in –20°C. Immunofluorescence was examined with epifluorescent microscope (Olympus IX70) (Fig. 1A only) or by confocal laser scanning microscopy (Leica TCS SP8). In multiple label experiments, channels were imaged sequentially to avoid bleed-through. Images were taken with Leica Confocal Software and analyzed with ImageJ or Imaris x64 8.3. Colocalization analysis was performed with Imaris with automatic thresholding based on point spread function width. For ImageJ analysis of localization of γ-secretase cleaved AβPP, thresholds were set by automatic thresholding by default on confocal images in the MAP2 or tau-1 channel. The mean intensity of the 369 channel was subsequently measured in the pixels that were above threshold in the MAP2 or tau-1 channel, respectively.

Aβ

$A\beta_{1\text{-}42}$ peptides (Tocris) or $A\beta_{1\text{-}42}$ HiLyte™ Fluor 555 labeled peptides (Aβ555) (AnaSpec) were reconstituted in DMSO to 250 μM, sonicated for 10 min and followed by 15 min of centrifugation at 12k rpm before adding the supernatant to the culture media in depicted final concentrations.

Antibodies and reagents

The following antibodies were used: 369 [28] IF 1:500; 6E10 (BioLegend, previously Covance SIG-39320) IF: 1:500; 12F4 (BioLegend, previously Covance SIG-39142) for immunofluorescence (IF) 1:250; Amyloidβ (1–42) (IBL, 18582); Amyloidβ (1–42) (Invitrogen, 700254) IF 1:1000; CAMKIIα (Millipore, 05–532) IF 1:500; DAPI (Sigma, D9542) IF 1:2000; drebrin (Abcam, ab11068) IF 1:1000; GAD67 (Millipore, MAB5406) IF 1:1000; MAP2 (Sigma, M4403) IF 1:1000; PSD-95 (Millipore, MAB1596) IF 1:200; somatostatin (Millipore, MAB354) IF 1:200; synapsin I (Sigma, S1939) IF 1:500; synaptophysin (Merck Millipore, MAB5258) IF 1:1000; tau-1 (Chemicon, MAB3420) IF 1:500; secondary antibodies conjugated to Alexa Fluor-488, –546, –647 (IF 1:500; Invitrogen). γ-secretase inhibitor N-[N-(3,5-difluorophenacetyl-l-alanyl)]-S-phenylglycine t-butyl ester (DAPT; Calbiochem) was diluted in culture medium to 250 nM.

Colocalization analysis

Colocalization analysis was performed using Imaris software. The colocalization channel displays the intensity of colocalized voxels as the square root of the product of the intensities of the original channels, hence the brightest pixels in the colocalization channel represent the pixels with the highest colocalization. Under conditions of proportional codistribution, the points of the scatter plot cluster around a straight line. However, lack of colocalization is reflected by distribution of points onto two separate groups, each showing varying levels of one probe with little or no signal from the other probe. Quantification of colocalization was done with automatic thresholding and was reported as percentage of colocalized material above threshold. Pearson's correlation coefficient (PCC) is based on an algorithm developed by Costes and Lockett at the National Institute of Health, NCI/SAIC [29]. PCC values range from 1 for two images whose fluorescence

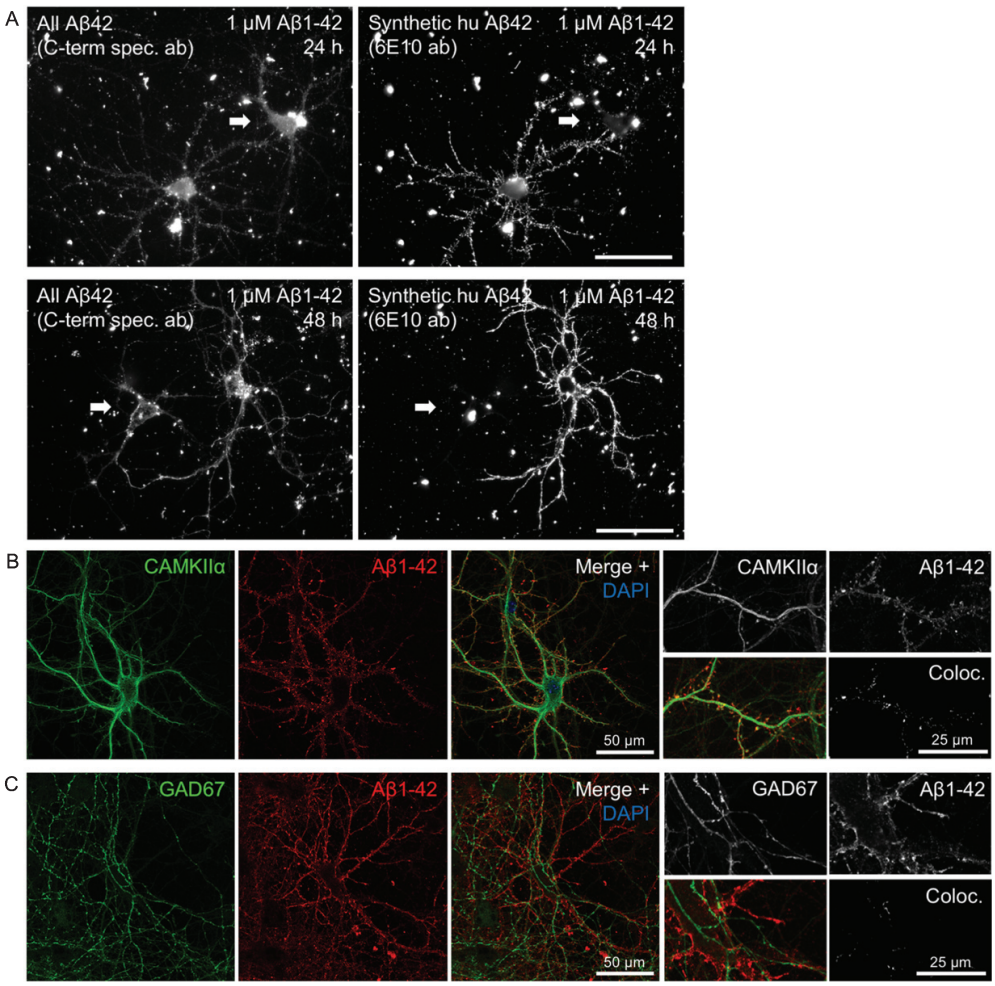


Fig. 1. Heterogeneity in $A\beta_{1\text{-}42}$ binding and internalization. A) Only certain neurons in culture accumulate synthetic $A\beta_{1\text{-}42}$ in a punctate pattern along the processes. Epifluorescent imaging of wt primary mouse neurons treated with 1 μM human $A\beta_{1\text{-}42}$ for 24 h or 48 h. Labeling with a C-terminal specific $A\beta_{x\text{-}42}$ antibody (left panels) showing both endogenous mouse $A\beta_{42}$ and the added human synthetic $A\beta_{1\text{-}42}$, displays two large neurons in each of these images. However, the exogenously added human $A\beta_{1\text{-}42}$, recognized by antibody 6E10 (right panels), accumulates predominantly only in one of the two neurons, including their processes. Note the brighter labeling with the high affinity antibody 6E10 of only one of the two neurons in the right image panels. Scale bars 50 μm. B-C) Accumulation of exogenously added $A\beta_{1\text{-}42}$ for 30 min is more pronounced in excitatory CamKII-positive compared to inhibitory GAD67-positive neurons. B) $A\beta_{1\text{-}42}$ accumulation in some but not all, and not exclusively in, neurons labeled with CamKIIα. Higher magnification images (right) with $A\beta_{1\text{-}42}$ in CamKIIα-positive synaptic terminals that appear more consistent with dendritic spines. C) $A\beta_{1\text{-}42}$ was not seen accumulating in any GAD67-positive neurons.

intensities are perfectly linearly related, to –1 for two images whose fluorescence intensities are perfectly, but inversely, related to one another. Values near zero reflect distributions that are uncorrelated with one another. Because PCC subtracts the mean intensity from the intensity of each pixel value, it is independent of signal levels and background. Thus, PCC can be measured without any form of preprocessing, making it relatively safe from user bias. Manders' Colocalization Coefficients (MCC) is the fraction of

the total probe fluorescence of one protein that colocalizes with the fluorescence of a second protein. MCC strictly measures co-occurrence independent of signal proportionality. It is necessary to first eliminate the background and this is done automatically in Imaris by the method developed by Costes [29].

Immunogold electron microscopy

Paraffin embedded brain sections (10 μm) of PS1cKO; AβPP Tg mice were deparaffinized, alcohol-dehydrated, and free-floating sections were incubated with 369 antibody (AβPP C-terminal epitope) by the immunogold-silver procedure with goat anti-rabbit IgG conjugated to 1 nm gold particles (Amersham Biosciences, Arlington, IL) in 1.01% gelatin and 0.08% bovine serum albumin in PBS. Transmission electron microscopy was performed on a Philips CM10 electron microscope. Immunogold electron microscopic analysis were performed as previously described [8].

Statistical analysis

Statistical analysis was performed with PRISM 6 software (Graph-Pad Software, San Diego, CA, USA) by using unpaired *t*-test. Data are expressed as mean ± SD. Differences were considered significant at $*p<0.05$, $**p<0.01$, $***p<0.001$, $****p<0.0001$.

RESULTS

Selective binding and internalization of exogenously added Aβ

Binding and uptake of synthetic human $A\beta_{1-42}$ ($huA\beta_{1-42}$) added to primary mouse neurons in culture is remarkably heterogeneous for different neurons. As an example, two neurons side-by-side can show completely different abilities to accumulate exogenous $huA\beta_{1-42}$ added for 24 h and 48 h to the culture medium (Fig. 1A). While the whole dendritic tree is labeled by $huA\beta_{1-42}$ in a punctate pattern in one neuron, an adjacent neuron (white arrow) is completely devoid of $huA\beta_{1-42}$ along its processes. In some cases, neurons negative for $huA\beta_{1-42}$ in their dendrites, do however show strong $huA\beta_{1-42}$-signal in their cell bodies (Fig. 1A). In general, $huA\beta_{1-42}$ accumulation in the cell body increases with time, with more neurons showing large amounts of $huA\beta_{1-42}$ in their cell bodies at 48 h compared to 24 h.

Neurons can broadly be classified as either excitatory or inhibitory. We therefore first asked whether Aβ binds preferentially to certain types of neurons, based on whether they express excitatory or inhibitory markers. We first confirmed that primary neurons incubated with fluorescently tagged $A\beta_{1-42}$ (Aβ555) for 30 min also preferentially accumulated only in select neurons consistent with the results obtained with untagged human Aβ shown in Fig. 1A. Immunofluorescent labeling of CAMKIIα, which recognizes the majority of glutamatergic neurons, shows that some but not all of the Aβ555-positive neurons co-label for CAMKIIα. However, not all CAMKIIα-positive cells have strong Aβ555-labeling. Figure 1B shows a CAMKIIα-positive cell with prominent Aβ555-labeling along its processes, with marked labeling also of terminals, which appear consistent with dendritic spines (Fig. 1B higher magnification). In contrast, no overlap was observed upon labeling Aβ555-treated cells with GAD67, a marker for GABAergic neurons, despite GAD67-positive processes often being very close or intertwined with Aβ555-positive processes (Fig. 1C).

Untreated transgenic AβPP/PS1 primary neurons in culture also display varying levels of endogenous $A\beta_{42}$ (Fig. 2), even though they all overexpress AβPPswe under the prion protein promoter. We therefore asked whether the excitatory or inhibitory type of individual neurons could affect the intracellular $A\beta_{42}$ levels. All CAMKIIα-positive cells (white filled arrows) have high levels of $A\beta_{42}$, with 27% of all $A\beta_{42}$ positive cells being CAMKIIα-positive. However so do many, but not all, CAMKIIα-negative cells as well (black arrows) (Fig. 2A, B). Many GAD67-positive neurons show similar high levels of $A\beta_{42}$ to CAMKIIα-positive neurons; in total about 26% of all $A\beta_{42}$ positive cells were GAD67-positive (Fig. 2C). There was also variability in labeling of endogenous $A\beta_{42}$ in somatostatin positive inhibitory neurons, which represent a subgroup of the GAD67-positive GABAergic neurons, with some showing low levels of $A\beta_{42}$, with 2% of all $A\beta_{42}$ positive cells being somatostatin positive and 44% of all somatostatin positive cells being positive for $A\beta_{42}$ (Fig. 2D).

The pattern of Aβ accumulation in neurons is more consistent with dendritic labeling

To determine whether added human $A\beta_{1-42}$ preferentially localizes to axons or dendrites, primary neurons were treated with 0.5 μM fluorescently-tagged $A\beta_{1-42}$ (Aβ555) for 30 min and subsequently

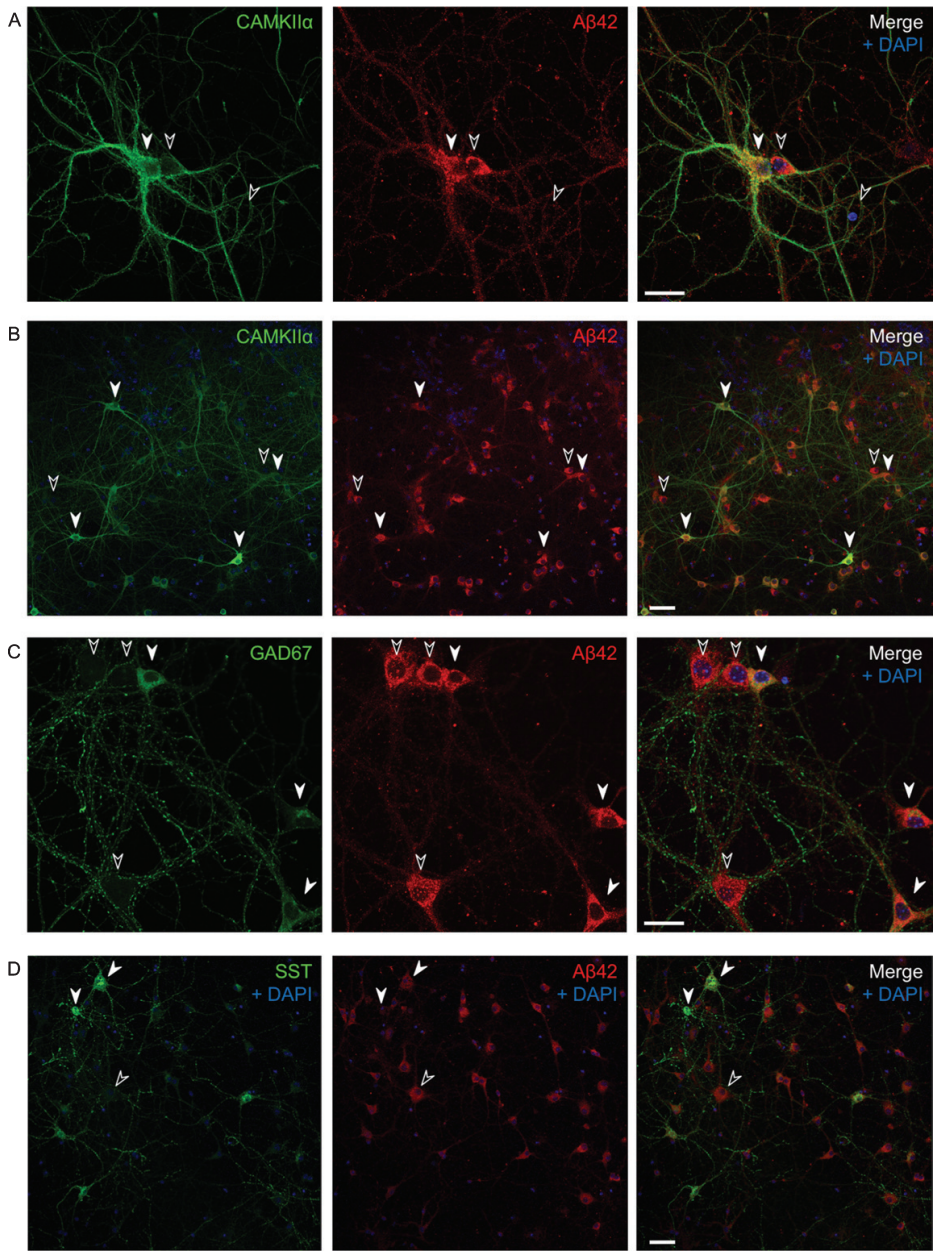


Fig. 2. Varying endogenous $A\beta_{42}$ levels in AβPP/PS1 primary neurons in culture. Immunofluorescent labeling of AβPP/PS1 primary neurons. A, B) All CAMKIIα-positive cells (white filled arrows) have high levels of $A\beta_{1\text{-}42}$; however, so do many, but not all, CAMKIIα-negative cells as well (black arrows). Also note that the two side by side neurons in (A) with varying levels of CAMKIIα (the positive to the left and the negative to the right) have comparable high levels of $A\beta_{1\text{-}42}$. C, D) Many GAD67-positive neurons show high levels of $A\beta_{42}$ (C), however, some somatostatin positive cells have lower levels of $A\beta_{42}$ (D). Scale bars 25 μm (A and C) and 50 μm (B and D).

labeled with tau-1 and MAP2 antibodies to label axons and dendrites, respectively (Fig. 3). Aβ555 did not clearly co-localize well with either tau-1 or MAP2, which could be due to these proteins not extending fully into synaptic terminals. However, the overall pattern of Aβ labeling appeared more similar to that observed with dendritic MAP2 rather than axonal tau-1 labeling. It appeared that $A\beta_{1-42}$ was present near to MAP2, or between MAP2 and tau-1 positive processes, suggesting accumulation at synaptic terminals and in particular dendritic spines.

Aβ binds and accumulates at pre- and post-synaptic sites

To test if $A\beta_{1-42}$ is accumulating at synapses and whether it has a preference to the pre- or post-synaptic side, neurons were treated with Aβ555 for 30 min and labeled with two sets of pre- and post-synaptic markers, respectively: synapsin I and PSD-95 (Fig. 4A) or synaptophysin and drebrin (Fig. 4B). Aβ555 was co-labeled with one pre- and one post-synaptic marker on the same coverslip. Two different sets of pre-and post-synaptic markers were used, since the intensity and prevalence of a specific marker could potentially influence the colocalization analysis. In the colocalization images (Fig. 4A, B, right panel) the brightest pixels in the colocalization channel represent the pixels with the highest colocalization. The scatter plots (Fig. 4C, D) show the intensity of the $A\beta_{1-42}$ channel plotted against the intensity of the respective pre- or post-synaptic channel for each pixel. Quantification of colocalization revealed that there is no significant difference in the percentage of material above threshold colocalized with Aβ555 between pre- and post-synaptic markers (Fig. 4C, D). PCC values between PSD-95 and synapsin I, and drebrin and synaptophysin, respectively, are not significantly changed (Fig. 4E, F). MCC values of $A\beta_{1-42}$ are also not significantly changed between pre- and post-synaptic markers (Fig. 4E, F). Taken together, these results with two different sets of pre- and post-synaptic markers support that Aβ555 does not have a clear-cut preference for either the pre- or post-synaptic site.

γ-secretase inhibition leads to earlier AβPP CTF accumulation at pre- than post-synaptic sites

The complex subcellular localization and anatomy in the brain of AβPP processing is further evident with the anatomically and pre- versus post-synaptic selective accumulation of AβPP CTFs with γ-secretase inhibition or absence of PS1. Accumulation of AβPP CTFs in pre-synaptic compartments in the CA1 region of hippocampus was previously reported in conditional PS1 knock-out mice over-expressing AβPP (cKO; AβPP Tg mice) [26]. However, there is an anatomy to this AβPP CTF accumulation, since in the CA3 region of hippocampus AβPP CTFs mainly accumulate in post- rather than pre-synaptic compartments in these PS1 cKO; AβPP Tg mice (Fig. 5A). This shows that AβPP CTF accumulation due to lack of PS1 activity can occur both at the pre- and post-synaptic sites. To further explore this selective accumulation of CTF, we next used immunofluorescent labeling of AβPP/PS1 cortical, including hippocampal, primary neurons treated with the γ-secretase inhibitor DAPT. Of note, 17 h of DAPT treatment revealed AβPP CTF-accumulation with the C-terminal specific AβPP antibody 369 in both pre- and post-synaptic compartments as labeled with synaptophysin and PSD-95, respectively. However, at early time points AβPP CTFs upon DAPT treatment were evident only in pre-synaptic compartments. Specifically, after 2 h with DAPT there was a marked increase of AβPP CTFs in pre-synaptic compartments of treated compared to untreated neurons (223% of untreated control, $p < 0.0001$). After 17 h of DAPT treatment, AβPP CTFs were further increased in pre-synaptic compartments (324% of untreated control, $p = 0.0001$) and were now also evident in post-synaptic compartments (202% of untreated control, $p = 0.02$) (Fig. 5B, C). Further, labeling with markers for axons and dendrites indicated that AβPP CTFs accumulate in a pattern more consistent with axons in neurons treated with DAPT for 17 h (Supplementary Figure 2). Taken together these data support the conclusion that γ-secretase cleavage of AβPP, as measured by AβPP CTF-accumulation after γ-secretase inhibition, occurs earlier and/or to a larger extent in pre-synaptic compartments compared to post-synaptic compartments in cortical primary neurons.

DISCUSSION

In the current study, we discuss and further explore the more complex anatomy in brain and subcellular localization in neurons of Aβ and AβPP. Specifically, we show that exogenous $A\beta_{1-42}$ accumulates in a punctate pattern along processes in a subset of CamKII-positive neurons but not in GAD67-positive

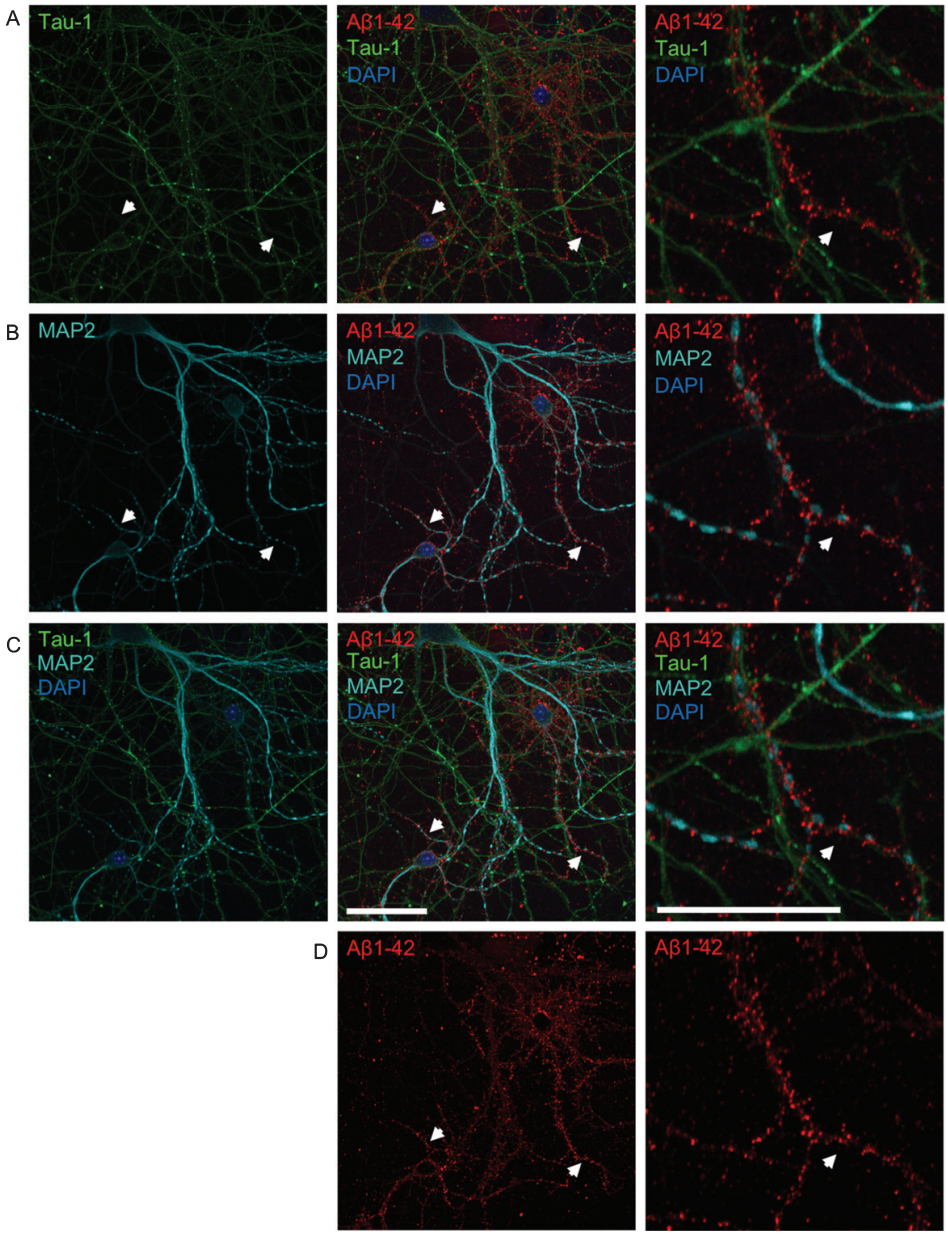


Fig. 3. The pattern of Aβ accumulation in neurons is more consistent with dendritic labeling. A-D) Double-labeling with axonal tau-1 (A) and dendritic MAP2 (B) markers of primary neurons treated with 0.5 μM of fluorescently tagged $Aβ_{1-42}$ (Aβ555) for 30 min. All images show the same field of view. Merged images of both tau-1, MAP2, $Aβ_{1-42}$, and DAPI are shown in row C. The panel to the far right show higher magnification images of the middle panel. The pattern of Aβ labeling (shown separately in row D) is more consistent with that of dendritic MAP2 than tau-1 labeling. White arrows denote MAP2-positive dendrites accumulating Aβ555, which are not positive for tau-1. High magnification images (right) show tau-1-positive axons devoid of Aβ555. Scale bars 50 μm.

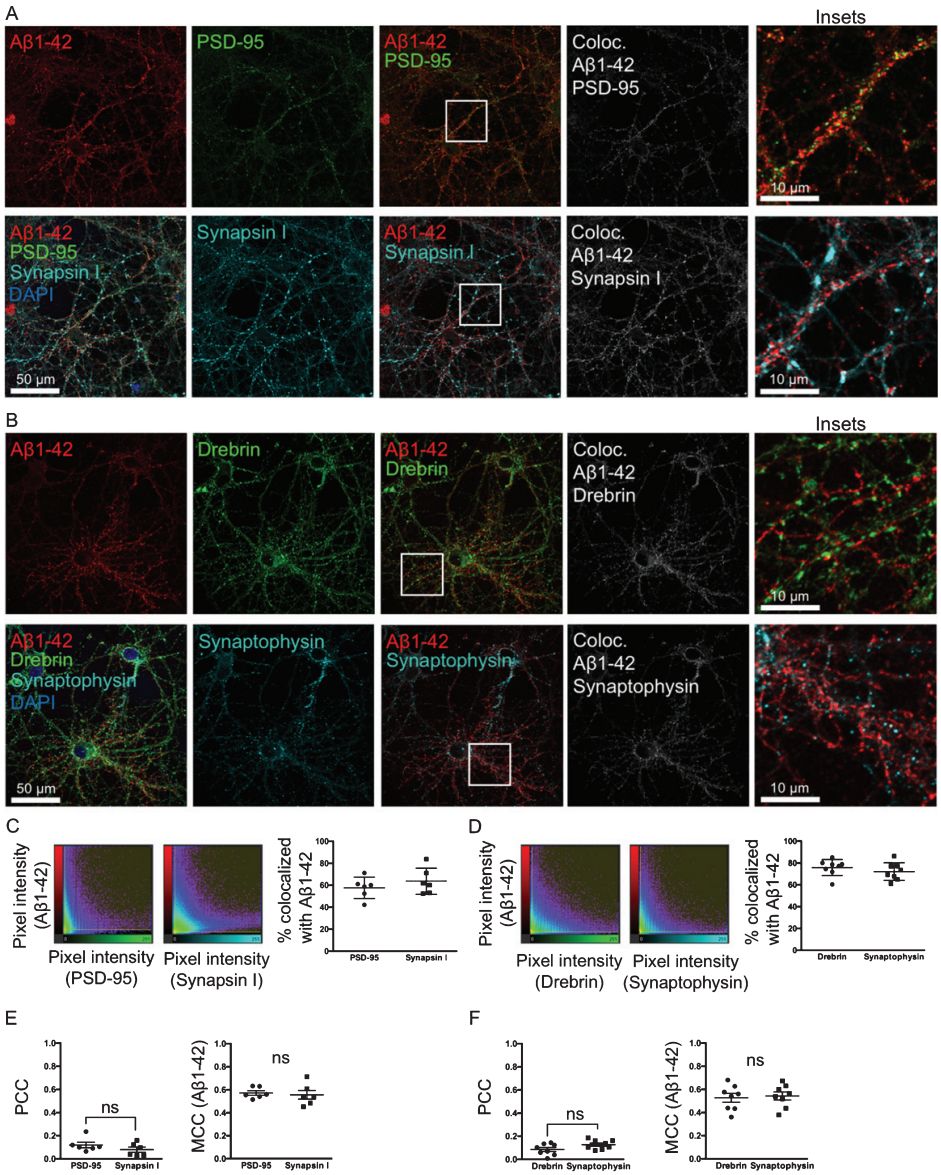


Fig. 4. Aβ binds and accumulates at both pre- and post-synaptic sites. A, B) Double-labeling with two different pre-synaptic and post-synaptic markers synapsin I and PSD-95 (A) and synaptophysin and drebrin (B), respectively, of primary neurons treated with 0.5 μM of fluorescently tagged $A\beta_{1\text{-}42}$ for 30 min. In the colocalization channel (right panel) the amount of colocalization is represented as such as the brighter the pixels, the higher the colocalization at that particular pixel. Scale bars 50 μm. C, D) The scatter plots show the intensity of the $A\beta_{1\text{-}42}$ channel plotted against the intensity of the respective pre- or post-synaptic channel for each pixel. Quantification shows no significant difference in the percentage of colocalization above threshold between Aβ555 and pre- or post-synaptic markers. E, F) Pearson's correlation coefficient (PCC) values between PSD-95 and synapsin I, and drebrin and synaptophysin, respectively, are not significantly different. Manders' Colocalization Coefficients (MCC) values for $A\beta_{1\text{-}42}$ are also not significantly different between pre- and post-synaptic markers.

neurons. We also demonstrate that exogenous $A\beta_{1-42}$ does not clearly have a selective preference to either the pre- or post-synaptic side in cultured neurons. However, the overall pattern of exogenous $A\beta_{1-42}$ accumulation in neurons is more consistent with dendritic labeling. Finally, we show with EM that γ-secretase inhibition leads to AβPP CTF accumulation at either the pre- or post-synaptic site depending on the anatomical localization in the hippocampus.

Amyloid deposition in the AD brain during the progression of the disease generally follows a similar pattern [30, 31], although variants occur such as the visual variant of AD [32]. It is possible that the specific vulnerability of certain brain areas and neurons in the AD brain are attributed to a preference of Aβ to accumulate in and/or bind to specific types of neurons. In fact, laser capture micro-dissection of individual neurons pooled from human brains showed that CA1 pyramidal neurons show much higher levels of endogenous $A\beta_{42}$ compared to cerebellar Purkinje neurons [33]. Moreover, it was also shown that less Aβ binds to cerebellar compared to cortical synaptosomes [34]. We show that added human $A\beta_{1-42}$ only accumulates in a subset of neurons in culture initially in a punctate pattern along their processes. This corroborates a previous study where Aβ diffusible oligomers (ADDLs) were shown to only bind at most half of neurons in hippocampal culture [10].

We demonstrate that accumulation of exogenously added $A\beta_{1-42}$ occurs in certain, but not all, excitatory CamKII-positive neurons. We did not find any such accumulation in processes of inhibitory GAD67-positive neurons, supporting previous studies [10, 34]. Many factors may play a role in the affinity of Aβ binding and uptake in different types of neurons. Aβ has been proposed to interact with numerous different putative receptors, including among many others the PrP_C receptor, metabotropic glutamate receptor 5 (mGluR5), a7 nicotinic acetylcholine receptor, immunoglobulin G Fcγ receptor II-b (FcγRIIb), mouse paired immunoglobulin- like receptor B (PirB), leukocyte immunoglobulin-like receptor (LilrB2) and Ephrin-like B receptor 2 (EphB2) [35–40]. In addition, AβPP has been shown to be important in the binding [41], toxicity [42, 43] and synapse altering effects of Aβ [6].

Overall, the pattern of Aβ accumulation in neurons treated with exogenous $A\beta_{1-42}$ appears to be more consistent with dendritic labeling compared to axonal. However, as dendrites are thicker than axons, the greater surface area might give the impression of more Aβ in dendrites, no matter whether it is due to "unspecific" binding and/or uptake via the plasma membrane or via a more regulated mechanism via one or several specific target molecules. Moreover, using two different sets of pre-and post-synaptic markers, we found no selective preference of exogenous $A\beta_{42}$ to either the pre- or post-synaptic side in cultured neurons. In contrast to our study, Lacor et al. [10] found that ADDLs colocalized with PSD-95. It is important to note that, colocalization analysis of Aβ with the pre- or post-synaptic site is very much dependent on the particular pre- or post-synaptic marker chosen to represent the synaptic sites. It is also likely that the concentration and conformation of Aβ will have an impact on the precise spatial targeting of added Aβ to synapses. Corroborating our results, a recent study showed endogenous non-fibrillar oligomeric Aβ within a subset of both pre- and post-synaptic sites in AβPP/PS1 mouse brains (labeled with synaptophysin and PSD-95, respectively) by transmission electron microscopy and array tomography [44]. It has been suggested that Aβ might have differential effects on the pre- and post-synaptic sides and that this effect depends on the concentration of Aβ [45]. Within a physiological range, small increases in Aβ might primarily facilitate pre-synaptic functions, resulting in synaptic potentiation [46, 47]. However, at abnormally high levels, Aβ could enhance LTD-related mechanisms, resulting in post-synaptic depression and loss of dendritic spines [48, 49].

As well as being endocytosed from the extracellular compartment, Aβ is also produced within neurons after γ-secretase cleavage of AβPP CTFs. Frykman et al. [50] reported the presence of active γ-secretase in preparations of synaptic vesicles and pre-synaptic membranes of rat brain. Sannerud et al. [27] reported that PS2 was exclusively present in the somatodendritic compartments, while PS1 localized to both axons and dendrites. Here we show by immuno-gold EM that AβPP CTF accumulation, due to lack of γ-secretase cleavage, occurs mainly in post-synaptic compartments in the CA3 region of hippocampus in PS1 cKO; AβPP Tg mice, while a previous report focusing on CA1 hippocampus described pre-synaptic accumulation [26]. This suggests an anatomical difference in the pre- versus post-synaptic γ-secretase activity in the brain. As the axons of CA3 neurons terminate in the CA1 region, a possible explanation for our results could be that CA3 neurons have particularly high γ-secretase cleavage of AβPP. This would in PS1 cKO; AβPP Tg mice leads to accumulation of AβPP CTFs both in the axon

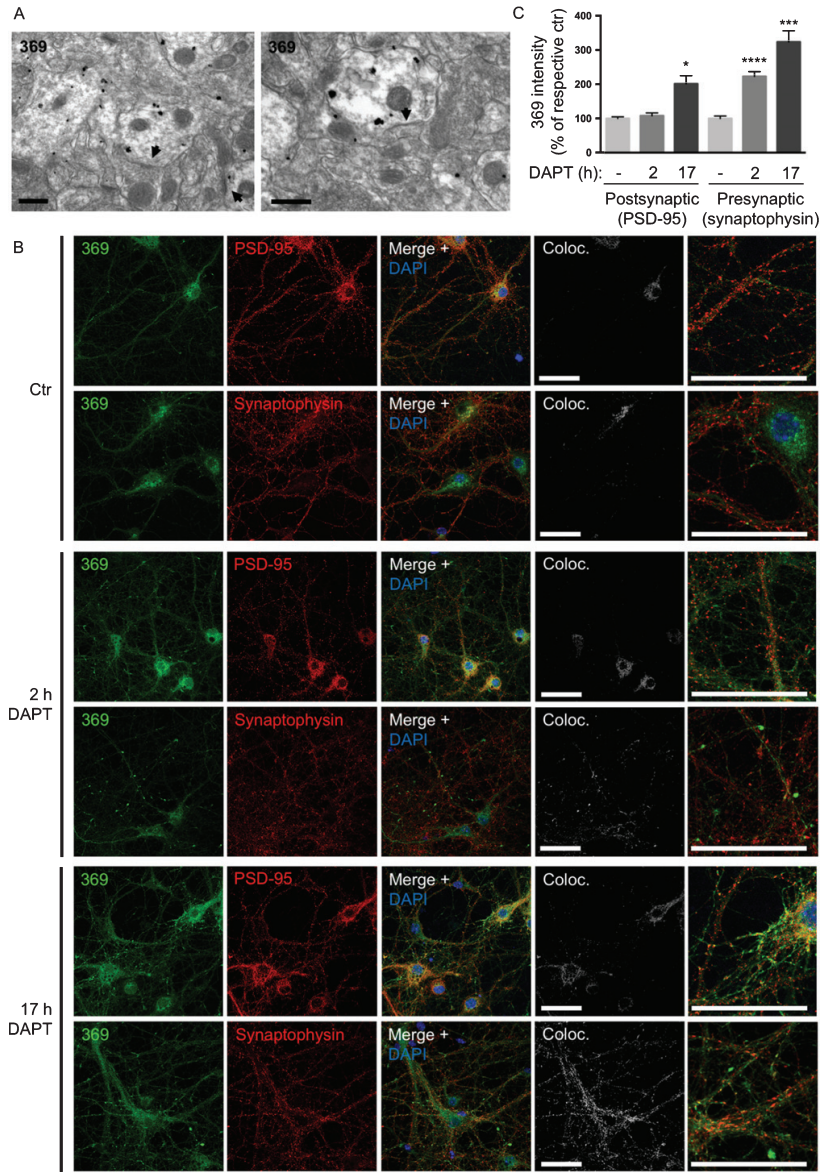


Fig. 5. γ-secretase inhibition leads to earlier AβPP CTF accumulation at pre- than post-synaptic sites. A) In the CA3 region of hippocampus AβPP CTFs are mainly accumulating in post-synaptic compartments in PS1 cKO; AβPP Tg mice. Arrowheads denote post-synaptic densities. Scale bars 500 nm. B) Immunofluorescent labeling of AβPP/PS1 primary cortical neurons treated with the γ-secretase inhibitor DAPT. AβPP CTF-accumulation is seen by C-terminal specific AβPP antibody 369 in both axons and dendrites after 17 h. However, with only 2 h of DAPT treatment, AβPP CTF-accumulation is evident only in pre-synaptic compartments. Scale bars 50 μm. C) Quantification of the intensity of antibody 369 labeling in post-synaptic compared to pre-synaptic compartments with DAPT-treatment indicates a relatively greater increase in pre-synapses, which is also evident earlier (at 2 h). Thresholds were set by automatic thresholding by default on confocal images in the MAP2 or tau-1 channel. The mean intensity of the antibody 369 channel was subsequently measured in the pixels that were above threshold in the MAP2 or tau-1 channel respectively. Values are presented as percentage of respective untreated control.

terminals of the CA3 neurons that terminate in pre-synaptic compartments in CA1 and in the dendrites of CA3 neurons in post-synaptic compartments of CA3. We also show by short term (2 h) treatment of chemical γ-secretase inhibitor that AβPP CTFs first and/or to a larger extent accumulate in pre-synaptic compartments in cortical neurons. However, after longer time points of DAPT treatment (17 h), AβPP CTFs are also evident in post-synaptic compartments. This suggests that either (1) only a small fraction of neurons accumulates AβPP CTFs in their post-synaptic compartments which is initially drowned out by most neurons not showing this, (2) a longer treatment duration being necessary to impact post-synaptic AβPP CTFs, and/or that AβPP CTFs first accumulate in pre-synaptic compartments that then only with time are transported to post-synaptic compartments. Another possible explanation of the preferential buildup of AβPP CTFs in the pre-synaptic compartment with γ-secretase inhibition could be faster degradation of AβPP CTFs in the post-synaptic compartment compared to the pre-synaptic compartment. AβPP CTFs have been shown to be degraded by the lysosome and since lysosomes are only found in the cell body of the neuron and not in the axon or dendrite, it appears less likely that the AβPP CTFs are degraded in either the axon or the dendrites. An additional possibility is that retrograde transport of AβPP CTF-containing multivesicular bodies to the cell body for degradation might be slower in axons compared to dendrites. However, vesicular trafficking of AβPP bearing a C-terminal tag typically appears more rapid in axons than dendrites [6].

AD is a complex disease of aging that is only gradually becoming better understood. The precise role of the Aβ peptide, which has been linked by pathological, genetic and biological lines of evidence to the disease, remains to be understood. Increasing evidence supports that like in other neurodegenerative diseases where synapses are sites of attack, the misfolding proteins linked to AD, Aβ and tau, also target synapses in this disease [8, 51]. How fundamental processes of aging make synapses vulnerable sites requires further work, although the wear and tear of synaptic activity and resulting oxidative, inflammatory, vascular and other stressors likely drive the vulnerabilities of synapses in age-related proteinopathies [52, 53].

Here we underscore the challenges in clearly differentiating Aβ binding to pre- compared to post-synaptic compartments and highlight anatomical differences in accumulation of AβPP metabolites. Synapse loss is considered the best pathological correlate of cognitive deficits in human AD [2]. Aβ accumulates at synapses and is associated with synaptic pathology [9] and leads to loss of synaptic markers such as PSD-95, GluR1 and synaptophysin [54]. Hence a better understanding of the subcellular site of Aβ involvement within neurons in AD will be important to understand the selective vulnerability and anatomical specificity of AD.

ACKNOWLEDGMENTS

We acknowledge Carlos Saura and Jie Shen for their generation of the PS1cKO. This study was supported by MultiPark, the Swedish Research Council and NIH grant R01-AG027140.

Authors' disclosures available online (http://j-alz.com/manuscript-disclosures/17-0262r1).

SUPPLEMENTARY MATERIAL

The supplementary material is available in the electronic version of this article: http://dx.doi.org/10.3233/JAD-170262.

REFERENCES

[1] DeKosky ST, Scheff SW (1990) Synapse loss in frontal cortex biopsies in Alzheimer's disease: Correlation with cognitive severity. *Ann Neurol* **27**, 457-464.

[2] Terry RD, Masliah E, Salmon DP, Butters N, DeTeresa R, Hill R, Hansen LA, Katzman R (1991) Physical basis of cognitive alterations in Alzheimer's disease: Synapse loss is the major correlate of cognitive impairment. *Ann Neurol* **30**, 572-580.

[3] Rajmohan R, Reddy PH (2016) Amyloid-beta and phosphorylated tau accumulations cause abnormalities at synapses of Alzheimer's disease neurons. *J Alzheimers Dis* **57**, 975-999.

[4] Li F, Calingasan NY, Yu F, Mauck WM, Toidze M, Almeida CG, Takahashi RH, Carlson GA, Flint Beal M, Lin MT, Gouras GK (2004) Increased plaque burden in brains of APP mutant MnSOD heterozygous knockout mice. *J Neurochem* **89**, 1308-1312.

[5] Kamenetz F, Tomita T, Hsieh H, Seabrook G, Borchelt D, Iwatsubo T, Sisodia S, Malinow R (2003) APP processing and synaptic function. *Neuron* **37**, 925-937.

[6] Tampellini D, Rahman N, Gallo EF, Huang Z, Dumont M, Capetillo-Zarate E, Ma T, Zheng R, Lu B, Nanus DM, Lin MT, Gouras GK (2009) Synaptic activity reduces intraneuronal Abeta, promotes APP transport to synapses, and protects against Abeta-related synaptic alterations. *J Neurosci* **29**, 9704-9713.

[7] Buckner RL, Snyder AZ, Shannon BJ, LaRossa G, Sachs R, Fotenos AF, Sheline YI, Klunk WE, Mathis CA, Morris JC, Mintun MA (2005) Molecular, structural, and functional characterization of Alzheimer's disease: Evidence for a rela-

tionship between default activity, amyloid, and memory. *J Neurosci* **25**, 7709-7717.

[8] Takahashi RH, Milner TA, Li F, Nam EE, Edgar MA, Yamaguchi H, Beal MF, Xu H, Greengard P, Gouras GK (2002) Intraneuronal Alzheimer abeta42 accumulates in multivesicular bodies and is associated with synaptic pathology. *Am J Pathol* **161**, 1869-1879.

[9] Takahashi RH, Almeida C, Kearney PF, Yu F, Lin MT, Milner TA, Gouras GK (2004) Oligomerization of Alzheimer's beta-amyloid within processes and synapses of cultured neurons and brain. *J Neurosci* **24**, 3592-3599.

[10] Lacor PN, Buniel MC, Chang L, Fernandez SJ, Gong Y, Viola KL, Lambert MP, Velasco PT, Bigio EH, Finch CE, Krafft GA, Klein WL (2004) Synaptic targeting by Alzheimer's-related amyloid beta oligomers. *J Neurosci* **24**, 10191-10200.

[11] Bilousova T, Miller CA, Poon WW, Vinters HV, Corrada M, Kawas C, Hayden EY, Teplow DB, Glabe C, Albay R, 3rd, Cole GM, Teng E, Gylys KH (2016) Synaptic amyloid-β oligomers precede p-Tau and differentiate high pathology control cases. *Am J Pathol* **186**, 185-198.

[12] Davies P, Maloney AJ (1976) Selective loss of central cholinergic neurons in Alzheimer's disease. *Lancet* **2**, 1403.

[13] DeKosky ST, Ikonomovic MD, Styren SD, Beckett L, Wisniewski S, Bennett DA, Cochran EJ, Kordower JH, Mufson EJ (2002) Upregulation of choline acetyltransferase activity in hippocampus and frontal cortex of elderly subjects with mild cognitive impairment. *Ann Neurol* **2**, 145-155.

[14] Perry EK, Blessed G, Tomlinson BE, Perry RH, Crow TJ, Cross AJ, Dockray GJ, Dimaline R, Arregui A (1981) Neurochemical activities in human temporal lobe related to aging and Alzheimer-type changes. *Neurobiol Aging* **2**, 251-256.

[15] Mesulam M (2004) The cholinergic lesion of Alzheimer's disease: Pivotal factor or side show? *Learn Mem* **11**, 43-49.

[16] Gouras GK, Tsai J, Naslund J, Vincent B, Edgar M, Checler F, Greenfield JP, Haroutunian V, Buxbaum JD, Xu H, Greengard P, Relkin NR (2000) Intraneuronal Abeta42 accumulation in human brain. *Am J Pathol* **156**, 15-20.

[17] Baker-Nigh A, Vahedi S, Davis EG, Weintraub S, Bigio EH, Klein WL, Geula C (2015) Neuronal amyloid-β accumulation within cholinergic basal forebrain in ageing and Alzheimer's disease. *Brain* **138**, 1722-1737.

[18] Braak H, Braak E (1995) Staging of Alzheimer's disease-related neurofibrillary changes. *Neurobiol Aging* **16**, 271-278; discussion 278-284.

[19] Gómez-Isla T, Price JL, McKeel DW Jr, Morris JC, Growdon JH, Hyman BT (1996) Profound loss of layer II entorhinal cortex neurons occurs in very mild Alzheimer's disease. *J Neurosci* **16**, 4491-4500.

[20] Kobro-Flatmoen A, Nagelhus A, Witter MP (2016) Reelin-immunoreactive neurons in entorhinal cortex layer II selectively express intracellular amyloid in early Alzheimer's disease. *Neurobiol Dis* **93**, 172-183.

[21] Snyder EM, Nong Y, Almeida CG, Paul S, Moran T, Choi EY, Nairn AC, Salter MW, Lombroso PJ, Gouras GK, Greengard P (2005) Regulation of NMDA receptor trafficking by amyloid-beta. *Nat Neurosci* **8**, 1051-1058.

[22] DeBoer SR, Dolios G, Wang R, Sisodia SS (2014) Differential release of β-amyloid from dendrite- versus axon-targeted APP. *J Neurosci* **34**, 12313-12327.

[23] Gouras GK (2013) Convergence of synapses, endosomes, and prions in the biology of neurodegenerative diseases. *Int J Cell Biol* **2013**, 141083.

[24] Ubelmann F, Burrinha T, Salavessa L, Gomes R, Ferreira C, Moreno N, Guimas Almeida C (2017) Bin1 and CD2AP polarise the endocytic generation of beta-amyloid. *EMBO Rep* **18**, 102-122.

[25] Sadleir KR, Kandalepas PC, Buggia-Prévot V, Nicholson DA, Thinakaran G, Vassar R (2016) Presynaptic dystrophic neurites surrounding amyloid plaques are sites of microtubule disruption, BACE1 elevation, and increased Aβ generation in Alzheimer's disease. *Acta Neuropathol* **32**, 235-256.

[26] Saura CA, Chen G, Malkani S, Choi SY, Takahashi RH, Zhang D, Gouras GK, Kirkwood A, Morris RG, Shen J (2005) Conditional inactivation of presenilin 1 prevents amyloid accumulation and temporarily rescues contextual and spatial working memory impairments in amyloid precursor protein transgenic mice. *J Neurosci* **25**, 6755-6764.

[27] Sannerud R, Esselens C, Ejsmont P, Mattera R, Rochin L, Tharkeshwar AK, De Baets G, De Wever V, Habets R, Baert V, Vermeire W, Michiels C, Groot AJ, Wouters R, Dillen K, Vints K, Baatsen P, Munck S, Derua R, Waelkens E, Basi GS, Mercken M, Vooijs M, Bollen M, Schymkowitz J, Rousseau F, Bonifacino JS, Van Niel G, De Strooper B, Annaert W (2016) Restricted location of PSEN2/γ-secretase determines substrate specificity and generates an intracellular Aβ pool. *Cell* **166**, 193-208.

[28] Buxbaum JD, Gandy SE, Cicchetti P, Ehrlich ME, Czernik AJ, Fracasso RP, Ramabhadran TV, Unterbeck AJ, Greengard P (1990) Processing of Alzheimer beta/A4 amyloid precursor protein: Modulation by agents that regulate protein phosphorylation. *Proc Natl Acad Sci U S A* **87**, 6003-6006.

[29] Costes SV, Daelemans D, Cho EH, Dobbin Z, Pavlakis G, Lockett S (2004) Automatic and quantitative measurement of protein-protein colocalization in live cells. *Biophys J* **86**, 3993-4003.

[30] Braak H, Braak E (1991) Neuropathological stageing of Alzheimer-related changes. *Acta Neuropathol* **82**, 239-259.

[31] Thal DR, Rüb U, Orantes M, Braak H (2002) Phases of A beta-deposition in the human brain and its relevance for the development of AD. *Neurology* **58**, 1791-1800.

[32] Levine DN, Lee JM, Fisher CM (1993) The visual variant of Alzheimer's disease: A clinicopathologic case study. *Neurology* **43**, 305-313.

[33] Hashimoto M, Bogdanovic N, Volkmann I, Aoki M, Winblad B, Tjernberg LO (2010) Analysis of microdissected human neurons by a sensitive ELISA reveals a correlation between elevated intracellular concentrations of Abeta42 and Alzheimer's disease neuropathology. *Acta Neuropathol* **119**, 543-554.

[34] Lacor PN, Buniel MC, Furlow PW, Clemente AS, Velasco PT, Wood M, Viola KL, Klein WL (2007) Abeta oligomer-induced aberrations in synapse composition, shape, and density provide a molecular basis for loss of connectivity in Alzheimer's disease. *J Neurosci* **27**, 796-807.

[35] Wang HY, Lee DH, D'Andrea MR, Peterson PA, Shank RP, Reitz AB (2000) beta-Amyloid(1-42) binds to alpha7 nicotinic acetylcholine receptor with high affinity. Implications for Alzheimer's disease pathology. *J Biol Chem* **275**, 5626-5632.

[36] Laurén J, Gimbel DA, Nygaard HB, Gilbert JW, Strittmatter SM (2009) Cellular prion protein mediates impairment of synaptic plasticity by amyloid-beta oligomers. *Nature* **457**, 1128-1132.

[37] Cissé M, Halabisky B, Harris J, Devidze N, Dubal DB, Sun B, Orr A, Lotz G, Kim DH, Hamto P, Ho K, Yu GQ, Mucke L (2011) Reversing EphB2 depletion rescues cognitive functions in Alzheimer model. *Nature* **469**, 47-52.

[38] Kam TI, Song S, Gwon Y, Park H, Yan JJ, Im I, Choi JW, Choi TY, Kim J, Song DK, Takai T, Kim YC, Kim KS, Choi SY, Choi S, Klein WL, Yuan J, Jung YK (2013) FcγRIIb mediates amyloid-β neurotoxicity and memory impairment in Alzheimer's disease. *J Clin Invest* **123**, 2791-2802.

[39] Kim T, Vidal GS, Djurisic M, William CM, Birnbaum ME, Garcia KC, Hyman BT, Shatz CJ (2013) Human LilrB2 is a β-amyloid receptor and its murine homolog PirB regulates synaptic plasticity in an Alzheimer's model. *Science* **341**, 1399-1404.

[40] Renner M, Lacor PN, Velasco PT, Xu J, Contractor A, Klein WL, Triller A (2010) Deleterious effects of amyloid β oligomers acting as an extracellular scaffold for mGluR5. *Neuron* **66**, 739-754.

[41] Fogel H, Frere S, Segev O, Bharill S, Shapira I, Gazit N, O'Malley T, Slomowitz E, Berdichevsky Y, Walsh DM, Isacoff EY, Hirsch JA, Slutsky I (2014) APP homodimers transduce an amyloid-β-mediated increase in release probability at excitatory synapses. *Cell Rep* **7**, 1560-1576.

[42] Lorenzo A, Yuan M, Zhang Z, Paganetti PA, Sturchler-Pierrat C, Staufenbiel M, Mautino J, Vigo FS, Sommer B, Yankner BA (2000) Amyloid beta interacts with the amyloid precursor protein: A potential toxic mechanism in Alzheimer's disease. *Nat Neurosci* **3**, 460-464.

[43] Shaked GM, Kummer MP, Lu DC, Galvan V, Bredesen DE, Koo EH (2006) Abeta induces cell death by direct interaction with its cognate extracellular domain on APP (APP 597-624). *FASEB J* **20**, 1254-1256.

[44] Pickett EK, Koffie RM, Wegmann S, Henstridge CM, Herrmann AG, Colom-Cadena M, Lleo A, Kay KR, Vaught M, Soberman R, Walsh DM, Hyman BT, Spires-Jones TL (2016) Non-fibrillar oligomeric amyloid-β within synapses. *J Alzheimers Dis* **53**, 787-800.

[45] Palop JJ, Mucke L (2010) Amyloid-beta-induced neuronal dysfunction in Alzheimer's disease: From synapses toward neural networks. *Nat Neurosci* **13**, 812-818.

[46] Abramov E, Dolev I, Fogel H, Ciccotosto GD, Ruff E, Slutsky I (2009) Amyloid-beta as a positive endogenous regulator of release probability at hippocampal synapses. *Nat Neurosci* **12**, 1567-1576.

[47] Puzzo D, Privitera L, Leznik E, Fà M, Staniszewski A, Palmeri A, Arancio O (2008) Picomolar amyloid-beta positively modulates synaptic plasticity and memory in hippocampus. *J Neurosci* **28**, 14537-14545.

[48] Walsh DM, Klyubin I, Fadeeva JV, Cullen WK, Anwyl R, Wolfe MS, Rowan MJ, Selkoe DJ (2002) Naturally secreted oligomers of amyloid beta protein potently inhibit hippocampal long-term potentiation in vivo. *Nature* **416**, 535-539.

[49] Wang HW, Pasternak JF, Kuo H, Ristic H, Lambert MP, Chromy B, Viola KL, Klein WL, Stine WB, Krafft GA, Trommer BL (2002) Soluble oligomers of β amyloid (1-42) inhibit long-term potentiation but not long-term depression in rat dentate gyrus. *Brain Res* **924**, 133-140.

[50] Frykman S, Hur JY, Frånberg J, Aoki M, Winblad B, Nahalkova J, Behbahani H, Tjernberg LO (2010) Synaptic and endosomal localization of active gamma-secretase in rat brain. *PLoS One* **5**, e8948.

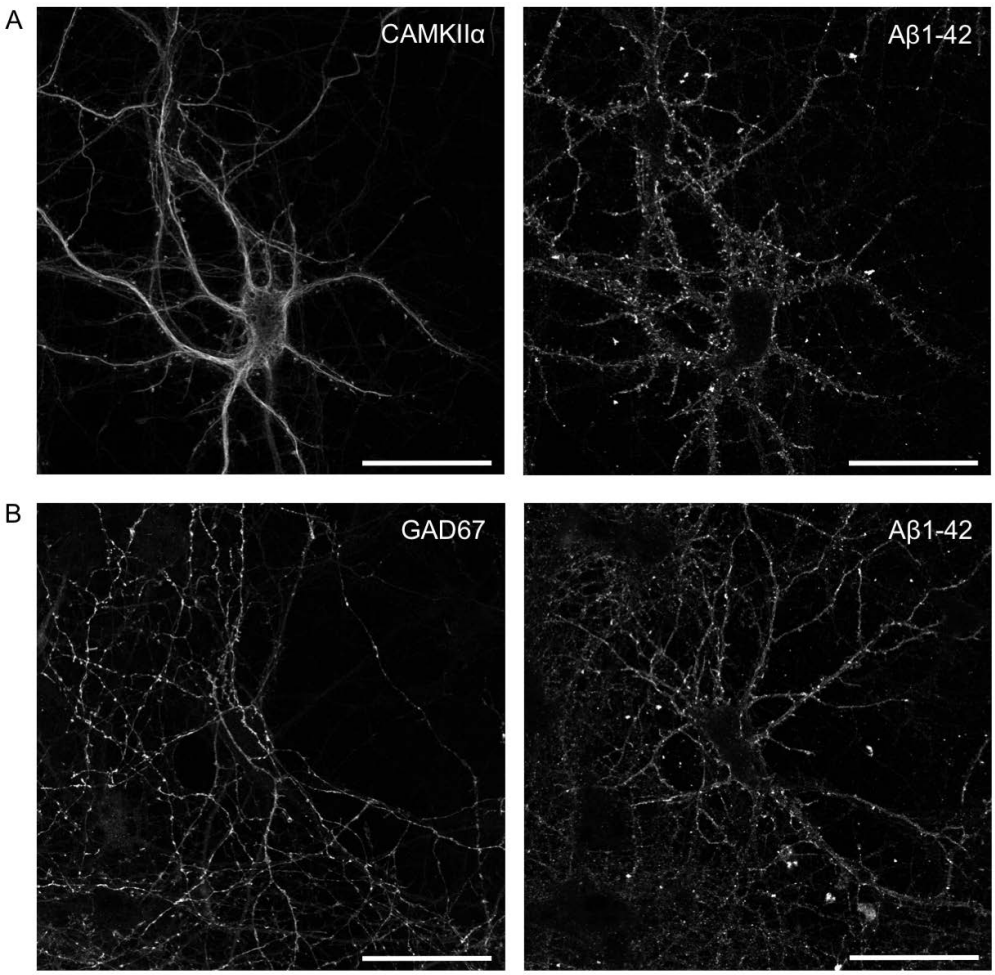
[51] Takahashi RH, Capetillo-Zarate E, Lin MT, Milner TA, Gouras GK (2010) Co-occurrence of Alzheimer's disease ß-amyloid and τ pathologies at synapses. *Neurobiol Aging* **31**, 1145-1152.

[52] Lin MT, Beal MF (2006) Mitochondrial dysfunction and oxidative stress in neurodegenerative diseases. *Nature* **443**, 787-795.

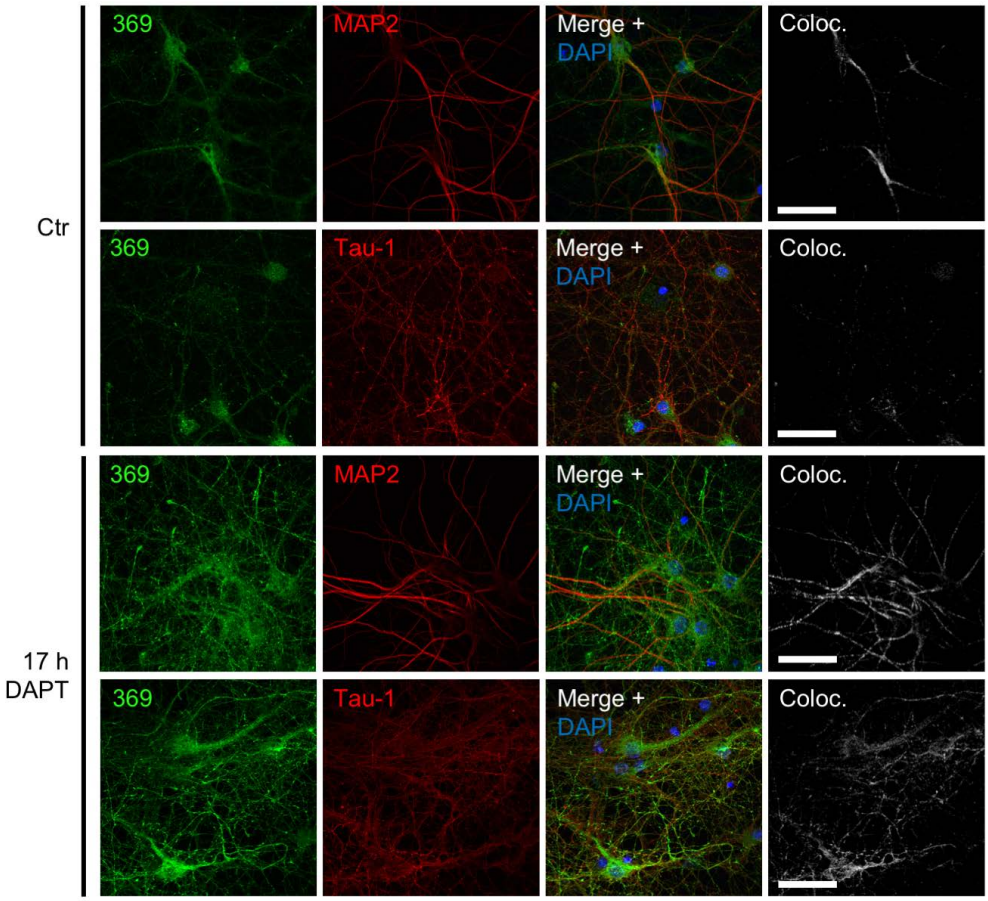
[53] Clark TA, Lee HP, Rolston RK, Zhu X, Marlatt MW, Castellani RJ, Nunomura A, Casadesus G, Smith MA, Lee HG, Perry G (2010) Oxidative stress and its implications for future treatments and management of Alzheimer disease. *Int J Biomed Sci* **6**, 225-227.

[54] Almeida CG, Tampellini D, Takahashi RH, Greengard P, Lin MT, Snyder EM, Gouras GK (2005) Beta-amyloid accumulation in APP mutant neurons reduces PSD-95 and GluR1 in synapses. *Neurobiol Dis* **20**, 187-198.

Supplementary Figure 1



Supplementary Figure 2



Paper II

© 2015. Published by The Company of Biologists Ltd | Journal of Cell Science (2015) 128, 2520-2528 doi:10.1242/jcs.170233

RESEARCH ARTICLE

ESCRTs regulate amyloid precursor protein sorting in multivesicular bodies and intracellular amyloid-β accumulation

James R. Edgar[1,2], Katarina Willén[3], Gunnar K. Gouras[3] and Clare E. Futter[1,*]

ABSTRACT

Intracellular amyloid-β (Aβ) accumulation is a key feature of early Alzheimer's disease and precedes the appearance of Aβ in extracellular plaques. Aβ is generated through proteolytic processing of amyloid precursor protein (APP), but the intracellular site of Aβ production is unclear. APP has been localized to multivesicular bodies (MVBs) where sorting of APP onto intraluminal vesicles (ILVs) could promote amyloidogenic processing, or reduce Aβ production or accumulation by sorting APP and processing products to lysosomes for degradation. Here, we show that APP localizes to the ILVs of a subset of MVBs that also traffic EGF receptor (EGFR), and that it is delivered to lysosomes for degradation. Depletion of the endosomal sorting complexes required for transport (ESCRT) components, Hrs (also known as Hgs) or Tsg101, inhibited targeting of APP to ILVs and the subsequent delivery to lysosomes, and led to increased intracellular Aβ accumulation. This was accompanied by dramatically decreased Aβ secretion. Thus, the early ESCRT machinery has a dual role in limiting intracellular Aβ accumulation through targeting of APP and processing products to the lysosome for degradation, and promoting Aβ secretion.

KEY WORDS: Amyloid precursor protein, Multivesicular body, Alzheimer's disease, ESCRT

INTRODUCTION

Alzheimer's disease is characterized by progressive loss of memory and cognitive function, and histologically characterized by neuronal loss, extracellular amyloid plaques, dystrophic neurites and neurofibrillary tangles of hyperphosphorylated Tau (Glenner, 1989; Goedert et al., 1988; Selkoe et al., 1986). Plaques are extracellular aggregates of Aβ peptides (Glenner and Wong, 1984) generated by sequential proteolysis of APP by β-site APP cleaving enzyme 1 (BACE1) and the γ-secretase complex. APP can alternatively be processed by α-secretase, which cleaves within the Aβ sequence, precluding Aβ formation.

Both the trans-Golgi network (TGN) and the endolysosomal pathway contain APP, BACE1 and γ-secretase, and are proposed sites of Aβ generation. Newly synthesized APP can traffic from the TGN to endosomes either directly through binding to the adaptor AP-4 (Burgos et al., 2010) or via the plasma membrane, and can also undergo retromer-dependent recycling to the TGN (Vieira et al., 2010). APP and its processing products have been localized to multivesicular bodies (MVBs) in Alzheimer's disease brains (Takahashi et al., 2004, 2002) and cultured neurons (Morel et al., 2013). MVBs have a number of fates including fusion with the lysosome, fusion with the cell surface for the release of intraluminal vesicles (ILVs) as exosomes, fusion with autophagosomes to generate amphisomes and the biogenesis of lysosome-related organelles such as melanosomes. In pigmented cells PMEL is targeted to ILVs where it undergoes proteolytic processing to generate amyloid striations upon which melanin is deposited (Berson et al., 2001).

Several populations of MVBs exist (White et al., 2006) and ILVs can be formed by different mechanisms (Edgar et al., 2014; Stuffers et al., 2009; Subra et al., 2007; Trajkovic et al., 2008; Wollert and Hurley, 2010). The endosomal sorting complexes required for transport (ESCRT) machinery, which is composed of four complexes (0–III), binds ubiquitylated cargo and generates ILVs that are delivered to lysosomes and degraded. APP can be ubiquitylated (Watanabe et al., 2012) in a manner that promotes its targeting to ILVs (Morel et al., 2013). Interfering with the potential interaction between early ESCRT components and APP has been reported to both increase (Morel et al., 2013) and decrease (Choy et al., 2012) Aβ secretion. Depleting later ESCRT components promotes APP traffic to the TGN and increased Aβ secretion (Choy et al., 2012). Intriguingly PMEL sorting onto ILVs is essential for its amyloidogenic processing but occurs independently of ESCRTs (Theos et al., 2006). The extent to which ESCRT-dependent targeting of APP to ILVs might play a similar positive role in Aβ production, or might reduce Aβ production by targeting APP to the lysosome and/or removing APP from the recycling pathway to the TGN, remains unclear.

Studies of the role of the ESCRT machinery in regulating APP traffic and Aβ production have been performed in a variety of cultured cell lines and primary neurons, in which intracellular Aβ is difficult to detect. Most studies have therefore analysed ESCRT roles in Aβ secretion, rather than intracellular accumulation. The importance of intracellular versus extracellular Aβ is a subject of considerable debate. Transgenic mice display intraneuronal Aβ at the same age as initial pathological manifestations and synaptic dysfunction, which is prior to the appearance of extracellular plaques (Oddo et al., 2003). In this study, we investigate the role of ESCRT-mediated sorting within MVBs in intracellular Aβ accumulation. We reveal a role for early ESCRT components in limiting intracellular Aβ accumulation by both promoting lysosomal targeting and promoting Aβ secretion.

RESULTS

APP is localized to the Golgi and ILVs of a subpopulation of MVBs in H4-APP cells

Immunofluorescent staining of H4 neuroglioma cells stably expressing human APP (H4-APP) with the antibody 6E10, which labels both APP and Aβ (hereafter anti-APP/Aβ antibody), revealed

[1]Department of Cell Biology, UCL Institute of Ophthalmology, London EC1 V9EL, UK. [2]Cambridge Institute for Medical Research, University of Cambridge, Cambridge CB2 0XY, UK. [3]Department of Experimental Medical Science, Lund University, Lund 22184, Sweden.

*Author for correspondence (c.futter@ucl.ac.uk)

This is an Open Access article distributed under the terms of the Creative Commons Attribution License (http://creativecommons.org/licenses/by/3.0), which permits unrestricted use, distribution and reproduction in any medium provided that the original work is properly attributed.

Received 18 February 2015; Accepted 21 May 2015

Journal of Cell Science

Journal of Cell Science (2015) 128, 2520-2528 doi:10.1242/jcs.170233

that there was a perinuclear pool that colocalized with the Golgi marker TGN46 (also known as TGOLN2), plus punctate staining, typical of endosomes and lysosomes (Fig. 1A). As no marker accurately distinguishes between MVBs and lysosomes, electron microscopy was used to determine the identity of the punctate staining. We previously showed that electron lucence, a diameter >200 nm, and one or more discrete ILVs in a single section plane defines MVBs that are functionally distinct from lysosomes, as they lack the capacity to degrade endocytosed EGF (Futter et al., 1996; Wherlock et al., 2004). Lysosomes are electron dense, can contain ILVs but also contain membrane whorls and can degrade endocytosed EGF (Futter et al., 1996; Wherlock et al., 2004). Immunoelectron microscopy showed that the majority of 6E10 staining was confined to the Golgi and MVBs, where most was on ILVs but some was on the limiting membrane (Fig. 1B). Analysis of the 6E10 gold distribution on MVBs revealed the labelling not to be randomly distributed but, rather, that it was confined to a subset (39%) of MVBs and that a second population of 6E10-negative MVBs existed (Fig. 1C). 6E10 staining was found on MVBs both sparsely and densely packed with ILVs, and so did not correlate with MVB maturation state. Lysosomes were not stained. 6E10 binds the first 16 residues of Aβ and thus detects full-length APP (fl-APP), the β C-terminal fragment (β-CTF) and Aβ. Similar results were obtained using another pan-Aβ antibody, 4G8 (data not shown). Several Aβ-specific antibodies tested on cell lines overexpressing APP showed no specific staining.

Western blotting H4-APP lysates using the 6E10 antibody showed the predominant species to be fl-APP with much less intense bands corresponding to the size of CTFs and little or no Aβ (Fig. 1D). These data suggest that, like many non-neuronal and neuronal cell lines, H4-APP cells produce very little Aβ and that the majority of the 6E10 signal detected by immunofluorescence and immunoelectron microscopy is likely to represent fl-APP. Consistent with this, treatment of H4-APP cells with the γ-secretase inhibitor DAPT, to prevent Aβ generation, caused no detectable change in 6E10 staining as assessed by immunoelectron microscopy (supplementary material Fig. S1A,B), and an antibody against the N-terminus of APP, which does not stain β-CTF or Aβ, showed the same dual localization to the Golgi and the ILVs of MVBs as 6E10 (supplementary material Fig. S1C,D).

To determine whether Aβ could be detected in a subset of MVBs in neurons, hippocampus from age-matched wild-type and Tg2576 mice, which overexpress Swedish mutant APP (sweAPP) and present detectable levels of intraneuronal deposits of Aβ (Takahashi et al., 2002), were stained with anti-Aβ antibodies and assessed by immunoelectron microscopy. 6E10 and Aβ40-specific antibodies localized to the ILVs of a subset of MVBs in the Tg2576 mice (Fig. 2).

APP traffics through EGFR-positive endosomes to lysosomes and is degraded

We have previously shown that EGFR traffics in a subpopulation of MVBs destined for the lysosome (White et al., 2006). To determine whether APP is trafficked in the same MVBs, cells were incubated with EGF-488 for 10 and 45 min when EGF–EGFR complexes are primarily localized to early endosomes and MVBs, respectively (Futter et al., 1996). Fig. 3A shows that a small proportion of punctate 6E10 staining colocalized with EGF after 10 min, suggesting that only a small proportion of 6E10-positive puncta are early endosomes (14% APP colocalized with EGF, Fig. 3B). However, after 45 min stimulation, the majority of 6E10-positive puncta contained EGF (37% of the total APP colocalized with EGF, the majority of the remainder was in the TGN). These data show that APP is trafficked in the same population of MVBs that deliver EGFR to the lysosome for degradation. Although in control cells, we did not detect APP in lysosomes (Fig. 1), treatment of H4-APP cells with the protease inhibitor leupeptin caused a time-dependent increase in the amount of APP within cathepsin-D-positive compartments (Fig. 3C,D). This indicates that APP can be

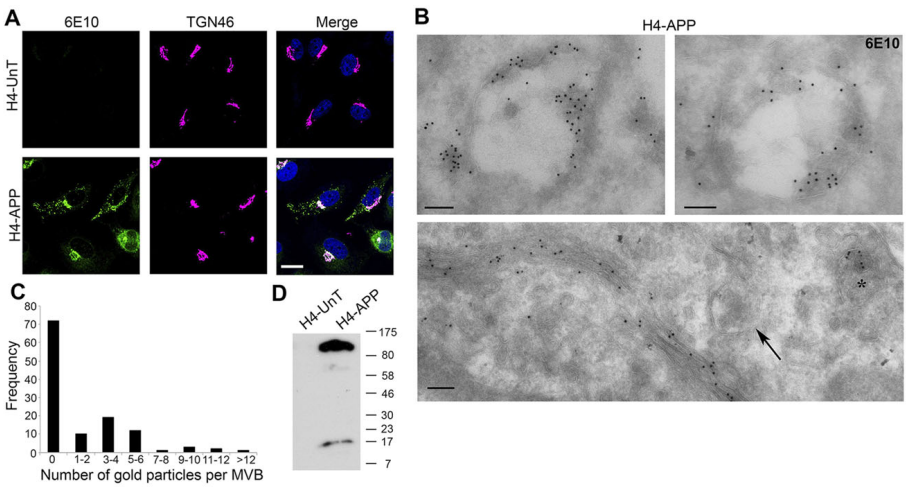


Fig. 1. APP localizes to the Golgi and ILVs of a subpopulation of MVBs. (A) Untransfected H4-UnT and H4-APP cells were stained for APP/Aβ (6E10; green), TGN46 (magenta) and DAPI (blue). Scale bar: 10 µm. (B) In ultrathin cryosections of H4-APP cells, 6E10 immunogold labelling is on a subset of MVBs (asterisks) and the Golgi, although some MVBs lack label (arrows). Scale bars: 100 nm. (C) Counting 6E10 gold particles per MVB (n=120) shows populations of 6E10 negative and positive MVBs (approximately four particles per MVB). (D) H4-UnT and H4-APP cells were western blotted with 6E10.

Journal of Cell Science

Journal of Cell Science (2015) 128, 2520-2528 doi:10.1242/jcs.170233

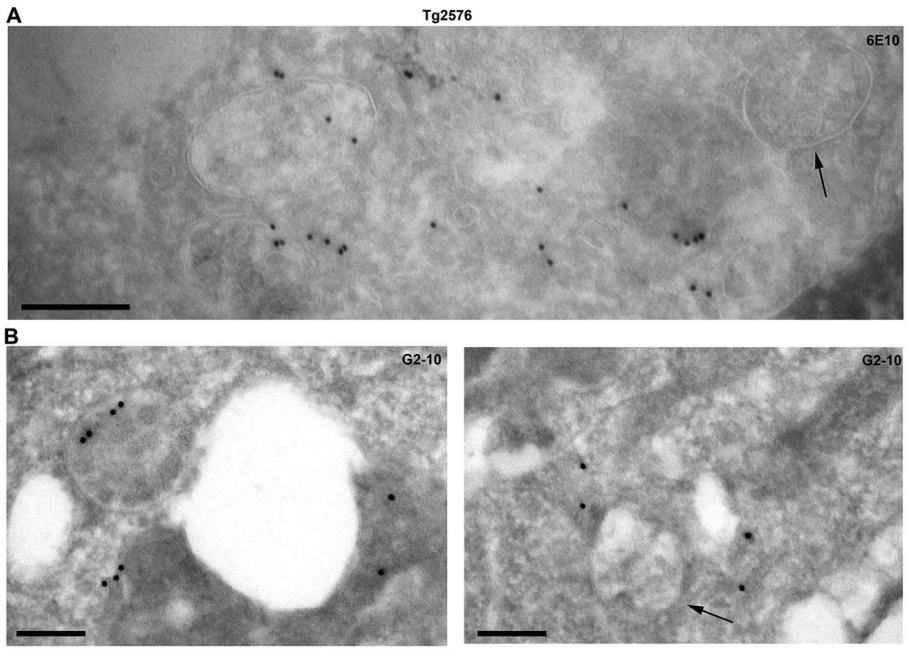


Fig. 2. APP and Aβ localizes to the ILVs of a subpopulation of MVBs in hippocampus of Tg2576 mice. Ultrathin sections of hippocampus of Tg2576 mice were stained with the anti-APP/Aβ antibody 6E10 (A) or Aβ40-specific antibody G2-10 (B). Arrows show MVBs negative of gold labelling. Scale bars: 200 nm.

trafficked to the lysosome but is rapidly degraded and only detectable following inhibition of lysosomal degradation.

Depletion of Hrs inhibits traffic of APP to ILVs

Targeting of EGFR to the ILVs of MVBs depends on EGFR-ubiquitylation-dependent engagement of the ESCRT machinery. To measure potential ubiquitylation of APP N2a-UnT and N2a-APP cells were transfected with ubiquitin–Myc and lysates were immunoprecipitated with 6E10. Blotting of the immunoprecipitations with anti-Myc antibody revealed that fl-APP can be ubiquitylated (supplementary material Fig. S2A) and there are several potential sites of APP ubiquitylation (supplementary material Fig. S2B). Depletion of the ESCRT0 component Hrs (also known as Hgs), which binds ubiquitylated cargo, caused APP to redistribute from ILVs to the limiting membrane of enlarged endosomes, as shown by immunoelectron microscopy (Fig. 4A), such that 31.5% of 6E10 gold particles localized to the limiting membrane in control cells increasing to 73.6% in Hrs-depleted cells. Immunofluorescence analysis showed that the 6E10-positive punctae were clearly enlarged in Hrs-depleted cells (Fig. 4B) and sometimes 6E10-positive 'rings' could be observed, as previously described (Choy et al., 2012). Some Hrs-depleted MVBs contained a population of unusually small ILVs, only detectable on glutaraldehyde-fixed specimens (Fig. 4A), as shown in our recent study on Hrs-depleted HeLa cells (Edgar et al., 2014).

Hrs and Tsg101 depletion reduce lysosomal delivery of APP

In order to determine whether depleting ESCRT components affected delivery of APP to lysosomes, we analysed the colocalization of APP with LAMP1. A change in the amount of co-staining of APP with LAMP1 upon ESCRT depletion could be caused by a change in the distribution of LAMP1 or by a change in the efficiency of delivery of APP to the lysosome. These two possibilities can be distinguished by incubation of the cells with leupeptin to inhibit lysosomal enzyme activity. This would be expected to have no effect on the distribution of LAMP1 but, as shown in Fig. 3, it increased APP signal in lysosomes by inhibiting degradation. Without leupeptin there was limited co-staining of APP with LAMP1 in control cells and cells treated with small interfering RNA (siRNA) against Hrs (siHrs) (~8 and 9%, respectively) (Fig. 5A,B). With leupeptin there was a 2-fold increase in APP co-staining with LAMP1 in control cells compared with only a 1.5-fold increase in siHrs-treated cells (Fig. 5A,C), indicating inhibition of lysosomal delivery of APP in Hrs-depleted cells. Although cells treated with siRNA against Tsg101 (siTsg101) displayed higher APP and LAMP1 colocalization in controls, there was only a 1.25-fold increase following leupeptin treatment, indicating a greater inhibition of APP delivery to lysosomes in siTsg101-treated cells (Fig. 5A,C).

Hrs or Tsg101 depletion reduces Aβ40 secretion but increases intracellular APP and Aβ

The effects of ESCRT depletion on Aβ accumulation and secretion was tested on N2a-APP cells, which secrete more Aβ than H4-APP cells and show a similar redistribution of APP to the perimeter membrane of enlarged MVBs, frequently visible as 'rings', upon Hrs or Tsg101 depletion (supplementary material Fig. S3). Depletion of

Journal of Cell Science

Journal of Cell Science (2015) 128, 2520-2528 doi:10.1242/jcs.170233

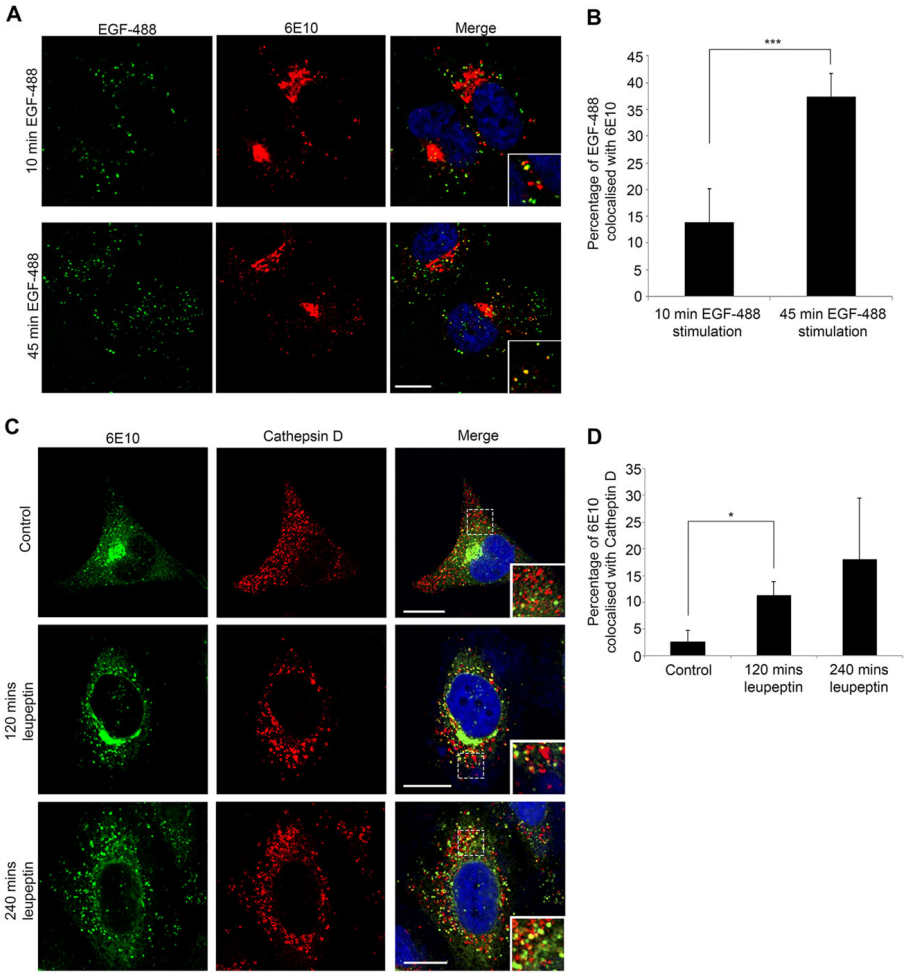


Fig. 3. APP traffics through the same MVBs as EGFR. (A) H4-APP cells stimulated with EGF–Alexa-Fluor-488 (EGF-488; green) for 10 or 45 min were stained for APP/Aβ with 6E10 (red). Scale bar: 5 µm. (B) Quantification of APP colocalization with EGF-488. (C) H4-APP cells treated with leupeptin were stained with 6E10 (green), cathepsin D (red) and DAPI (blue). Scale bars: 10 µm. (D) Quantification of 6E10 colocalization with cathepsin D. All results are mean±s.d. (n=3 separate experiments). *P<0.05, ***P<0.005 (Student's t-test).

Hrs or Tsg101 led to a 73% and 80% reduction in secreted Aβ40 levels respectively, as measured by ELISA of media samples (Fig. 6A), without any corresponding decrease in release of the intracellular enzyme lactate dehydrogenase (LDH) (Fig. 6B). Secreted Aβ levels do not necessarily reflect intracellular Aβ levels and so intracellular and secreted Aβ were analysed by western blotting, which, though challenging, allows distinction between fl-APP and processing products (Gouras et al., 2012). Western blotting of medium from N2a-APP cells showed reduced secreted Aβ levels following Hrs or Tsg101 depletion (Fig. 6C,D), in agreement with the ELISA results. Western blotting of cell lysates showed an increase in APP levels upon Hrs or Tsg101 depletion consistent with reduced delivery of APP to the lysosome (Fig. 6E,F). Interestingly, although α- and β-CTF levels were unchanged by Hrs or Tsg101 depletion (Fig. 6E), the intracellular levels of Aβ were dramatically increased following Hrs depletion (Fig. 6E,G). It is not possible to directly measure the effects of ESCRT depletion on Aβ generation, as the intracellular Aβ levels are a balance between production, degradation and secretion. However the intracellular Aβ accumulation that accompanied reduced Aβ secretion upon Hrs depletion suggests that Hrs-dependent targeting of APP to ILVs is not necessary for Aβ production but that Hrs and Tsg101 are involved in Aβ secretion.

Journal of Cell Science (2015) 128, 2520-2528 doi:10.1242/jcs.170233

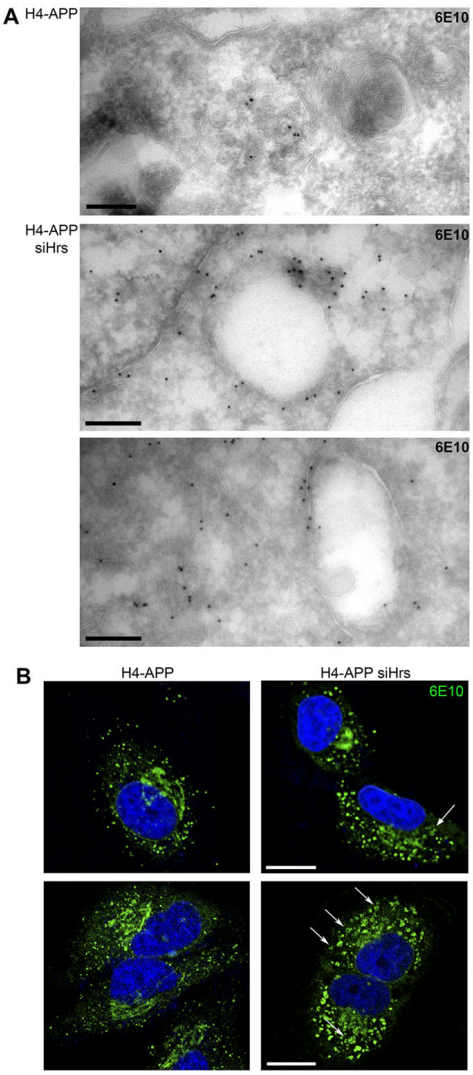


Fig. 4. Redistribution of APP from ILVs to the limiting membrane of MVBs after Hrs depletion. (A) Cryosections of H4-APP and Hrs-depleted H4-APP cells (siHrs) were stained for APP/Aβ with 6E10 (upper two panels, cells fixed with 4% PFA; lower panel, cells fixed with 4% PFA and 0.2% glutaraldehyde). Scale bars: 200 nm. (B) Confocal microscopy reveals 6E10-positive endosomal rings following Hrs depletion (arrows). Scale bars: 5 µm.

DISCUSSION

Despite the clinical importance of Aβ, the role of the endocytic pathway versus the TGN and the role of sorting within MVBs in regulating the intracellular accumulation and secretion of Aβ remain unclear. In keeping with previous studies, we found that APP localized predominantly to endosomes and the TGN, and now show that, within the endocytic pathway, APP is found mainly on the ILVs of a subset of MVBs. Sorting of APP onto ILVs could promote Aβ production by providing favourable conditions for amyloidogenic processing, as it does for PMEL in melanogenic cells. Consistent with this hypothesis, we found Aβ40 on the ILVs of MVBs in mouse brain from Tg2576 mice. Alternatively sorting of APP to ILVs could prevent intracellular Aβ accumulation by targeting APP and/or its processing products for lysosomal degradation. Consistent with this hypothesis, we found APP in EGFR-containing MVBs, an MVB subpopulation that normally fuses with lysosomes, and lysosomal accumulation of APP in cells treated with protease inhibitor.

To determine whether sorting of APP onto ILVs has a positive or negative effect on Aβ accumulation, we aimed to inhibit the ILV sorting machinery and analyse the effects on intracellular Aβ levels. EGFR is targeted to the ILVs of MVBs by ubiquitylation-dependent interaction with the ESCRT machinery. In contrast, PMEL, which depends on sorting to ILVs for amyloidogenic processing, is targeted to ILVs independently of ubiquitylation and the ESCRT machinery (Theos et al., 2006; van Niel et al., 2011). That APP traffics predominantly in the same MVBs that traffic EGFR implied that the ESCRT machinery was involved in APP sorting. However, ESCRT-dependent and -independent ILV sorting mechanisms are not entirely segregated within separate populations of MVBs. van Niel et al. (van Niel et al., 2011) have shown that the C-terminal fragment of PMEL that remains after amyloidogenic processing is targeted to the lysosome in an ESCRT-dependent manner and we have recently shown that Hrs-dependent and Hrs-independent ILVs can form in the same MVB (Edgar et al., 2014).

Several studies, including our own, show that APP can be ubiquitylated (Morel et al., 2013; Watanabe et al., 2012) and, hence, could potentially engage the ESCRT machinery. A previous study has shown that depletion of the ESCRT0 component Hrs or the ESCRTI component Tsg101 leads to the retention of APP in early endosomes at the expense of the TGN (Choy et al., 2012) and proposed a role for Hrs and Tsg101 in retromeric traffic of APP to the TGN. Another recent study presented evidence for a role for the ESCRT machinery in sorting APP to ILVs. Expression of a poorly ubiquitylated mutant APP or depletion of the phosphoinositide 3-kinase (PI3K) Vps34 and its effector Hrs inhibits sorting of APP to ILVs (Morel et al., 2013). Here, we show that depletion of Hrs or Tsg101 inhibit sorting of APP to ILVs of a subset of MVBs, directly demonstrating a role for the ESCRT machinery in sorting APP to ILVs.

Thus, two amyloidogenic proteins, PMEL and APP, are sorted onto ILVs by different mechanisms. ESCRT-independent sorting of PMEL to ILVs promotes amyloidogenic processing. Does sorting of APP onto ILVs, serve a similar purpose, albeit utilizing a different machinery, or does ESCRT-dependent ILV sorting target APP and its processing products to the lysosome and, thereby, reduce Aβ accumulation? Consistent with the latter possibility, we found that Hrs or Tsg101 depletion increased cellular APP levels and inhibited APP delivery to the lysosome. Morel et al. proposed that ESCRT-mediated ILV targeting limits Aβ production after finding that silencing Vps34, or expressing ubiquitylation-deficient APP, increased Aβ secretion (Morel et al., 2013). However, here, we found that Hrs or Tsg101 depletion reduced Aβ secretion. Choy et al. also found reduced Aβ secretion on Hrs or Tsg101 depletion but found increased Aβ secretion on depletion of the later ESCRT components CHMP and Vps34 (Choy et al., 2012). This enhanced

Journal of Cell Science

Journal of Cell Science (2015) 128, 2520-2528 doi:10.1242/jcs.170233

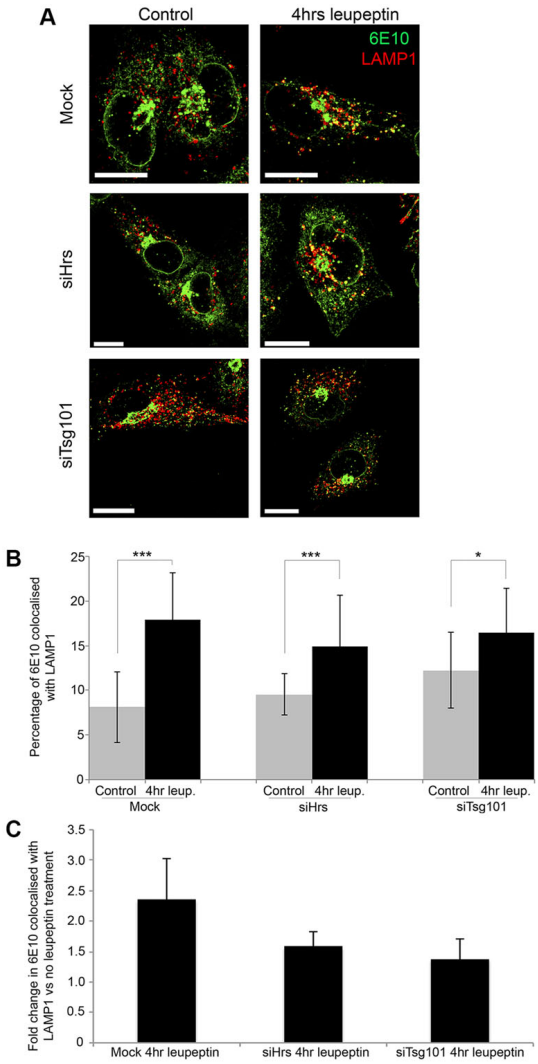


Fig. 5. Reduced lysosomal delivery after Hrs/Tsg101 depletion. (A) H4-APP cells depleted of Hrs (siHrs) or Tsg101 (siTsg101) were treated with or without leupeptin and stained with 6E10 (green) and LAMP1 (red). Scale bars: 5 µm. (B) Quantification of 6E10 colocalization with LAMP1 (using Velocity). Results are mean±s.d. of three experiments. *P<0.05, ***P<0.005 (Student's t-test). (C) Fold change (mean±s.d., n=2 separate experiments) of 6E10 colocalized with LAMP1.

Aβ secretion required retromer-dependent redistribution of APP to the TGN and these authors concluded that the TGN was the major site of Aβ production. How can treatments likely to reduce ESCRT-dependent sorting of APP to ILVs enhance Aβ secretion in one study (Morel et al., 2013) and reduce them in others (Choy et al., 2012) (and the current study)? Although differences in cell types might underlie these apparent differences (HEK293 cells in Choy et al. and Hela cells in Morel et al.), we can add a key component that was absent from previous studies. As well as Aβ secretion, we measured intracellular Aβ levels. Although depletion of Hrs inhibited Aβ secretion, intracellular Aβ levels were considerably increased. Although we cannot eliminate the possibility that Hrs depletion affects Aβ production, the elevated intracellular Aβ levels imply that Hrs-dependent sorting to ILVs does not promote Aβ generation. Aβ found on ILVs could arise from Aβ generation on the perimeter membrane of the MVB and subsequent sorting onto ILVs, or γ-cleavage could occur on ILVs as well as on the perimeter membrane. The previous immunoelectron microscopy findings showing that Aβ42 in neurons normally localizes preferentially to the MVB limiting membranes is consistent with Aβ generation on the MVB perimeter membrane (Takahashi et al., 2002). Intracellular Aβ levels depend on the

Journal of Cell Science (2015) 128, 2520-2528 doi:10.1242/jcs.170233

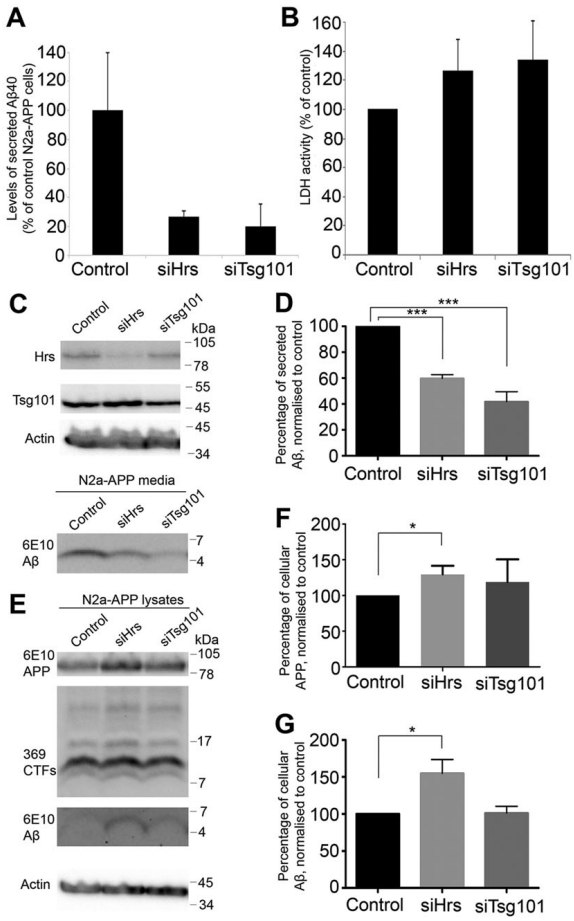


Fig. 6. Reduced Aβ40 secretion and increased intracellular APP and/or Aβ after depletion of Hrs or Tsg101. (A) ELISA shows reduced Aβ40 secretion in N2a-APP cells depleted of of Hrs (siHrs) or Tsg101 (siTsg101). (B) Hrs or Tsg101 depletion does not affect release of LDH activity into culture medium. (C–G) N2a-APP cells were depleted of Hrs or Tsg101 and media (C,D) and cell lysates (E–G) were analysed by western blotting. All results are mean±s.d. of three experiments. **P*<0.05, ****P*<0.005 (Student's *t*-test).

balance between Aβ generation and Aβ degradation and secretion. Hrs or Tsg101 depletion might increase Aβ levels by inhibiting lysosomal delivery of APP or β-CTF, increasing the time that they reside in MVBs, but also increasing Aβ accumulation through reduced Aβ secretion.

What is the role of Hrs and Tsg101 in Aβ secretion? Although the major fate of ESCRT-dependent ILVs is degradation in the lysosome, Aβ accumulation in MVBs could affect that fate. Consistently, a defect in EGFR degradation has been observed upon Aβ accumulation within MVBs (Almeida et al., 2006). One alternative MVB fate is fusion with the cell surface and release of ILVs as exosomes, and exosome-associated Aβ has been found (Rajendran et al., 2006). Interestingly, one exosome population has been shown to be generated independently of ESCRTs (Trajkovic et al., 2008), but depletion of Hrs and Tsg101 has recently been shown to reduce some exosome production (Colombo et al., 2013; Tamai et al., 2012, 2010), and ubiquitylated proteins have been found in exosomes (Buschow et al., 2005). Thus, reduced exosome secretion could contribute to the reduced Aβ secretion upon depletion of Hrs or Tsg101. Additionally, non-exosome-associated Aβ within the MVB lumen could be released upon MVB fusion with the plasma membrane and Hrs or Tsg101 could play a role in this fusion. Another possible fate of MVBs is fusion with autophagosomes in a process that participates in autophagic degradation (Lamb et al., 2013). The accumulation of autophagic vacuoles in Alzheimer's disease brain (Nixon et al., 2005) and mouse Alzheimer's disease models (Yu et al., 2005) suggests a link between Aβ accumulation and autophagy. ESCRT proteins are required for efficient autophagic degradation (Rusten and Simonsen, 2008), but, in an intriguing recent development, genetic ablation of autophagy by knockout of Atg7 has been shown to dramatically reduce Aβ secretion (Nilsson et al., 2013; Nilsson and Saido, 2014). Clearly the relationship between ESCRT-mediated sorting of APP onto ILVs, autophagy and Aβ secretion is a major subject for future study.

Journal of Cell Science

Understanding the molecular mechanisms that regulate intracellular Aβ accumulation is crucial to understanding early Alzheimer's disease pathogenesis. Increasing evidence indicates that intracellular Aβ accumulation in Alzheimer's-disease-vulnerable neurons initiates synaptic dysfunction prior to the presence of amyloid plaques. Our data indicate a key role for early ESCRT components in limiting intracellular Aβ accumulation by sorting APP onto ILVs of MVBs for lysosomal degradation and promoting Aβ secretion.

MATERIALS AND METHODS

Reagents

Anti-APP/Aβ antibodies were mouse 6E10 and 4G8, against residues 3–8 and 17–24 of Aβ respectively (Covance), rabbit 369 against CTF (Buxbaum et al., 1990), and mouse G2-10 (Aβ40-specific) and P2-1 (N-terminus) (Millipore). Sheep anti-TGN46 (AbD Serotec), rabbit anti-Cathepsin D (Upstate), -LAMP1 (Ab24170 - Abcam), -Myc (Abcam), and mouse anti-Hrs (Enzo Lifesciences) and Tsg101 (Genetex) antibodies were used. Leupeptin and cycloheximide (Sigma) were used at 50 μg/ml and 40 μg/ml, respectively.

Cell culture

Human H4 neuroglioma cells (H4) cells from ATCC were cultured in Dulbecco's modified Eagle's medium (DMEM) with 10% fetal calf serum (FCS). N2a mouse neuroblastoma cells (generously provided by Gopal Thinakaran and Sangram Sisodia – University of Chicago) were cultured in 47.5% DMEM, 47.5% OptiMem and 5% FCS, with 0.4 mg/ml Geneticin (Invitrogen).

Western blotting

Western blotting to analyse knockdown efficiencies were performed as previously described (Edgar et al., 2014). To perform western blotting for Aβ, medium was collected and cells were harvested in ice-cold PBS. Cell pellets were lysed in 6% SDS, 1% β-mercaptoethanol, sonicated and heated at 95°C. Centrifuged (10,600 ***g*** for 10 min) supernatants were electrophoresed, transferred to PVDF membranes (Millipore), and boiled in PBS. Blocking and antibody incubations were in 0.1% Tween-20 (PBST) with 5% milk powder. Immunoreactions were visualized by chemiluminescence (Pierce) and quantified with Image Lab (Bio-Rad).

Co-immunoprecipitation

The ubiquitin–Myc construct was a kind gift from Sylvie Urbe (University of Liverpool, UK). Cells were scraped in lysis buffer containing 10 mM NEM and lysates incubated with 10 μg of primary antibody for 4 h and then protein G beads (Santa Cruz Biotechnology) for 1 h. Washed pellets were boiled in reducing sample buffer and analysed by SDS-PAGE and western blotting.

RNA interference

Cells were transfected using Oligofectamine (Invitrogen) with 20 μM negative control siRNA (Mammalian AllStar negative siRNA), or human Hrs or Tsg101 (Razi and Futter, 2006), murine Hrs ON-TARGETplus SMARTpool siRNA or murine Tsg101 ON-TARGETplus SMARTpool siRNA sequences (Quiagen).

Cryo-immunoelectron microscopy

Cultured cells were prepared and sectioned as described (Edgar et al., 2014). For mouse brains, 10-month-old mice expressing human-sweAPP (Tg2576 mice; Hsiao et al., 1996) and wild-type littermates were perfusion fixed with 4% PFA. 50-μm vibratome sections of hippocampus were dissected and embedded in 12% gelatin before preparation as above. Sections were immunogold labelled (Slot et al., 1991) and visualized with a JEOL1010 transmission electron microscope with a Gatan digital camera and Digital Micrograph software. All animal experiments were approved by the Animal Ethical Committee of Lund University (Sweden).

Immunofluorescence

Cells were fixed with 4% PFA, permeabilized with 0.1% saponin, and then blocking, antibody incubations and washes were in 1% BSA and 0.01% saponin in PBS. Coverslips were mounted in DAPI-containing medium Prolong gold anti-fade reagent (Invitrogen). For EGF-trafficking experiments, cells were serum starved for 90 min before incubation with 200 ng/ml EGF–Alexa-Fluor-488 (Molecular Probes).Cells were visualized using a Leica TCS SP2 AOBS confocal microscope using a 63× oil immersion lens. Images were analysed using Methamorph Image Analysis or Velocity software.

Human Aβ40 ELISA

Human Aβ40 secreted over 48 h was measured in culture medium by ELISA (Invitrogen).

Competing interests

The authors declare no competing or financial interests.

Author contributions

J.R.E. and K.W. designed and performed experiments, analysed data and wrote the manuscript. G.K.G. and C.E.F. conceived the project, analysed the data and wrote the manuscript.

Funding

This work was supported by the Alzheimer's Society; the Wellcome Trust (to C.E.F.); the Swedish Research Council; and MultiPark (to G.K.G.). Deposited in PMC for immediate release.

Supplementary material

Supplementary material available online at
http://jcs.biologists.org/lookup/suppl/doi:10.1242/jcs.170233/-/DC1

References

Almeida, C. G., Takahashi, R. H. and Gouras, G. K. (2006). Beta-amyloid accumulation impairs multivesicular body sorting by inhibiting the ubiquitin-proteasome system. *J. Neurosci.* **26**, 4277-4288.

Berson, J. F., Harper, D. C., Tenza, D., Raposo, G. and Marks, M. S. (2001). Pmel17 initiates premelanosome morphogenesis within multivesicular bodies. *Mol. Biol. Cell* **12**, 3451-3464.

Burgos, P. V., Mardones, G. A., Rojas, A. L., daSilva, L. L. P., Prabhu, Y., Hurley, J. H. and Bonifacino, J. S. (2010). Sorting of the Alzheimer's disease amyloid precursor protein mediated by the AP-4 complex. *Dev. Cell* **18**, 425-436.

Buschow, S. I., Liefhebber, J. M. P., Wubbolts, R. and Stoorvogel, W. (2005). Exosomes contain ubiquitinated proteins. *Blood Cells Mol. Dis.* **35**, 398-403.

Buxbaum, J. D., Gandy, S. E., Cicchetti, P., Ehrlich, M. E., Czernik, A. J., Fracasso, R. P., Ramabhadran, T. V., Unterbeck, A. J. and Greengard, P. (1990). Processing of Alzheimer beta/A4 amyloid precursor protein: modulation by agents that regulate protein phosphorylation. *Proc. Natl. Acad. Sci. USA* **87**, 6003-6006.

Choy, R. W.-Y., Cheng, Z. and Schekman, R. (2012). Amyloid precursor protein (APP) traffics from the cell surface via endosomes for amyloid beta (Abeta) production in the trans-Golgi network. *Proc. Natl. Acad. Sci. USA* **109**, E2077-E2082.

Colombo, M., Moita, C., van Niel, G., Kowal, J., Vigneron, J., Benaroch, P., Manel, N., Moita, L. F., Théry, C. and Raposo, G. (2013). Analysis of ESCRT functions in exosome biogenesis, composition and secretion highlights the heterogeneity of extracellular vesicles. *J. Cell Sci.* **126**, 5553-5565.

Edgar, J. R., Eden, E. R. and Futter, C. E. (2014). Hrs- and CD63-dependent competing mechanisms make different sized endosomal intraluminal vesicles. *Traffic.* **15**, 197-211.

Futter, C. E., Pearse, A., Hewlett, L. J. and Hopkins, C. R. (1996). Multivesicular endosomes containing internalized EGF-EGF receptor complexes mature and then fuse directly with lysosomes. *J. Cell Biol.* **132**, 1011-1023.

Glenner, G. G. (1989). The pathobiology of Alzheimer's disease. *Annu. Rev. Med.* **40**, 45-51.

Glenner, G. G. and Wong, C. W. (1984). Alzheimer's disease: initial report of the purification and characterization of a novel cerebrovascular amyloid protein. *Biochem. Biophys. Res. Commun.* **120**, 885-890.

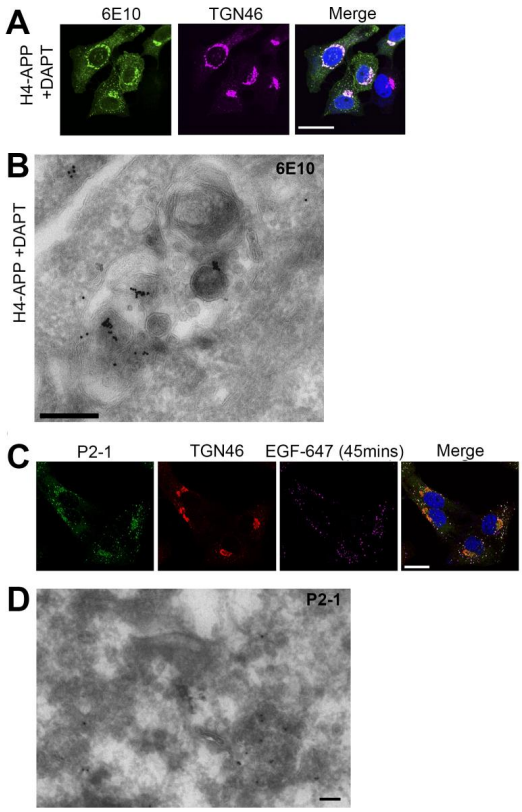
Goedert, M., Wischik, C. M., Crowther, R. A., Walker, J. E. and Klug, A. (1988). Cloning and sequencing of the cDNA encoding a core protein of the paired helical filament of Alzheimer disease: identification as the microtubule-associated protein tau. *Proc. Natl. Acad. Sci. USA* **85**, 4051-4055.

Gouras, G. K., Willén, K. and Tampellini, D. (2012). Critical role of intraneuronal Abeta in Alzheimer's disease: technical challenges in studying intracellular Abeta. *Life Sci.* **91**, 1153-1158.

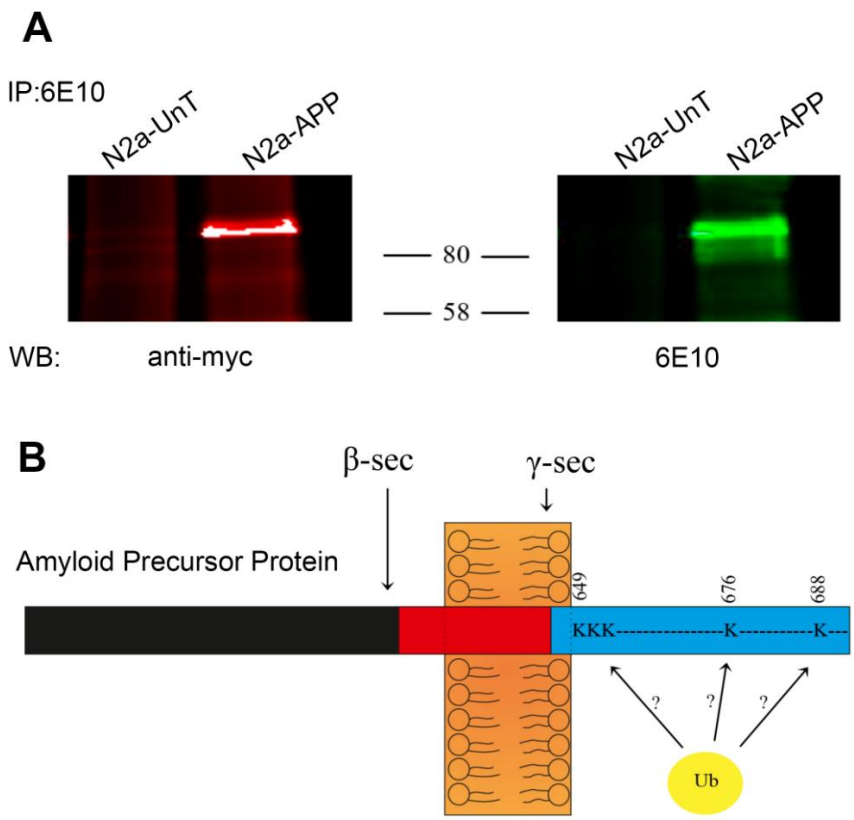
Hsiao, K., Chapman, P., Nilsen, S., Eckman, C., Harigaya, Y., Younkin, S., Yang, F. and Cole, G. (1996). Correlative memory deficits, Abeta elevation, and amyloid plaques in transgenic mice. *Science* **274**, 99-103.

Lamb, C. A., Dooley, H. C. and Tooze, S. A. (2013). Endocytosis and autophagy: Shared machinery for degradation. *BioEssays* **35**, 34-45.
Morel, E., Chamoun, Z., Lasiecka, Z. M., Chan, R. B., Williamson, R. L., Vetanovetz, C., Dall'Armi, C., Simoes, S., Point Du Jour, K. S., McCabe, B. D. et al. (2013). Phosphatidylinositol-3-phosphate regulates sorting and processing of amyloid precursor protein through the endosomal system. *Nat. Commun.* **4**, 2250.
Nilsson, P. and Saido, T. C. (2014). Dual roles for autophagy: degradation and secretion of Alzheimer's disease Abeta peptide. *BioEssays* **36**, 570-578.
Nilsson, P., Loganathan, K., Sekiguchi, M., Matsuba, Y., Hui, K., Tsubuki, S., Tanaka, M., Iwata, N., Saito, T. and Saido, T. C. (2013). Abeta secretion and plaque formation depend on autophagy. *Cell Rep.* **5**, 61-69.
Nixon, R. A., Wegiel, J., Kumar, A., Yu, W. H., Peterhoff, C., Cataldo, A. and Cuervo, A. M. (2005). Extensive involvement of autophagy in Alzheimer disease: an immuno-electron microscopy study. *J. Neuropathol. Exp. Neurol.* **64**, 113-122.
Oddo, S., Caccamo, A., Shepherd, J. D., Murphy, M. P., Golde, T. E., Kayed, R., Metherate, R., Mattson, M. P., Akbari, Y. and LaFerla, F. M. (2003). Triple-transgenic model of Alzheimer's disease with plaques and tangles: intracellular Abeta and synaptic dysfunction. *Neuron* **39**, 409-421.
Rajendran, L., Honsho, M., Zahn, T. R., Keller, P., Geiger, K. D., Verkade, P. and Simons, K. (2006). Alzheimer's disease beta-amyloid peptides are released in association with exosomes. *Proc. Natl. Acad. Sci. USA* **103**, 11172-11177.
Razi, M. and Futter, C. E. (2006). Distinct roles for Tsg101 and Hrs in multivesicular body formation and inward vesiculation. *Mol. Biol. Cell* **17**, 3469-3483.
Rusten, T. E. and Simonsen, A. (2008). ESCRT functions in autophagy and associated disease. *Cell Cycle* **7**, 1166-1172.
Selkoe, D. J., Abraham, C. R., Podlisny, M. B. and Duffy, L. K. (1986). Isolation of low-molecular-weight proteins from amyloid plaque fibers in Alzheimer's disease. *J. Neurochem.* **46**, 1820-1834.
Slot, J. W., Geuze, H. J., Gigengack, S., Lienhard, G. E. and James, D. E. (1991). Immuno-localization of the insulin regulatable glucose transporter in brown adipose tissue of the rat. *J. Cell Biol.* **113**, 123-135.
Stuffers, S., Sem Wegner, C., Stenmark, H. and Brech, A. (2009). Multivesicular endosome biogenesis in the absence of ESCRTs. *Traffic* **10**, 925-937.
Subra, C., Laulagnier, K., Perret, B. and Record, M. (2007). Exosome lipidomics unravels lipid sorting at the level of multivesicular bodies. *Biochimie* **89**, 205-212.
Takahashi, R. H., Milner, T. A., Li, F., Nam, E. E., Edgar, M. A., Yamaguchi, H., Beal, M. F., Xu, H., Greengard, P. and Gouras, G. K. (2002). Intraneuronal Alzheimer abeta42 accumulates in multivesicular bodies and is associated with synaptic pathology. *Am. J. Pathol.* **161**, 1869-1879.
Takahashi, R. H., Almeida, C. G., Kearney, P. F., Yu, F., Lin, M. T., Milner, T. A. and Gouras, G. K. (2004). Oligomerization of Alzheimer's beta-amyloid within processes and synapses of cultured neurons and brain. *J. Neurosci.* **24**, 3592-3599.
Tamai, K., Tanaka, N., Nakano, T., Kakazu, E., Kondo, Y., Inoue, J., Shiina, M., Fukushima, K., Hoshino, T., Sano, K. et al. (2010). Exosome secretion of dendritic cells is regulated by Hrs, an ESCRT-0 protein. *Biochem. Biophys. Res. Commun.* **399**, 384-390.
Tamai, K., Shiina, M., Tanaka, N., Nakano, T., Yamamoto, A., Kondo, Y., Kakazu, E., Inoue, J., Fukushima, K., Sano, K. et al. (2012). Regulation of hepatitis C virus secretion by the Hrs-dependent exosomal pathway. *Virology* **422**, 377-385.
Theos, A. C., Truschel, S. T., Tenza, D., Hurbain, I., Harper, D. C., Berson, J. F., Thomas, P. C., Raposo, G. and Marks, M. S. (2006). A lumenal domain-dependent pathway for sorting to intralumenal vesicles of multivesicular endosomes involved in organelle morphogenesis. *Dev. Cell* **10**, 343-354.
Trajkovic, K., Hsu, C., Chiantia, S., Rajendran, L., Wenzel, D., Wieland, F., Schwille, P., Brugger, B. and Simons, M. (2008). Ceramide triggers budding of exosome vesicles into multivesicular endosomes. *Science* **319**, 1244-1247.
van Niel, G., Charrin, S., Simoes, S., Romao, M., Rochin, L., Saftig, P., Marks, M. S., Rubinstein, E. and Raposo, G. (2011). The tetraspanin CD63 regulates ESCRT-independent and -dependent endosomal sorting during melanogenesis. *Dev. Cell* **21**, 708-721.
Vieira, S. I., Rebelo, S., Esselmann, H., Wiltfang, J., Lah, J., Lane, R., Small, S. A., Gandy, S., da Cruz e Silva, E. F. and da Cruz e Silva, O. A. B. (2010). Retrieval of the Alzheimer's amyloid precursor protein from the endosome to the TGN is S655 phosphorylation state-dependent and retromer-mediated. *Mol. Neurodegener.* **5**, 40.
Watanabe, T., Hikichi, Y., Willuweit, A., Shintani, Y. and Horiguchi, T. (2012). FBL2 regulates amyloid precursor protein (APP) metabolism by promoting ubiquitination-dependent APP degradation and inhibition of APP endocytosis. *J. Neurosci.* **32**, 3352-3365.
Wherlock, M., Gampel, A., Futter, C. and Mellor, H. (2004). Farnesyltransferase inhibitors disrupt EGF receptor traffic through modulation of the RhoB GTPase. *J. Cell Sci.* **117**, 3221-3231.
White, I. J., Bailey, L. M., Aghakhani, M. R., Moss, S. E. and Futter, C. E. (2006). EGF stimulates annexin 1-dependent inward vesiculation in a multivesicular endosome subpopulation. *EMBO J.* **25**, 1-12.
Wollert, T. and Hurley, J. H. (2010). Molecular mechanism of multivesicular body biogenesis by ESCRT complexes. *Nature* **464**, 864-869.
Yu, W. H., Cuervo, A. M., Kumar, A., Peterhoff, C. M., Schmidt, S. D., Lee, J.-H., Mohan, P. S., Mercken, M., Farmery, M. R., Tjernberg, L. O. et al. (2005). Macroautophagy–a novel Beta-amyloid peptide-generating pathway activated in Alzheimer's disease. *J. Cell Biol.* **171**, 87-98.

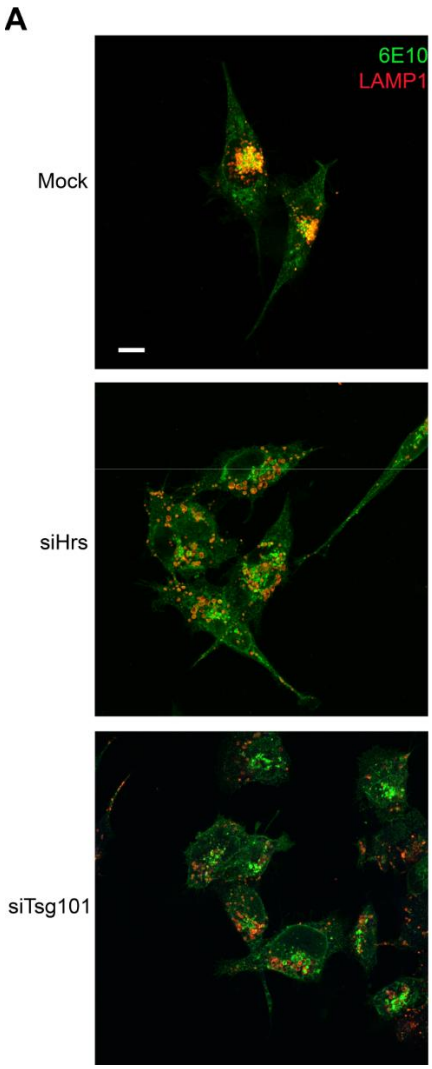
Journal of Cell Science



Supplementary Figure 1 – Inhibition of y-secretease does not alter 6E10, and the N-terminus of APP displays the same localization at 6E10. (A) H4-APP cells were treated with the y-secretase inhibitor DAPT (1 ng/ml, 18 hours) before being fixed and analysed by immunofluorescence. Cells were stained with the anti-APP/Aβ antibody 6E10 (green) and an anti-TGN46 antibody (magenta). Scale bar 10μm. (B) Cells were similarly treated with DAPT and processed for cryosectioning. Thawed cryosections were stained with the anti-APP/Aβ antibody 6E10. Scale bar 200nm. (C) H4-APP or untransfected cells were fixed and stained with the N-terminal APP antibody, P2-1 (green) and imaged by confocal microscopy. Scale bar 10μm. (D) H4-APP cells were fixed and prepared for cryosectioning. Ultrathin cryosections were stained using the anti-N-terminal APP antibody, P2-1. Scale bars 100nm.



Supplementary Figure 2 – APP undergoes ubiquitination. (A) N2a-UnT and N2a-APP cells transfected with a myc-tagged ubiquitin construct were lysed and immunoprecipitated using anti-APP/Aβ antibody, 6E10. Pull-downs were Western blotted with anti-myc antibody. (B) Schematic of potential sites of ubiquitination within APP.



Supplementary Figure 3 - N2a-APP cells display similar morphology to H4-APP cells following siHrs or siTsg101 depletion. N2a-APP cells were depleted for Hrs or Tsg101 and stained for APP (green) and LAMP1 (red). Scale bar 10μm.

Paper III

Willén et al. Molecular Neurodegeneration (2017) 12:61
DOI 10.1186/s13024-017-0203-y

Molecular Neurodegeneration

RESEARCH ARTICLE Open Access

Aβ accumulation causes MVB enlargement and is modelled by dominant negative VPS4A

Katarina Willén[1], James R. Edgar[2,3], Takafumi Hasegawa[4], Nobuyuki Tanaka[5], Clare E. Futter[3] and Gunnar K. Gouras[1*]

Abstract

Background: Alzheimer's disease (AD)-linked β-amyloid (Aβ) accumulates in multivesicular bodies (MVBs) with the onset of AD pathogenesis. Alterations in endosomes are among the earliest changes associated with AD but the mechanism(s) that cause endosome enlargement and the effects of MVB dysfunction on Aβ accumulation and tau pathology are incompletely understood.

Methods: MVB size and Aβ fibrils in primary neurons were visualized by electron microscopy and confocal fluorescent microscopy. MVB-dysfunction, modelled by expression of dominant negative VPS4A (dnVPS4A), was analysed by biochemical methods and exosome isolation.

Results: Here we show that AD transgenic neurons have enlarged MVBs compared to wild type neurons. Uptake of exogenous Aβ also leads to enlarged MVBs in wild type neurons and generates fibril-like structures in endocytic vesicles. With time fibrillar oligomers/fibrils can extend out of the endocytic vesicles and are eventually detectable extracellularly. Further, endosomal sorting complexes required for transport (ESCRT) components were found associated with amyloid plaques in AD transgenic mice. The phenotypes previously reported in AD transgenic neurons, with net increased intracellular levels and reduced secretion of Aβ, were mimicked by blocking recycling of ESCRT-III by dnVPS4A. DnVPS4A further resembled AD pathology by increasing tau phosphorylation at serine 396 and increasing markers of autophagy.

Conclusions: We demonstrate that Aβ leads to MVB enlargement and that amyloid fibres can form within the endocytic pathway of neurons. These results are consistent with the scenario of the endosome-lysosome system representing the site of initiation of Aβ aggregation. In turn, a dominant negative form of the CHMP2B-interacting protein VPS4A, which alters MVBs, leads to accumulation and aggregation of Aβ as well as tau phosphorylation, mimicking the cellular changes in AD.

Keywords: Alzheimer's disease, Amyloid, Endocytosis, Multivesicular body, Tau

Background

Alzheimer's disease (AD) is characterized by progressive decline in cognitive function, anatomical selective loss of synapses and neurons, and aggregation of the β-amyloid peptide (Aβ) in amyloid plaques and hyperphosphorylated tau in neurofibrillary tangles (NFTs). Although plaques are extracellular aggregates of Aβ, accumulation of Aβ42, the most pathogenic Aβ peptide, begins within neurons in AD [1–3] and in AD transgenic mouse models [4–6]. In AD transgenic mice, cognitive, physiological and structural impairments appear prior to plaques [7–9] and are accompanied by intraneuronal Aβ peptide accumulation, supporting that accumulation of intraneuronal Aβ peptides is one of the earliest events in AD pathogenesis [10].

Abnormalities in the endocytic pathway are also among the earliest pathological features reported in AD, preceding the classical pathological markers of Aβ plaques and NFTs [11]. Specifically, enlargement of Rab5-positive early endosomes and Rab7-positive late endosomes were reported in AD [12, 13], as well as progressive accumulation

* Correspondence: gunnar.gouras@med.lu.se
[1]Department of Experimental Medical Science, Lund University, 221 84 Lund, Sweden
Full list of author information is available at the end of the article

BioMed Central

© The Author(s). 2017 **Open Access** This article is distributed under the terms of the Creative Commons Attribution 4.0 International License (http://creativecommons.org/licenses/by/4.0/), which permits unrestricted use, distribution, and reproduction in any medium, provided you give appropriate credit to the original author(s) and the source, provide a link to the Creative Commons license, and indicate if changes were made. The Creative Commons Public Domain Dedication waiver (http://creativecommons.org/publicdomain/zero/1.0/) applies to the data made available in this article, unless otherwise stated.

of multivesicular bodies (MVBs), lysosomes and autophagic vacuoles [14]. The amyloidogenic cleavage of APP occurs predominantly in endosomes [15–19]. Proteins in the amyloidogenic pathway (APP, the β-site APP cleaving enzyme (BACE1) and the γ-secretase that generates the Aβ peptides) are transmembrane proteins that traffic through the secretory pathway as well as the endocytic pathway. Immuno-electron microscopy revealed that particularly the limiting membrane of MVBs are the normal location of Aβ42 in neurons of the brain and are the sites of Aβ accumulation during AD pathogenesis [20], especially at synapses [5]. Sorting of EGFR via the MVB pathway was impaired by endosomal Aβ accumulation in cultured AD transgenic neurons [21]. Translocation into MVBs appeared particularly affected, suggesting Aβ dependent dysfunction of the late endosomal sorting complexes required for transport (ESCRT) pathway in AD.

The ESCRTs are a set of proteins conserved from yeast to mammals that regulate and drive formation of the intraluminal vesicles of MVBs. They assemble into distinct subcomplexes: ESCRT-0, ESCRT-I, ESCRT-II and ESCRT-III. Their sequential action directs the sorting of ubiquitinated transmembrane proteins and the inward budding of intraluminal vesicles (ILVs) into the lumen of endosomes, thereby generating MVBs that then either deliver membrane-associated cargo to the lysosome for degradation, release the intraluminal vesicles (then called exosomes) via fusion with the plasma membrane or traffic cargo back to the Golgi apparatus. ESCRT-III subunits, among them CHMP2B, are inactive monomers in the cytoplasm [22] that assemble on endosomal membranes in an ordered manner to generate the transient ESCRT-III complex. CHMP2B, linked genetically to frontotemporal dementia (FTD) and AD [23, 24], directly interacts with and recruits the VPS4 AAA−ATPase complex that disassembles ESCRT-III, and genome-wide association studies for late onset AD identified an association with VPS4B [25].

Given the cumulative genetic, biological and pathological evidence implicating Aβ in AD, and the early accumulation of Aβ in MVBs in AD, we set out to test our first hypothesis (1) that Aβ can cause the abnormal endosomal phenotype seen in AD. To determine this, we investigated the effects of Aβ on MVB size and Aβ aggregation in late endosomes. Since Aβ accumulates particularly at the outer limiting membrane of MVBs where ESCRTs reside and since ESCRT dysfunction leads to endosomal enlargement we also tested our second hypothesis (2) that Aβ causes dysfunction of the ESCRT pathway. This was investigated by examining changes in ESCRT proteins in primary neurons, as well as modulating the late ESCRT pathway to examine how this influences Aβ accumulation.

Here we provide experimental evidence of Aβ-dependent MVB enlargement as well as Aβ aggregation within late endocytic compartments of neurons. Consistent with the scenario of MVBs representing the site of initiation of Aβ aggregation, the accumulation of neuronal ESCRT components was evident in amyloid plaques. Moreover, dysfunction of ESCRT-III, modelled by dominant negative VPS4A (dnVPS4A) mimicked the Aβ accumulation and aggregation in MVBs as well as the enlarged late endosomal size seen in AD. These results support a novel scenario where a vicious cycle of ESCRT-dependent late endosomal dysfunction causes further Aβ accumulation as well as AD-pathogenic tau phosphorylation.

Methods

Cell culture

Primary neuronal cultures were generated from B6.Cg-Tg (APPswe, PSEN1dE9)85Dbo/Mmjax mice (APP/PS1) AD transgenic (tg) and wild-type (wt) mouse embryos. The APP sequence in APP/PS1 encodes a chimeric mouse/human APP (Mo/HuAPP695swe) that was humanized by modifying three amino acids, and introducing the Swedish AD mutation. The PS1 sequence encodes human presenilin 1 lacking exon 9 (dE9) that models AD-associated mutations in PS1. Both APPswe and PS1 are independently controlled by the prion protein promoter. Primary neuronal cultures were prepared from cortices and hippocampi of embryonic day 15 embryos as previously described [9]. In brief, E15 brain tissue was dissociated by trypsinization and trituration in DMEM with 10% fetal bovine serum (Gibco). Dissociated neurons were cultured on poly-D-lysine (Sigma) coated plates or glass coverslips (Bellco Glass Inc.) and were maintained until 12 and 19 DIV in neurobasal medium (Gibco), B27 supplement (Gibco), glutamine (Invitrogen) and antibiotics (ThermoScientific).

Wild type mouse N2a neuroblastoma cells (N2a) or N2a cells stably transfected with the 670/671 Swedish mutation human APP (Swe) [26] or wild-type α-synuclein with HA-Tag (α-syn) were grown on 10 cm dishes or coverslips.

Electron microscopy

Cells were grown on Thermanox coverslips (Nalgene, Nunc) and fixed with 2% PFA, 2.5% glutaraldehyde in 0.1 M cacodylate. Cells were then secondarily fixed with 1% osmium tetroxide followed by incubation with 1% tannic acid to enhance contrast. Cells were dehydrated using increasing percentages of ethanol before being embedded onto Epoxy resin (Agar scientific, UK) stubs. Coverslips were cured overnight at 65 °C. Ultrathin sections were cut using a diamond knife mounted to a Reichert ultracut S ultramicrotome and sections were collected onto copper grids. Grids were post-stained with drops of lead citrate. Sections were viewed on a FEI Tecnai transmission electron microscope (Eindhoven, The Netherlands) at a working voltage of 80 kV. BSA-gold was prepared as previously described [27]. For quantification of MVB diameter, MVBs

were defined as organelles containing intraluminal vesicles and monomeric rather than flocculated BSA-gold.

Aβ1-42 peptides (Sigma) were incubated at 37 °C for 1 h to induce fibril formation in vitro. Grids were inverted onto the drops of Aβ1-42, negatively stained with 2% uranyl acetate, washed with water and dried on filter paper before being viewed by EM.

Transfection and constructs

Cells were transfected using Lipofectamine 2000 (Invitrogen) for N2a cells or Lipofectamine 3000 (Invitrogen) for primary neurons. N2a cells were transfected in Opti-MEM while primary neurons were transfected directly in their growth medium. The plasmids p3xFLAG-CMV-10-hVPS4A-wt and p3xFLAG-CMV-10-hVPS4A-dn E228Q were generated as described [28]. The control plasmids p3xFLAG-CMV-7-BAP Control Plasmid was purchased from Sigma-Aldrich and pcDNA3-CMV-GFP from Addgene. pcDNA3-synapsin-FLAG-wtVPS4 and pcDNA3-synapsin-FLAG-dnVPS4 were constructed from pcDNA3-synapsin-FLAG and PCR products from the p3xFLAG-CMV-10-hVPS4A-wt and p3xFLAG-CMV-10-hVPS4A-dn respectively. Control plasmid pAAV-synapsin-GFP was purchased from Addgene.

Antibodies and reagents

The following antibodies were used (see also Additional file 1: Table S1): 369 [29] (Buxbaum et al., 1990) for Western blot (WB) 1:1000; 6E10 (BioLegend, previously Covance SIG-39320) IF: 1:500, WB 1:1000; 12F4 (BioLegend, previously Covance SIG-39142) for immunofluorescence (IF) 1:250; Amyloidβ (1-42) (IBL, 18,582); Amyloidβ (1-42) (Invitrogen, 700,254) IF 1:1000; beta-actin (Sigma, A 5316) WB 1:2000; CD63 (ThermoFisher Scientific, MAI-19281) WB 1:1000; CHMP2B (Abcam, ab33174) IF 1:250, WB 1:1000; Clavestin-1 + 2 (Bioss, bs-6569R-A647) IF 1:250; DAPI (Sigma, D9542) IF 1:2000; drebrin (Abcam, ab11068) IF 1:1000; FLAG (Biolegend, 637,302) IF 1:1000, (Sigma, F1804) WB 1:1000; Flotillin-1 (BD Biosciences, 610,821) IF 1:400; GM130 (BD Biosciences, 610,822) IF: 1:500; GSK3β (Cell Signaling Technology, 12,456) IF 1:400; pGSKα/β (Cell Signaling Technology, 9331S) WB 1:1000; HA-Tag (Cell Signaling Technology, 3724) WB 1:1000; Hrs and Hrs-2 (Enzo, ALX-804-382-C050) IF 1:100; LAMP1 (Abcam, ab24170) IF 1:1000; LAMP1 (Abcam, ab25245) IF: 1:1500; LC3β (Cell Signaling Technology, 2775) WB 1:1000; Amyloid fibrils OC (Merck Millipore, AB2286) IF 1:1000; P2:1 (ThermoFisher Scientific, OMA1-03132) IF 1:500; Phospho-tau pSer396 (ThermoFisher, 44-752G); Rab7 (Abcam, ab50533) IF 1:500; Synaptophysin (Merck Millipore, MAB5258) IF 1:1000; Tsg101 (Genetex, GTX70255) IF 1:250, WB 1:1000; VPS4 (SantaCruz, sc-133,122) IF 1:100, WB 1:1000; secondary antibodies conjugated to Alexa Fluor-488, −546, −647 (IF 1:500; Invitrogen) or to HRP (WB 1:2000; R&D Systems, Minneapolis, MN).

Bafilomycin A (Sigma), torin 1 (Tocris) or rapamycin (Fisher BioReagents) were added to pre-warmed culture media at appropriate concentrations. Starvation media for induction of autophagy was 33% Opti-MEM in Hank's Balance Salt solution (HBSS). Aβ1-40 or Aβ1-42 peptides (Tocris) were reconstituted in DMSO to 250 μM, sonicated for 10 min and followed by 15 min of centrifugation at 12 k rpm before adding the supernatant to the culture media for the depicted times. All experiments used 0.5 μM of Aβ1-40 or Aβ1-42, except for EM and LAMP-1 positive vesicle size experiments that used 5 μM and 1 μM respectively.

Cell immunofluorescence

Cultured neurons at 12 DIV or N2a cells were fixed in 4% paraformaldehyde (PFA) in phosphate buffered saline (PBS) with 0.12 M sucrose for 20 min, permeabilized and blocked in PBS containing 2% normal goat serum (NGS), 1% bovine serum albumin (BSA), and 0.1% saponin at room temperature (RT) for 1 h, and then immunolabelled in 2% NGS in PBS overnight at 4 °C. After appropriate washing, coverslips were mounted with SlowfadeGold (Invitrogen). Immunofluorescence was examined by confocal laser scanning microscopy (Leica TCS SP8 or Zeiss LSM 510). In multiple label experiments, channels were imaged sequentially to avoid bleed-through. Images were taken with Leica Confocal Software or Zeiss ZEN software and analysed with ImageJ or Imaris 7.6. LAMP1-positive vesicles in pyramidal neurons were quantified by measuring the diameter of the five largest LAMP1-positive vesicles per cell, imaged by confocal microscopy in z-stacks, (n= >45 LAMP1-positive vesicles). All fluorescent labelling of cells was performed $n \geq 3$; and in the case of primary neurons from different embryos.

Brain immunofluorescence

Mice were anesthetized with isoflurane and perfused transcardially with saline followed by 4% PFA in 0.1 M PBS (pH 7.4) at RT. After dissection, brains were postfixed by immersion in 4% PFA in 0.1 M PBS (pH 7.4) at 4 °C for 2 h or overnight. After fixation, brains were cut in 40 μm thick sections with a sliding microtome. Sections were kept in storage buffer composed of 30% sucrose and 30% ethylene glycol in PBS at −20 °C. Free-floating sections were blocked for 1 h in RT with serum and triton-X and then incubated in primary antibodies overnight at 4 °C, followed by appropriate fluorescent Alexa secondary antibodies for 1 h at RT.

Western blot

Medium was collected and centrifuged and cells were washed twice, harvested in ice cold PBS, and centrifuged. Cell pellets were lysed with 6% sodium dodecyl sulfate

(SDS) containing 10 μl/ml β-mercaptoethanol, sonicated, and then heated at 95 °C for 6 min. After centrifugation, supernatants and medium were mixed with loading buffer, heated at 95 °C for 5 min and loaded into 10–20% Tricine gels (Invitrogen). Samples were subjected to electrophoresis and transferred to polyvinylidine difluoride membranes (Millipore). Membranes were blocked in PBS containing 0.1% Tween-20 (PBST) and 5% milk, and incubated in primary antibodies overnight and then with HRP-conjugated secondary antibodies for 1 h diluted in PBS containing 0.1% Tween-20 (PBST) and 5% milk. The immunoreaction was visualized by a chemiluminescence system (Pierce or BioRad). Bands were quantified using Image Lab (Bio-Rad Laboratories). For visualization of Aβ, membranes were boiled in PBS for 5 min prior to blocking. For analysis of exosomes, WB was performed as above but without β-mercaptoethanol in the 6% SDS lysis buffer.

For analysis of LC3β cells were lysed in RIPA buffer (Thermo Fisher Scientific) with protease inhibitor and phosphatase inhibitor (Thermo Fisher Scientific). Lysates with NuPAGE LDS sample buffer and NuPAGE reducing agent were loaded on NuPAGE 4-12% BisTris gels and run with NuPAGE MES SDS buffer (Invitrogen).

For analysis of α-synuclein in medium, total protein was extracted using a trichloroacetic acid (TCA)/acetone precipitation protocol. Briefly, freshly collected samples were cleared by centrifugation at 10000 rpm for 10 min to pellet debris and intact cells. The supernatant was transferred to a new tube and added with ¼ volume of ice-cold 20% TCA followed by incubation on ice for 3 h. The proteins were pelleted by centrifugation at 14000 rpm and washed twice with cold acetone.

For native conditions, cell pellets were lysed on ice in NativePAGE sample buffer (1X, Life Technologies) containing 1% digitonin (Life Technologies) and Halt proteinase inhibitor cocktail (1X, Thermo Scientific) by pipetting up and down and incubating on ice for 15 min. Lysates were centrifuged at 20000 x g for 30 min at 4 °C and protein concentrations of the supernatants were determined with BCA assay. Equal amounts of protein were loaded on a 3-12% NativePAGE Novex Bis-Tris gel (Life Technologies).

Exosome isolation and analysis

Exosomes were purified from cell culture medium by differential ultracentrifugation as described previously [30]. Briefly, Swe N2a cells were cultured and transfected for 48 h in exosome-free medium. Collected medium was depleted of cells and cellular debris by sequential low speed centrifugation. Exosomes were then isolated by centrifugation of the collected supernatant at 100,000×g at 4 °C for 70 min. The resultant pellet was washed in PBS and centrifuged for 70 min at 100,000×g at 4 °C.

Statistical analysis

Statistical analysis was performed with PRISM 6 software (Graph-Pad Software, San Diego, CA, USA) by using unpaired t-test or ANOVA with Tukey's multiple comparisons test or ANOVA with Dunnett's multiple comparisons test. All data are expressed as the mean ± SD. Differences were considered significant at $^{*}p < 0.05$, $^{**}p < 0.01$, $^{***}p < 0.001$, $^{****}p < 0.0001$.

Results

Aβ-dependent MVB enlargement

Endogenous Aβ42 is present in both dendrites and axons of cultured primary APP transgenic neurons and localizes especially with markers of late endosomes/MVBs [21]. In order to examine whether increased levels of Aβ can lead to the enlarged endosomal phenotype seen in AD, MVB size was compared between APP/PS1 transgenic and wt primary mouse neurons. Cells were incubated with BSA-gold 2 h (h) before fixation to confirm identity of the endocytic compartments. Remarkably, electron micrographs showed a significantly greater MVB diameter (52% increase; $p < 0.001$) in APP/PS1 transgenic compared to wt neurons at 12 days in vitro (DIV) (Fig. 1a and b) consistent with the larger diameter of endosomes described in human AD. Since full length APP, β-CTFs, Aβ and the presenilin mutation in the APP/PS1 transgenic neurons potentially all could be the cause of this effect, wt neurons at 12 DIV were treated with freshly prepared human synthetic Aβ1-40 or Aβ1-42 for 48 h, to test if Aβ was sufficient to induce the endosomal enlargements. The neurons demonstrated a 69% and 114% increase in the diameter of MVBs with Aβ1-40 or Aβ1-42 treatment, respectively ($p < 0.001$; Fig. 1c and d) as measured on EM images compared to controls. Further, an increased size by 165% of LAMP1-positive late endosomes/lysosomes was already evident by immunofluorescent labelling at 3 h in pyramidal neurons treated with Aβ1-42 ($p < 0.0001$, Fig. 1e and f). LAMP1-changes at different time points of Aβ1-42 treatment, ranging from 30 s to 48 h, are shown in Additional file 2: Figure S1B. Taken together, our results indicate that enlarged MVBs, one of the earliest pathological features in AD, can be caused by Aβ, which however does not rule out important contributions also of other APP components such as β-CTFs.

Fibril-like structures in endocytic organelles of wild-type neurons treated with Aβ

Interestingly, fibril-like structures were apparent by EM in endocytic organelles of wt primary neurons incubated with synthetic human Aβ1-42 for 48 h that were not seen in untreated neurons (Fig. 2a), and were more prominent in neurons treated with Aβ1-42 than Aβ1-40. For comparison, Aβ1-42 fibrilized in vitro showed similar size and morphology of fibrils on EM as in the endocytic vesicles

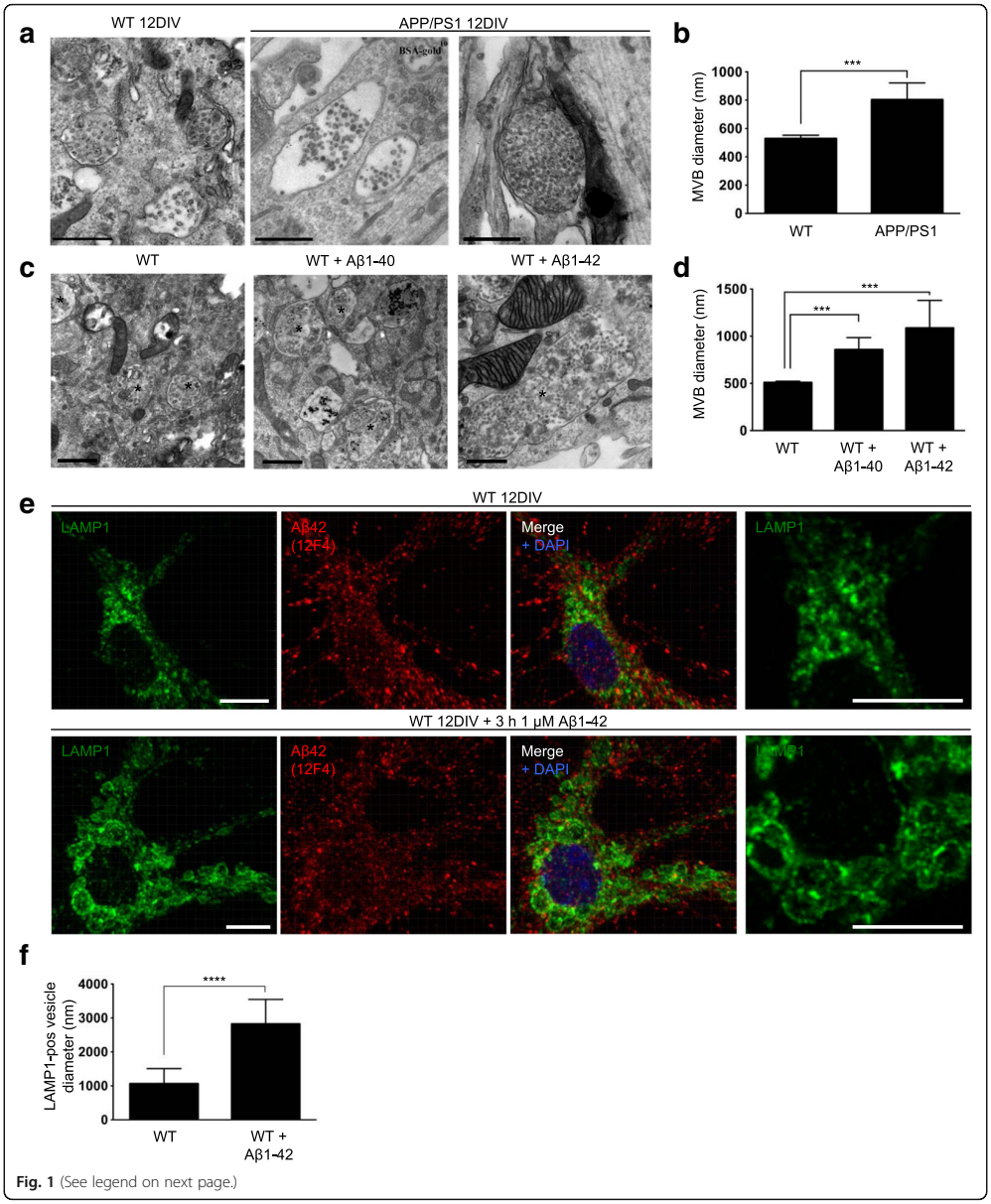


Fig. 1 (See legend on next page.)

(See figure on previous page.)
Fig. 1 Aβ increases MVB diameter in primary neurons. **a** Electron microscopy reveals that APP/PS1 AD transgenic compared to wt mouse primary neurons have significantly larger MVBs at 12 DIV. Scale bar 500 nm. **b** Quantification of A shows an increase of 52% in MVB diameter in Tg compared to wt neurons, $n > 94$ MVBs per group; *** $p < 0.001$. **c** Exogenously added monomeric Aβ1-40 or Aβ1-42 to wt primary neurons at 12 DIV leads to increased MVB diameter at 48 h on EM images. MVBs are marked with an asterisk. Scale bar 500 nm. **d** Quantification of C, $n > 45$ MVBs per group; *** $p < 0.001$. **e** Shorter time-points of exogenously added monomeric Aβ1-42 already leads to increased size of LAMP1-positive vesicles 3 h after treatment in wt mouse neurons at 12 DIV; 3D-rendering with Imaris from confocal z-stack. High magnification image of LAMP1 labelling from a single focal plane to the right. Scale bar 10 μm. **f** Quantification of E shows significant increase in diameter of LAMP1-positive vesicles after addition of Aβ. The diameters of the five largest LAMP1-positive vesicles per pyramidal neuron were measured in the z-stacks; $n > 10$ neurons per treatment; **** $p < 0.0001$

(Fig. 2b). Loss of endolysosomal impermeability was also seen with Aβ1-42 treatment of neurons with BSA-gold leaking out into the cytoplasm (Fig. 2c). To further investigate the fibril-like structures, wt murine neurons were treated with elevated levels of human Aβ1-42 at different time points and immunolabelled with the conformational dependent Aβ antibody OC to label amyloid fibrils and fibrillar oligomers [31] and antibody 6E10 to specifically label the added human Aβ. Using the same parameters as in the EM experiments, neurons treated with Aβ1-40 only led to weak OC antibody labelling compared to vehicle treated cells, while Aβ1-42 treated neurons showed robust OC labelling (Additional file 3: Figure S2).

Already at 45 min of treatment with 0.5 μM Aβ1-42 (Fig. 2d) and up to 24 h of incubation, antibodies OC and 6E10 revealed an almost completely overlapping vesicular pattern of labelling, indicating that the amyloid fibrils and/or fibrillar oligomers consisted of Aβ1-42, which was particularly prominent along neuronal processes. Of note, OC labelling increased in intensity with time of treatment with Aβ1-42. Interestingly, at 48 h the OC positive structures were enlarged and elongated, displaying a part that was human Aβ antibody 6E10 positive and an extension that was 6E10 negative (Fig. 2e). Surface labelling of non-permeabilized cells revealed that the elongated OC labelling at 48 h was now to a certain extent extracellular, whereas the punctate OC and 6E10 co-labelling at 24 h was generally intracellular (Fig. 2f). This suggests that with time, fibrils extend out of neurites into the extracellular space and/or that organelles containing the fibrils fuse with the plasma membrane. To better define the subcellular site of Aβ aggregation, cells were double labelled with OC antibody and the late endosomal/lysosomal marker LAMP1. At 45 min colocalization with OC was evident in small LAMP1-positive vesicles in the processes but not in the larger LAMP1-positive vesicles in the cell soma (Additional file 4: Figure S3A). Since lysosomes normally do not localize to axons and dendrites, other than their very proximal part, this suggests that Aβ42 starts to aggregate in late endosomes/MVBs of neurites. At 48 h, OC and LAMP1 still colocalized mainly in neuronal processes, but in LAMP1-positive structures that now appeared somewhat enlarged and irregular in their shape. Elongated OC-positive structures could be seen extending out from the more punctate LAMP1 labelling (Fig. 2g and Additional file 4: Figure S3A). The late endosomal marker Rab7 indicated that at least a subset of the vesicular OC labelling at 24 h colocalized with Rab7 positive late endocytic compartments in neurites (Additional file 4: Figure S3C). Taken together these data indicate that Aβ1-42 can be taken up by neurons in culture and forms amyloidogenic fibrils and/or fibrillar oligomers in late endocytic compartments particularly within neuronal processes that eventually appear to extend extracellularly.

Aβ1-42 induces changes in the native state of ESCRT-III complex component CHMP2B

Given prior evidence supporting that sorting via the MVB pathway was impaired by Aβ accumulation in cultured AD transgenic neurons and that Aβ dependent translocation into MVBs seemed affected [21], we next investigated possible dysfunction of the ESCRT pathway in models of AD. In APP/PS1 transgenic primary neurons Aβ42 was found associated with CHMP2B-positive vesicles (Fig. 3a). In young 3-month-old Tg19959 mice, a different transgenic mouse model of β-amyloidosis harbouring the Swedish and Indiana APP mutations, CHMP2B immunolabelling was most prominent in the area of hippocampus and entorhinal cortex that also expressed increased levels of Aβ/APP (Additional file 5: Figure S4A-B). Although levels of total CHMP2B and VPS4 were not significantly changed in wt compared to APP/PS1 primary neurons lysed in 6% SDS (Additional file 5: Figure S4C), levels of high molecular weight complexes of CHMP2B on blue native polyacrylamide gel electrophoresis were increased in APP/PS1 neurons treated with Aβ1-42 for 3 h (Fig. 3b). Other ESCRT proteins were not resolved on native gels, likely due to masking of antibody epitopes under native conditions.

ESCRT components localize to amyloid plaques

Since AD transgenic neurons showed an increased diameter of MVBs and treatment with Aβ1-42 led to prominent fibril-like structures in late endocytic organelles, and as prior immuno-EM work has indicated early Aβ accumulation in dystrophic neurites [10], we next examined whether aggregating Aβ42 in endosomes might lead to the presence of ESCRT components in amyloid plaques. Indeed, APP/PS1 transgenic mice with plaque pathology demonstrated that the ESCRT-III associated protein VPS4

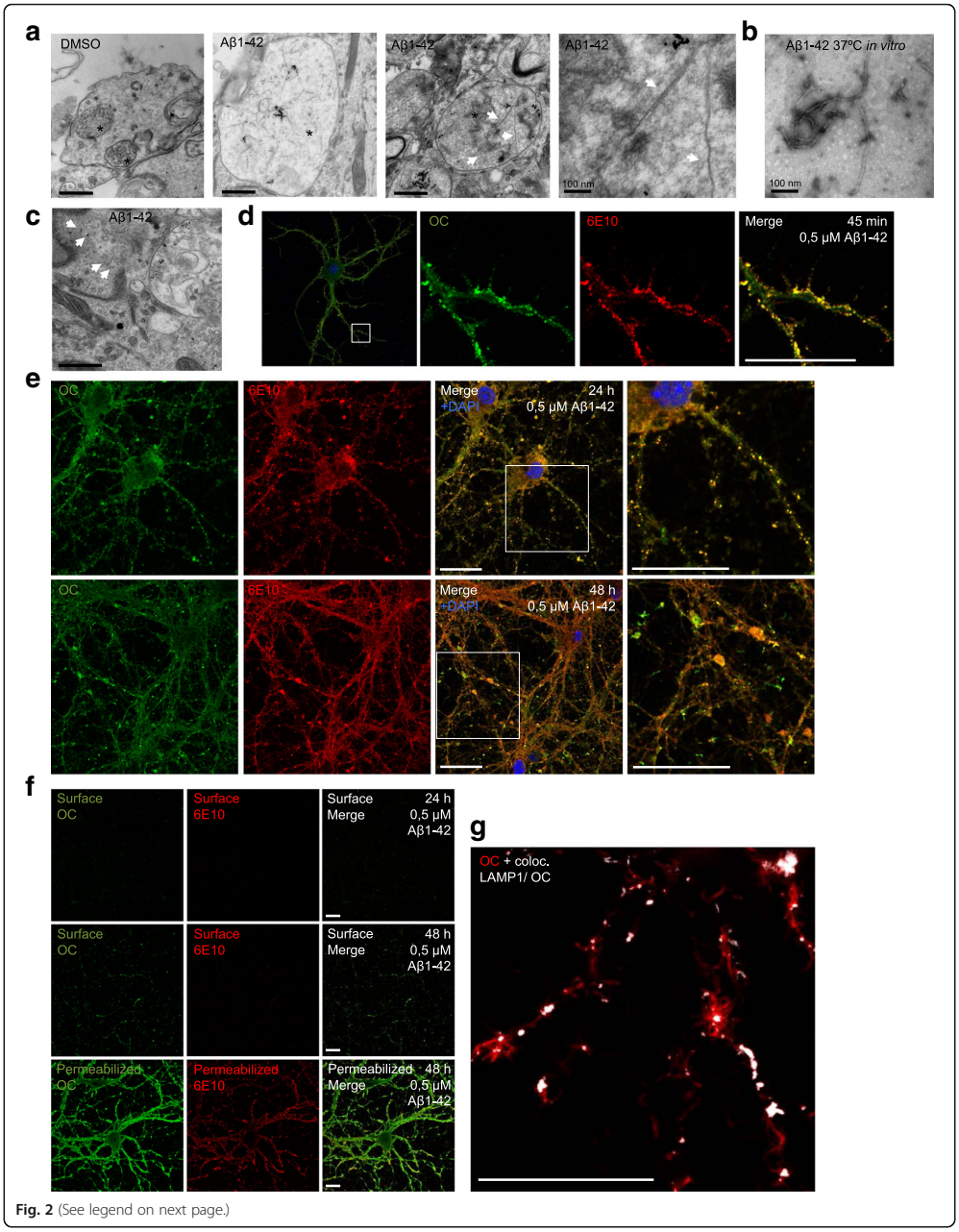


Fig. 2 (See legend on next page.)

(See figure on previous page.)
Fig. 2 Fibril-like structures in endocytic organelles of wild-type neurons treated with Aβ1-42. **a** Wt primary neurons treated at 12 DIV with Aβ for 48 h induced fibril-like structures in endocytic organelles with Aβ1-42. BSA-gold was added to cells 2 h before fixation to delineate endocytic organelles (*marked with asterisk*). Scale bar 500 nm. High magnification image to the right, scale bar 100 nm. **b** Aβ1-42 peptides incubated in vitro at 37 °C for 1 h to induce fibril formation, imaged with EM. Scale bar 100 nm. **c** BSA-gold (white arrows) was found in the cytosol in Aβ1-42 treated neurons, indicating loss of endolysosomal impermeability due to Aβ1-42. Scale bar 500 nm. **d** OC antibody labelling for fibrillar oligomers and/or fibrils is seen in a vesicular pattern in processes after 45 min treatment with 0.5 μM of Aβ1-42 and colocalizes with human Aβ antibody 6E10 confirming that fibrils consist of the added human Aβ1-42. Scale bar 10 μm. **e** Feeding 0.5 μM of Aβ1-42 to wt primary neurons at 12 DIV at 24 h vs 48 h. At 24 h most of the OC labelling was also antibody 6E10 positive. At 48 h the outer aspects of OC positive structures were 6E10 negative. Scale bar 20 μm. **f** Weak surface labelling of non-permeabilized neurons shows that OC and 6E10 antibody positive structures were intracellular after 24 h of treatment with Aβ1-42 (*upper panel*). At 48 h extracellular OC antibody labelling was now more visible consistent with penetration of the plasma membrane by the elongated OC positive fibrils (*middle panel*). Strong OC and 6E10 antibody labelling of permeabilized cells after fixation but before immunolabelling, shows that the vast majority of added human Aβ1-42 (antibody 6E10) and OC antibody positive fibrils and/or fibrillar oligomers are inside neurons (*lower panel*). Scale bar 20 μm. **g** After 48 h of treatment with 0.5 μM Aβ1-42, OC antibody labelling was seen extending out from LAMP1-positive structures in the processes. The image shows OC with the superimposed colocalizing channel for LAMP1 and OC. For the complete image with separate channels see Additional file 3: S2A. Scale bar 20 μm

was markedly increased in plaques (Fig. 3c and Additional file 5: Figure S4D), where it partially colocalized with Aβ42. ESCRT–I component Tsg101, a marker of MVBs, also showed increased labelling in plaques (Fig. 3d). In contrast, labelling of CHMP2B and the earlier ESCRT-0 component Hrs appeared decreased in plaques compared to surrounding brain parenchyma (Additional file 5: Figure S4E-F). Brain sections were also co-labelled with an antibody against clavestin-1 and 2 (Fig. 3d), which are neuron-specific proteins in the endo-lysosomal pathway [32]. The strong colocalization between Tsg101 and clavesin-1 and 2 in amyloid plaques supports the neuronal origin of ESCRT components in plaques. Moreover, much of the strong Aβ42 labelling outside of plaques in AD transgenic brain occurred in vesicle-like structures of dystrophic neurites that also contained clavesin-1 and 2 and Tsg101, consistent with accumulation of Aβ42 within endosomal compartments of neurons. To confirm these results in a different AD transgenic mouse model of β-amyloidosis, Tg19959 mice were examined with the onset of plaque pathology. In early plaques of 3-month-old Tg19959 mice Tsg101 (Fig. 3e) and VPS4 (not shown) also colocalized strongly with Aβ42.

Blocking VPS4A increases intracellular accumulation and decreases secretion of Aβ

In order to model the effect of dysfunctional ESCRT-dependent MVBs on Aβ accumulation, a dominant negative, E228Q ATPase-deficient form of VPS4A (dnVPS4A) was expressed for 24 h in N2a neuroblastoma cells harbouring stably transfected human Swedish mutant APP. N2a cells were used here because of their high transfection efficiency compared to primary neurons. To assess that N2a cells react to Aβ1-42 in a similar manner as primary neurons, N2a cells were treated with exogenously added Aβ1-42 for different time points. N2a cells treated with Aβ1-42 also exhibited increased size of LAMP1-positive vesicles (Additional file 6: Figure S5). The ATPase VPS4 is a key component of the ESCRT machinery as it is the only energy-consuming enzyme, promotes disassembly and recycling of ESCRT-III oligomers, and is recruited to the ESCRT-III complex by direct interaction with CHMP2B. We found that the expression of dnVPS4A markedly increased the intracellular pool of Aβ by 424% ($p < 0.001$, Fig. 4a and d) while concurrently decreasing the amounts of Aβ secreted into the medium by 87% ($p < 0.0001$, Fig. 4c and d). DnVPS4A also increased higher molecular weight bands between 17 kDa and 34 kDa that might represent Aβ oligomers within cells (Fig. 4a) as they were not seen with C-terminal specific APP antibody 369 (Fig. 4b). In addition, dnVPS4A increased the levels of APP within cells by 149% ($p < 0.05$) and secreted APPα in conditioned media by 149% ($p < 0.05$). Overexpression of wild type VPS4A (wtVPS4A) also significantly reduced secretion of Aβ by 72% ($p < 0.001$), although not to the extent of the dominant negative construct. Such a partially dominant negative effect of over-expressing wtVPS4 has been described [28].

Confocal immunofluorescence microscopy of Swe N2a cells transfected with dnVPS4A confirmed the increase of Aβ and full-length APP (Fig. 4e). Increased labelling by immunofluorescent microscopy with the conformational antibody OC in dnVPS4A-transfected cells confirmed the increase in Aβ oligomers and showed that the fibrillar oligomers and/or fibrils labelled by antibody OC colocalized with enlarged vesicles labelled positive for dnVPS4A protein and flotillin-1 (Fig. 4f and g). Triple labelling revealed that Aβ42 accumulated in enlarged vesicles positive for the MVB marker Tsg101 in dnVPS4A expressing cells labelled by the FLAG-tag (Fig. 4h). Thus, dysfunctional MVBs accumulate Aβ42 that, at least in part, is in an oligomeric and/or fibrillar form. In contrast to effects on Aβ and in agreement with a prior report [28], dnVPS4A increased secretion of α-synuclein in α-syn N2a cells without altering the total pool of intracellular α-synuclein (Additional file

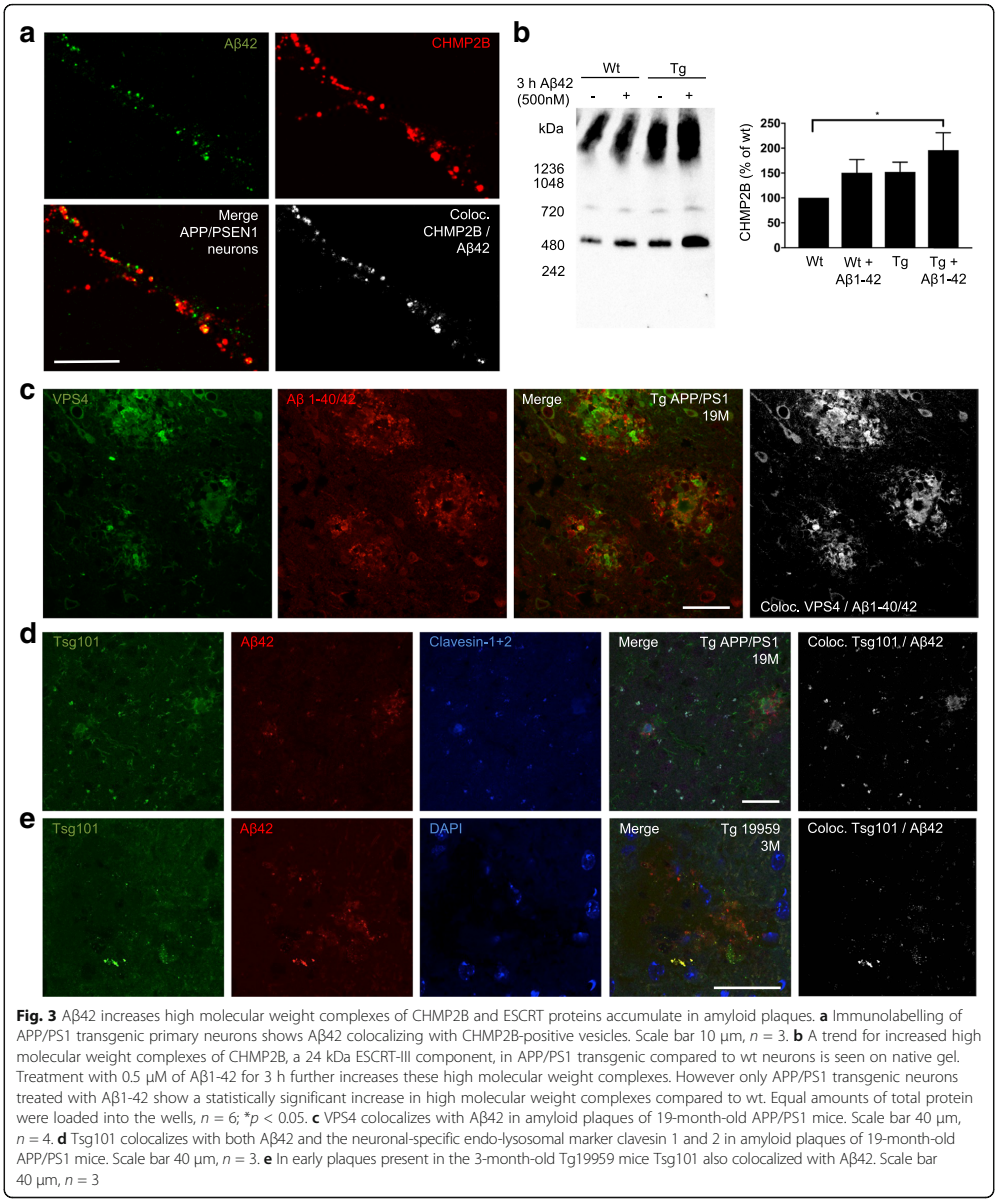


Fig. 3 Aβ42 increases high molecular weight complexes of CHMP2B and ESCRT proteins accumulate in amyloid plaques. **a** Immunolabelling of APP/PS1 transgenic primary neurons shows Aβ42 colocalizing with CHMP2B-positive vesicles. Scale bar 10 μm, $n = 3$. **b** A trend for increased high molecular weight complexes of CHMP2B, a 24 kDa ESCRT-III component, in APP/PS1 transgenic compared to wt neurons is seen on native gel. Treatment with 0.5 μM of Aβ1-42 for 3 h further increases these high molecular weight complexes. However only APP/PS1 transgenic neurons treated with Aβ1-42 show a statistically significant increase in high molecular weight complexes compared to wt. Equal amounts of total protein were loaded into the wells, $n = 6$; $^*p < 0.05$. **c** VPS4 colocalizes with Aβ42 in amyloid plaques of 19-month-old APP/PS1 mice. Scale bar 40 μm, $n = 4$. **d** Tsg101 colocalizes with both Aβ42 and the neuronal-specific endo-lysosomal marker clavesin 1 and 2 in amyloid plaques of 19-month-old APP/PS1 mice. Scale bar 40 μm, $n = 3$. **e** In early plaques present in the 3-month-old Tg19959 mice Tsg101 also colocalized with Aβ42. Scale bar 40 μm, $n = 3$

7: Figure S6). Since the CMV-FLAG-dnVPS4A induced toxicity in primary neurons, we constructed a plasmid under the weaker synapsin promoter. Expressing dnVPS4A under this synapsin promoter in wt or APP/PS1 primary neurons showed increased labelling of Aβ42 (Fig. 4i), supporting that dysfunctional ESCRT-dependent MVB formation leads to increased levels of Aβ within neurons.

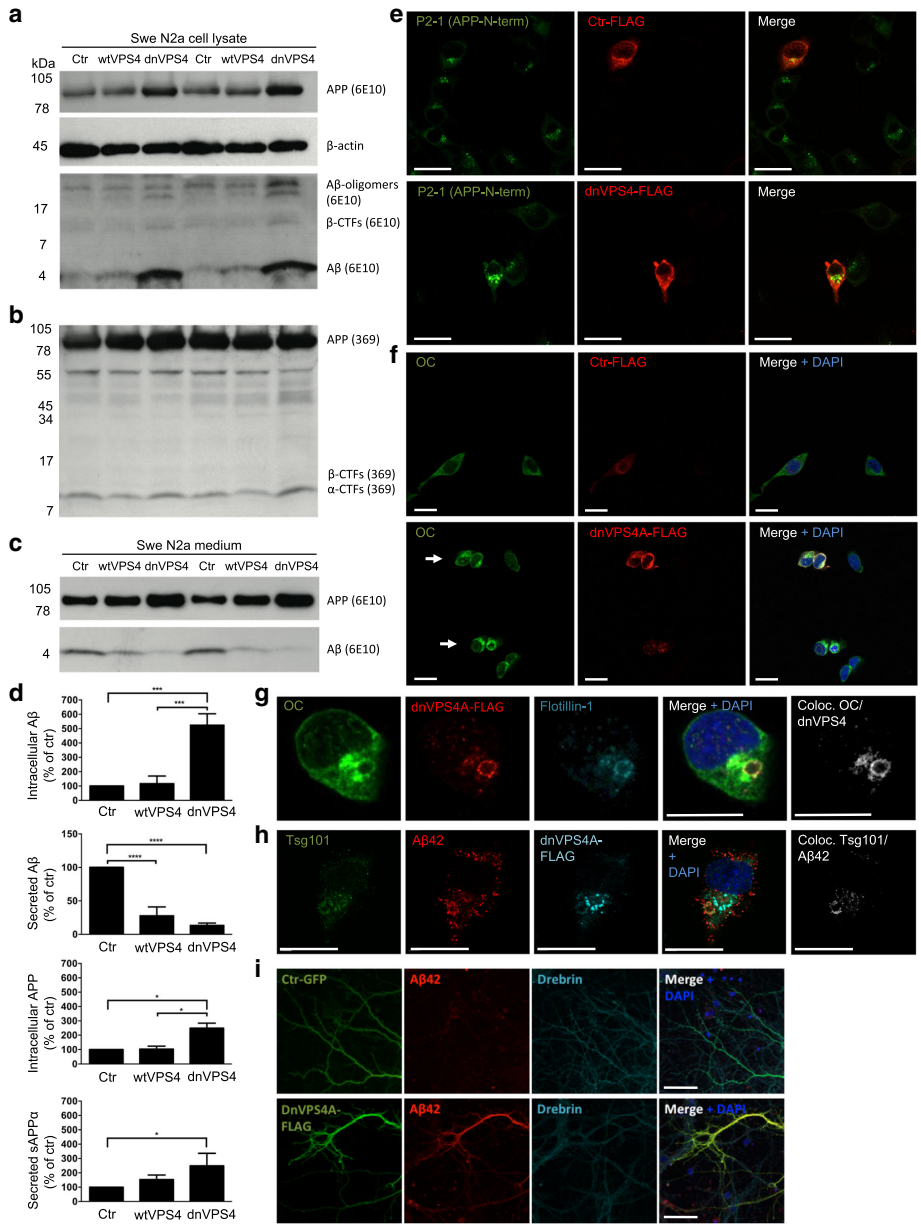


Fig. 4 (See legend on next page.)

(See figure on previous page.)
Fig. 4 DnVPS4A causes increased accumulation and reduced secretion of Aβ42. Expression of control plasmid (ctr), wtVPS4A (wtVPS4) or the ATP hydrolysis deficient mutant dnVPS4A (dnVPS4) in Swe N2a cells (A-H) or wt primary mouse neurons (I) for 24 h. **a** Representative Western blot of APP, SDS-stable oligomeric Aβ species, β-CTFs and monomeric Aβ in cell lysate probed with antibody 6E10, and β-actin for protein normalization. **b** Western blot analysis of full length APP, β-CTFs and α-CTFs in cell lysate probed with the C-terminal specific APP antibody 369. **c** Western blot analysis of secreted αAPP (sAPPα) and Aβ in cell medium with antibody 6E10. **d** Densitometric quantification of A and C demonstrates that expression of dnVPS4, but not wtVPS4, increases intracellular Aβ compared to ctr. On the other hand, both wtVPS4A and dnVPS4A reduces secreted Aβ compared to ctr, although to a greater extent with dnVPS4A. DnVPS4 increases both cellular and secreted APP. Values are normalized against actin and expressed as percentage of control, $n > 3$; $^{*}p < 0.05$, $^{**}p < 0.01$, $^{***}p < 0.001$, $^{****}p < 0.0001$. **e** Cellular full length APP is increased in cells transfected with dnVPS4A-FLAG (lower panel) compared to control plasmid Ctr-FLAG (*upper panel*). Scale bar 25 μm. **f** Antibody OC labelling of fibrillar oligomers and fibrils is increased in cells transfected with dnVPS4A (*arrows*) compared to control plasmid. Scale bar 25 μm. **g** Antibody OC labelling in dnVPS4-transfected cells is associated with enlarged vesicles positive for flotillin-1. Scale bar 15 μm. **h** Aβ42 accumulation in vesicles positive for ESCRT protein Tsg101 in dnVPS4A-transfected cells. Scale bar 25 μm. **i** Wt primary neurons at 12 DIV transfected with synapsin-dnVPS4A-FLAG or control synapsin-GFP plasmid for 24 h, immunolabelled for Aβ42 and the post-synaptic protein drebrin shows that Aβ42 labelling is increased with expression of dnVPS4A but not with control plasmid. Scale bar 50 μm

Increased cellular levels of Aβ with dysfunctional MVBs is mimicked by inhibiting lysosomal degradation

The increased intracellular levels of Aβ with dnVPS4A could be due to changes in the production of Aβ, reduced secretion and/or reduced fusion of MVBs with the lysosome for degradation. In order to investigate the turnover of APP and Aβ, Swe N2a were treated with the protein synthesis inhibitor cycloheximide (Additional file 8: Figure S7A-B and Additional file 9: Figure S8D). This revealed a rapid turnover of APP in cell lysates with a half-life of about 45 min, while cellular Aβ had a half-life of about 4 h. In contrast, the degradation of APP and Aβ in conditioned media was slower, not reaching 50% of control levels within 6 h of cycloheximide treatment. To investigate the role of lysosomal degradation, Swe N2a cells were treated for 24 h with 5 nM bafilomycin A1 (BafA1), which inhibits the vacuolar H+ ATPase. BafA1 treatment had the same effects on Aβ as dnVPS4A, markedly increasing intracellular levels of Aβ and reducing the secretion of Aβ (Fig. 5a-b and Additional file 9: Figure S8A-D). These results suggest that dnVPS4A blocks MVBs with Aβ on route to lysosomes for degradation. Consistently, when the endo-lysosomal pH gradient was blocked with BafA1, dnVPS4A transfected cells no longer showed higher cellular levels of Aβ than the wtVPS4A or GFP transfected cells (Fig. 5c). Hence, when the ability of lysosomes to degrade Aβ is abolished, blocking Aβ on route to the lysosomes via dnVPS4 does not lead to further Aβ accumulation.

To investigate the secretion of Aβ via fusion of MVBs with the plasma membrane and concomitant release of exosomes, exosomes from dnVPS4A-transfected Swe N2a cells were isolated and analysed (Fig. 5d). Secretion of exosomes was not prevented but instead increased by dnVPS4A in Swe N2a cells, possibly due to upregulation of ESCRT independent (CD63 dependent) MVB formation [33–35].

Blocking ESCRT dependent ILV formation increases pathological tau phosphorylation

A major question in AD is how Aβ links to tau pathology. MVBs are necessary for the sequestration of GSK3 [36] which phosphorylates tau at serine 396 (S396). Both elevated tau phosphorylation at S396 [37] and hyperactive GSK3 is implicated in AD [38, 39]. Therefore, we examined the effects of dnVPS4A on tau phosphorylation. Tau phosphorylation at residue S396 was significantly increased by 56% with dnVPS4A ($p < 0.05$; Fig. 6a and b), suggesting increased activation of GSK3β and increased GSK3β dependent phosphorylation of tau caused by dysfunctional ESCRT dependent MVBs. Immunofluorescence microscopy revealed increased GSK3β labelling of cells upon dnVPS4A transfection (Additional file 10: Figure S9A), although changes in total GSK3β or phosphorylated GSK3α/β (S21/9) levels were not detected by Western blot in cell lysates of Swe N2a cells transfected with dnVPS4A (Additional file 10: Figure S9B). One possible explanation for this apparent discrepancy is that the active GSK3β in the cytosol and early endosomes (facing the cytosol) is easier to visualize with immunofluorescence than the sequestered GSK3β inside the ILVs of MVBs.

Autophagy induction partially rescues the intracellular accumulation of Aβ

Since autophagic organelles are markedly increased in AD and autophagy is thought to be impaired in the disease [14], we next examined LC3β-II and p62, markers of autophagy, in dnVPS4A transfected cells accumulating intracellular Aβ. Expression of dnVPS4A in Swe N2a cells showed increased levels of LC3β-II, which correlate with increased numbers of autophagosomes in the cell, by 35% ($p < 0.05$, Fig. 7a) and increased levels of p62 by 52% ($p < 0.05$, Fig. 7b). Inducing autophagy by 1 μM Rapamycin ($p < 0.01$, Fig. 7c), 250 nM Torin1 or starvation (Fig. 7d) reduced the dnVPS4A-induced increase in intracellular Aβ. Thus, in the setting of dysfunctional MVBs with Aβ that is inefficiently trafficked to

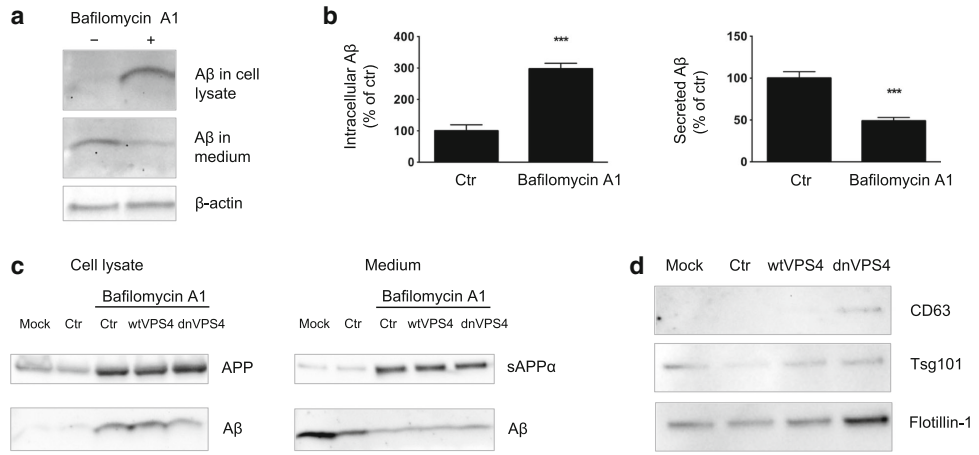


Fig. 5 Increased cellular levels of Aβ with dnVPS4A expression is consistent with decreased lysosomal degradation. **a** Bafilomycin A1 (BafA1) treatment had similar effects on Aβ as dnVPS4a, markedly increasing intracellular levels of Aβ and reducing Aβ secretion. Representative Western blot analysis of cell lysates and cell medium from Swe N2a cells treated with 5 nM BafA1 for 24 h and blotted for 6E10 for Aβ and β-actin. **b** Densitometric quantification of A. Values are normalized against actin and expressed as percentage of untreated control, $n = 3$, *** $p < 0.001$. **c** When the ability of lysosomes to degrade Aβ is abolished by BafA1, blocking Aβ on route to the lysosomes via dnVPS4 does not lead to further Aβ accumulation. Representative Western blots are shown of lysates (*left*) and medium (*right*) from Swe N2a cells treated with 5 nM BafA1 6 h after transfection with mock (no plasmid), control plasmid ctrGFP, wtVPS4A or dnVPS4A. Cells were collected 24 h post-transfection, $n = 3$. **d** Western blot analysis of isolated exosomes secreted from Swe N2a cells transfected with mock (no plasmid), ctrGFP, wtVPS4 or dnVPS4 for 48 h. Representative blots demonstrate that exosome secretion is not reduced with dnVPS4. Instead, increased amounts of CD63, an exosomal marker postulated to be involved in ESCRT independent ILV formation, is seen in the exosomal fraction from dnVPS4 transfected cells. Flotillin-1, an exosomal marker associated with cholesterol-enriched lipid rafts is also increased in the exosomal fraction from dnVPS4 transfected cells, while the ESCRT-I protein and exosomal marker Tsg101 is not changed, $n = 3$

lysosomes for degradation and/or inefficiently secreted, stimulation of autophagy is associated with decreased cellular Aβ.

Discussion

Over the past years, the view of the role of Aβ in the pathogenesis of AD has been changing. Rather than merely aggregation of extracellular Aβ, a complex and interrelated biology of intra- and extra-cellular pools of Aβ has emerged. Progressive intraneuronal Aβ accumulation and impaired secretion of Aβ were reported in AD transgenic neurons with time in culture [9, 40] and plaque-independent, Aβ-dependent synapse damage and memory impairment correlated with this intracellular pool of Aβ but not plaques in AD-transgenic mice [41]. Our working hypothesis is that dystrophic neurites with accumulating intraneuronal Aβ, initially within MVBs, are a nidus of plaque formation [10], with an important contribution of secreted Aβ originating also from hyperactive neurons.

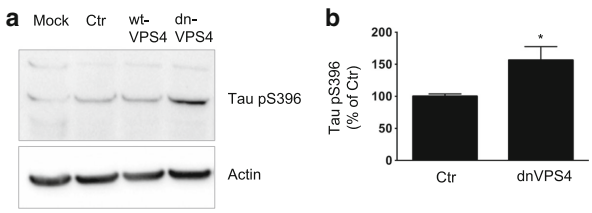


Fig. 6 Blocking ESCRT dependent ILV formation increases tau phosphorylation at serine 369 (S396). **a** Western blot of transfected N2a Swe cells demonstrates increased tau phosphorylation at S396 with expression of dnVPS4A. **b** Quantification of A shows a 56% increase in levels tau phosphorylated at S396 with dnVPS4A; values are normalized against actin and expressed as percentage of ctrGFP, ($n = 5$, *$p < 0.05$)

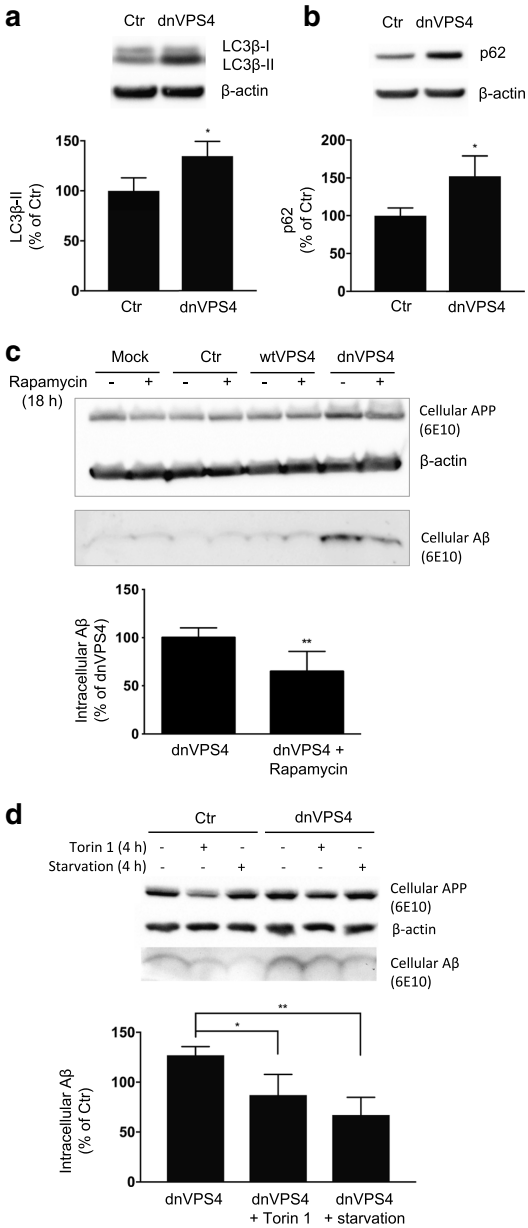


Fig. 7 (See legend on next page.)

(See figure on previous page.)
Fig. 7 Induction of autophagy partially rescues dnVPS4A induced intracellular accumulation of Aβ. **a** Expression of dnVPS4A increases levels of LC3β-II, an indicator of autophagy, by 35% ($n = 3$, $^{*}p < 0.05$). Representative blot (above) and quantification (below); values are normalized against actin and expressed as percentage of ctrGFP. **b** dnVPS4A increases levels of p62, an indicator of autophagy, by 52% ($n = 3$, $^{**}p < 0.01$). Representative blot (above) and quantification (below); values are normalized against actin and expressed as percentage of ctrGFP. **c** Chemically induced autophagy by Rapamycin partially rescues the increase in intracellular Aβ from dnVPS4A. 6 h after transfection Swe N2a cells were treated with 1 μM Rapamycin and harvested 24 h post-transfection. Representative blot (above) and quantification (below) demonstrating 35% reduction in intracellular Aβ by Rapamycin on dnVPS4 transfected cells. Values are normalized against actin and expressed as percentage of dnVPS4 ($n = 6$, $^{**}p < 0.01$). **d** Induced autophagy by torin 1 or by starvation significantly reduces intracellular Aβ to levels in dnVPS4 transfected cells. Values are normalized against actin and expressed as percentage of control transfected cells ($n = 3$, $^{*}p < 0.05$, $^{**}p < 0.01$)

Here we provide novel molecular insights into endosomal alterations with AD pathogenesis. Enlarged endosomes have been observed to be among the earliest cellular changes in AD and the related AD pathology that develops in Down syndrome [12]. It has been reported that the enlarged phenotype in early endosomes and lysosomes in AD is independent of Aβ and instead only dependent on APP β-CTFs [42, 43]. We now provide evidence that MVB size is increased in AD transgenic neurons, and that this phenotype of increased late endosomal size can be recapitulated in wt neurons with addition of exogenous Aβ. These data support that Aβ can induce endosomal enlargement, but do not exclude an important role also for APP β-CTFs. Although we only measured the size of MVBs with EM, it is likely that also other endocytic compartments including lysosomes and early endosomes were affected. The large LAMP1-positive vesicles seen and measured on confocal images (Fig. 1f) with Aβ treatment, likely also include lysosomes and autolysosomes.

We show by EM fibrillar-like structures inside abnormal MVBs/late endocytic/lysosomal compartments in neurons treated with Aβ1-42, and immunofluorescent labelling further indicates that MVBs/late endocytic compartments contain aggregated Aβ1-42. We cannot fully exclude the possibility that these aggregates begin to form in the cell culture medium and then are taken up by the cells. However, the acidic pH environment and high peptide concentration in a limited space promote amyloid aggregation [44], a milieu that is found inside MVBs. In line with this, it was shown in SHSY5Y cells that synthetic Aβ1-42 added to cell culture medium at 1 μM was taken up and formed aggregates of Aβ inside these cells, while only monomers could be found in the cell culture medium even after 5 days [45]. Overall, these results are consistent with the notion that aggregation of Aβ1-42 is promoted inside acidic endocytic compartments. Friedrich et al. (2010) [46] demonstrated in a macrophage cell line, bundles of Aβ1-40 fibrils in MVBs that penetrated the MVB membrane and leaked into the cytoplasm. We now present the first experimental evidence of Aβ42 aggregates developing inside MVBs/late endocytic/lysosomal compartments of cultured neurons.

We also found evidence of loss of endolysosomal impermeability with Aβ1-42 treatment of neurons, in line with reports in non-neuronal cells [47]. Further, we show that Aβ fibrillar oligomers/fibrils are visible inside neurons in a vesicular pattern as early as 45 min after addition of Aβ1-42 to the cell medium, that are not seen when only labelling the cell surface. Remarkably, at later time points intracellular aggregates are larger and extend into elongated structures that appear to penetrate the plasma membrane or are potentially even secreted or extruded into the extracellular space. Of note, the part of the elongated OC antibody positive structures that developed with time and no longer colabeled with the human Aβ specific antibody, might represent (1) Aβ where the N-terminal antibody binding sites become inaccessible to the antibody, (2) endogenous mouse Aβ aggregation and/or (3) incorporation of other amyloidogenic proteins. We demonstrate the ESCRT proteins VPS4A and Tsg101 in plaques of two different AD transgenic mouse models. Moreover, these ESCRT proteins strongly colocalized with a neuronal specific marker of the endo-lysosomal pathway, indicating the neuronal origin of the ESCRT proteins in plaques. Previously the lysosomal hydrolases cathepsin D and β-hexosaminidase A were shown to colocalize with Aβ in a subgroup of diffuse plaques of AD and DS patients [48] consistent with an endo-lysosomal origin of aggregated Aβ. However, whether these lysosomal proteins were derived from glial cells or neurons was not determined in that study.

Expression of VPS4 mutants deficient in ATP hydrolysis, such as the dominant negative VPS4 E228Q used in this study, leads to enlarged vesicles defined as a class E phenotype, resulting from disruption of ESCRT-III recycling [49–51]. VPS4 acts after the membrane scission step to recycle ESCRT-III proteins back to monomers, so that they are available to start a second wave of ILV formation [52]. One might speculate that Aβ disturbs this recycling leading to enlarged endocytic vesicles.

We show that inhibition of the late ESCRT machinery component VPS4A mimics AD pathogenesis by causing a marked increase in intracellular accumulation of Aβ and a concomitant decrease in secreted Aβ, consistent with what was reported in cultures of AD-transgenic compared to wt neurons [40]. Choy et al., 2012, reported that depletion of Hrs and Tsg101 in HEK293 cells stably expressing APP695 reduced Aβ secretion [53] and Edgar et al. (2015) found reduced Aβ40 secretion and increased intracellular Aβ when depleting APP overexpressing N2a cells of Hrs or Tsg101

[54], consistent with a role for the ESCRT machinery in preventing intracellular Aβ accumulation. However, in contrast to reduced Aβ secretion on depletion of early ESCRTs, Choy et al. found increased Aβ40 secretion upon VPS4A depletion with siRNA [53]. The difference with our demonstration of reduced Aβ secretion upon expression of dnVPS4 might be explained by the different cell types and methods of altering VPS4A that were used.

We provide evidence that the reduced secretion of Aβ with dnVPS4 was not due to reduced exosome secretion, since total exosome secretion was increased with dnVPS4A. Multiple mechanisms of ILV formation have been identified, but the relationship between different populations of ILVs and MVBs remains unclear. Both ESCRT-dependent and ESCRT-independent mechanisms of MVB biogenesis exist in mammalian cells. A competitive relationship between ESCRT-dependent and -independent mechanisms of ILV formation within single MVBs has been suggested, with upregulation of CD63-dependent ILV formation from ESCRT depletion [33–35]. It was shown in HeLa-CIITA-OVA cells that depletion of VPS4B increased the secretion of CD63 positive exosomes [55], in line with our results of increased amounts of CD63 positive exosomes with dnVPS4A. It is interesting to note that in our EM data from APP/PS1 neurons and in wt neurons treated with Aβ1-42, we saw both enlarged MVBs with many ILVs as well as enlarged MVBs with few ILVs. One can speculate that these might represent two different subsets of MVBs; it is possible that ESCRT-dependent ILV formation is disturbed by Aβ/APP, resulting in enlarged and empty MVBs, and potentially subsequent up-regulation of CD63 dependent ILVs formation resulting in MVBs filled with many ILVs. Others have reported that formation of ILVs destined for exosomal release was not ESCRT dependent, while ESCRTs were necessary for ILVs destined for degradation in the lysosome [56].

The intraneuronal pool of Aβ can have a dual origin, namely the production of Aβ from APP inside neurons and uptake of Aβ from the extracellular space that is secreted by other cells and/or the same neuron. Although we saw a net increase in intracellular Aβ levels with the expression of dnVPS4A supporting impaired degradation of Aβ and APP, we can not rule out that the production of Aβ from APP inside neurons was unaffected. In the OC antibody positive dnVPS4A-transfected cells, the enlarged vesicles also colocalized with increased labelling of flotillin-1 (Fig. 4g), hence associating with cholesterol-enriched lipid microdomains. Interestingly, ATPase-defective mammalian VPS4 was reported to localize to aberrant late endosomes accumulating cholesterol, due to impaired cholesterol trafficking [50] and retention of cholesterol in late endosomal/lysosomal compartments was reported to be associated with alterations in APP processing [57].

Our data also demonstrate that defective MVBs, modelled by dnVPS4A, leads to increased tau phosphorylation at serine 396 (S396). This site is phosphorylated by GSK3β; hence the increased tau phosphorylation could be due to impaired GSK3β sequestration into MVBs. Immunofluorescent labelling of GSK3β was increased with dnVPS4A (Additional file 10: Figure S9A), although total levels of GSK3β or GSK3α/β phosphorylated at serine 21/9 were not changed by Western blot. Hence, we cannot fully conclude that defective sequestration of GSK3β into MVBs is responsible for the increased levels of tau phosphorylation that we see with dnVPS4. However, consistent with our results, Tg APP-V7171 mice with the London mutation were found to have increased phosphorylation of tau at S396 and increased GSK3β activity, but no change in total levels of GSK3β and GSK3β phosphorylated at serine 9 [58].

We show that Aβ aggregation can initiate inside nerve cells from vesicular accumulation of Aβ. Aberrant endosomal trafficking has been linked genetically and biologically to a number of neurodegenerative diseases. Proteins involved in endocytosis are also prominent among genes linked to AD [11]. Interestingly, CD2AP, which is genetically linked to late onset AD and has been reported to affect MVB biogenesis and ILV formation [59], was recently reported to elevate levels of intracellular Aβ in dendrites [60]. While the ESCRT-III protein CHMP2B was first genetically linked to FTD [23], copy number variation in CHMP2B has since been reported in a family with familial Alzheimer's disease [24] and genome-wide association studies for late onset AD identified an association with VPS4B [25]. Moreover, immunoreactivity for CHMP2B is increased in neurons of hippocampus in another characteristic neuropathology of AD, granulovacuolar degeneration (GVD) [61]. CHMP2B-positive GVDs were reported to colocalize to a greater extent with the late endosomal/lysosomal marker LAMP1 than to the lysosomal marker cathepsin D or to the autophagic markers LC3 and p62, suggesting a late endosomal origin of GVDs or that they accumulate at the nexus of autophagic and endocytic pathways [62]. It is interesting to note that we found CHMP2B immunoreactivity particularly in hippocampus and medial temporal lobe of 3-month-old Tg19959 mice before plaque pathology, the two areas that are the first to have GVD-affected neurons in AD [63].

Conclusions

Neuropathological studies have pointed to an early and aberrant accumulation and aggregation of Aβ within neurons in AD, in particular in dystrophic neurites. Cell biological studies that model this aggregation in neurons are valuable in delineating the molecular mechanisms of Aβ-related synaptic dysfunction. We propose a model where elevated

levels of Aβ42 cause enlarged and defective MVBs, possibly via effects on ESCRT-III components. Alternatively, MVB dysfunction, as modelled by the expression of dnVPS4A, can lead to accumulation of Aβ in enlarged endocytic compartments. These results support a scenario where disturbances in the MVB pathway caused by Aβ42, or vice versa, could turn into a vicious cycle where more Aβ42 accumulates and oligomeric and fibrillar aggregates form. Our findings that ESCRT components colocalize with Aβ42 in amyloid plaques in two different mouse models of AD support the scenario that aggregated Aβ42 in MVBs/late endocytic compartments, potentially together with ESCRT-components could serve as seeds for plaques.

Additional files

Additional file 1: Table S1. List of antibodies. (PDF 35 kb)

Additional file 2: Figure S1. (A) EM image of an enlarged MVB in wt neurons treated with Aβ1-42. This image shows an example of an enlarged MVB with very few ILVs. (B) Confocal analysis of changes in size of LAMP1-positive structures in Aβ1-42 treated wt primary neurons with time. Scale bar 40 μm. (PDF 8949 kb)

Additional file 3: Figure S2. (A) Confocal analysis of wt primary neurons show that untreated (DMSO) cells have no OC labelling, while cells incubated with Aβ1-40 for 48 h have low levels of OC labelling. However, cells incubated with Aβ1-42 display very strong OC labelling. (PDF 4679 kb)

Additional file 4: Figure S3. (A) The early relatively weak OC labelling at 45 min of Aβ1-42 treatment colocalizes with LAMP1 labelling in the neurites, but not with the large LAMP1-positive structures in the cell soma. Confocal analysis of wt primary neurons treated with Aβ1-42 for 45 min. Scale 20 μm. (B) After 48 h of Aβ1-42 treatment, OC labelling is stronger and colocalizes partly with LAMP1-positive structures that appear enlarged and irregular in their shape. Elongated OC-positive structures extend out from such punctate LAMP1 labelling in the neuronal processes. Scale 20 μm. (C) At high magnification, antibody OC labelling can be seen colocalizing with the late endocytic marker Rab7 in neuronal processes of wt neurons treated for 24 h with Aβ1-42. Scale bar 5 μm. (PDF 269 kb)

Additional file 5: Figure S4. ESCRT proteins in primary neurons and plaques. (A-B) In young 3-month-old Tg19959 mice, CHMP2B immunolabelling is increased in areas of hippocampus (a) and entorhinal cortex (b) that also have increased labelling of APP/Aβ (6E10). Scale bar 40 μm, $n = 4$. (C) Western blot analysis of APP/PS1 compared to wt primary neurons at 12 DIV lysed in 6% SDS shows that protein levels of CHMP2B and VPS4 are not significantly changed, although there is a trend for increased levels of CHMP2B in APP/PS1 neurons, $n > 6$. Protein levels are expressed as percentage of control and are corrected against actin. (D) VPS4 colocalizes with Aβ42 in a vesicular pattern in 19-month-old wt mice (upper panel), $n = 3$. In 19-month-old APP/PS1 mice VPS4 accumulates in and around amyloid plaques (lower panel, white arrows). Scale bar 40 μm, $n = 4$. (E) Decreased labelling of CHMP2B in plaques (white arrows) in 19-month-old APP/PS1 mice. Some colocalization of CHMP2B is seen in Aβ/APP (6E10) positive cells (grey arrows). Scale bar 40 μm, $n = 3$. (F) Labelling of early ESCRT-0 component Hrs is decreased in amyloid plaques compared to surrounding brain parenchyma. Scale bar 40 μm, $n = 2$. (PDF 13619 kb)

Additional file 6: Figure S5. Aβ1-42 increases the diameter of LAMP-1 positive vesicles in N2a cells. Confocal images of exogenously added monomeric Aβ1-42 incubated for different time points, ranging from 15 min to 48 h, in N2a cells. 3D-rendering with Imaris from confocal z-stack. Colocalization of OC labelling and LAMP1 labelling can be seen from 45 min of Aβ treatment. The last image is from a single focal plane showing OC labelling inside an enlarged LAMP1-positive structure as well as OC labelling that appears to localize at the cell surface. Scale bar 10 μm. (PDF 375 kb)

Additional file 7: Figure S6. DnVPS4A increases secretion but does not change levels of intracellular α-syn. (A) Western blot analysis of α-syn N2a cells transfected with dnVPS4A shows increased levels of extracellular α-synuclein without altering the total pool of intracellular α-synuclein. (B) Quantification of A. Values are normalized against actin and expressed as percentage of control, $n = 3$; $^{*}p < 0.05$, $^{**}p < 0.01$. (C) Overexposed WB membrane for secreted α-synuclein (same as above) with increased intensity to better visualize the bands. (PDF 1607 kb)

Additional file 8: Figure S7. (A) Western blot analysis of APP and Aβ in Swe N2a cells treated with 40 μg/ml cycloheximide (CHX) at different times in hours (h) before harvest. Cell culture media was replaced with fresh media 24 h before harvest. For quantification, values are normalized against actin and expressed as percentage of control, $n = 3$; $^{*}p < 0.05$, $^{**}p < 0.01$, $^{***}p < 0.001$, $^{****}p < 0.0001$ (ANOVA with Dunnett's multiple comparisons test, compared to ctr). (B) Confocal images of 6E10 and Golgi marker GM130 in Swe N2a cells treated with 40 μg/ml CHX for the depicted times. (PDF 2263 kb)

Additional file 9: Figure S8. (A) Western blot analysis of APP and Aβ in Swe N2a cells treated with 5 nM bafilomycin A1 (BafA1) at different time points (h) before harvest. Cell culture media was replaced with fresh media 24 h before harvest. (B) Quantification of A. Values are normalized against actin and expressed as percentage of control, $n = 3$; $^{*}p < 0.05$, $^{**}p < 0.01$, $^{***}p < 0.001$, $^{****}p < 0.0001$ (ANOVA with Dunnett's multiple comparisons test, compared to ctr). (C) Confocal images of 6E10 and LAMP1 labelling in Swe N2a cells treated with 5 nM bafilomycin A1 for the depicted times. At 24 h there is a build up of both 6E10 labelling and punctate LAMP1-positive structures. (D) Western blot analysis of APP and Aβ in Swe N2a cells treated with 5 nM bafilomycin A1 (BafA1) 24 h before harvest and 40 μg/ml cycloheximide (CHX) at different time points (h) before harvest. Cell culture media was replaced with fresh media 24 h before harvest, before the addition of Baf A1. (PDF 1310 kb)

Additional file 10: Figure S9. (A) 3D images show increased GSK3β labelling in dnVPS4-expressing N2a Swe compared to cells transfected with control plasmid. Rab7 labelling is also increased in dnVPS4 expressing cells. Scale bar 15 μm. (B) Western blot analysis of cell lysates of Swe N2a cells transfected with dnVPS4A showing no changes in total GSK3β or phosphorylated GSK3α/β (serine 21/9). (PDF 5570 kb)

Abbreviations

AD: Alzheimer's disease; APP: Amyloid precursor protein; APP/PS1: B6.Cg-Tg (APPswe,PSEN1dE9)85Dbo/Mmjax mice; BACE1: Beta-secretase 1; BafA1: Bafilomycin A1; BSA: Bovine serum albumin; DIV: Days in vitro; dnVPS4A: Dominant negative VPS4A; EM: Electron microscopy; ESCRT: Endosomal sorting complexes required for transport; FTD: Frontotemporal dementia; ILV: Intraluminal vesicle; MVB: Multivesicular bodies; NFTs: Neurofibrillary tangles; NGS: Normal goat serum; PBS: Phosphate buffered saline; PBST: PBS containing 0.1% Tween-20; PFA: Paraformaldehyde; PS1: Presenilin 1; RT: Room temperature; SDS: Sodium dodecyl sulfate; TCA: Trichloroacetic acid; tg: AD transgenic; wtVPS4A: Wild type VPS4A

Acknowledgements

We thank Drs. Gopal Thinakaran and Sangram Sisodia at the University of Chicago for sharing their stably transfected human APP N2a cells. We also thank Bodil Israelsson at Lund University for technical support.

Funding

This study was supported by MultiPark, Parkinsonsfonden and the Swedish Research Council.

Availability of data and materials

The datasets used and/or analysed during the current study are available from the corresponding author on reasonable request.

Authors' contributions

KW and GKG conceived the study; KW performed and analysed all experiments except for the EM imaging, which was performed and analysed by JRE and CEF; TH and NT supplied the p3xFLAG-CMV-10-hVPS4A-wt and p3xFLAG-CMV-10-hVPS4A-dn plasmids; KW wrote the paper, with input and editing provided by GKG, JRE and CEF. All authors read and approved the final manuscript.

Ethics approval
All animal experiments were approved by the Animal Ethical Committee of Malmö and Lund, reference number M40-14.

Consent for publication
Not applicable.

Competing interests
The authors declare that they have no competing interests.

Publisher's Note
Springer Nature remains neutral with regard to jurisdictional claims in published maps and institutional affiliations.

Author details
[1]Department of Experimental Medical Science, Lund University, 221 84 Lund, Sweden. [2]Cambridge Institute for Medical Research, University of Cambridge, Cambridge CB2 0XY, UK. [3]UCL Institute of Ophthalmology, London EC1V 9EL, UK. [4]Division of Neurology, Department of Neuroscience and Sensory Organs, Tohoku University Graduate School of Medicine, Sendai 980-8574, Japan. [5]Division of Cancer Biology and Therapeutics, Miyagi Cancer Center Research Institute, Natori 981-1293, Japan.

Received: 6 February 2017 Accepted: 15 August 2017
Published online: 23 August 2017

References
1. Cataldo AM, Petanceska S, Terio NB, Peterhoff CM, Durham R, Mercken M, Mehta PD, Buxbaum J, Haroutunian V, Nixon RA. Abeta localization in abnormal endosomes: association with earliest Abeta elevations in AD and down syndrome. Neurobiol Aging. 2004;25:1263–72.
2. D'Andrea MR, Nagele RG, Wang HY, Peterson PA, Lee DHS. Evidence that neurones accumulating amyloid can undergo lysis to form amyloid plaques in Alzheimer's disease. Histopathology. 2001;38:120–34.
3. Gouras GK, Tsai J, Naslund J, Vincent B, Edgar M, Checler F, Greenfield JP, Haroutunian V, Buxbaum JD, Xu H, Greengard P, Relkin NR. Intraneuronal Ab42 accumulation in human brain. Am J Pathol. 2000;156:15–20.
4. Oakley H, Cole SL, Logan S, Maus E, Shao P, Craft J, Guillozet-Bongaarts A, Ohno M, Disterhoft J, Van Eldik L, Berry R, Vassar R. Intraneuronal beta-amyloid aggregates, neurodegeneration, and neuron loss in transgenic mice with five familial Alzheimer's disease mutations: potential factors in amyloid plaque formation. J Neurosci. 2006;26:10129–40.
5. Takahashi RH, Milner TA, Li F, Nam EE, Edgar MA, Yamaguchi H, Beal MF, Xu H, Greengard P, Gouras GK. Intraneuronal Alzheimer Abeta42 accumulates in multivesicular bodies and is associated with synaptic pathology. Am J Pathol. 2002;161:1869–79.
6. Wirths O, Multhaup G, Czech C, Blanchard V, Moussaoui S, Tremp G, Pradier L, Beyreuther K, Bayer TA. Intraneuronal Abeta accumulation precedes plaque formation in beta-amyloid precursor protein and presenilin-1 double-transgenic mice. Neurosci Lett. 2001;306:116–20.
7. Billings LM, Oddo S, Green KN, McGaugh JL, LaFerla FM. Intraneuronal Abeta causes the onset of early Alzheimer's disease-related cognitive deficits in transgenic mice. Neuron. 2005;45:675–88.
8. Chapman PF, White GL, Jones MW, Cooper-Blacketer D, Marshall VJ, Irizarry M, Younkin L, Good MA, Bliss TV, Hyman BT, Younkin SG, Hsiao KK. Impaired synaptic plasticity and learning in aged amyloid precursor protein transgenic mice. Nat Neurosci. 1999;2:271–6.
9. Takahashi RH, Almeida CG, Kearney PF, Yu F, Lin MT, Milner TA, Gouras GK. Oligomerization of Alzheimer's beta-amyloid within processes and synapses of cultured neurons and brain. J Neurosci. 2004;24:3592–9.
10. Gouras GK, Tampellini D, Takahashi RH, Capetillo-Zarate E. Intraneuronal beta-amyloid accumulation and synapse pathology in Alzheimer's disease. Acta Neuropathol. 2010;119:523–41.
11. Peric A, Annaert W. Early etiology of Alzheimer's disease: tipping the balance toward autophagy or endosomal dysfunction? Acta Neuropathol. 2015;129:363–81.
12. Cataldo AM, Peterhoff CM, Troncoso JC, Gomez-Isla T, Hyman BT, Nixon RA. Endocytic pathway abnormalities precede amyloid beta deposition in sporadic Alzheimer's disease and down syndrome: differential effects of APOE genotype and presenilin mutations. Am J Pathol. 2000;157:277–86.
13. Cataldo AM, Mathews PM, Boiteau AB, Hassinger LC, Peterhoff CM, Jiang Y, Mullaney K, Neve RL, Gruenberg J, Nixon RA. Down syndrome fibroblast model of Alzheimer-related endosome pathology: accelerated endocytosis promotes late endocytic defects. Am J Pathol. 2008;173:370–84.
14. Nixon RA, Wegiel J, Kumar A, Yu WH, Peterhoff C, Cataldo A, Cuervo AM. Extensive involvement of autophagy in Alzheimer disease: an immuno-electron microscopy study. J Neuropathol Exp Neurol. 2005;64:113–22.
15. Small SA, Gandy S. Sorting through the cell biology of Alzheimer's disease: intracellular pathways to pathogenesis. Neuron. 2006;52:15–31.
16. De Strooper B, Vassar R, Golde T. The secretases: enzymes with therapeutic potential in Alzheimer disease. Nat Rev Neurol. 2010;6:99–107.
17. Rajendran L, Annaert W. Membrane trafficking pathways in Alzheimer's disease. Traffic. 2012;13:759–70.
18. Sannerud R, Declerck I, Peric A, Raemaekers T, Menendez G, Zhou L, Veerle B, Coen K, Munck S, De Strooper B, Schiavo G, Annaert W. ADP ribosylation factor 6 (ARF6) controls amyloid precursor protein (APP) processing by mediating the endosomal sorting of BACE1. Proc Natl Acad Sci U S A. 2011;108:E559–68.
19. Sannerud R, Esselens C, Ejsmont P, Mattera R, Rochin L, Tharkeshwar AK, De Baets G, De Wever V, Habets R, Baert V, Vermeire W, Michiels C, Groot AJ, Wouters R, Dillen K, Vints K, Baatsen P, Munck S, Derua R, Waelkens E, Basi GS, Mercken M, Vooijs M, Bollen M, Schymkowitz J, Rousseau F, Bonifacino JS, Van Niel G, De Strooper B, Annaert W. Restricted location of PSEN2/γ-Secretase determines substrate specificity and generates an intracellular Aβ pool. Cell. 2016;166:193–208.
20. Langui D, Girardot N, El Hachimi KH, Allinquant B, Blanchard V, Pradier L, Duyckaerts C. Subcellular topography of neuronal Abeta peptide in APPxPS1 transgenic mice. Am J Pathol. 2004;165:1465–77.
21. Almeida C, Takahashi H, Gouras GK. Beta-amyloid accumulation impairs multivesicular body sorting by inhibiting the ubiquitin-proteasome system. J Neurosci. 2006;26:4277–88.
22. Babst M, Katzmann DJ, Estepa-Sabal EJ, Meerloo T, Emr SD. Escrt-III: an endosome-associated heterooligomeric protein complex required for mvb sorting. Dev Cell. 2002;3:271–82.
23. Skibinski G, Parkinson NJ, Brown JM, Chakrabarti L, Lloyd SL, Hummerich H, Nielsen JE, Hodges JR, Spillantini MG, Thusgaard T, Brandner S, Brun A, Rossor MN, Gade A, Johannsen P, Sørensen SA, Gydesen S, Fisher EM, Collinge J. Mutations in the endosomal ESCRTIII-complex subunit CHMP2B in frontotemporal dementia. Nat Genet. 2005;37:806–8.
24. Hooli BV, Kovacs-Vajna ZM, Mullin K, Blumenthal MA, Mattheisen M, Zhang C, Lange C, Mohapatra G, Bertram L, Tanzi RE. Rare autosomal copy number variations in early-onset familial Alzheimer's disease. Mol Psychiatry. 2014;19:676–81.
25. Jones L, Holmans PA, Hamshere ML, Harold D, Moskvina V, Ivanov D, Pocklington A, Abraham R, Hollingworth P, Sims R, Gerrish A, Pahwa JS, Jones N, Stretton A, Morgan AR, Lovestone S, Powell J, Proitsi P, Lupton MK, Brayne C, Rubinsztein DC, Gill M, Lawlor B, Lynch A, Morgan K, Brown KS, Passmore PA, Craig D, McGuinness B, Todd S, Holmes C, Mann D, Smith AD, Love S, Kehoe PG, Mead S, Fox N, Rossor M, Collinge J, Maier W, Jessen F, Schürmann B, Heun R, Kölsch H, van den Bussche H, Heuser I, Peters O, Kornhuber J, Wiltfang J, Dichgans M, Frölich L, Hampel H, Hüll M, Rujescu D, Goate AM, Kauwe JS, Cruchaga C, Nowotny P, Morris JC, Mayo K, Livingston G, Bass NJ, Gurling H, McQuillin A, Gwilliam R, Deloukas P, Al-Chalabi A, Shaw CE, Singleton AB, Guerreiro R, Mühleisen TW, Nöthen MM, Moebus S, Jöckel KH, Klopp N, Wichmann HE, Rüther E, Carrasquillo MM, Pankratz VS, Younkin SG, Hardy J, O'Donovan MC, Owen MJ, Williams J. Genetic evidence implicates the immune system and cholesterol metabolism in the aetiology of Alzheimer's disease. PLoS One. 2010;5:e13950.
26. Thinakaran G, Teplow DB, Siman R, Greenberg B, Sisodia SS. Metabolism of the "Swedish" amyloid precursor protein variant in neuro2a (N2a) cells. Evidence that cleavage at the "beta-secretase" site occurs in the golgi apparatus. J Biol Chem. 1996;271:9390–7.
27. Slot JW, Geuze HJ. A new method of preparing gold probes for multiple-labeling cytochemistry. Eur J Cell Biol. 1985;38:87–93.
28. Hasegawa T, Konno M, Baba T, Sugeno N, Kikuchi A, Kobayashi M, Miura E, Tanaka N, Tamai K, Furukawa K, Arai H, Mori F, Wakabayashi K, Aoki M, Itoyama Y, Takeda A. The AAA-ATPase VPS4 regulates extracellular secretion and lysosomal targeting of α-synuclein. PLoS One. 2011;6:e29460.
29. Buxbaum JD, Gandy SE, Cicchetti P, Ehrlich ME, Czernik AJ, Fracasso RP, Ramabhadran TV, Unterbeck AJ, Greengard P. Processing of Alzheimer beta/A4 amyloid precursor protein: modulation by agents that regulate protein phosphorylation. Proc Natl Acad Sci U S A. 1990;87:6003–6.

30. Théry C, Amigorena S, Raposo G, Clayton A. Isolation and characterization of exosomes from cell culture supernatants and biological fluids. Curr Protoc Cell Biol. 2006;30(3.22):3.22.1–3.22.29.
31. Kayed R, Head E, Sarsoza F, Saing T, Cotman CW, Necula M, Margol L, Wu J, Breydo L, Thompson JL, Rasool S, Gurlo T, Butler P, Glabe CG. Fibril specific, conformation dependent antibodies recognize a generic epitope common to amyloid fibrils and fibrillar oligomers that is absent in prefibrillar oligomers. Mol Neurodegener. 2007;2:18.
32. Katoh Y, Ritter B, Gaffry T, Blondeau F, Höning S, McPherson PS. The clavesin family, neuron-specific lipid- and clathrin-binding sec14 proteins regulating lysosomal morphology. J Biol Chem. 2009;284:27646–54.
33. Stuffers S, Sem Wegner C, Stenmark H, Brech A. Multivesicular endosome biogenesis in the absence of ESCRTs. Traffic. 2009;10:925–37.
34. van Niel G, Charrin S, Simoes S, Romao M, Rochin L, Saftig P, Marks MS, Rubinstein E, Raposo G. The tetraspanin CD63 regulates ESCRT-independent and -dependent endosomal sorting during melanogenesis. Dev Cell. 2011;21:708–21.
35. Edgar JR, Eden ER, Futter CE. Hrs- and CD63-dependent competing mechanisms make different sized endosomal intraluminal vesicles. Traffic. 2014;15:197–211.
36. Taelman VF, Dobrowolski R, Plouhinec JL, Fuentealba LC, Vorwald PP, Gumper I, Sabatini DD, De Robertis EM. Wnt signaling requires sequestration of glycogen synthase kinase 3 inside multivesicular endosomes. Cell. 2010;143:1136–48.
37. Kimura T, Whitcomb DJ, Jo J, Regan P, Piers T, Heo S, Brown C, Hashikawa T, Murayama M, Seok H, Sotiropoulos I, Kim E, Collingridge GL, Takashima A, Cho K. Microtubule-associated protein tau is essential for long-term depression in the hippocampus. Philos Trans R Soc Lond Ser B Biol Sci. 2013;369:20130144.
38. Hooper C, Killick R, Lovestone S. The GSK3 hypothesis of Alzheimer's disease. J Neurochem. 2008;104:1433–9.
39. Dunning CJ, McGauran G, Willén K, Gouras GK, O'Connell DJ, Linse S. Direct high affinity interaction between Aβ42 and GSK3α stimulates hyperphosphorylation of tau. A new molecular link in Alzheimer's disease? ACS Chem Neurosci. 2016;7:161–70.
40. Tampellini D, Rahman N, Lin MT, Capetillo-Zarate E, Gouras GK. Impaired beta-amyloid secretion in Alzheimer's disease pathogenesis. J Neurosci. 2011;31:15384–90.
41. Tampellini D, Capetillo-Zarate E, Dumont M, Huang Z, Yu F, Lin MT, Gouras GK. Effects of synaptic modulation on beta-amyloid, synaptophysin, and memory performance in Alzheimer's disease transgenic mice. J Neurosci. 2010;30:14299–304.
42. Kim S, Sato Y, Mohan PS, Peterhoff C, Pensalfini A, Rigoglioso A, Jiang Y, Nixon RA. Evidence that the rab5 effector APPL1 mediates APP-βCTF-induced dysfunction of endosomes in down syndrome and Alzheimers disease. Mol Psychiatry. 2016;21:707–16.
43. Lauritzen I, Pardossi-Piquard R, Bourgeois A, Pagnotta S, Biferi MG, Barkats M, Lacor P, Klein W, Bauer C, Checler F. Intraneuronal aggregation of the β-CTF fragment of APP (C99) induces Aβ-independent lysosomal-autophagic pathology. Acta Neuropathol. 2016;132:257–76.
44. Burdick D, Soreghan B, Kwon M, Kosmoski J, Knauer M, Henschen A, Yates J, Cotman C, Glabe C. Assembly and aggregation properties of synthetic Alzheimer's A4/beta amyloid peptide analogs. J Biol Chem. 1992;267:546–54.
45. Hu X, Crick SL, Bu G, Frieden C, Pappu RV, Lee JM. Amyloid seeds formed by cellular uptake, concentration, and aggregation of the amyloid-beta peptide. Proc Natl Acad Sci U S A. 2009;1(106):20324–9.
46. Friedrich RP, Tepper K, Rönicke R, Soom M, Westermann M, Reymann K, Kaether C, Fändrich M. Mechanism of amyloid plaque formation suggests an intracellular basis of Aβ pathogenicity. Proc Natl Acad Sci U S A. 2010;107:1942–7.
47. Yang AJ, Chandswangbhuvana D, Margol L, Glabe CG. Loss of endosomal/lysosomal membrane impermeability is an early event in amyloid Abeta1-42 pathogenesis. J Neurosci Res. 1998;52:691–8.
48. Cataldo AM, Barnett JL, Mann DM, Nixon RA. Colocalization of lysosomal hydrolase and beta-amyloid in diffuse plaques of the cerebellum and striatum in Alzheimer's disease and Down's syndrome. J Neuropathol Exp Neurol. 1996;55:704–15.
49. Babst M, Wendland B, Estepa EJ, Emr SD. The Vps4p AAA ATPase regulates membrane association of a Vps protein complex required for normal endosome function. EMBO J. 1998;11:2982–93.
50. Bishop N, Woodman P. ATPase-defective mammalian VPS4 localizes to aberrant endosomes and impairs cholesterol trafficking. Mol Biol Cell. 2000;11:227–39.
51. Dores MR, Chen B, Lin H, Soh UJ, Paing MM, Montagne WA, Meerloo T, Trejo J. ALIX binds a YPX(3)L motif of the GPCR PAR1 and mediates ubiquitin-independent ESCRT-III/MVB sorting. J Cell Biol. 2012;197:407–19.
52. Wollert T, Wunder C, Lippincott-Schwartz J, Hurley JH. Membrane scission by the ESCRT-III complex. Nature. 2009;458:172–7.
53. Choy RW, Cheng Z, Schekman R. Amyloid precursor protein (APP) traffics from the cell surface via endosomes for amyloid β (Aβ) production in the trans-Golgi network. Proc Natl Acad Sci U S A. 2012;109:E2077–82.
54. Edgar JR, Willén K, Gouras GK, Futter CE. ESCRTs regulate amyloid precursor protein sorting in multivesicular bodies and intracellular amyloid-β accumulation. J Cell Sci. 2015;128:2520–8.
55. Colombo M, Moita C, van Niel G, Kowal J, Vigneron J, Benaroch P, Manel N, Moita LF, Théry C, Raposo G. Analysis of ESCRT functions in exosome biogenesis, composition and secretion highlights the heterogeneity of extracellular vesicles. J Cell Sci. 2013;126:5553–65.
56. Trajkovic K, Hsu C, Chiantia S, Rajendran L, Wenzel D, Wieland F, Schwille P, Brügger B, Simons M. Ceramide triggers budding of exosome vesicles into multivesicular endosomes. Science. 2008;319:1244–7.
57. Runz H, Rietdorf J, Tomic I, de Bernard M, Beyreuther K, Pepperkok R, Hartmann T. Inhibition of intracellular cholesterol transport alters presenilin localization and amyloid precursor protein processing in neuronal cells. J Neurosci. 2002;22:679–89.
58. Terwel D, Muyllaert D, Dewachter I, Borghgraef P, Croes S, Devijver H, Van Leuven F. Amyloid activates GSK-3beta to aggravate neuronal tauopathy in bigenic mice. Am J Pathol. 2008;172:786–98.
59. Kim JM, Wu H, Green G, Winkler CA, Kopp JB, Miner JH, Unanue ER, Shaw AS. CD2-associated protein haploinsufficiency is linked to glomerular disease susceptibility. Science. 2003;300:1298–300.
60. Ubelmann F, Burrinha T, Salavessa L, Gomes R, Ferreira C, Moreno N, Guimas AC. Bin1 and CD2AP polarise the endocytic generation of beta-amyloid. EMBO Rep. 2017;18:102–22.
61. Yamazaki Y, Takahashi T, Hiji M, Kurashige T, Izumi Y, Yamawaki T, Matsumoto M. Immunopositivity for ESCRT-III subunit CHMP2B in granulovacuolar degeneration of neurons in the Alzheimer's disease hippocampus. Neurosci Lett. 2010;477:86–90.
62. Funk KE, Mrak RE, Kuret J. Granulovacuolar degeneration (GVD) bodies of Alzheimer's disease (AD) resemble late-stage autophagic organelles. Neuropathol Appl Neurobiol. 2011;37:295–306.
63. Thal DR, Del Tredici K, Ludolph AC, Hoozemans JJ, Rozemuller AJ, Braak H, Knippschild U. Stages of granulovacuolar degeneration: their relation to Alzheimer's disease and chronic stress response. Acta Neuropathol. 2011;122:577–89.

Submit your next manuscript to BioMed Central and we will help you at every step:

- We accept pre-submission inquiries
- Our selector tool helps you to find the most relevant journal
- We provide round the clock customer support
- Convenient online submission
- Thorough peer review
- Inclusion in PubMed and all major indexing services
- Maximum visibility for your research

Submit your manuscript at
www.biomedcentral.com/submit



Table S1

Antibody	Target Epitope	Species and type	Dilution (WB)	Dilution (IF)	Source	Cat. #
369	Human/mouse full length APP, α/β CTFs, APP C-terminus	Rabbit polyclonal	1:1000		Buxbaum et al. 1990 [29]	
6E10	Human Aβ, full length APP, sAPPα, β CTF, a.a. 3-8 of Aβ	Mouse monoclonal	1:1000	1:500	BioLegend	previously Covance SIG-39320
12F4	Human/mouse Aβx-42, C-terminus specific	Mouse monoclonal		1:250	BioLegend	Previously Covance SIG-39142
Amyloidβ (1-42)		Rabbit polyclonal		1:250	IBL	18582
Amyloidβ (1-42)	Human/mouse Aβx-42, C-terminus specific	Rabbit polyclonal		1:1000	Invitrogen	700254
β-actin		Mouse monoclonal	1:2000		Sigma	A 5316
CD63		Mouse monoclonal	1:1000		ThermoFisher Scientific	MAI-19281
CHMP2B		Rabbit polyclonal	1:1000	1:250	Abcam	ab33174
Clavestin-1+2		Rabbit polyclonal		1:250	Bioss	bs-6569R-A647
DAPI				1:1500	Sigma	D9542
Drebrin		Rabbit polyclonal		1:1000	Abcam	ab11068
FLAG	DYKDDDDK	Rat	1:1000	1:1000	Biolegend	637302
Flotillin-1		Mouse monoclonal		1:400	BD Biosciences	610821
GM130		Mouse monoclonal		1:500	BD Biosciences	610822
GSK3β		Rabbit monoclonal	1:1000	1:400	Cell Signaling Technology	12456
pGSKα/β		Rabbit polyclonal	1:1000		Cell Signaling Technology	9331S
HA-Tag		Rabbit monoclonal	1:1000		Cell Signaling Technology	3724
Hrs and Hrs-2		Mouse monoclonal		1:100	Enzo	ALX-804-382-C050
LAMP1		Rabbit polyclonal		1:1000	Abcam	ab24170
LAMP1		Rat monoclonal		1:1500	Abcam	ab25245
LC3β		Rabbit polyclonal	1:1000		Cell Signaling Technology	2775
OC	Amyloid fibrils	Rabbit polyclonal		1:1000	Merck Millipore	AB2286
P2:1	Human APP, N-terminus, a.a. 104-118 of APP	Mouse monoclonal		1:500	ThermoFisher Scientific	OMA1-03132
Phospho-tau pSer396		Rabbit polyclonal	1:1000		ThermoFisher	44-752G
Rab7		Mouse monoclonal		1:500	Abcam	ab50533
Synapto-physin		Mouse monoclonal		1:1000	Merck Millipore	MAB5258
Tsg101		Mouse monoclonal		1:250	Genetex	GTX70255
VPS4		Mouse monoclonal	1:1000	1:100	SantaCruz	sc-133122

Figure S1

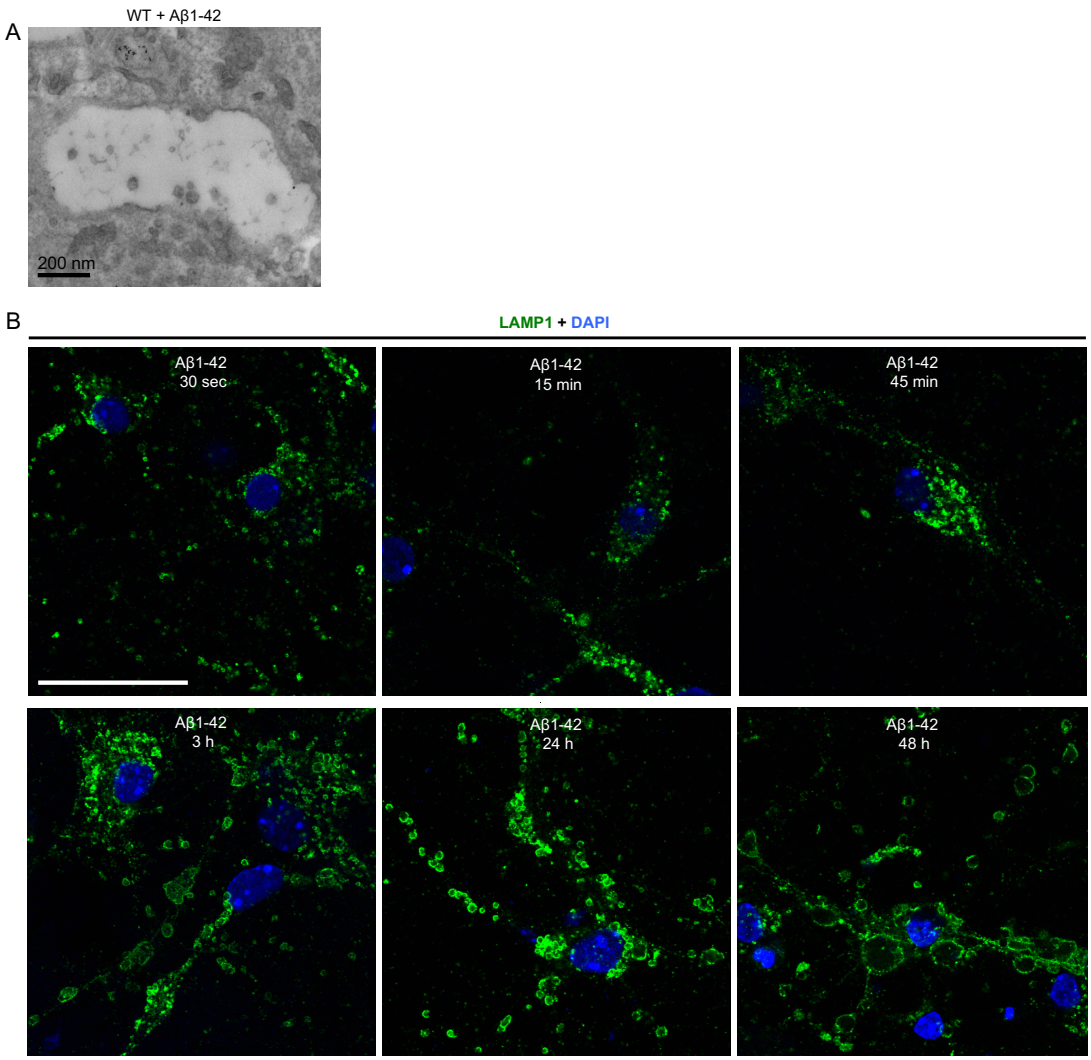

A
WT + Aβ1-42
200 nm
B
LAMP1 + DAPI
Aβ1-42
30 sec
Aβ1-42
15 min
Aβ1-42
45 min
Aβ1-42
3 h
Aβ1-42
24 h
Aβ1-42
48 h

Figure S2

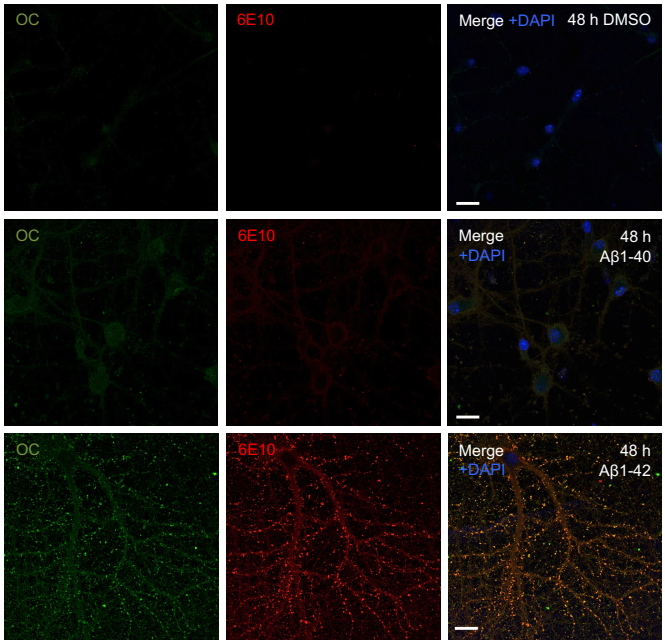

OC
6E10
Merge +DAPI 48 h DMSO
OC
6E10
Merge
+DAPI
48 h
Aβ1-40
OC
6E10
Merge
+DAPI
48 h
Aβ1-42

Figure S3

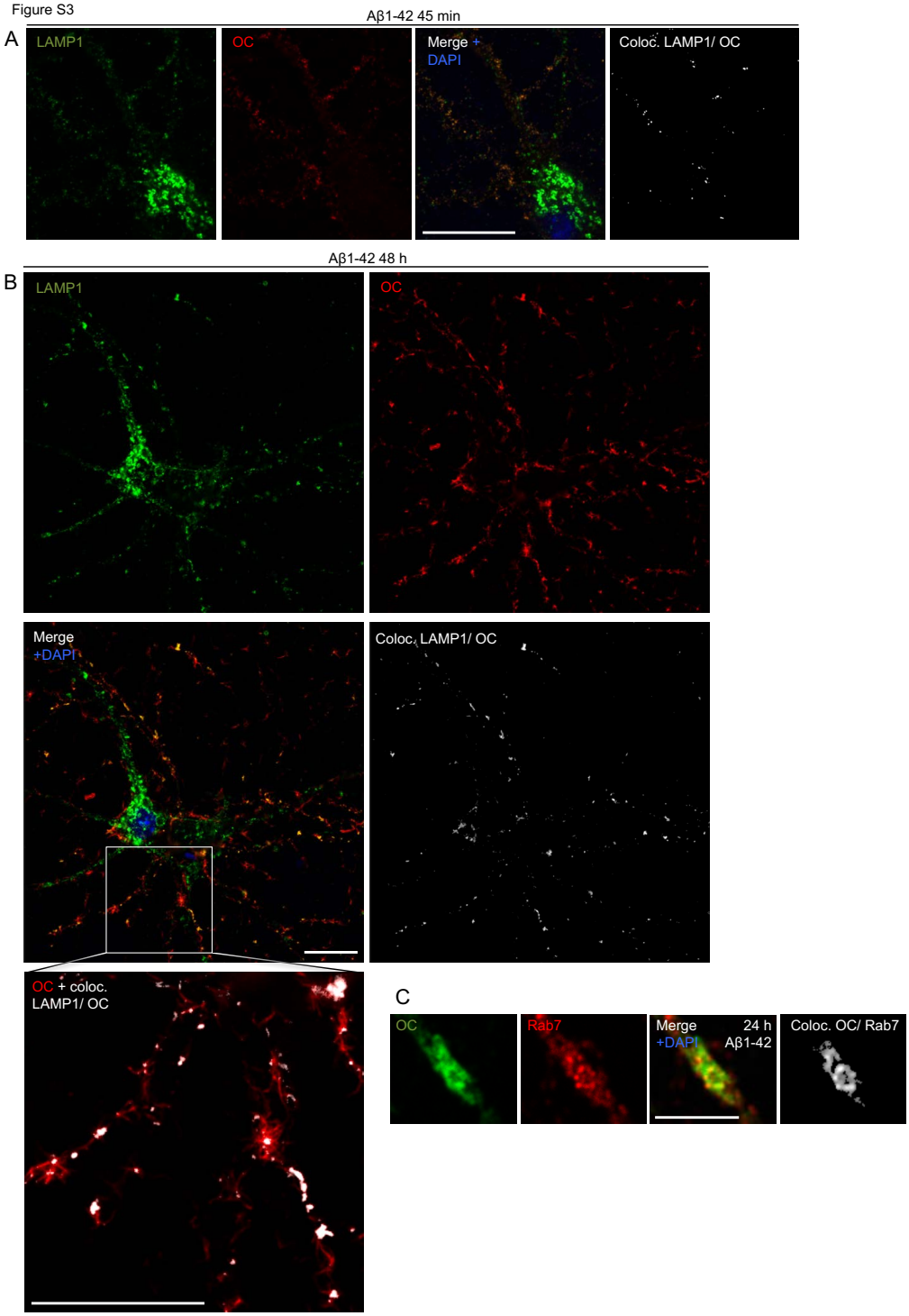

A
Aβ1-42 45 min
LAMP1
OC
Merge +
DAPI
Coloc. LAMP1/ OC
B
Aβ1-42 48 h
LAMP1
OC
Merge
+DAPI
Coloc. LAMP1/ OC
OC + coloc.
LAMP1/ OC
C
OC
Rab7
Merge
+DAPI
24 h
Aβ1-42
Coloc. OC/ Rab7

Figure S4

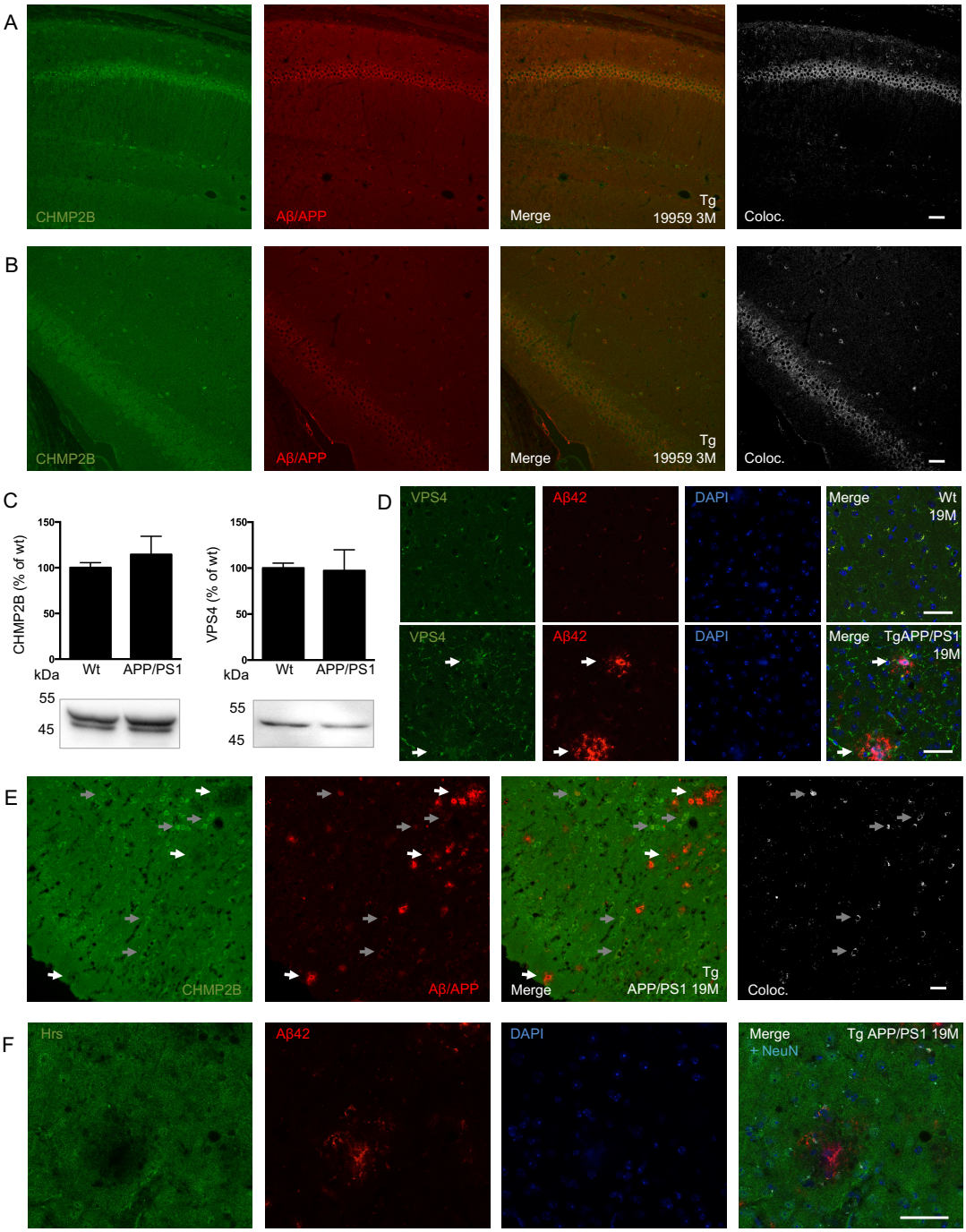

A
CHMP2B
Aβ/APP
Merge
Tg
19959 3M
Coloc.
B
CHMP2B
Aβ/APP
Merge
Tg
19959 3M
Coloc.
C
CHMP2B (% of wt)
150
100
50
0
kDa
Wt
APP/PS1
55
45
VPS4 (% of wt)
150
100
50
0
kDa
Wt
APP/PS1
55
45
D
VPS4
Aβ42
DAPI
Merge
Wt
19M
VPS4
Aβ42
DAPI
Merge
TgAPP/PS1
19M
E
CHMP2B
Aβ/APP
Merge
Tg
APP/PS1 19M
Coloc.
F
Hrs
Aβ42
DAPI
Merge
+ NeuN
Tg APP/PS1 19M

Figure S5

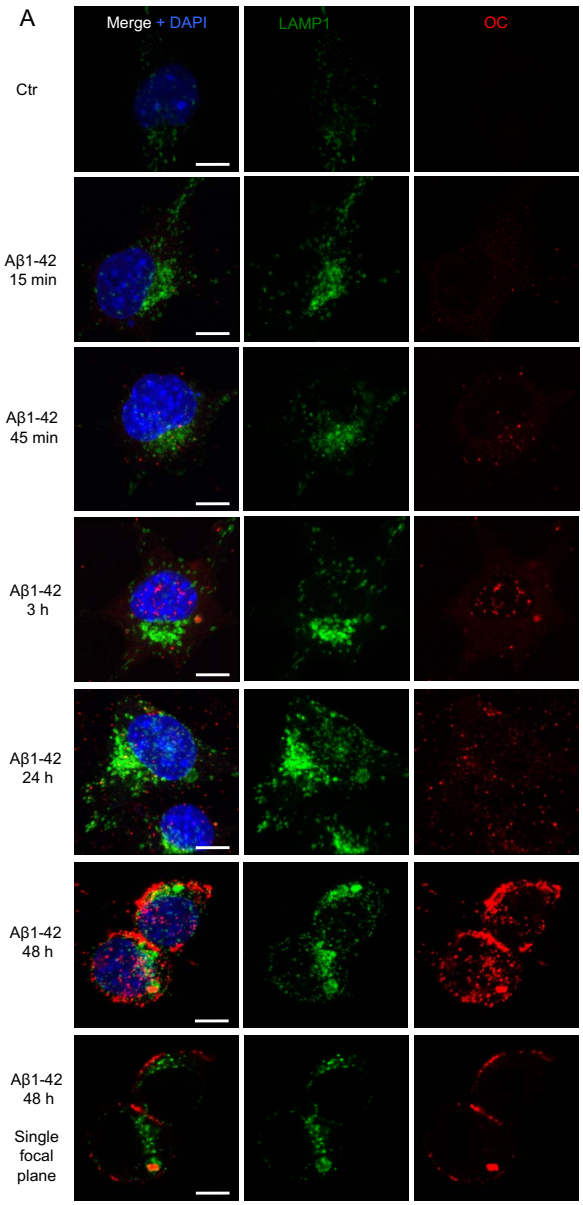

A
Merge + DAPI
LAMP1
OC
Ctr
Aβ1-42
15 min
Aβ1-42
45 min
Aβ1-42
3 h
Aβ1-42
24 h
Aβ1-42
48 h
Aβ1-42
48 h
Single
focal
plane

Figure S6

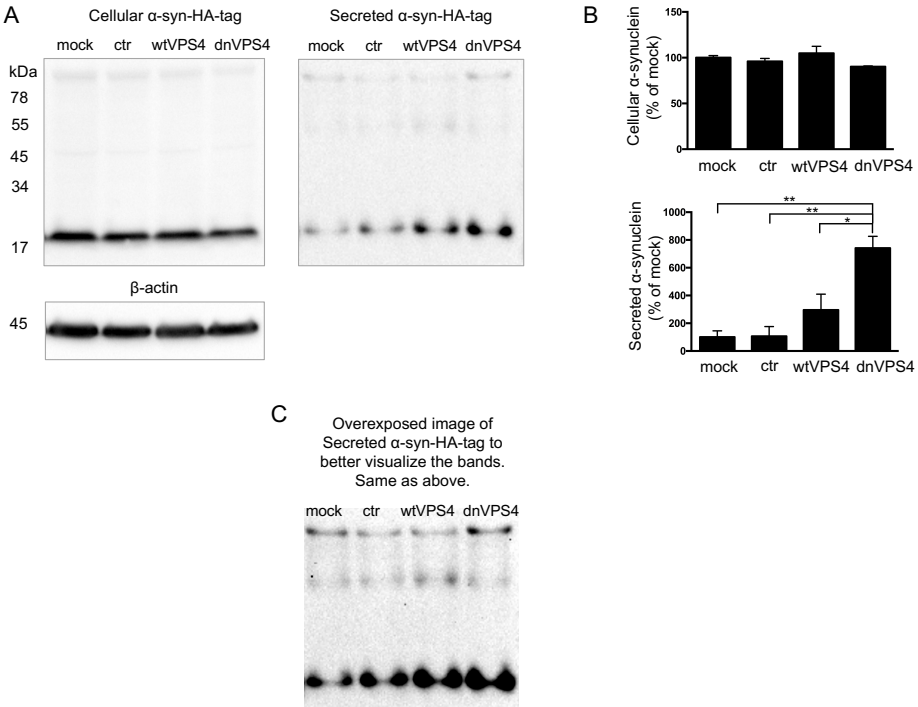

A
Cellular α-syn-HA-tag
Secreted α-syn-HA-tag
mock ctr wtVPS4 dnVPS4
mock ctr wtVPS4 dnVPS4
kDa
78
55
45
34
17
β-actin
45
B
Cellular α-synuclein (% of mock)
150
100
50
0
mock ctr wtVPS4 dnVPS4
Secreted α-synuclein (% of mock)
1000
800
600
400
200
0
**
**
*
mock ctr wtVPS4 dnVPS4
C
Overexposed image of Secreted α-syn-HA-tag to better visualize the bands. Same as above.
mock ctr wtVPS4 dnVPS4

Figure S7

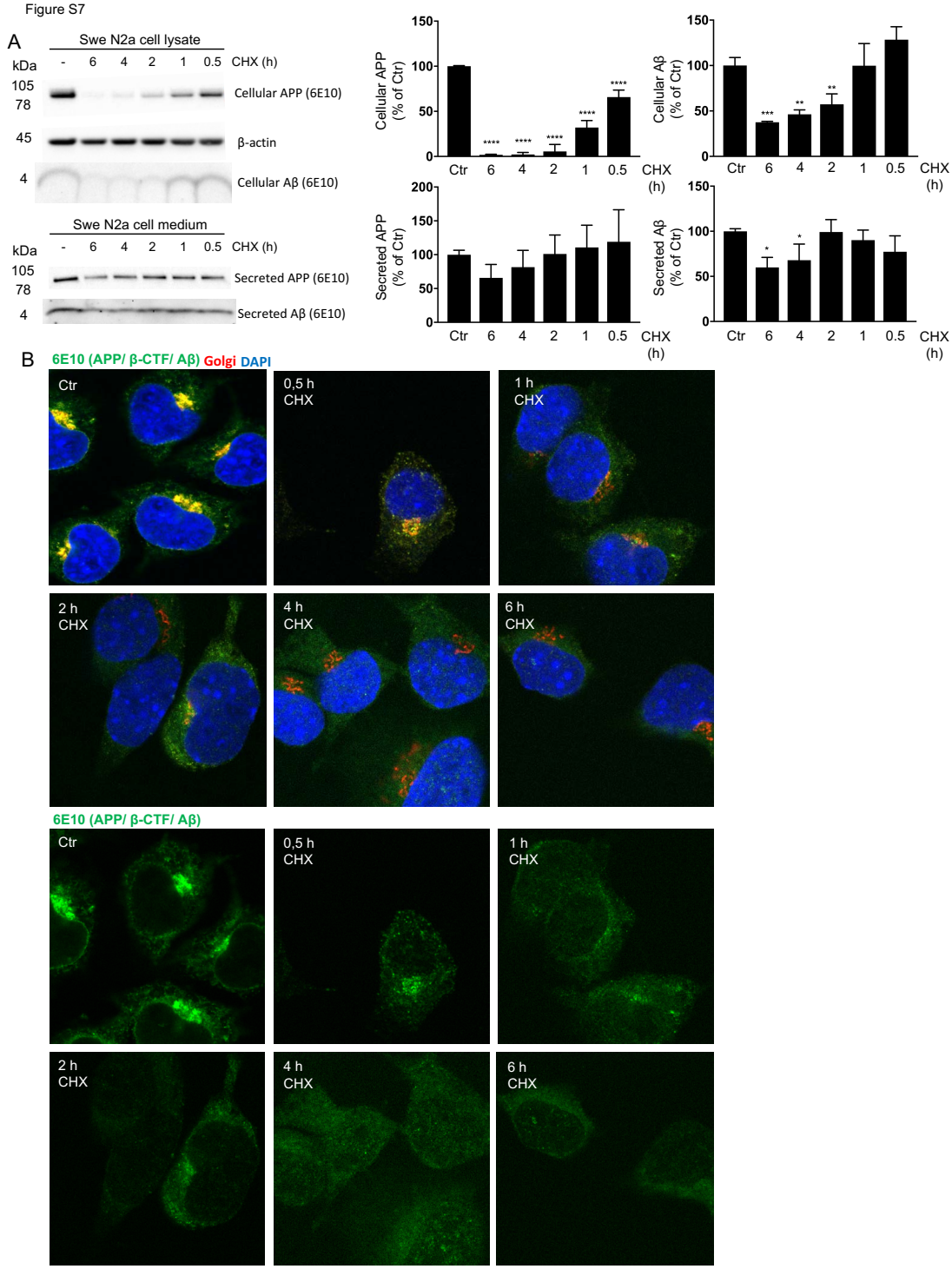

A
Swe N2a cell lysate
kDa
- 6 4 2 1 0.5 CHX (h)
105
78
Cellular APP (6E10)
45
β-actin
4
Cellular Aβ (6E10)
Swe N2a cell medium
kDa
- 6 4 2 1 0.5 CHX (h)
105
78
Secreted APP (6E10)
4
Secreted Aβ (6E10)
Cellular APP (% of Ctr)
Cellular Aβ (% of Ctr)
Secreted APP (% of Ctr)
Secreted Aβ (% of Ctr)
Ctr 6 4 2 1 0.5 CHX (h)
B
6E10 (APP/ β-CTF/ Aβ) Golgi DAPI
Ctr
0,5 h CHX
1 h CHX
2 h CHX
4 h CHX
6 h CHX
6E10 (APP/ β-CTF/ Aβ)
Ctr
0,5 h CHX
1 h CHX
2 h CHX
4 h CHX
6 h CHX

Figure S8

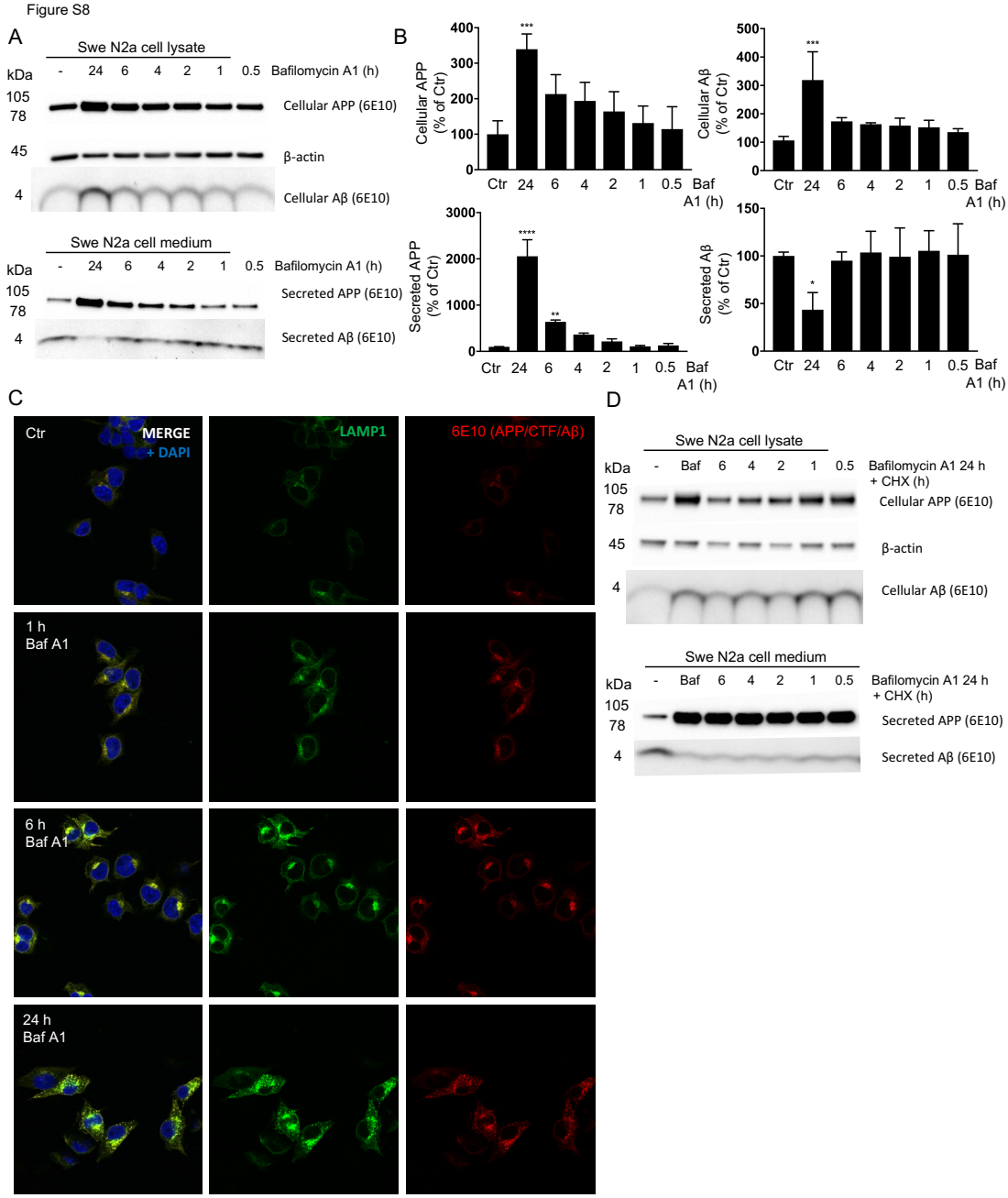
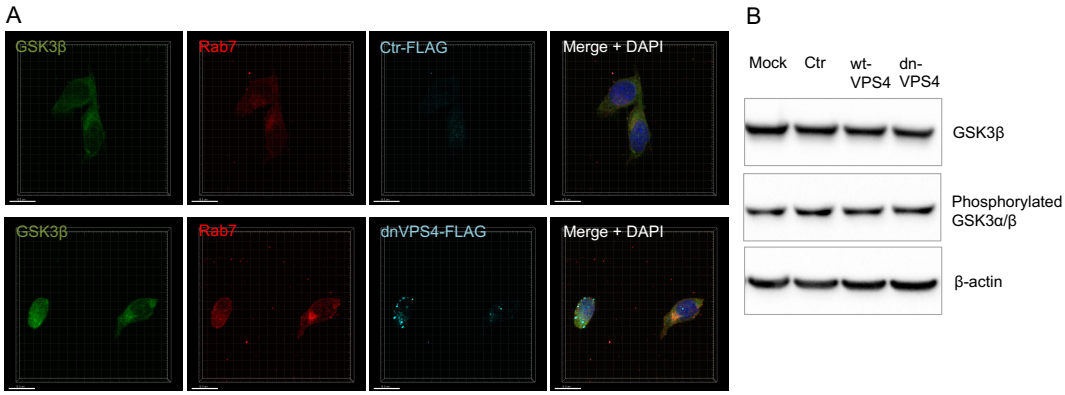

A
Swe N2a cell lysate
kDa
- 24 6 4 2 1 0.5 Bafilomycin A1 (h)
105
78
Cellular APP (6E10)
45
β-actin
4
Cellular Aβ (6E10)
Swe N2a cell medium
kDa
- 24 6 4 2 1 0.5 Bafilomycin A1 (h)
105
78
Secreted APP (6E10)
4
Secreted Aβ (6E10)
B
Cellular APP (% of Ctr)
Cellular Aβ (% of Ctr)
Secreted APP (% of Ctr)
Secreted Aβ (% of Ctr)
Ctr 24 6 4 2 1 0.5 Baf A1 (h)
C
Ctr
MERGE + DAPI
LAMP1
6E10 (APP/CTF/Aβ)
1 h Baf A1
6 h Baf A1
24 h Baf A1
D
Swe N2a cell lysate
kDa
- Baf 6 4 2 1 0.5 Bafilomycin A1 24 h + CHX (h)
105
78
Cellular APP (6E10)
45
β-actin
4
Cellular Aβ (6E10)
Swe N2a cell medium
kDa
- Baf 6 4 2 1 0.5 Bafilomycin A1 24 h + CHX (h)
105
78
Secreted APP (6E10)
4
Secreted Aβ (6E10)

Figure S9


A
GSK3β
Rab7
Ctr-FLAG
Merge + DAPI
GSK3β
Rab7
dnVPS4-FLAG
Merge + DAPI
B
Mock
Ctr
wt-VPS4
dn-VPS4
GSK3β
Phosphorylated GSK3α/β
β-actin

Paper IV

nature COMMUNICATIONS

ARTICLE

Received 31 May 2016 | Accepted 25 Jan 2017 | Published 13 Mar 2017

DOI: 10.1038/ncomms14726 OPEN

Pre-plaque conformational changes in Alzheimer's disease-linked Aβ and APP

O. Klementieva[1], K. Willén[1], I. Martinsson[1], B. Israelsson[1], A. Engdahl[2], J. Cladera[3], P. Uvdal[2,4] & G.K. Gouras[1]

Reducing levels of the aggregation-prone Aβ peptide that accumulates in the brain with Alzheimer's disease (AD) has been a major target of experimental therapies. An alternative approach may be to stabilize the physiological conformation of Aβ. To date, the physiological state of Aβ in brain remains unclear, since the available methods used to process brain tissue for determination of Aβ aggregate conformation can in themselves alter the structure and/or composition of the aggregates. Here, using synchrotron-based Fourier transform infrared micro-spectroscopy, non-denaturing gel electrophoresis and conformational specific antibodies we show that the physiological conformations of Aβ and amyloid precursor protein (APP) in brain of transgenic mouse models of AD are altered before formation of amyloid plaques. Furthermore, focal Aβ aggregates in brain that precede amyloid plaque formation localize to synaptic terminals. These changes in the states of Aβ and APP that occur prior to plaque formation may provide novel targets for AD therapy.

[1] Experimental Dementia Research Unit, Department of Experimental Medical Science, Lund University, 22184 Lund, Sweden. [2] MAX IV Laboratory, Lund University, 22100 Lund, Sweden. [3] Department of Biochemistry and Molecular Biology, Universitat Autònoma de Barcelona, 08193 Bellaterra, Spain. [4] Chemical Physics, Department of Chemistry, Lund University, 22100 Lund, Sweden. Correspondence and requests for materials should be addressed to O.K. (email: oxana.klementieva@med.lu.se) or to G.K.G. (email: gunnar.gouras@med.lu.se).

Studies on the aggregation state of β-amyloid peptide (Aβ) in brain typically have relied on brain tissue being processed by techniques including homogenization, high-speed centrifugation and/or enrichment, all of which may themselves trigger alterations in protein structure and state of assembly of aggregation-prone proteins. Moreover, assaying whole-brain homogenate can make it difficult to detect localized pathology, which may occur in the early stages of the disease, before gradually progressing through the brain over time. A central question in AD concerns the mechanism by which Aβ structure contributes to neuropathology[1]. The up to 42/43 amino acid long Aβ peptides, cleaved from within the larger amyloid precursor protein (APP), are generally thought to normally exist in brain as monomers that then with age abnormally aggregate to insoluble fibrils in AD brain. Increasingly, soluble oligomers have been viewed as the neurotoxic form of Aβ. Various structures of Aβ oligomers are seen as important in AD, including particularly dimers, trimers, dodecamers and larger amyloid beta-derived diffusible ligands. However, studies on Aβ in brain tissue have generally relied on standard SDS gel electrophoresis or other methods, which can alter native protein conformations. Thus, at present, no consensus exists regarding the structures of Aβ species in brain associated with disease pathogenesis.

Here, to analyse the early changes in Aβ structure in brains of AD transgenic mouse models of β-amyloidosis, we used the non-destructive techniques of synchrotron-based two-dimensional Fourier transform infrared micro-spectroscopy imaging (μFTIR) and blue native polyacrylamide gel electrophoresis (BN-PAGE) complemented with 3D confocal immunofluorescence microscopy.

BN-PAGE is a separation method that is sensitive to alterations in the conformation of a protein and is therefore useful for the study of protein aggregation. Combined with western blot it provides higher sensitivity to detect Aβ than gel filtration or sucrose density ultra-centrifugation. μFTIR detects vibrations of main-chain carbonyl groups that occur in the wavenumber range of 1,600 to 1,700 cm^{-1} (Amide I region)[2], allowing for the detection of specifically β-sheet structures[3]. Importantly, no tissue processing is required, and non-volatile tissue components that could be affected or lost during chemical processing remain *in situ* and contribute to the infrared spectrum[2–4]. μFTIR permits for the acquisition of spectra from samples as low as 100 pg (ref. 5); however, μFTIR is a non-destructive technique, since mid-IR photons are too low in energy (0.05–0.5 eV) to either break chemical bonds or to cause ionization[6,7]. Using FTIR it was shown that amyloid fibrils and native β-sheet proteins produce different Amide I bands[8], as they differ by the structural variability of the residues constructing their sheets, the average number of strands per sheet, and twist angles. Different morphologies of purified amyloid fibrils and native β-sheet proteins were confirmed *in vitro* by cryo-electron microscopy[9]. Although *in vitro* and *in vivo* environments are of course different and ideal controls for the FTIR experiments of brain tissue are challenging, μFTIR has been used to specifically detect amyloid fibrils in tissue sections[10,11]. Here we provide evidence of localized β-sheet elevations in brain tissue of AD transgenic mice using μFTIR that precede amyloid plaque formation. In addition, using BN-PAGE we show the loss of a low molecular weight Aβ complex and emergence of higher weight Aβ and APP complexes in AD transgenic mouse brains that occur concomitant with this pre-plaque rise in β-sheet content by μFTIR.

Results

Pre-plaque β-sheet transition in transgenic AD models. To focus on the development of amyloid pathology, we used young AD transgenic Tg19959 mice harbouring two familial AD mutations in the amyloid precursor protein (APP), which show initial amyloid plaques at or just before 3 months of age[12]. μFTIR spectral maps were recorded in chemically unprocessed brain sections of Tg19959 and wild-type mice at 1, 2 and 3 months of age (Fig. 1). We verified that the sample preparation used for our μFTIR imaging of cryo-dried brain tissue did not introduce artificial β-sheet formation, since change of β-sheet did not occur with cryo-drying of synthetic Aβ42 preparations (Supplementary Fig. 1). The increase in intensity of a band around 1,627 cm^{-1} in the amide I region of the infrared spectra (red on the μFTIR maps; Fig. 1a) correlated with the age of Tg19959 mice and is indicative of increased β-sheet structures already developing between 1 and 2 months, which is before amyloid plaque formation as determined by thioflavin S (ThS) staining. To better resolve the peak positions for β-sheet structures at around 1,627 cm^{-1} and the band centred at 1,656 cm^{-1} (a frequency characteristic of α-helical structures), we performed a second derivative analysis[10,13]. The second derivative spectra of wild type and 1 month-old Tg animals displayed a peak at around 1,640 cm^{-1}, which together with the less intense bands above 1,675 cm^{-1}, can be assigned to the intra-molecular β-sheet structures of native proteins[10,11]. The second derivative spectra of AD transgenic animals are characterized by a peak at about 1,627 cm^{-1}, due to inter-molecular β-sheet structures. The inter-molecular β-sheet content increased only in AD transgenic and not in wild-type mouse brains at these ages (Fig. 1b–g). This type of intermolecular β-sheet structure has been described as amyloid aggregates in brain tissue samples analysed by μFTIR (refs 11,14). However, β-sheet content in brain sections of 1-month-old Tg19959 mice was similar to those of wild-type mice. Immunolabelling of post-fixed brain sections adjacent to the FTIR brain sections with a C-terminal specific Aβ42 antibody indicated age-related increases of Aβ42 in transgenic but not wild-type mouse brain tissue. Of note, Aβ42 labelling in 2 month-old Tg19959 mice was punctate, and therefore not consistent with pre-fibrillar diffuse plaques, whereas β-sheet structures detected by μFTIR appear over significantly wider areas of cortex (Supplementary Fig. 2a), which likely is to some extent due to the lower spatial resolution of μFTIR. To complement the μFTIR data, we used the conformation-specific antibody OC (ref. 15) and ThS, which are both considered indicators of fibrillar amyloid structures. However, the adjacent Tg19959 brain sections to those showing early β-sheet structures by FTIR did not show evidence of amyloid fibrils with antibody OC or ThS (Supplementary Figs 3 and 4). The absence of ThS and OC antibody labelling may be due to the low concentration of fibrils and/or dye specificity, that ThS and OC labelling do not detect all types of fibrils[16,17], or due to a non-fibrillar nature of the β-sheet structures.

FTIR measurements of a model compound (synthetic Aβ1-40 monomers) showed a peak at 1,640 cm^{-1} (Fig. 2a), which corresponds to unstructured Aβ40 monomers in the experimental solution (buffered D_2O)[18]. This signature was not observed for Aβ40 oligomers and fibrils, suggesting that unstructured monomers were not present in the samples. Instead, Aβ40 oligomers show a peak at about 1,630 cm^{-1}, which indicates the presence of β-sheets[18]. However, the electron microscopy, small angle X-ray scattering and ThT spectroscopy data support the non-fibrillar nature of these Aβ40 oligomers: lack of thin (12–15 nm), elongated (100–1,000 nm) and branched structures, which are characteristics of fibrils[19] (Fig. 2b–d). These data corroborate previously published experimental data[18] and although the secondary structure of *in vitro*-generated Aβ oligomers cannot be a true prototype for oligomers that may form *in vivo* in the complex environment of the brain, these data support the hypothesis that the β-structures detected in brain

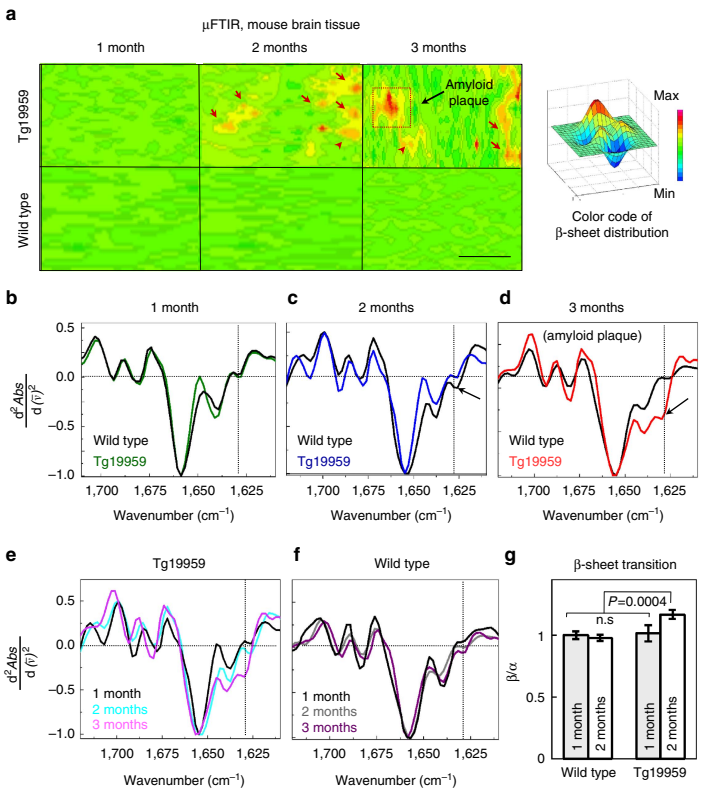


Figure 1 | Early β-structural transition in transgenic AD mouse brains. (**a**) FTIR maps were integrated for the β-sheet spectral region at 1,635–1,620 cm^{-1} to visualize absorption intensities for the β-sheet content in brain sections of Tg19959 (upper panels) and wild type (lower panels) mice at 1, 2 and 3 months, respectively. β-sheet content is shown in red (arrows). Maps are representative; $N=3$; N represents the number of animals per genotype/age. Scale bar, 50 μm. (**b**) Averaged and normalized 2nd derivatives of the Amide I absorption band; β-sheet structures in 1-month Tg19959 mice are similar to those in wild-type mice; averages were taken from 20 to 40 FTIR measurement positions per brain section and 3 brain sections per genotype/age). (**c**) Averaged and normalized 2nd derivatives of FTIR spectra taken from areas with increased β-sheet content in the corresponding μFTIR maps in **a**. The corresponding FTIR absorbance spectra with elevated β-sheet content are shown in Supplementary Fig. 2. The red arrow shows an increase in β-sheet content in Tg19959 mouse brain. Vertical dashed lines indicate the centre of the β-peaks. Horizontal dashed lines indicate (x, $y=0$). (**d**) Same as in **c**, but for 3 month-old Tg19959 mice, with spectra taken from an area with high β-sheet content (indicated by red dotted square on the corresponding μFTIR map). (**e**) The overlap of the second derivatives corresponding to Tg19959 mice at different ages more clearly shows the progressive increase in β-content with age. (**f**) In comparison the overlap of the second derivatives corresponding to wild-type mice at different ages is similar. FTIR spectra are representative; FTIR spectra from different animals of the same age and genotype are shown in Supplementary Fig. 2c. (**g**) Statistical analysis of β-sheet content measured as the average of the ratio of peak intensities between 1,635 and 1,620 cm^{-1} (β-sheet) to 1,656 cm^{-1} (α-helix) in Tg19959 and wild-type mice as a function of age. Protein aggregation in wild-type mice is taken as 100%. ANOVA ($P<0.01$) followed by Bonferroni's *post-hoc* comparisons test ($P<0.01$). $N=9$; N represents the number of brain sections. Data are represented as mean ± s.d.

tissue of Tg19959 mice at 2 months of age may originate from non-fibrillar (non-ThT and non-OC positive) β-sheet Aβ species formed in brain tissue prior to amyloid plaques.

To model the above findings in brain in a cellular system, we examined Aβ aggregation in AD transgenic neurons in culture, which show Aβ accumulation with time, similar to what occurs in brain with ageing[20]. μFTIR showed elevation of β-sheet structures in AD transgenic neurons between 12 and 19 days *in vitro*, compared to wild type neurons, respectively (Fig. 3a–c). Although age of neurons in culture[21] is not directly comparable to age of neurons in brain, these results support the conclusion that β-sheet structures can be formed within neurons.

Early changes in Aβ/APP complexes in AD transgenic mice. To analyse changes in the native conformation of Aβ and APP in brain tissue BN-PAGE and subsequent western blot using different Aβ and/or APP specific antibodies was performed. For molecular weight estimation of native Aβ on BN-PAGE we used synthetic Aβ1-42, which runs as a mixture of monomers, dimers, trimers and tetramers. Interestingly, Aβ in brain of wild-type and

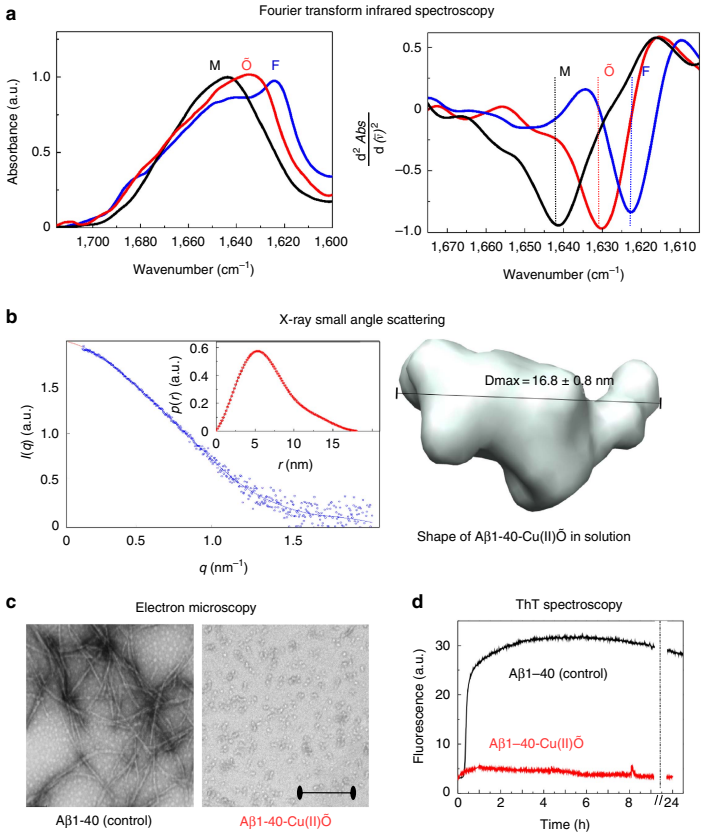


Figure 2 | Non-fibrillar Aβ1-40 oligomers with β-sheet quaternary structure. (**a**) Left panel: normalized FTIR spectra of Aβ1-40 monomers (M) in 10 mM Hepes/D_2O pD11, fibrils (F) after 24 h incubation in 10 mM Hepes pD7.4 and Aβ1-40-Cu(II)-induced oligomers (Aβ1-40-Cu(II)Ō) after 24 h incubation at 37 °C, pD7.4. Graphs show the Amide I region. Right panel: Second derivatives show a band centred at around 1,623 cm^{-1} (blue, F) indicative of the existence of fibrillar β-structures. A broader band is centred around 1,643 cm^{-1} (black, M), which can be assigned to a mixture of unordered and helical structures. A band centred at 1,630 cm^{-1} (red, Ō) is indicative of the existence of β-sheet structure. (**b**) SAXS analysis of the Aβ1-40 Cu(II)Ō. In the graph: blue line shows the best fit for the model (spheres) calculated using GNOM (ref. 4); the blue circles correspond to the experimental data. Inset: pair distribution function p(r) with a single peak that corresponds to the quasi-globular shape with $D_{max} = 16.8 \pm 0.8$ nm. *De novo* three-dimensional reconstruction of the scattering entity of Aβ1-40-Cu(II)Ō using DAMMIN (ref. 4) after 10 independent DAMMIN reconstructions. A line indicates the maximum dimension (D_{max}). Scale bar, 200 nm. (**c**) Electron microscopy images show that after incubation for 24 h at 37 °C, Aβ1-40 (control) formed amyloid fibrils (right image) while Aβ1-40-Cu(II)Ō formed spherical aggregates. EM images are representative; 6–10 images were acquired for each EM grid. (**d**) Aβ1-40 aggregation was evaluated by ThT fluorescence; the change in ThT fluorescence showed that 25 μM Aβ1-40 Cu(II)Ō do not form fibrils (red), whereas a control sample, 25 μM Aβ1-40 alone, does form fibrils (black). ThT fluorescence was monitored during 24 h of incubation at 37 °C in 10 mM Hepes pH 7.4. The dashed line indicates a time point of sample collection for EM and FTIR. Kinetics are representative; at least three repeats were done.

1-month-old AD transgenic mice runs as a band closest to the 20 kDa low molecular weight marker on BN-PAGE (Fig. 4a,b; Supplementary Fig. 5a), as well as a higher molecular weight smear, which we show below, is however consistent with APP. This Aβ band corresponds to synthetic Aβ1-42 tetramers running on the same BN-PAGE (Fig. 4 and Supplementary Fig. 5). Remarkably, at and after 2 months of age there was a drop in the intensity of this Aβ band in AD transgenic mouse brains on BN-PAGE concomitant with an increase in Aβ aggregation evident as a high molecular weight smear between 100–500 kDa. Blotting with antibody 369 against the C-terminus of APP/CTFs and 22C11 against the N-terminus of APP suggests that this Aβ tetramer band that drops at 2 months in AD transgenic mouse brain does not correspond to other APP fragments (Supplementary Fig. 5b). Overall, these results support the conclusion that under physiological conditions Aβ in brain initially exists as a low molecular weight protein complex consistent with Aβ tetramers. With the age-related increase in Aβ in AD

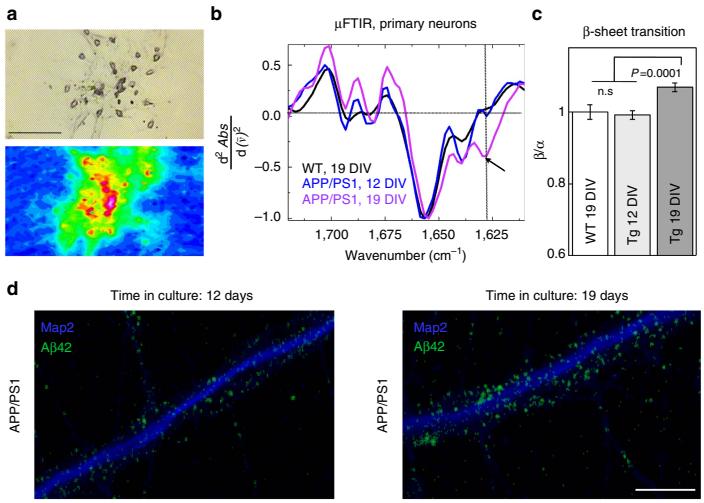


Figure 3 | β-sheet aggregation in cultured AD transgenic primary neurons. (**a**) Bright field image (upper panel) and FTIR map (lower panel) of AD neurons cultured for 19 DIV on a FTIR sample support. Scale bar, 50 μm. (**b**) Averaged and normalized second derivatives of FTIR spectra taken from APP/PS1 neurons at 12 and 19 DIV, and wild-type neurons at 19 DIV. Arrows indicate the β-sheet peak, which is evident only in APP/PS1 neurons at 19 DIV. (**c**) Statistical analysis of protein aggregation measured as the average of the protein aggregation ratios of 1,628 cm^{-1} (β-structures) to 1,656 cm^{-1} (α-structures) in AD transgenic and wild-type neurons as a function of days *in vitro*. β-sheet content in wild-type neurons is taken as 100%. ANOVA ($P<0.01$) followed by Bonferroni's *post-hoc* comparisons test ($P<0.01$); *N* represents the number of neurons (50 cells per genotype/age). Data are represented as mean ± s.d. (**d**) High-resolution confocal microscopy images of immunofluorescently labelled Aβ42 (green) using antibody 12F4 and the dendritic marker MAP2 (blue) reveal increases in Aβ42 labelling between 12 and 19 DIV. Scale bar is 1 μm.

transgenic mice, this Aβ complex is then reduced as Aβ forms higher molecular weight aggregates. Strikingly, this change in the initial state of Aβ occurs concomitantly with the increase of β-structured content detected by μFTIR.

We next analysed the molecular weight of APP in brains by BN-PAGE (Fig. 4c; Supplementary Fig. 5c). Remarkably, the molecular weight patterns of APP also changed between 1 and 2 months in brains of Tg19959 mice before the appearance of amyloid plaques. Specifically, on BN-PAGE, APP in the membrane soluble fraction of Tg19959 mouse brains at 1 month of age runs similarly to APP in wild-type mouse brains as two bands, which appear to correspond to APP monomers and dimers[22]. In contrast, at 2 months of age, APP in Tg19959 mouse brains changes to three bands with molecular weights that correspond to about 140, 240 and 480 kDa. The appearance of the additional 480 kDa band supports that APP may aggregate as well. Interestingly, after 2 months of age, Tg19959 mouse brains show a smear with a molecular weight corresponding to 240–480 kDa on BN-PAGE using Aβ N-terminus antibody 82E1, which could suggest an interaction between Aβ and APP (ref. 23). Similar high-molecular weight Aβ was also observed on BN-PAGE in aged APP23 AD transgenic mice[24].

To investigate whether there is an age-dependent interaction between Aβ and APP, Tg19959 mouse brains were immunoprecipitated with the human-specific APP antibody P2-1 followed by dot blotting with the Aβ42 specific antibody 12F4, which indicated an age-dependent increase in the association of Aβ42 with APP (data not shown). To experimentally examine the interaction of Aβ42 with APP, transgenic and wild-type mouse neurons were treated with 1 μM synthetic human Aβ1-42 for 24 h. After treatment, BN-PAGE followed by Western blot with human Aβ/CTF antibody 82E1 and Aβ/APP antibody 6E10 revealed the added human Aβ as a band at 240 kDa, corresponding to the molecular weight of APP, only in the APP overexpressing AD transgenic neurons but not the wild-type neurons (Supplementary Fig. 6a). Furthermore, Aβ immunolabelling of neurons treated with 1 μM synthetic Aβ1-42 showed a greater binding of Aβ1-42 to the cell surface of AD transgenic than to wild-type neurons (Supplementary Fig. 6b). Taken together these data support an interaction between Aβ and APP, and indicate that AD related protein aggregation is a complex process during which the physiological states of both Aβ and APP are affected.

Aβ aggregation and synapse pathology. To further define the localization of these pre-plaque β-aggregates and to evaluate potential pathological consequences of early Aβ-aggregation in brain, 1, 2 and 3 month-old Tg19959 mouse brain sections were labelled with antibodies directed against Aβ42 and synaptophysin or drebrin, markers of pre- and post-synaptic compartments, respectively. Three-dimensional confocal microscopy revealed that AD transgenic mouse brains show progressive Aβ42 accumulation in synaptic compartments (Fig. 5a; Supplementary Figs 7 and 8). In particular, post-synaptic Aβ42 labelling increased in AD transgenic mouse brains. In 1-month-old Tg19959 and wild-type mouse brains synaptic Aβ42 labelling is much less evident compared to older Tg19959 mice, consistent with prior immuno-electron microscopy of another AD transgenic mouse model[25]. The increase of Aβ42 labelling at two months of age is concomitant with the FTIR and biochemical data showing increases in Aβ aggregation with age in these AD

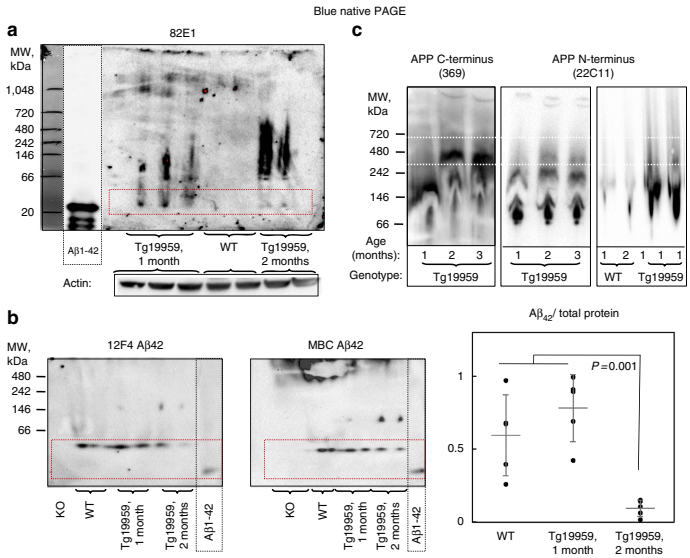


Figure 4 | Native Aβ and APP complexes in Tg19959 mouse brains change with age. (**a**) Blue native polyacrylamide gel electrophoresis (BN-PAGE) and subsequent Western blot of membrane-associated TBST fractions of mouse brain homogenates at 1 and 2 months of age. As detected by the human specific 82E1 antibody, human Aβ (dotted red box) in the Tg19959 mouse brain appears consistent with Aβ1-42 tetramers as well as a smear at higher molecular weights. Synthetic human Aβ1–42 was used as a molecular weight marker and positive control (dotted black box; underexposed). (**b**) BN-PAGE of membrane-associated fractions of mouse brain homogenates at 1 and 2 months of age and subsequent Western blotting with Aβ42 specific antibodies 12F4 and MBC42 detect the presence of low molecular weight Aβ42 bands (dotted red boxes). The low molecular weight Aβ42 band appears specific, since no band is observed in brain tissue homogenate from APP knockout mice. Statistical analysis of Aβ42 in brain homogenate: ANOVA ($P<0.01$) followed by Bonferroni's *post-hoc* comparisons test ($P<0.01$); grey lines indicate the mean ± s.d.; N of 4 represents number of independent experiments. (**c**) Native APP in Tg19959 mouse brains changes with age. BN-PAGE and subsequent blotting with antibody 369 against the C-terminus of APP/CTFs and 22C11 against the N-terminus of APP show alterations in the molecular weight of APP with a 480 kDa band appearing at 2 months of age in Tg19959 mice (dotted white boxes), which is not seen in WT or 1 month old Tg19959 mice. Total protein concentrations were determined using the BCA assay and further controlled by a parallel SDS PAGE blotted with β-actin; protein loaded was 100 μg per well in all experiments. Blots are representative, $N=3$.

transgenic mice. Interestingly, with the increasing synaptic Aβ in Tg19959 mouse brains at two months of age, the overlap of Aβ42 with the presynaptic protein synaptophysin also became more evident. Moreover, at 3 months of age, when amyloid fibrils detected by antibody OC are even more evident in synapses of AD transgenic mouse brains, the pre- and post-synaptic proteins appear to overlap more; such an increased overlap of the pre- and post-synaptic markers suggests localized synaptic abnormalities (Supplementary Fig. 7). The presence of Aβ in synapses of wild-type mouse brains, and its early accumulation in synapses in transgenic mice, supports the conclusion that synapses are the sites where physiological Aβ starts to accumulate and aggregate, thereby mediating synapse dysfunction in pre-plaque AD brain. Taken together our results demonstrate alterations in the native states of Aβ and APP with pre-plaque β-aggregation, which is concomitant with synaptic alterations in a transgenic mouse model of β-amyloidosis.

Discussion

Here we provide evidence that the physiological conformation of Aβ in brain on BN-PAGE is consistent with synthetic Aβ1-42 tetramers. Of note, tetramers were also the preferred state of freshly prepared Aβ1-42 run on the native gels (Fig. 4a; Supplementary Fig. 5a). Native gels are less accurate when it comes to molecular weight, and running the same synthetic Aβ1-42 preparations on semi-denaturing and SDS–polyacrylamide gel electrophoresis (SDS–PAGE) gels showed progressive loss of the tetramer band, and indicated that this tetramer band runs closer to a 14 kD molecular weight marker (not shown). We also noticed that the Aβ42 specific antibodies detected the band consistent with Aβ42 tetramers in brain but not the synthetic Aβ1-42 tetramers (Fig. 4b). We previously reported that Aβ42 specific antibodies react predominantly to Aβ1-42 monomers[20]. However, the observations in Fig. 4b suggest that the structure of the Aβ band that appears consistent with a tetramer in brain differs from synthetic Aβ1-42 tetramers. It is possible that, for example, associated lipid components and/or N- and/or C-terminally modified Aβ peptides contribute to this difference between this low molecular weight Aβ complex in brain compared to synthetic Aβ42.

Importantly, we demonstrate that the loss of this physiological state of Aβ in AD transgenic mouse brain before plaque formation is concomitant with the appearance of increased β-sheet content by FTIR; however this is not ThS or OC antibody positive, pointing to a non-fibrillar character of early β-sheet formation. Although, the differences between transgenic and wild type animals in the μFTIR spectra related to β-structures and

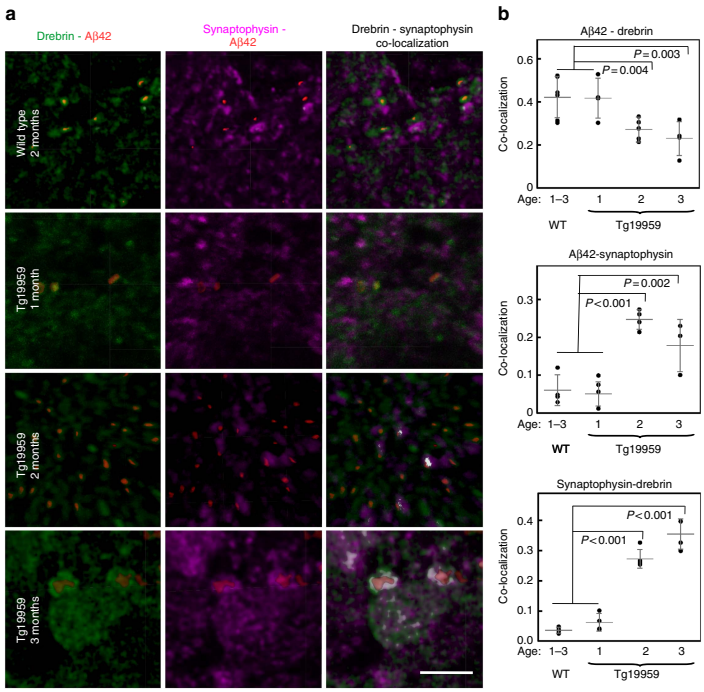


Figure 5 | Aβ42 disrupts the cytoarchitecture of dendritic terminals in Tg19959 mouse brains with age. (**a**) High-resolution confocal microscopy images of immunofluorescently labelled Aβ42 (red), the post-synaptic protein drebrin (green) and the pre-synaptic protein synaptophysin (magenta) in 2-month-old wild type, and 1–3 months-old Tg19959 mouse brain cortex. Iso-surface rendering of Aβ42 more clearly reveals Aβ42 within drebrin positive compartments. Note the presence of Aβ42 also in wild-type mice and the increasing levels of Aβ42 with age in Tg19959 mice. In the far left panel, the white colour shows co-localization of drebrin and synaptophysin, which is evident in 2 and 3 month-old Tg19959 mice. Scale bar is 2 µm. For an overview, low magnification images are shown in Supplementary Fig. 8. (**b**) Statistical analysis of the co-localization of Aβ42 with pre- and post- synaptic markers, as well as for the overlap of synaptophysin with drebrin: ANOVA ($P<0.01$) followed by Bonferroni's *post-hoc* comparisons test ($P<0.01$); 1 is equal to 100% of co-localization, grey lines indicate the mean ± s.d., $N=4$.

age-related increases in Aβ42 are evident, development of new antibodies which are both specific to β-structures and to Aβ will be helpful to determine whether the β-sheet structures detected by µFTIR in brain tissue of transgenic animals originate from Aβ42. Further, we present evidence consistent with aggregation of APP concomitant with Aβ pathogenesis, which may be contributing to the pre-plaque increase in β-structure. Since the increase of Aβ is concomitant with an apparent change in APP structure, and since *in vitro* experiments support that Aβ may bind APP, it is possible that binding of Aβ may cause changes in APP structure that interfere with physiological processing of APP. Dystrophic neurites, associated with amyloid plaques, are known to accumulate APP, as well as Aβ42 and the β-site amyloid precursor protein cleaving enzyme 1, supporting the concept that such dystrophies are the nidus of amyloid plaque formation[20,25].

It is of considerable interest that the destabilization and loss of the native state of normally tetrameric transthyretin has been found to promote subsequent aggregation of transthyretin into the β-sheet rich pathologic amyloid found in patients with transthyretin amyloidosis. Moreover, pharmacological stabilization of the physiological transthyretin tetramers led to the approval of the first drug that slows down the progression of an amyloidosis in the clinic[26–28]. Growing evidence also suggests that the native oligomeric structure of α-synuclein associated with Parkinson's disease is a tetramer[29]. Thus, the current study supports the concept that the native and physiological conformations of proteins linked pathologically and genetically to AD might also be altered in the disease. Stabilization of the physiological structure might therefore be considered among novel therapeutic approaches.

Methods

Animals. All mouse experiments were compliant with the requirements of the Ethical Committee of Lund University. Experimental AD transgenic mouse group: female Tg19959 mice, which harbour Swedish and Indiana familial AD mutations (KM670/671NL and V717F) in human APP under the control of the hamster PrP promoter[12]. Control group: female C57/B6SJL wild-type mice. Primary neuronal cultures were derived from cerebral cortex and hippocampus of Tg (hAPPswe, PSEN1dE9)85Dbo/Mmjax (APP/PS1; Jackson Labs) or wild-type mice at embryonic day 15 as described[30]. All mice were screened for the presence of the human APP695 transgene by PCR.

Experimental design. Brain material (sections or homogenates) of female Tg19959 and wild-type mice at 1, 2 and 3 month of age, N of 3–4 animals per genotype/age, were collected for the study. Brain sections were used for µFTIR and immunofluorescence imaging; brain homogenates (cortex) were used for biochemical studies.

Experimental procedures. Female Tg19959 and wild-type mice were killed at 1, 2 and 3 month of age. Mice were deeply anaesthetized with 100 mg kg^{-1} 1:10 ketamine:xylazine administered by intraperitoneal injection. For μFTIR and biochemical analysis, animals were first perfused transcardially with phosphate-buffered saline (PBS), and then brains were removed from skulls and deeply frozen in liquid nitrogen. For immunohistochemistry, brains were fixed by transcardial perfusion with PBS followed by 4% paraformaldehyde (PFA) in 0.1 M PBS (pH 7.4) at room temperature (RT) and post-fixed by immersion in 4% PFA in 0.1 M PBS at 4 °C overnight.

Aβ1-40 and Aβ1-42 peptides. Synthetic Aβ1-40 (DAEFRHDSGYEVHHQKLVF FAEDVGSNKGAIIGLMVGGVV) was purchased from JPT (Germany). Stock solution of 500 μM synthetic Aβ1-40 (JPT) was prepared in 10 mM HEPES (Sigma-Aldrich) with 0.02% NH_3 at pH 11 (pH of the non-aggregated peptide stock); aliquots were kept at − 80 °C until use. Aβ1-40 oligomers were prepared in the presence of ions of Cu(II) as described[31], with a minor change: Cu_2SO_4 was added in a stoichiometric ratio to Aβ1-40 stock solution, and then pH was changed to pH 7.4 to allow Aβ aggregation.

Small angle x-ray scattering (SAXS) analysis of the Aβ1-40 Cu(II)-induced oligomers was done at the beamline X33 EMBL DESY synchrotron (Germany). SAXS data was acquired for 1 mg ml^{-1} Aβ1-40-Cu(II)O in 10 mM Hepes pH 7.4 after 24 h of incubation at 37 °C before the experiment. The fit for the model (spheres) was calculated using GNOM (ref. 32). *De novo* three-dimensional reconstruction of the scattering entity of Aβ1-40-Cu(II)-induced oligomers was performed using DAMMIN (ref. 32) after 10 independent DAMMIN reconstructions.

Synthetic Aβ1-42 (DAEFRHDSGYEVHHQKLVFFAEDVGSNKGAIIGLMVG GVVIA) was purchased from Tocris Bioscience (USA). The peptides were dissolved in cold DMSO (Sigma–Aldrich) at a concentration of 250 μM, divided into aliquots of 50 μl and kept at at − 80 °C until use. Recombinant Aβ1-42 (M-DAEFRHDSGYEVHHQKLVFFAEDVGSNKGAIIGLMVGGVVIA), 20 μM in 20 mM phosphate buffer (pH 7.4), was a gift of Prof. Sara Linse (Lund University). Recombinant Aβ1-42 was prepared and purified as described[33], and kept on ice until use (1–2 h).

Fibril growth assays were initiated by placing the 96-well plate at 37 °C under quiescent conditions. The ThT fluorescence was measured through the bottom of the plate every 60 s with a 440 nm excitation filter and a 480 nm emission filter in a plate reader (Fluostar Omega BMG Labtech). To monitor fibril formation, Thioflavin T (ThT) kinetic assays were used. For ThT kinetics, 20 μM Aβ1-42 was incubated in the presence 6 μM ThT at 37 °C without agitation in a 96-well plate of black polystyrene with a clear bottom and PEG coating (Corning 3881). Since ThT fluorescence intensity at 480 nm is proportional to the mass of amyloid fibrils, the kinetic evaluation of the aggregation reactions showed that after several hours of incubation, Aβ1-42 formed β-sheet fibrils. For μFTIR measurements, in parallel to the ThT kinetic assays, Aβ1-42 was incubated without adding ThT in low-bind Eppendorf tubes at 37 °C under quiescent conditions.

Synchrotron-based μFTIR. Approximately 20 μm thick coronal brain cryosections were mounted onto clean 1 × 1 mm^2 CaF_2 windows (Crystran Ltd.); to avoid protein degradation sections were stored at − 80 °C until measurements as described[2]. Sections were cryo-dried before measurements. Primary neurons were seeded directly on CaF_2 spectrophotometric windows and grown for 12 or 19 days. Cultures were washed with PBS, fixed for 20 min with 4% PFA in PBS, washed with 20 mM phosphate buffer (PB) and stored at − 80 °C until measurements. Samples with neurons were dried before measurements. Samples of Aβ1-42 monomers and fibrils were prepared in the same way as the μFTIR samples from brain tissues. Approximately 5 μL drops of monomeric and fibrillar Aβ1-42 fractions were placed on CaF_2 spectrophotometric windows, snap frozen and cryo-dried before measurements were taken.

μFTIR spectroscopy was performed at beamline D7, MAX-IV Laboratory, Lund University, Sweden as described[34,35]. μFTIR spectra were collected from mouse brain sections of cortex and CA1 hippocampus (as shown in Supplementary Fig. 2a). The instrument set-up combines a Hyperion 3,000 microscope and a Bruker IFS66/v FTIR spectrometer. First, μFTIR maps were recorded in off-line mode using a conventional thermal light source for 'overview mapping' of larger tissue areas (4–6 mm^2) using 50 μm aperture diameter. Since the brightness of conventional thermal infrared sources is inherently limited near the diffraction limit, a synchrotron infrared source, which is about 100–1,000 times brighter than a conventional thermal source, was used. The high flux density of the synchrotron source allows smaller regions to be probed with an acceptable S/N ratio[4]. FTIR spectra were collected from cultured neurons at MAX-IV Laboratory and the SOLEIL synchrotron (Gif-sur-Yvette, France) using the SMIS beamline (Supplementary Fig. 2d). The measuring range was 900 − 4,000 cm^{-1} and the spectra collection was done in transmission mode at 4 cm^{-1} resolution, 8 × 8 μm^2 aperture dimensions, from 500 to 1,000 co-added scans. Background spectra were collected from a clean area of the same CaF_2 window.

FTIR spectral analysis. Analysis of FTIR spectra was performed using the OPUS software (Bruker). After atmospheric compensation, spectra exhibiting strong Mie scattering were eliminated. For all spectra, a linear baseline correction was applied from 1,200 to 2,000 cm^{-1}. After background subtraction and vector normalization, derivation of the spectra to the second order was used to increase the number of discriminative features to eliminate the baseline contribution. Derivation of the spectra was achieved using a Savitsky – Golay algorithm with a nine-point filter and a polynomial order of two. The β-aggregation level of proteins was studied by calculating the peak intensity ratio between 1,620 and 1,640 cm^{-1}, corresponding to β-sheet structures and the maximum corresponding mainly to α-helical content at 1,656 cm^{-1}. An increase in the 1,620–1,640 cm^{-1} component is considered a signature of amyloid fibrils[10,11,14,36]. We were not able to detect changes in the range of 1,690 cm^{-1} that were previously described to differentiate antiparallel and parallel Aβ in a study on purified Aβ using FTIR (ref. 37), likely due to the greater complexity of the tissue samples.

Immunohistochemistry. PFA fixed mouse brains were cut into 40 μm thick sections on a Leica SM 2010R freezing microtome. Sections were kept in storage buffer composed of 30% sucrose and 30% ethylene glycol in PBS at − 20 °C until use. Dual and triple immunolabelling combined with ThS of free-floating sections were done as described in ref. 38 using optimal working dilutions recommended by the manufacturer. Amyloid fibrils were visualized with rabbit polyclonal antibody OC (Merck Millipore, AB2286); the free Aβ42 C-terminus was recognized by antibody 12F4 (BioLegend, Covance SIG-39142, 1/1,000); antibody 22C11 (Merck Millipore, MAB 348) was used for the human/mouse APP N-terminus. For pre-synaptic and post-synaptic labelling mouse monoclonal synaptophysin antibody (Merck Millipore, MAB5258) and rabbit polyclonal drebrin antibody (Abcam, AB11068) were used respectively. All primary antibodies are summarized in Supplementary Table 1. For dual and triple label ThS staining, sections were incubated in 0.001% ThS in 70% ethanol for 20 min, and then rinsed sequentially with 70, 95 and 100% ethanol after immunofluorescent labelling as described[38].

Confocal microscopy. Images were obtained using a Leica TCS SP8 confocal microscope (Leica Microsystems) equipped with Diode 405/405 nm and Argon (405, 488, 552 and 638 nm) lasers with an HP PL APO 63x/NA1.2 water immersion objective. Autoquant (MediaCybernetics) was used for image deconvolution. Two-dimensional images obtained by confocal microscopy were quantified and reconstructed into 3D volumetric data sets using Imaris (Bitplane). Semi-opaque iso-surfaces were defined individually for each channel from the deconvolved data and rendered as semi-opaque, solid surfaces.

Biochemical analysis of mouse brain tissue. Forebrains were homogenized in five volumes of buffer composed of 20 mM Tris–HCl, 50 mM NaCl pH 7.8 and HaltTM protease inhibitor cocktail (Thermo Fisher Scientific). After 30 min incubation on ice, a first fraction was collected as a TBS dispersible fraction. A TBS-T membrane-bound fraction was collected after the TBS insoluble pellet was re-suspended in 1% Triton, 20 mM Tris–HCl, 50 mM NaCl at pH 7.4, incubated 30 min on ice and centrifuged. To avoid artificial protein aggregation or segregation, brain homogenates were centrifuged at low speed, at 10,000 *g*, at 4 °C for 30 min as described[24]. Protein amounts were determined using BCA protein assay (ThermoFisher Scientific). The protein load was also controlled by a parallel SDS–PAGE blotted with β-actin (Sigma A5316, 1/5,000). Samples were used immediately for BN- or SDS–PAGE and co-immunoprecipitation assays. For BN-PAGE, only freshly prepared samples of 100 μg total protein in 4 × Native PAGE sample buffer (Invitrogen) were electrophoretically resolved in a precast native 4–16% Bis-Tris gel (Invitrogen) according to the manufacturer's protocol. Native-Mark unstained protein standards (Invitrogen) were used as molecular weight markers. Before protein transfer, the gels were washed with running buffer containing 1% SDS for 20 min. The protein load was also controlled by a parallel SDS–PAGE blotted with β-actin (Sigma A5316, 1/5,000). For SDS–PAGE, brain homogenates (50 μg of total protein) were electrophoretically resolved in a precast NuPAGE 4–12% Bis-Tris gel system (Invitrogen). Proteins were transferred from BN and SDS gels onto polyvinylidene difluoride (PVDF) membranes (iBlotR, NovexR, Life Technologies). Unstained molecular weight markers were visualized using Ponceau S (SigmaAldrich) and digitally marked due to faint bands on the blue membranes. Membranes were boiled in PBS, pH 7.4 in a microwave oven for 5 min, and washed in PBS-TweenTM (Medicago). To block unspecific binding, membranes were incubated in 5% non-fat dry milk (Sigma) diluted in PBS-Tween for 1 h at RT. For immunodetection, membranes were incubated for 24 h at 4 °C with primary antibodies against Aβ/APP: 6E10 and 4G8 (BioLegend, Covance #SIG-39300 and #SIG-39220 respectively, 1/1,000), human/mouse APP N-terminus: 22C11 (Merck Millipore, MAB 348, 1/1,000), human APP: P2-1 (Thermo Fisher Scientific, 1/1,000), and human/mouse APP C-terminus antibody 369 (Supplementary Table, 1/1,000). The Aβ N-terminus was recognized by Aβ/APP monoclonal antibody 82E1 (IBL International #18582, 1/1,000), and the Aβ42 C-terminus was recognized by Aβ42 end-specific antibody from Life Technologies (#700254, 1/1,000) and 12F4 (BioLegend, Covance, SIG-39142, 1/1,000); MBCAβ42 (1/1,000); Chemicon (#AB5078, 1/1,000); primary antibodies are summarized in Supplementary Table 1. Blots were developed with enhanced chemiluminescence (SuperSignalR West Femto) detection system (Thermo Fisher Scientific). Synthetic Aβ1-42 (Tocris Bioscience) was used as positive and/or

negative control. All BN-PAGE blots were developed with standard chemiluminescence exposure times of 2–5 min, up to maximum exposure times of 1 h to detect even minor amounts of Aβ. All western blots were performed at least three times; only for the confirmation of the Aβ band in Fig. 3b, three additional Aβ antibodies were used to confirm the 3 blots done with antibody 82E1 and to show that this Aβ includes Aβ42. For quantification, 4 gels blotted with Aβ42 antibodies were pooled together.

Statistical analysis. One-way ANOVA followed by Bonferroni's *post-hoc* comparison tests were performed in all statistical analysis. Since no significant differences were found in the wild-type brains, the data from all the wild types were pooled and used in the statistical calculations. Statistics with a value of $P<0.01$ were considered significant.

Data availability. The data that support the findings of this study are available from the corresponding authors on reasonable request.

References

1. Marshall, K. E., Marchante, R., Xue, W.-F. & Serpell, L. C. The relationship between amyloid structure and cytotoxicity. *Prion* **8,** 192–196 (2014).
2. Baker, M. J. *et al.* Using Fourier transform IR spectroscopy to analyze biological materials. *Nat. Protoc.* **9,** 1771–1791 (2014).
3. Miller, L. M. & Dumas, P. From structure to cellular mechanism with infrared microspectroscopy. *Curr. Opin. Struct. Biol.* **20,** 649–656 (2010).
4. Kretlow, A. *et al.* FTIR-microspectroscopy of prion-infected nervous tissue. *Biochim. Biophys. Acta* **1758,** 948–959 (2006).
5. Diem, M., Romeo, M., Boydston-White, S., Miljković, M. & Matthäus, C. A decade of vibrational micro-spectroscopy of human cells and tissue (1994–2004). *Analyst* **129,** 880–885 (2004).
6. Holman, H.-Y. N., Martin, M. C. & McKinney, W. R. Synchrotron-based FTIR spectromicroscopy: cytotoxicity and heating considerations. *J. Biol. Phys.* **29,** 275–286 (2003).
7. Andrew Chan, K. L. & Kazarian, S. G. Attenuated total reflection Fourier-transform infrared (ATR-FTIR) imaging of tissues and live cells. *Chem. Soc. Rev.* **45,** 1850–1864 (2016).
8. Zandomeneghi, G., Krebs, M. R. H., McCammon, M. G. & Fändrich, M. FTIR reveals structural differences between native β-sheet proteins and amyloid fibrils. *Protein Sci.* **13,** 3314–3321 (2004).
9. Jimenez, J. L. *et al.* The protofilament structure of insulin amyloid fibrils. *Proc. Natl Acad. Sci.* **99,** 9196–9201 (2002).
10. Ami, D. *et al. In situ* characterization of protein aggregates in human tissues affected by light chain amyloidosis: a FTIR microspectroscopy study. *Sci. Rep.* **6,** 29096 (2016).
11. Miller, L. M., Bourassa, M. W. & Smith, R. J. FTIR spectroscopic imaging of protein aggregation in living cells. *Biochim. Biophys. Acta BBA–Biomembr.* **1828,** 2339–2346 (2013).
12. Li, F. *et al.* Increased plaque burden in brains of APP mutant MnSOD heterozygous knockout mice. *J. Neurochem.* **89,** 1308–1312 (2004).
13. de Aragão, B. J. G. & Messaddeq, Y. Peak separation by derivative spectroscopy applied to ftir analysis of hydrolized silica. *J. Braz. Chem. Soc* **19,** 1582–1594 (2008).
14. Benseny-Cases, N., Klementieva, O., Cotte, M., Ferrer, I. & Cladera, J. Microspectroscopy (μFTIR) reveals co-localization of lipid oxidation and amyloid plaques in human Alzheimer disease brains. *Anal. Chem.* **86,** 12047–12054 (2014).
15. Kayed, R. *et al.* Fibril specific, conformation dependent antibodies recognize a generic epitope common to amyloid fibrils and fibrillar oligomers that is absent in prefibrillar oligomers. *Mol. Neurodegener.* **2,** 18 (2007).
16. Elkins, M. R. *et al.* Structural polymorphism of Alzheimer's β-amyloid fibrils as controlled by an E22 Switch: a solid-state NMR study. *J. Am. Chem. Soc.* **138,** 9840–9852 (2016).
17. Groenning, M. Binding mode of Thioflavin T and other molecular probes in the context of amyloid fibrils—current status. *J. Chem. Biol.* **3,** 1–18 (2010).
18. Benseny-Cases, N., Cócera, M. & Cladera, J. Conversion of non-fibrillar β-sheet oligomers into amyloid fibrils in Alzheimer's disease amyloid peptide aggregation. *Biochem. Biophys. Res. Commun.* **361,** 916–921 (2007).
19. Toyama, B. H. & Weissman, J. S. Amyloid structure: conformational diversity and consequences. *Annu. Rev. Biochem.* **80,** 557–585 (2011).
20. Takahashi, R. H. *et al.* Oligomerization of Alzheimer's β-Amyloid within processes and synapses of cultured neurons and brain. *J. Neurosci.* **24,** 3592–3599 (2004).
21. Martin, M. G. *et al.* Cholesterol loss enhances TrkB signalling in hippocampal neurons aging *in vitro*. *Mol. Biol. Cell* **19,** 2101–2112 (2008).
22. Eggert, S., Midthune, B., Cottrell, B. & Koo, E. H. Induced dimerization of the amyloid precursor protein leads to decreased amyloid- protein production. *J. Biol. Chem.* **284,** 28943–28952 (2009).
23. Kedikian, G. *et al.* Secreted amyloid precursor protein and holo-APP bind amyloid β through distinct domains eliciting different toxic responses on hippocampal neurons. *J. Neurosci. Res.* **88,** 1795–1803 (2010).
24. Rijal Upadhaya, A. *et al.* Dispersible amyloid β-protein oligomers, protofibrils, and fibrils represent diffusible but not soluble aggregates: their role in neurodegeneration in amyloid precursor protein (APP) transgenic mice. *Neurobiol. Aging* **33,** 2641–2660 (2012).
25. Takahashi, R. H. *et al.* Intraneuronal Alzheimer Aβ42 accumulates in multivesicular bodies and is associated with synaptic pathology. *Am. J. Pathol.* **161,** 1869–1879 (2002).
26. Buxbaum, J. N. & Reixach, N. Transthyretin: the servant of many masters. *Cell Mol. Life Sci.* **66,** 3095–3101 (2009).
27. Kelly, J. W. Alternative conformations of amyloidogenic proteins govern their behavior. *Curr. Opin. Struct. Biol.* **6,** 11–17 (1996).
28. Peterson, S. A. *et al.* Inhibiting transthyretin conformational changes that lead to amyloid fibril formation. *Proc. Natl Acad. Sci. USA* **95,** 12956–12960 (1998).
29. Selkoe, D. *et al.* Defining the Native State of α-Synuclein. *Neurodegener. Dis.* **13,** 114–117 (2014).
30. Tampellini, D. *et al.* Synaptic activity reduces intraneuronal Abeta, promotes APP transport to synapses, and protects against Abeta-related synaptic alterations. *J. Neurosci.* **29,** 9704–9713 (2009).
31. Ha, C., Ryu, J. & Park, C. B. Metal ions differentially influence the aggregation and deposition of Alzheimer's beta-amyloid on a solid template. *Biochemistry* **46,** 6118–6125 (2007).
32. Petoukhov, M. V. *et al.* New developments in the *ATSAS* program package for small-angle scattering data analysis. *J. Appl. Crystallogr.* **45,** 342–350 (2012).
33. Arosio, P., Cukalevski, R., Frohm, B., Knowles, T. P. J. & Linse, S. Quantification of the concentration of Aβ42 propagons during the lag phase by an amyloid chain reaction assay. *J. Am. Chem. Soc.* **136,** 219–225 (2014).
34. Lindgren, J. *et al.* Microspectroscopic evidence of cretaceous bone proteins. *PLoS ONE* **6,** e19445 (2011).
35. Lindgren, J. *et al.* Molecular preservation of the pigment melanin in fossil melanosomes. *Nat. Commun.* **3,** 824 (2012).
36. Kong, J. & Yu, S. Fourier Transform Infrared Spectroscopic Analysis of Protein Secondary Structures. *Acta Biochim. Biophys. Sin.* **39,** 549–559 (2007).
37. Cerf, E. *et al.* Antiparallel β-sheet: a signature structure of the oligomeric amyloid β-peptide. *Biochem. J.* **421,** 415–423 (2009).
38. Capetillo-Zarate, E. *et al.* High-resolution 3D reconstruction reveals intra-synaptic amyloid fibrils. *Am. J. Pathol.* **179,** 2551–2558 (2011).

Acknowledgements

We thank Vladimir Denisov and Sara Linse for critical input to this manuscript. We thank Per Persson for the access to FTIR equipment. This work was funded by grants from Alzheimerfonden, Interreg Öresund-Kattegat-Skagerrak (EU), the Swedish Research Council, MultiPark and the Segerfalk, Anna-Lisa Rosenberg and Åhléns foundations.

Author contributions

O.K., G.K.G. designed experiments, analysed data and wrote the manuscript. G.K.G. supervised the research. O.K., K.W., I.M. and B.I. performed experiments. A.E. and P.U. assisted in μFTIR data acquisition and discussed the FTIR results. J.C. supervised the experiments described in Figure 2. All authors discussed the results and contributed to the scientific discussion.

Additional information

Supplementary Information accompanies this paper at http://www.nature.com/naturecommunications

Competing financial interests: The authors declare no competing financial interests.

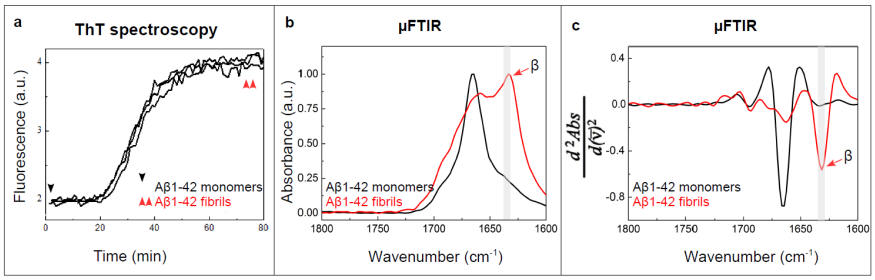
Reprints and permission information is available online at http://npg.nature.com/reprintsandpermissions/

How to cite this article: Klementieva, O. *et al.* Pre-plaque conformational changes in Alzheimer's disease-linked Aβ and APP. *Nat. Commun.* **8,** 14726 doi: 10.1038/ncomms14726 (2017).

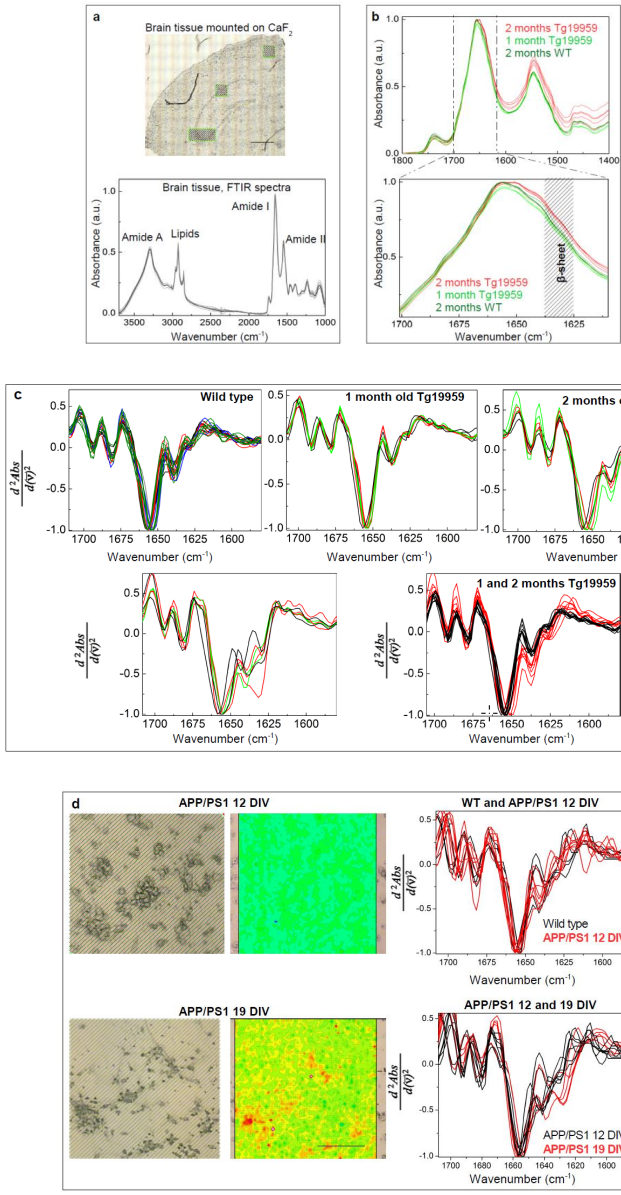
Publisher's note: Springer Nature remains neutral with regard to jurisdictional claims in published maps and institutional affiliations.

This work is licensed under a Creative Commons Attribution 4.0 International License. The images or other third party material in this article are included in the article's Creative Commons license, unless indicated otherwise in the credit line; if the material is not included under the Creative Commons license, users will need to obtain permission from the license holder to reproduce the material. To view a copy of this license, visit http://creativecommons.org/licenses/by/4.0/

© The Author(s) 2017

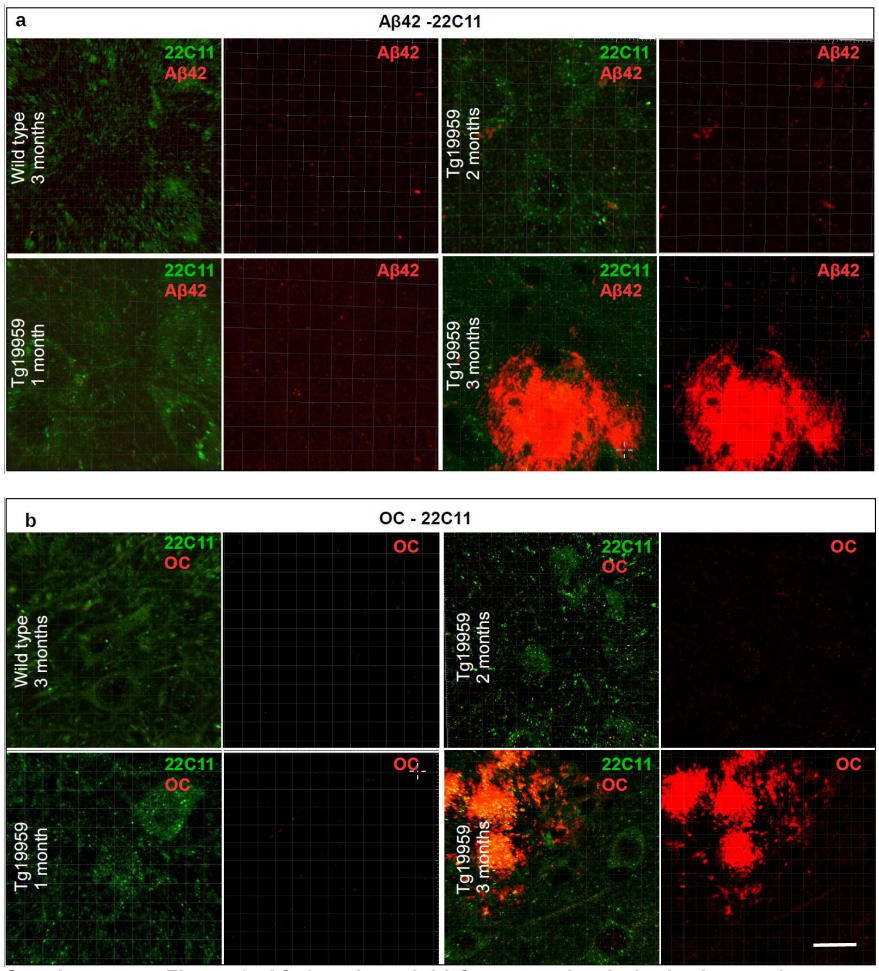


Supplementary Figure 1. Sample preparation used for μFTIR does not induce artificial β-aggregation. (a) Thioflavin T (ThT) kinetic assays of 20 μM Aβ1-42 fibril formation in the presence 6 μM ThT at 37°C. Since ThT fluorescence intensity at 480 nm is proportional to the mass of amyloid fibrils, the increase of ThT fluorescence shows that after several hours of incubation, Aβ1-42 formed β-sheet fibrils. The ThT fluorescence experiments were repeated three times. In parallel to the ThT kinetic assays, Aβ1-42 was incubated without adding ThT in low-bind Eppendorf tubes at 37°C under quiescent conditions. For μFTIR, 5 μL drops of samples of monomeric and fibrillar fractions were placed on CaF_2 spectrophotometric windows, and then all samples were snap frozen and cryo-dried. Monomeric Aβ1-42 was collected at 4°C, before the temperature switch. Fibrillar Aβ1-42 were collected after ThT fluorescence reached a plateau indicating the presence of mature fibrils in the suspension as indicated by red arrows. **(b)** Normalised representative μFTIR absorbance spectra taken from monomeric and fibrillar Aβ1-42 samples. Background spectra were collected from a clean area of the same CaF_2 window. **(c)** As shown by second derivatives of FTIR spectra, a characteristic peak for β-sheet structures was evident only for fibrillar Aβ1-42 (grey bar) but not for monomers of Aβ1-42, supporting that the sample preparation for μFTIR does not introduce artificial β-sheet formation. Experiments were repeated for 3 independent sample preparations.

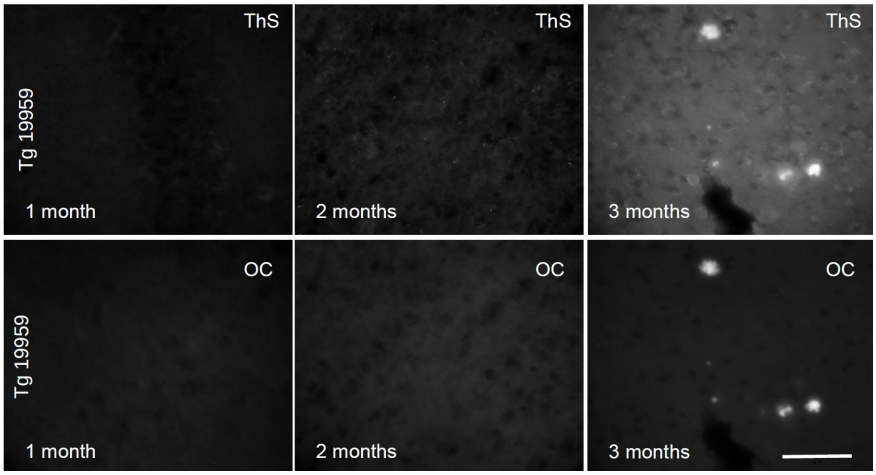


Supplementary Figure 2. FTIR absorbance spectra of Tg19959 and wild-type mouse brain sections. (a) An overview of a brain tissue slice placed on a CaF_2 window (upper panel). Brain tissue was snap frozen, cryostat sectioned, mounted on CaF_2 windows, and stored at -80°C until use. Dashed squares show the positions of µFTIR measurements. Scale

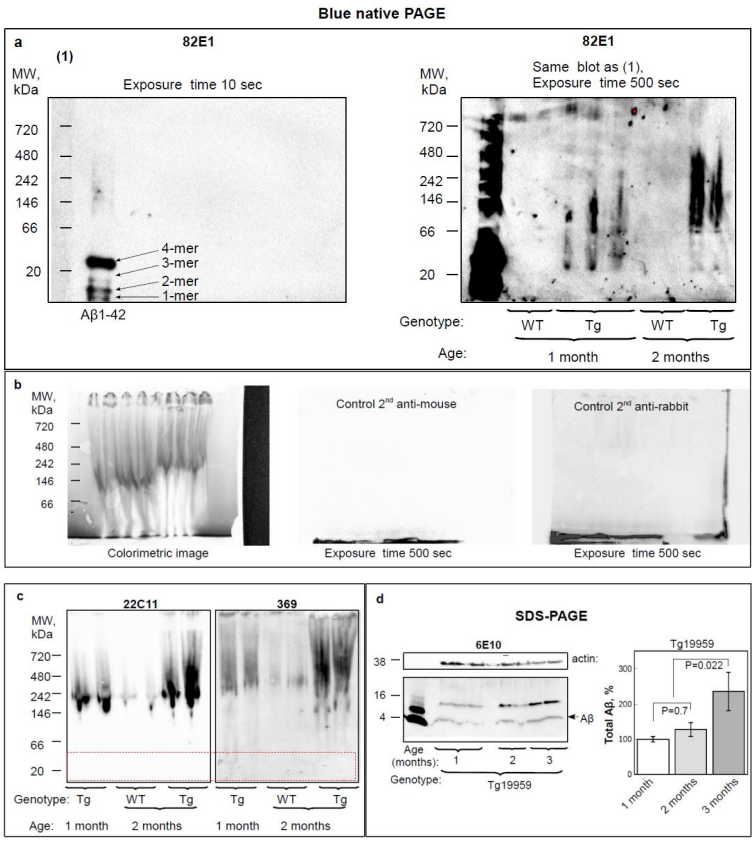
bar is 700 µm. Lower panel: Baseline corrected and normalized FTIR absorbance spectra of mouse brain tissue recorded with an aperture of 8×8 μm^2; the instrument resolution was set at 4 cm^{-1}; 250 - 1000 co-added scans per spectrum (5 to 10 spectra per age) **(b)** Baseline corrected and normalized FTIR absorbance spectra of Tg19959 and wild-type mice. A shoulder corresponding to β-sheet structures is indicated by a grey bar. **(c)** Normalised 2nd derivatives of FTIR spectra from brain tissue, spectra of one colour corresponds to one animal. **(d)** Left panels: an overview of a neuron grown on a CaF_2 window (left panels). Neurons were fixed and stored at -80°C until use. Middle panels: µFTIR maps integrated for the β-sheet spectral region at 1640-1620 cm^{-1} show absorption intensities for the β-sheet content in AD transgenic neurones at different times in culture, β-sheet content appears as red spots. Scale bar is 100 µm. Right panels: Normalised 2nd derivatives of FTIR spectra taken from APP/PS1 neurons at 12 and 19 DIV, and wild-type neurons at 19 DIV (panels 3 and 5).



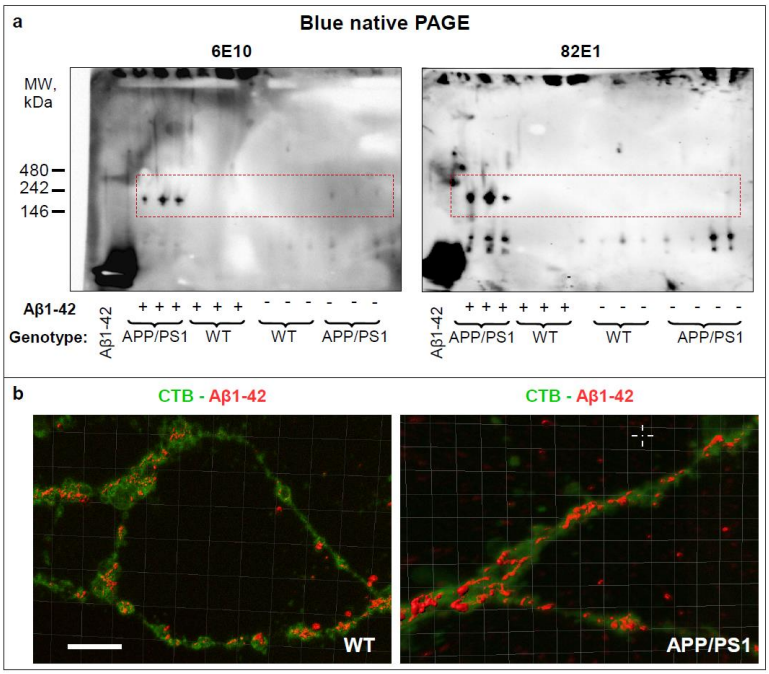
Supplementary Figure 3. Aβ42 and amyloid β-aggregation in brain tissue of Tg19959 mice. (a) Aβ42 in brain tissue with age as revealed by an Aβ42 specific antibody (Invitrogen 700254). **(b)** Amyloid fibrils in Tg19959 brain tissue revealed by OC antibody. OC positive amyloid plaques are visible in Tg19959 mouse brain tissue at the age of 3 months. Wild-type mouse brain was set as a threshold. Neuronal cells are visualised using antibody 22C11 against the N-terminus of APP. Images are representative, N=3 per genotype/age. Scale bar is 10 μm.



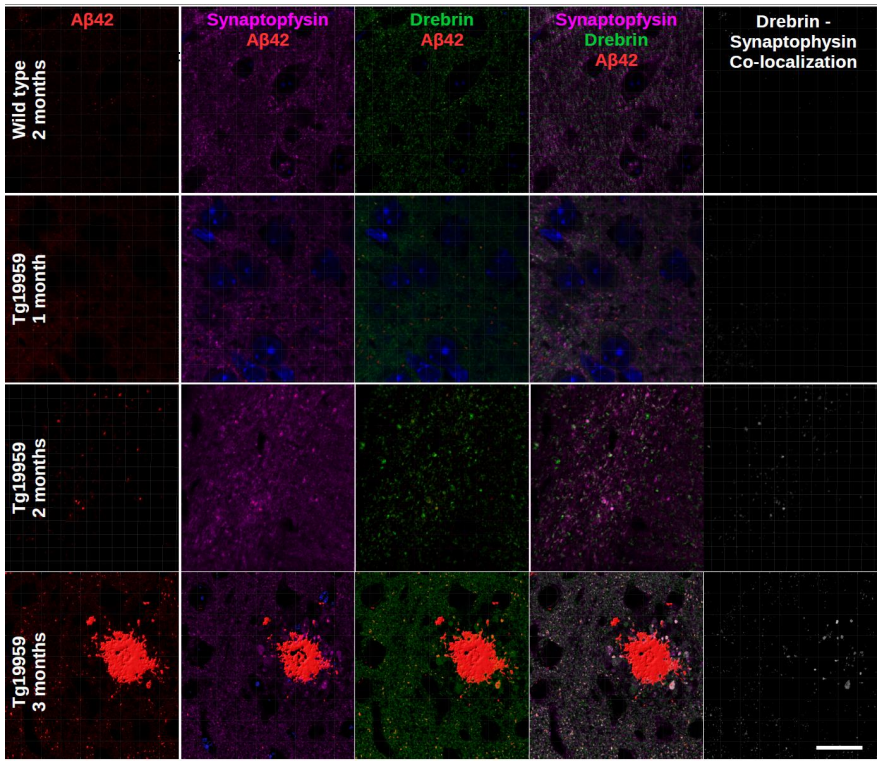
Supplementary Figure 4. Amyloid-β fibrillization in brain tissue of Tg19959 mice. Adjacent sections of the brain tissue sections used for FTIR measurements were double-labelled with OC and ThS. Double labelling visualised amyloid plaques in Tg19959 mouse brain tissue only at the age of 3 months. Scale bar is 50 µm. Wild-type mouse brain was set as a threshold. Images are representative, N=3 per genotype/age.



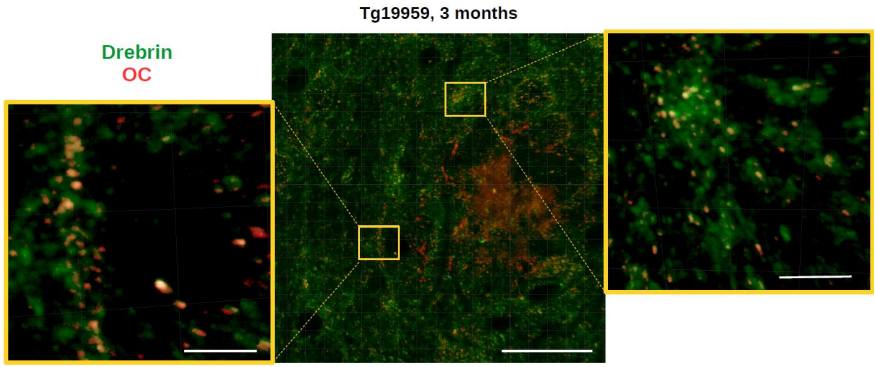
Supplementary Figure 5. Un-cropped versions of BN-PAGE western blots shown in Fig 4. (a) BN-PAGE and subsequent Western blot of membrane-associated TBST fractions of wild-type and Tg19959 mouse brain homogenates at 1 and 2 months of age. Aβ detected by human specific 82E1 antibody as shown in underexposed (1) and overexposed (2) versions. Synthetic human Aβ1–42 peptide was used as a size marker and positive control. **(b)** No cross-reactivity is evident as revealed by a WB with only secondary antibodies. **(c)** Un-cropped blots showing that the LMW Aβ band does not correspond to any APP fragments as revealed by antibodies against the APP N- (22C11) and C- (369) termini (red box). **(d)** As expected, SDS-PAGE shows increasing amounts of Aβ (arrowhead) in protein extracts from Tg19959 mouse brains as revealed by antibody 6E10. Statistical analysis of monomeric Aβ in brain homogenates is with ANOVA ($P < 0.01$) followed by *Bonferroni's post-hoc* comparisons test ($P < 0.01$); mean ± SD. ($N = 4$ per genotype/age).



Supplementary Figure 6. Role of APP in Aβ binding. (a) Wild-type and APP/PS1 primary neurons were treated with 1 μM of Aβ1-42 for 24 hours. The added Aβ1-42 was detected by BN-PAGE followed by Western blot with human-specific Aβ antibody 82E1 and human-specific Aβ/APP antibody 6E10; bands which are consistent with the molecular weight of APP are shown in the red boxes, N=3 embryos. **(b)** Immunofluorescent confocal microscopy images of wild-type and APP/PS1 primary neurons treated with 1 μM Aβ1-42 for 1 hour. Untreated neurons were set as a threshold. Aβ1-42 was detected by antibody 82E1 (red). Neuronal membranes were stained with the dye Cholera toxin subunit B1 (CTB) specific to GM1 gangliosides abundantly present in the cell membrane (green); scale bar is 1 μM.



Supplementary Figure 7. Aβ42 alters the cytoarchitecture of synaptic terminals in Tg19959 mouse brains with age. Aβ42 in brain tissue slides was labelled with an Aβ42 specific antibody (Invitrogen 700254) and is shown in red; at 3 months an amyloid plaque is clearly evident, while punctate Aβ42 increases are detectable already at 2 months. The middle panels show the pre- synaptic marker synaptophysin (magenta), the post-synaptic marker drebrin (green) and Aβ42 (red). The white puncta in the far right panel shows co-localization of drebrin and synaptophysin, which is evident in 2 and 3 month-old Tg19959 mice. Around the plaque in the 3-month-old Tg19959 mouse, the locations of these even more enlarged puncta (compared to at 2 months) are consistent with that of dystrophic neurites. Images are representative, N=3 per age/genotype. Scale bar is 10 µm.



Supplementary Figure 8. Amyloid aggregation in dendritic terminals of Tg19959 mouse brains. Double labelling with OC and the post–synaptic marker drebrin (green) revealed amyloid fibrils (OC, red) co-localized (yellow) with the post-synaptic protein drebrin (green) at the age of 3 months. Wild-type mouse brain was used to set the threshold. Images are representative, N=3. Scale bars: left panel: 1.5 µm, middle panel: 10 µm, right panel: 2µm.

Supplementary Table 1. List of primary antibodies

Antibody	Target Epitope	Species and type	Dilution (WB)	Dilution (IF)	Source	Cat. #
369	Human/mouse full length APP, α/βAPP, α/β CTF, APP C-terminus	Rabbit polyclonal	1:1000		Buxbaum et al. (1990)[1]	
6E10	Human Aβ, full length APP, α/βAPP, α/β CTF, a.a. 3-8 of Aβ	Mouse monoclonal	1:1000		BioLegend	Previously Covance catalog# SIG-39320
22C11	Human APP, N-terminus, a.a. 66-81 of APP	Mouse monoclonal	1:1000		Merck Millipore	ab348
P2-1	Human APP, N-terminus, a.a.104-118 of APP	Mouse monoclonal	1:1000		ThermoFisher	OMA1-03132
82E1	Human Aβ1-x, N-terminus specific, a.a. 1-4 of Aβ	Mouse monoclonal	1:1000	1:200	IBL International	10323
12F4	Human/mouse Aβx-42, C-terminus specific	Mouse monoclonal	1:1000	1:200	BioLegend	Previously Covance catalog# SIG-39142
MBC Aβ42	Human/mouse Aβx-42, C-terminus specific	Mouse monoclonal	1:1000		Kindly provided by Dr. Haruyasu Yamaguchi[2]	
Aβ42	Human/mouse Aβx-42, C-terminus specific	Rabbit polyclonal		1:200	Invitrogen	700254
OC	Amyloid fibrils	Rabbit polyclonal		1:1000	Merck Millipore	ab2286
Synaptophysin	Synaptophysin			1:1000	BioLegend	MAB5258
Drebrin	Drebrin	Rabbit polyclonal		1:1000	Abcam	ab11068
Cholera toxin Subunit B	Ganglioside GM1	Alexa Fluor 488 conjugate		1:1000	Molecular probes	C-34775
Map2	Map2	Chicken polyclonal		1:1500	Abcam	ab5392

Supplementary References

1. Buxbaum, J. D. *et al.* Processing of Alzheimer beta/A4 amyloid precursor protein: modulation by agents that regulate protein phosphorylation. *Proc Natl Acad Sci USA* 87, 6003–6006 (1990).

2. Takahashi, R. H. *et al.* Intraneuronal Alzheimer Aβ42 accumulates in multivesicular bodies and is associated with synaptic pathology. *Am. J. Pathol.* 161, 1869–1879 (2002).

Printed by Media-Tryck, Lund 2017 NORDIC ECOLABEL, 3041 0903



LUND UNIVERSITY
Faculty of Medicine

Department of Experimental Medical Science

Lund University, Faculty of Medicine
Doctoral Dissertation Series 2017:177
ISBN 978-91-7619-559-8
ISSN 1652-8220

